AN EXPERIMENTAL STUDY OF ACOUSTICALLY EXCITED, VORTEX DRIVEN, COMBUSTION INSTABILITY WITHIN A REARWARD FACING STEP COMBUSTOR

Thesis by

Duane A. Smith

In Partial Fulfillment of the Requirements
for the Degree of
Doctor of Philosophy

California Institute of Technology
Pasadena, California
1985

(Submitted 18 March 1985)

ACKNOWLEDGEMENTS

Over my years at Caltech, I have had the priviledge of working along side many talented individuals; therefore, I would like to express my thanks to all of them for their help and generosity. In particular, I am indebted to my advisor, Dr. Zukoski, whose enthusiastic support and guidance were invaluable. In addition, I would like to acknowledge Dr. Marble for his useful suggestions during this period.

My thanks are extended to Vigor Yang, for his computer data acquisition skill, and to Joe Humphrey for his acoustic modeling expertise. The technical support of George Lundgren, George Wilson, and Howard McDonald in construction of the experimental apparatus is appreciated, as well as Harry Hamaguchi's photographic work.

Finally, I want to express a special thanks to my wife, Sarah, for her support throughout my graduate work, enabling me to accomplish my dream. I can only hope that she will share my pride in its fulfillment, as much as she did my frustrations along the way.

This research was supported under AFSOR Grant No. 80-0286.

ABSTRACT

An internal feedback mechanism, capable of sustaining combustion instabilities, is investigated inside a small laboratory combustor in which the flame is stabilized behind a rearward facing step. Pressure and optical measurements are employed to define the acoustic field and heat release rate within the combustor, while shadowgraph records are used to visualize the reacting, kinematic flow field.

The acoustic flow field creates an unsteady flow inside the combustor, which produces an unsteady heat addition. When this fluctuating heat release is in the appropriate phase relationship with the pressure oscillation, energy is supplied to the acoustic field, and the strong acoustic oscillations are sustained.

As a result of the strong acoustic oscillations present during combustion instability, the flow surges into the combustor periodically, and large vortices are formed at the acoustic frequency which produce the large velocity fluctuation in the vicinity of the flameholder. The magnitude of the velocity fluctuation, relative to the mean flow speed, determines whether or not the vortex will form. The frequency of the combustion instability appears to be directly proportional to the amplitude of the velocity fluctuation so that the actual magnitude of the velocity fluctuation determines the instability frequency. The dependence of the instability frequency upon the velocity fluctuation creates the possibility of exciting a large range of frequencies.

Continued existence of the combustion instability depends upon the mean flow speed, fuel type, and fuel-air ratio.

TABLE OF CONTENTS

LIST OF FIGURES

LIST OF SYMBOLS

A_1	cross-sectional area of combustion chamber
A_2	cross-sectional area of inlet
A_3	cross-sectional area of plenum chamber
A_e	cross-sectional area of inductance
a	local acoustic velocity
a_1	acoustic velocity in combustion chamber
a_2	acoustic velocity in inlet
a_3	acoustic velocity in plenum chamber
a_e	acoustic velocity in inductance
K	modified wave number, $k/(1-M^2)$
K_1	modified wave number in combustion chamber
K_2	modified wave number in inlet
K_3	modified wave number in plenum chamber
k	local wave number, Ω/a
k_1	wave number in combustion chamber
k_2	wave number in inlet
k_3	wave number in plenum chamber
L	maximum length of the recirculation zone
LC	axial length of the combustor
L_e	length of recirculation zone
LI	axial length of the inlet
LP	axial length of the plenum chamber
l_e	axial length of the inductance
M	local Mach number
m_e	mass of fluid in the inductance region

P^+	right traveling wave
P^-	left traveling wave
P_1^+ , P_1^-	traveling waves in the combustion chamber
P_2^+ , P_2^-	traveling waves in the inlet
P_3^+ , P_3^-	traveling waves in the plenum chamber
p	pressure
p'	fluctuation pressure
p_0	local static pressure
p_1	pressure in the combustion chamber
p_2	pressure in the inlet
p_3	pressure in the plenum chamber
q'	fluctuating heat release rate
t	time
u	streamwise velocity
u_1	streamwise velocity in combustion chamber
u_2	streamwise velocity in inlet
u_3	streamwise velocity in plenum chamber
u_e	streamwise velocity in inductance
V	average velocity in the mixing layer
V_c	cold gas velocity outside the mixing layer
x	axial distance
x_0	origin of the mixing layer
α	imaginary portion of the complex frequency
β_c	blow off parameter
β_e	reflectance condition at combustor exit
β_p	reflectance condition at plenum chamber entrance

ΔE	change in acoustic energy
γ	specific heat ratio
δ	visual thickness of the mixing layer
δ'	mixing layer growth rate
ρ	fluid density
τ_c	chemical time delay
Ω	complex frequency, $\omega + i\alpha$
ω	real portion of the complex frequency

CHAPTER 1

INTRODUCTION

1.1 Combustor Concept

Numerous investigations have been undertaken to examine the combustion processes occurring inside high intensity combustion systems. These high intensity burners are characterized by flame stabilization which is maintained at flow velocities greater than the normal propagation velocity of the flame. To ensure continuous combustion in these systems, the flame is anchored, or sustained, by recirculation of some of the burnt products in the separated flow region behind a bluff body, or obstacle, placed in the mean flow. These obstacles are commonly called flameholders. One particular combustor, often used in ramjet combustion systems, stabilizes the flame in the wake region downstream of an abrupt change in the container contour as shown in Figure 1.1.

A small scale two-dimensional laboratory combustor was prepared to simulate the combustion processes occurring inside a ramjet type engine as illustrated in Figure 1.2. Behind the rearward facing step, flame stabilization is achieved by mixing the fresh reactants with the hot products of combustion inside the two-dimensional mixing layer formed downstream of the flameholder. This mixing layer appears to be similar to an isothermal layer and is composed of vortices which grow by entrainment of fluid and pairing with neighboring vortices. Once the flame has been anchored, or stabilized, it spreads across the length of

the combustor burning the remaining reactants.

Many high-intensity combustors are plagued by large vibrations created by pressure oscillations excited inside the combustor. The magnitude of the vibrations are frequently large enough to damage the payload aboard the vehicle, and sometimes of sufficient magnitude to entirely destroy the vehicle. The primary cause of these instabilities hinges on the fact that heat released during the combustion process supplies a substantial amount of energy to the mean flow field, creating instabilities through an internal feedback mechanism between the acoustically generated pressure field and the fluctuating heat addition. Consequently, the combustion processes may feed enough energy into the pressure field, producing large amplitude oscillations which are capable of destroying the properties associated with stable burning. The aim of the current work is to develop physical insight into the problem by describing the feedback mechanism observed during unstable combustion.

1.2 Background

Early work examining the flow field behind bluff body flameholders was presented by Zukoski (1954). His studies show the kinematic flow field and blowoff characteristics of flames stabilized behind several different types of flameholders. Continuing the line of work, Rogers and Marble (1956) succeeded in exciting large pressure fluctuations in a small combustor with the flame stabilized behind a "V" shaped flameholder. During their investigation, they discovered an instability mode which was referred to as screech. Under screeching conditions, the flow field behind the flameholder is transformed from a smooth mixing

layer to a series of vortices which are shed alternately from the flameholder edges.

The flow field, downstream of the flameholder in the current study, consist of a reacting, reattaching, turbulent shear layer. Recently many investigators have become interested in the flow field characteristics exhibited by planar turbulent shear flows and reattaching turbulent shear layers. Brown and Roshko (1974) discovered that large coherent structures are an inherent characteristic of planar turbulent mixing layers. After examining the effects of large density gradients across the layer, they conclude the growth of the vortical structures are meagerly affected by the large density differences between the two fluid streams. Ho and Huang (1982) studied the influence of periodic forcing upon turbulent shear flows in a water channel. Results of this study illustrate that the growth of the mixing layer may be enhanced by periodic forcing at the proper frequencies. Perturbations applied to both flow streams result in simultaneous merging of discrete individual vortices within the shear layer. The subsequent spreading rate of the mixing layer increases markedly, leading them to conclude the periodic forcing would be an effective method to manipulate the growth of mixing layers.

Eaton and Johnston (1980) conducted an experimental study examining the isothermal reattaching turbulent mixing layer formed behind a two-dimensional rearward facing step. A pulsed wire anemometer was employed to measure the mean velocity and turbulence profiles at different longitudinal positions. Their results indicate the reattaching turbulent mixing layer grows almost identically to the planar mixing layer studied by Brown and Roshko in the initial stages of formation.

However, as the layer develops, the influence of the wall boundary condition is felt, and the layer curves sharply toward the wall. The reattachment point, or location where the layer impinges against the wall, was found to be a function of the initial boundary layer condition and occurs 5 to 7 step heights downstream.

Several experimenters have studied different aspects of reacting flow fields as found in various ramjet combustion systems. Only a few individuals have examined in detail the reacting flow field behind a rearward facing step. Ganji and Sawyer (1980) studied characteristics of a two-dimensional, reattaching, reacting shear layer to establish how lean premixed flames affect pollutants. Results from their flow visualization indicated that the reacting mixing layer consisted of coherent structures similar to the type described by Brown and Roshko. However, as the fuel fraction of the combustible mixture was increased toward stoichiometric proportions, the characteristics of the flow field changed to their surprise. Instead of a mixing layer forming downstream of the step, a very large vortical structure was formed periodically. During this phenomenon, denoted as chugging, a rise in the pressure fluctuation inside the combustor was observed, which caused the incoming flow to reverse directions, leading Ganji to conclude that chugging leads to a flashback condition. Keller (1982) and Vaneveld (1984) looked at the chugging mode in this combustor more closely. Keller examined transition from smooth combustion to chugging by changing the fuel-air ratio in a step function manner. Vaneveld studied the secondary effects leading to flashback by inverting the hot and cold gas streams. He found that the buoyancy effects were negligible,and that a contour change, downstream of the step, broke up the chugging

phenomenon.

Pitz (1981) used the Ganji and Sawyer experimental facilities to explore the stable burning properties of this combustor employing a laser-Doppler velocimeter. He studied both the non-reacting and reacting cases. In the reacting case to ensure smooth combustion and thus a stable planar turbulent reattaching shear layer, steel wool was inserted into the upstream piping. Measurements of the layer growth, entrainment, and reattachment are discussed in this work and in a following paper by Pitz and Daily (1983). In the reacting flow field, a noticeable shortening of the reattachment length, of up to 30 percent, was observed.

Within the literature discussed here, I have found no attempt to propose, or examine, the feedback mechanism between the combustion processes and the oscillating pressure field inside ramjet combustion systems, and this is the major emphasis of the current work.

1.3 Scope of Work

The primary purpose of this work is to propose a mechanism which is capable of sustaining combustion instabilities inside ramjet type combustion systems. This includes exploring the effects of acoustic conditions, flow speed, and fuel-air ratio upon the instability mechanism and its development. To accomplish this goal, the following objectives are laid out:

EXPERIMENTAL:

Design and construct a test combustor apparatus to simulate a ramjet type combustion system.

Develop pressure instrumentation to measure the acoustic pressure field inside the combustor.

Design a system to visualize the reacting kinematic flow field inside the combustor.

Develop an optical apparatus capable of monitoring the local flame emission.

THEORETICAL:

Develop an analytical model of the test combustor apparatus to determine the normal acoustic resonant modes of the system.

Predict the acoustic fluctuating pressure throughout the apparatus given an experimentally determined pressure at a specific location.

Predict the fluctuating velocity inside the apparatus using the pressure measurement.

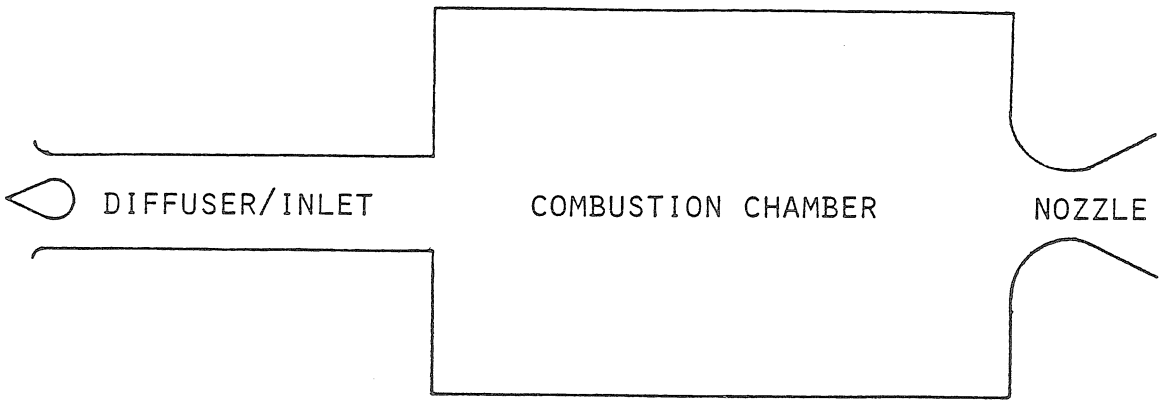

Figure 1.1 Ramjet Engine

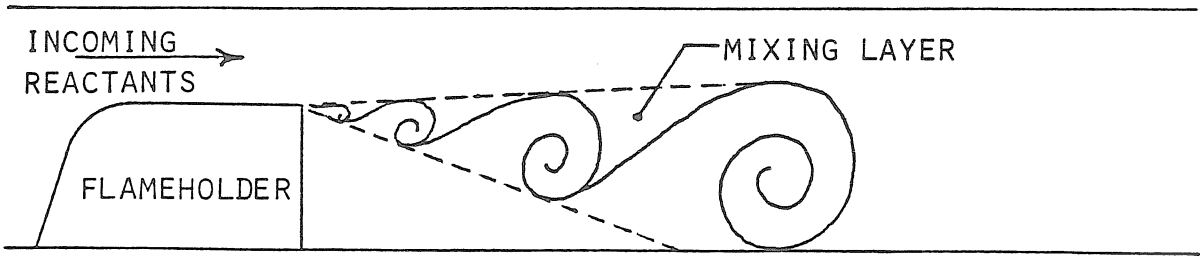

Figure 1.2 Laboratory Test Combustor

CHAPTER 2

EXPERIMENTAL APPARATUS AND PRINCIPALS OF OPERATION

2.1 Combustor Facility

The experimental study of combustion processes in the "ramjet" type combustor required construction of a small-scale combustor facility which is shown in Figure 2.1. A traditional blow-down supply system is used to furnish the combustible gas mixture. The high pressure fuel and air streams each pass through dual dome pressure regulators to ensure accurate pressure upstream of sonic nozzles used to control the flow rate. The total pressure at the inlet of these axis-symmetric, converging nozzles determines the mass flow entering the combustor when the exit nozzle Mach number is unity. Each nozzle inlet area is made much larger than the exit area so that the pressure of the gas measured at the nozzle inlet is a good estimate of the total pressure. Furthermore, the ratio of the fuel nozzle exit area to air nozzle exit area is sized such that a stoichiometric fuel-air ratio is delivered when the same upstream total pressures are used. With this design feature, the mass flow rate to the combustor can be monitored easily and accurately; moreover, the flow rate can be changed rapidly without fear of extinguishing the flame due to poor reactant control because both the fuel and air pressures are changed concurrently.

After passing through the flow metering system, the fuel and air streams impinge and begin to mix. With a prevaporized combustible mixture, a temperature rise created by a spark or combustor flashback

would markedly increase the local reaction rate. The density change associated with the temperature of burning the reactants would be in the order of 7:1. This sudden expansion would cause instrumentation damage and possible structural failure of the plumbing hardware. In the event of uncontrolled combustion a rupture disc is installed for venting the system and protecting the equipment when mixed reactants are present.

The combustible mixture enters the 15.2 cm. diameter plenum chamber through a porous cone structure to enhance production of a uniform, axis-symmetric velocity profile as shown in Figure 2.2. Six screens (about 25 mesh) are placed at the downstream portion of the plenum chamber to reduce the turbulence level of the mean flow. A contracting segment is fitted to the plenum exit which smoothly changes the axis-symmetric geometry to a two-dimensional one compatible with the combustor. The gas is accelerated through this 9.4:1 contraction as it flows into the inlet. The reactants enter the combustor and the flame is stabilized behind the rearward facing step.

The fuel-air mixture ratio delivered to the combustor can be continuously changed. The remote dome pressure regulators, located in the air and fuel lines, are activated by control regulators mounted in the operator panel. The nitrogen output pressure from a single control regulator controls the two furthest downstream regulators in the air and fuel supply lines for delivery of stoichiometrically mixed air and fuel as mentioned before. When the proper flow rate has been established, a 3-way valve is used to separate the two dome regulators. Now, the additional control regulator manipulates the nitrogen pressure, delivered to the remote fuel regulator, so that the mixture ratio can be set to any desired value.

2.1.1 Combustor Design

The design for the combustor requires access for pressure measurements, flow visualization, and optical measurements. Adequate flow visualization dictated the use of a two-dimensional geometry; consequently, a rectangular channel is chosen as the body contour for the combustor. This channel is mounted to the plenum chamber assembly as shown in Figure 2.2.

The combustor upper and lower walls are fabricated so that the inner steel liner of the combustor is cooled by water flowing inside an outer aluminum cooling jacket. The side walls of the combustor are segmented and secured to the upper and lower walls by a window frame structure. This provides flexibility to the experimenter. A water cooled metal side wall can be inserted for long duration experiments, or Vycore glass walls can be utilized for flow visualization and optical measurements. The region of burning is of variable length, up to 81 centimeters, with a cross-sectional area of 2.54 cm by 7.62 cm.

The rearward facing step flame holder is attached to the lower wall. Its position can be changed so that the combustor length is variable. The flame holder spanned the entire width of the duct and is 1.91 cm high, 7.62 cm wide, and 7.62 cm long. Immediately downstream of the flame holder the igniter is installed. It is mounted in the lower wall and is formed by a stainless steel rod surrounded by a ceramic insulator. When a high electric potential is applied to the steel rod, a spark is generated. This spark ignites the premixed fuel and air mixture so that the flame can be stabilized.

A common externally sized port is used for instrumentation access

to the combustor. This common mount is convenient because a measurement device can be moved to any location without fear of cooling water leaking into the burner or combustion products escaping. Ten access ports are mounted in the upper wall and four ports are located in the lower wall. This design has proven to be adequately versatile for measurements and observations performed during the combustion experiments.

2.1.2 Pressure Instrumentation

In order to measure the average static pressure and rapidly fluctuating pressure in the combustor apparatus, two types of pressure measurement equipment are employed. Small diameter metal tubes are flush mounted into the combustor wall to measure static pressure. Plastic hoses, connected between the metal tubes and a Scanvalve switch, enable measurements of pressures, at several different locations, to be made with a single pressure transducer. Over a period of a couple of seconds, the static pressure distribution, involving up to 11 measurements, can be determined easily, employing this motorized Scanvalve switch arrangement.

The measurements of time varying pressure in the combustor is more difficult. The adiabatic flame temperature from a premixed methane-air flame is nearly 2000 Kelvin. Any material exposed to this extreme heat would quickly disintegrate; therefore, a transducer of sturdy construction is needed in addition to a mounting technique that maintains the transducer at a reasonable temperature. A constant moderate temperature not only keeps the transducer structurally intact,

but limits the change of frequency response due to thermal heating. An integrated circuit, piezoelectric pressure transducer, PCB model 106B, was chosen for measurements of the oscillating pressure. This type of transducer features a miniature voltage amplifier combined with the piezoelectric measurement element. A high-level, low-noise output signal is generated by this type of transducer with a fixed voltage sensitivity independent of cable length or capacitance. The sensitivity of the transducer is 300 mv/psi (.04 mv/Pa). A small battery operated power supply provides the proper electric current to the transducer,and the variable gain output of this power unit ensures adequate voltage levels sufficient for computer based data acquisition.

Each pressure transducer is mounted in a cavity to protect the pressure sensitive surface from extreme temperatures and rapid overpressurization. The cavity and transducer mounting are bored into the common instrumentation plugs which are inserted through the water jacket and threaded into the combustor wall. Consequently, each transducer and the gas trapped in the cavity volume are cooled by water flowing around the plug. The pressure transducer is 1.31 centimeters in diameter, defining the cavity's cross-sectional area. The gas in the cavity is joined to the combustor via 5 small holes. The size of the holes is kept small, 0.159 cm. diameter, to protect the transducer from rapid pressure rises in the combustor by limiting the amount of gas passing through them.

Measurements of the oscillating pressure are easiest to interpret if the pressure measured at the surface of the transducer is identical to the pressure disturbance inside the combustor. Therefore, for the sake of convenience, the region of gas between the combustor and

transducer must not alter the pressure magnitude or phase. The length of the connecting holes could be designed so that the lengths were less than a centimeter and, thus, short with respect to the 1 to 2 meter wavelengths of the pressure oscillations. Consequently, a Helmholtz resonator analogy would be appropriate to use in calculating the acoustic properties of the transducer mounting. Given the above mentioned constraints, choosing a cavity volume of .0853 cubic centimeters and 5 connecting holes with lengths of .90 centimeters provides an interface designed with a 5500 hertz resonant frequency. The measurements of the cavity's resonant frequency compared favorably with this design prediction. The resonant frequency was measured to be 5240 hertz, only about one percent different than predicted. Consequently, no compensation for differences between the measured and source pressure are needed with this design for disturbances below approximately 800 hertz.

2.1.3 Radiation Instrumentation

The pressure oscillations observed inside the combustor apparatus are sustained by energy released during the chemical reaction process. Examination of the manner in which the heat is generated locally is mandatory for understanding the complex coupling between the pressure oscillations and combustion processes occurring inside the burner. The localized heat release is influenced by the fluctuating acoustic pressure field. To sustain large pressure fluctuations, the heat release must occur at the same frequency as the pressure oscillations. Consequently, the time response of an instrument to measure heat release

must be much less than the period of acoustic oscillation.

Unfortunately, a technique for the direct measurement of the rate at which heat is released during the exothermic combustion process is not available. However, an approximate method based upon flame radiation can be employed. The governing idea behind this method relies on the fact that the magnitude of the radiation, produced by burning of a small premixed combustible mass, is related to the local heat release rate. The radiation emission can be measured with an optical technique which easily meets the time response criterion.

This method has been employed by several experimenters. For example, John and Summerfield (1957) suggest the ideal measurement would identify a substance confined to the reaction zone itself. Thus, observation of the radiant emission from free radicals such as CH, C2, and CO2 is very useful in studying chemical reaction processes in the flame region. John, Wilson, and Summerfield (1955) examined the effects of mixture ratio upon the ratio of two of these emitters, CH/C2. In fact, they found the emitter ratio to be a unique function of the fuel-air ratio and provided them with a way to study the heat release as a function of the flame's local stoichiometry. Some experimenters, such as Hurle (1968), have calibrated the light emission from the C2 free radical in terms of the fuel flow rate of reactants. He found a linear relationship existed between the emission and the flow rate. This experiment was duplicated at Caltech by Huot, Frost, and Lim (1982). In their work, a somewhat lesser linear dependence was found. However, in either set of experiments, a monatonic relationship existed between the heat release rate and flame radiation, and in general, the emission from the flame varied approximately linearly with respect to the flow rate.

The linear relationship existed for either a narrow spectral band (Hurle, Price, Sugden, and Thomas 1968, and Huot, Frost, and Lim 1982), or broad band flame radiation (Huot, Frost, and Lim 1982).

Thus, the current study assumes that the intensity of radiation emitted from a small region of reacting gas indicates at least qualitatively the rate of heat release in that region. In other words, the intensity of light emitted from the burning gas can be used to compare the heat release rate between different experimental operating conditions.

A photomultiplier tube, RCA model 8645, is used to measure the radiation emitted from the flame because of its high frequency response and broad band spectral coverage. The photomultiplier views the burner through an optical arrangement which observed the entire height and width of the combustor, but limits the axial length view to approximately .64 centimeters (Figure 2.3). The total system is mounted on a moveable traverse mechanism which allows detailed examination of the heat release rate throughout the entire length of the combustor.

2.2 Data Acquisition System

One objective of the experiment is to obtain accurate time-resolved measurements of the fluctuating pressure and light emission observed in the test combustor under different operating conditions. An estimate of the frequency and magnitude of these fluctuating signals would be the most useful information to obtain. Since the pressure and radiation arise from acoustic oscillations, the measured signals are periodic functions which may be decomposed into a combination of elementary

sinusoids. Such a Fourier series representation of the signals is most commonly obtained using a Fast Fourier Transform algorithm to compute a spectrum from a digitized time record. Consequently, a computerized data acquisition system is very attractive. Now, any number of experimental parameters can be measured sequentially by a controlling computer in the proper format for data reduction.

Surveying the experimental parameters of interest requires six channels of time-varying data and four channels of steady-state data. The time-varying data consist of pressures measured at five different locations and observations of the light radiation from the flame at a specific location. The time-varying pressures are required for acoustic analysis while the radiation intensity is employed to study the local periodic heat released rate of the flame. Additionally steady data, such as the reactant's temperature and pressure, are monitored to evaluate the flow rate and stoichiometry delivered to the combustor.

The computer data acquisition system employed to collect the data is based upon the Hewlett Packard 2100A computer. The computer controls a 16-channel Preston multiplexer/converter utilized for data digitation. Digitation of a continuous time signal consists of two separate operations. First, sampling of the time-varying signal is made at discrete time intervals. For these experiments the multiplexer speed is set to obtain 62,500 samples per second, or a corresponding channel sampling rate of 10,417 samples per second. Excessive data points are eliminated by choosing this sampling rate, yet confusion between low and high frequency components of the data or aliasing is avoided. The second operation, quantitation, involves converting the output voltage from the transducer to a binary number compatible with computer storage

and manipulation. The Preston unit converts a 10 volt full-scale signal to a word equal to 2**15 or 32,768. Inaccurate quantification was avoided by amplifying the electrical signals generated from the transducers to a point in which the background noise was a small fraction of the output signal; in other words, amplified to a level in which a change of the measured quantity in time produced a signal level change greater than the system noise level.

2.2.1 Data Acquisition Procedure and Data Analysis

The combustion process produces pressure oscillations whose amplitude changes with time. This random character makes it impossible to predict the exact value of pressure at a future instant of time. Thus, the random sampled data must be classified in a statistical sense so that statistical functions, such as the Power Spectral Density, can be used to accurately estimate the spectral composition of a finite discrete data record. As discussed in Bendat and Piersol (1971), formulas derived for data processing of discrete time series are obtained by assuming the sampled data records represent ergodic random processes. An ergodic process describes a stationary random process in which the time averaged properties are equal to the ensemble averaged values. Subsequently, the values of power spectral density in a stationary process are invariant over different samples of a parameter. If such a condition exists, then the frequencies of the pressure oscillation can be determined by calculating the time averages from a single sample function.

Its fortunate that most physical systems are generally stationary.

The easiest method to determine the stationarity of random data is to look carefully at the physics of the problem. When the basic physical circumstances which cause a phenomenon are constant with time, then the stationarity of the observed measurements can generally be accepted without further analysis. In an experimental test, the mass flow rate, reactant temperature, and stoichiometry delivered to the combustor are fixed. If the combustor is operated under steady state conditions, then the resulting data are consequently assumed to be stationary for analysis purposes. However, if the flow rate is varied during data acquisition, then the characteristics controlling the physical combustion processes and fluid dynamics would change, causing a nonstationary data record.

After classifying the type of data record generated during the experimental test of the combustor as stationary, an accurate analysis of the frequency content may be obtained. As mentioned earlier, the Power Spectral Density function is an important descriptive analysis of stationary random data. This function describes the general frequency content of the data in terms of the spectral density of its mean square value. The total area under the power spectrum curve is equivalent to the mean square value of the stationary random data sample.

After the combustor was ignited and the flame stabilized, an estimate of the power spectrum was obtained through a three step data analysis procedure. To begin, data are sampled at a rate of 10,417 samples per second, or a sample interval of 96 microseconds. Under these sampling conditions, the Nyquist frequency is 5208 hertz. A sinusoid, whose frequency is greater than this Nyquist frequency, will appear as a lower frequency in the Power Spectral Density function.

This phenomenon is referred to as aliasing (Bendat and Piersol, 1971). For example, suppose the power spectrum contained a component at 700 hertz. Energy at this frequency could be the result of oscillations at this frequency or oscillations at 2n(fc) +/- 700 hertz, where fc is the Nyquist frequency, and n is an indexing integer. So, oscillations at 9,716 hertz, 11,116 hertz, 20,132 hertz, 21,532 hertz, and so forth, would show up as energy at 700 hertz in the power spectrum. During the initial combustor inspections, no frequencies were observed greater than the Nyquist frequency so that aliasing is avoided and presents no problems.

The second step involves leakage reduction by shaping the time series segments, described next in step three, at each end to reduce error in the frequency domain results (Oatnes, 1978). The selected shaping is of the form of a cosine taper over one-tenth of the length of each end of the data segment. The shaping suppresses the inaccuracy of the Fourier Transform caused by sampling non-integer periods of sinusoids.

Step three is the computation of the power spectrum estimate using a Fast Fourier Transform computer code written by E. O. Brigham (1974). To obtain a smooth accurate estimate of the spectral density function, segment averaging is employed. The input time signal is divided into 25 smaller time segments which are cosine tapered and each analyzed by the FFT. The 25 results are averaged together to produce a smooth spectrum. The computed Power Spectral Density function has an effective bandwidth resolution of 5 cycles per second and normalized standard error of 0.2 under the described sampling conditions.

2.3 Flow Field Visualization

The shadow technique is very useful for direct viewing of flow phenomena containing large density gradients; therefore, this method is employed to observe the reacting kinematic flow field inside the combustor. During the combustion process, huge changes in temperature occur as well as changes in composition. The resulting refractive index variation, created by these disturbances, is primarily caused by temperature changes as discussed in Weinberg (1963). The shadow pattern, produced from the temperature changes, is formed by redistributing the illumination provided from the collimated incident light beam. Thus, shadowgraphy produces images of the flow field without hindering or interfering with the mean flow or combustion processes.

As mentioned earlier, the combustion processes are established in a premixed combustible mixture containing methane and air. The luminous flame zone generated by these premixed, prevaporized reactants is pale blue in color. The absence of yellow light indicates that no, or very little, soot is formed. Thus, absorption of the illuminating light within the flame zone is minimized and a clear shadowgraph image is created.

The resultant shadow effect depends on the relative deflection of the incident light rays passing through the combustor and not on the absolute deflection of the rays. In other words, if all the rays are deflected equally, then no shadow image would be created. Consequently, the shadowgraph technique is useful for flow visualization but not appropriate for measuring actual refractive index distributions.

In order to observe the relative deflection of the light rays, the shadow plane is naturally located at a position slightly outside the combustor. Since the shadow plane and disturbance within the combustor are not coincident, the shadow image appears different in size, as compared to the combustor body image, when they are both focused onto the recording film plane. Consequently, care must be taken when utilizing the photographs of the kinematic flow field for elementary quantitative analysis.

2.3.1 Spark Shadowgraph System

A typical focused shadowgraph system was designed to photograph the instantaneous reacting combustor flow field. The focused system varies from the traditional shadowgraph system in that optical elements are placed between the shadow plane and the film plane to allow control of the image size. The insertion of the lenses or mirrors not only changes the magnification of the image, so that different recording devices can be used, but also moves the image plane far from the test section so that heat from the combustor will not damage the photographic recording equipment.

The shadowgraph apparatus is illustrated in the sketch of Figure 2.4. The light source used in this system is generated by a spark produced from the rapid discharge of a capacitor bank across an air gap. The spark created by the unit is cylindrical in nature with a diameter of 1 millimeter and a length of about 4 millimeters. The spark is viewed along the axis of the cylinder placed at the focus of a 15 centimeter diameter, front surface, spherical mirror. The collimated

light beam is now projected through the combustor perpendicular to the center line axis and parallel to the top and bottom walls.

The shadowgraph image formed from the collimated beam is observed at a position about 15 centimeters outside the combustor. This image is focused onto the film plane of a camera by another 15 centimeter diameter, spherical mirror. The optical path required to create the appropriate shadowgraph image size is quite large; consequently, flat mirrors are used to fold the light beam path to conserve laboratory space. Nevertheless, the long path is an advantage. The increased distance between the flame and the film plane minimizes the impact of the light emission from the flame upon the light sensitive film surface.

The observable region is limited to 15 centimeters by the spherical mirrors; consequently, surveying the complete combustor length would require moving the entire system 15 centimeters at a time. By mounting the focusing spherical mirror, flat mirrors, and camera on a moveable optical pallet, the major components of the optical system can be translated in a fixed orientation so that the entire combustor is available for examination without time consuming realignment.

Overall, very clear polaroid photographs are produced using this system. The duration of the spark source was measured to be less than two microseconds. Considering the short duration of the light source, and the absence of inertia of the shadowgraph process, the photographs are essentially instantaneous records of the reacting kinematic flow field. For example, consider the distance traveled by an element of fluid moving at the highest dump plane velocity, 70 m/sec. During the duration of the illuminating spark light source, the fluid would have traveled 0.14 millimeters. The field of view is 15 centimeters long by

2.54 centimeters high. So, the fluid particle travels about one half of one percent of the minimum viewing distance. Clear photographs result because the impact of this motion upon the photograph is negligible. The flow speed for this example is the largest encountered during experimentation. Therefore, the above calculations represent the worst conditions. In addition, the sudden expansion, at the rear of the flameholder, reduces the velocity of the fluid as it is convected downstream. Consequently, the distance the fluid travels during the exposure period becomes even less, leading to even clearer images as the fluid moves downstream inside the combustion chamber.

The spark shadowgraph photographs are used for the initial combustor examination. A time history of the flow field is assembled by taking a photograph of the flow field and marking the time at which it was taken on an oscilloscope. The reference time for the photographs is determined from the time-varying pressure oscillation at the flameholder. A subsequent collage of random photographs can be assembled in a time sequence to produce a crude evolutionary picture of the flow field.

2.3.2 High Speed Cinematography

To obtain a nearly continuous time record of the flow field inside the combustor, a high-speed motion picture camera is employed. Inserting several lenses into the optical path reduces the shadow image size so that it may be recorded on 16 mm film using a HYCAM camera. In the shadowgraph apparatus described in the previous section, the spark light source is replaced by a continuous, high-intensity light source

manufactured by the Ealing Company. All the light produced by the high-intensity light source is focused onto the film so the camera could be operated at maximum speed. The resulting shadowgraph images of the flow field can be recorded at a rate of 8000 frames per second. This framing rate provides adequate time resolution of the flow phenomena.

The exposure time corresponding to the aforementioned framing rate is approximately 50 microseconds. This exposure time is 25 times larger than before when the spark source is used. Consequently, the distance traveled by a gas particle is 25 times greater. The pictures of the flow field taken with the HYCAM are naturally not as clear as the spark shadowgraphs. Minimal image blurring created by movement of the gas during the film exposure period is observed. Nevertheless, the high-speed visual recording of the flow field was quite successful.

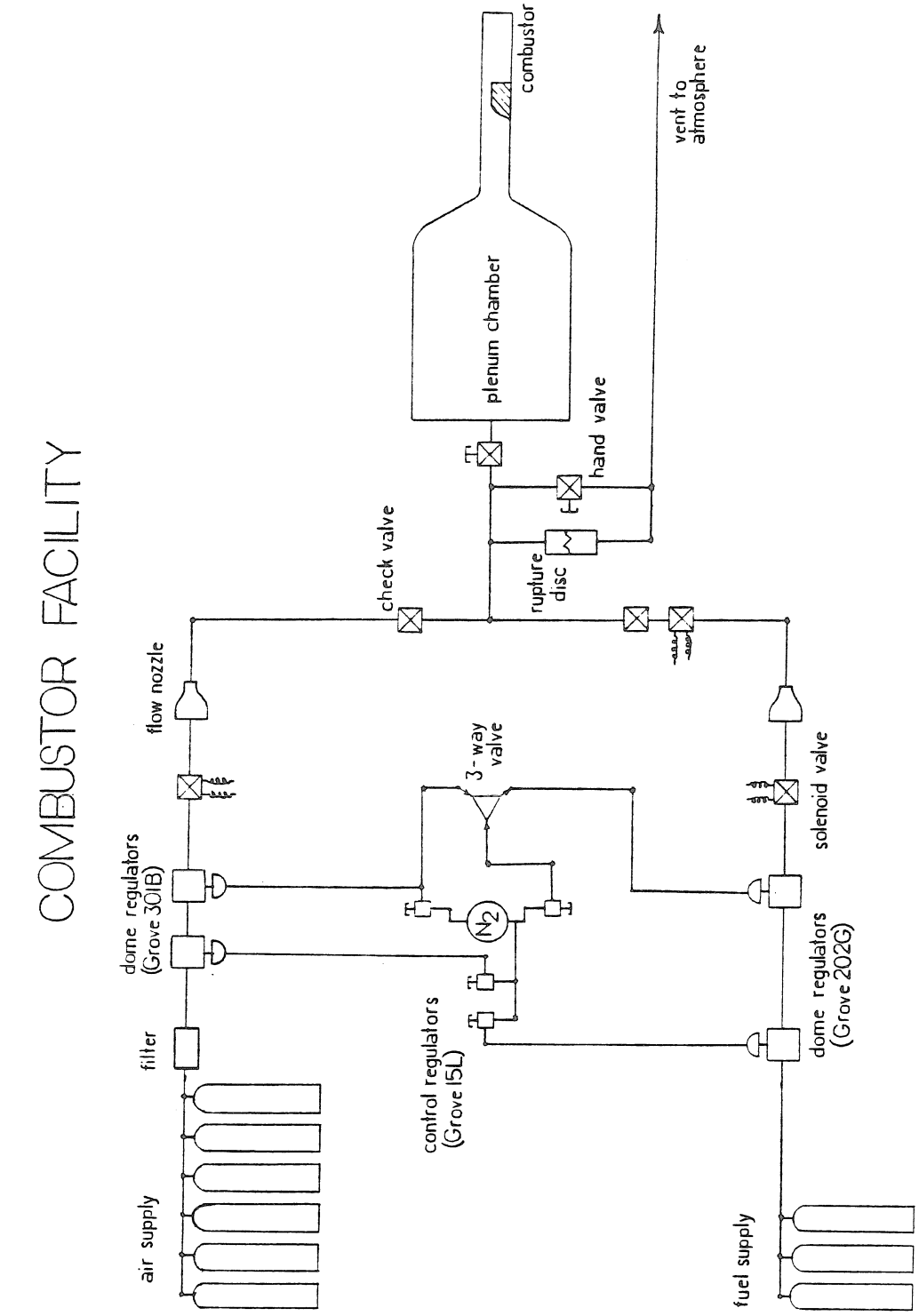

Figure 2.1 Combustion Laboratory

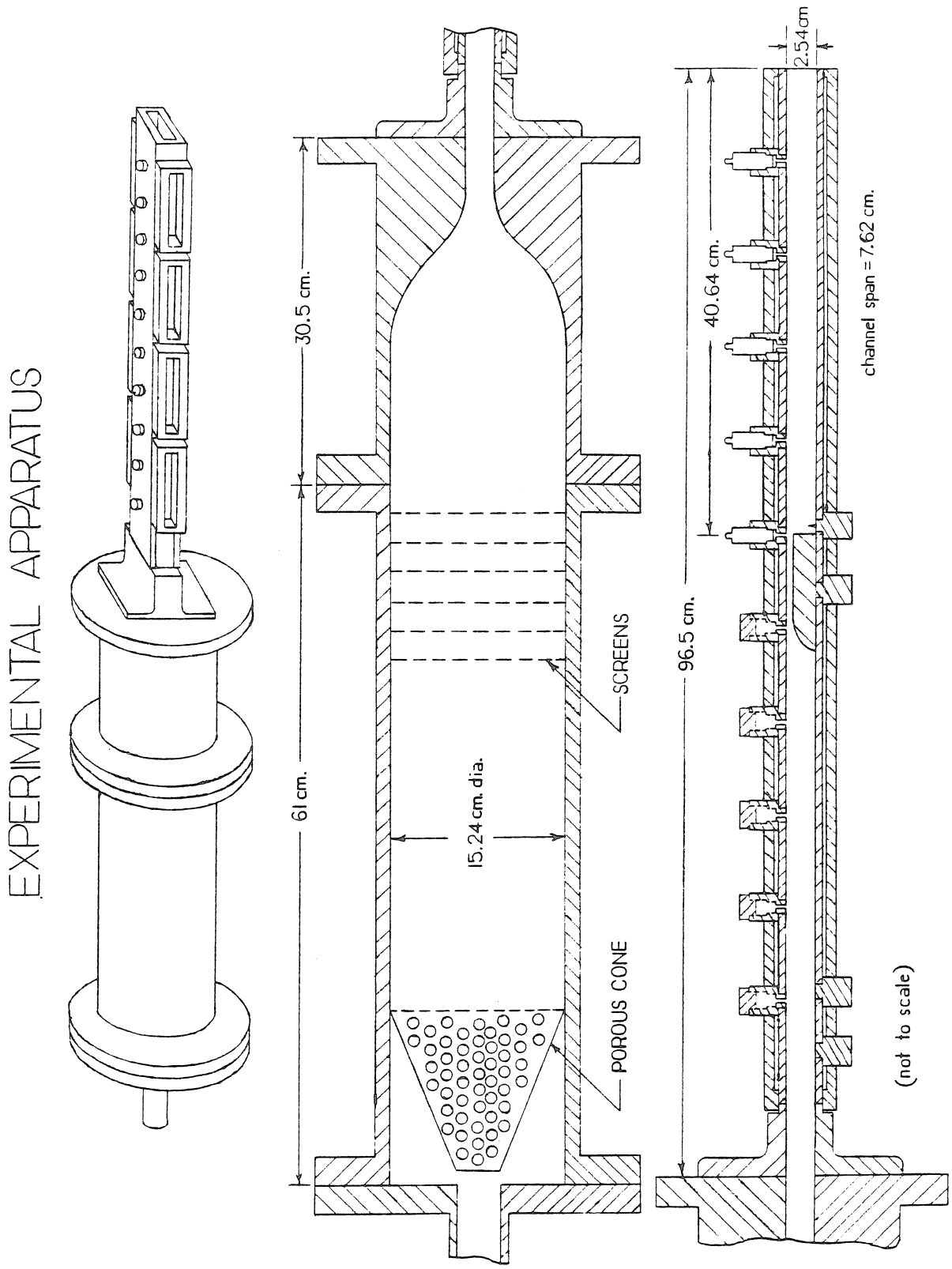

Figure 2.2 Laboratory Combustor Design

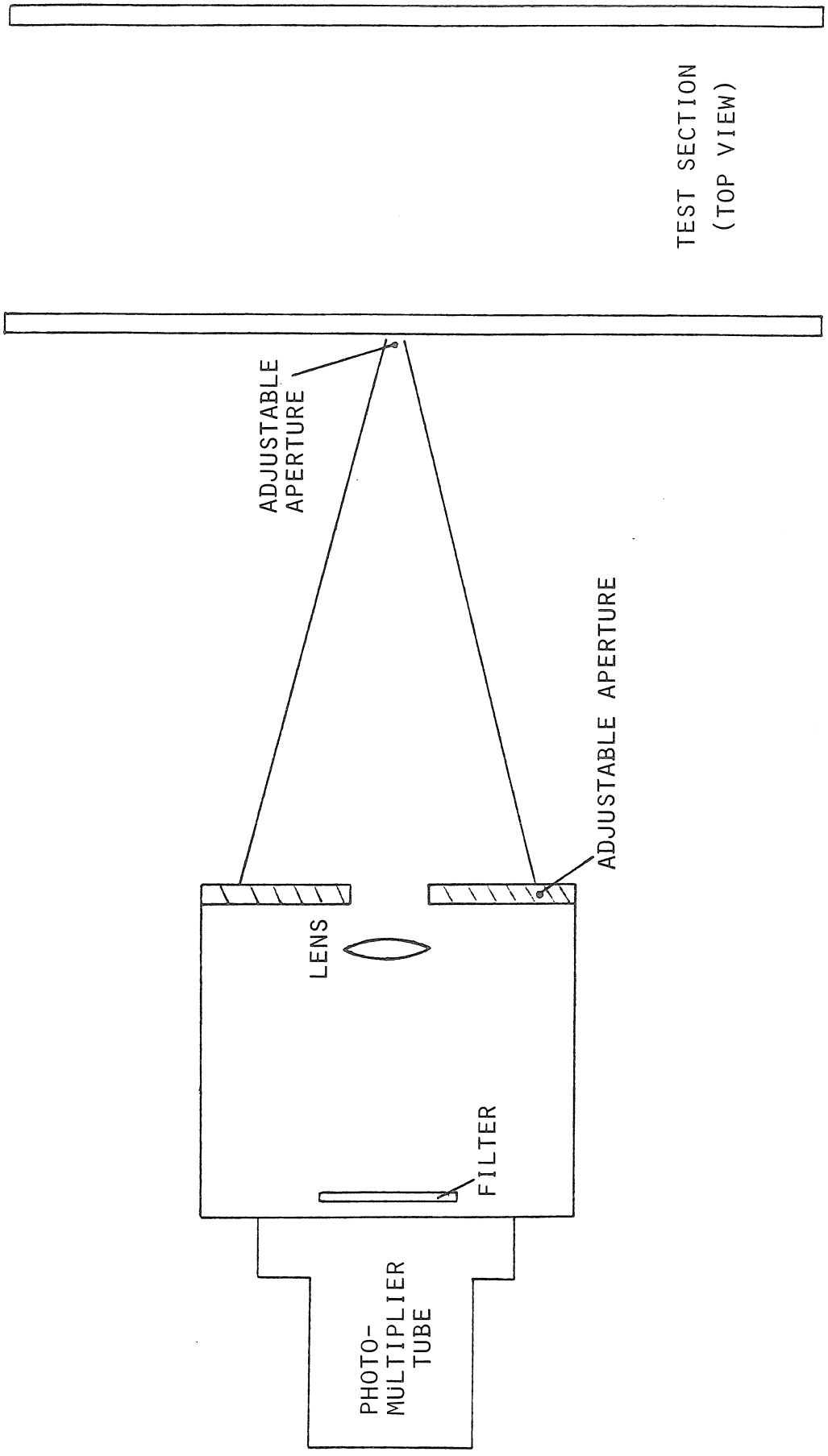

Figure 2.3 Optical Apparatus used for Flame Emission Measurements

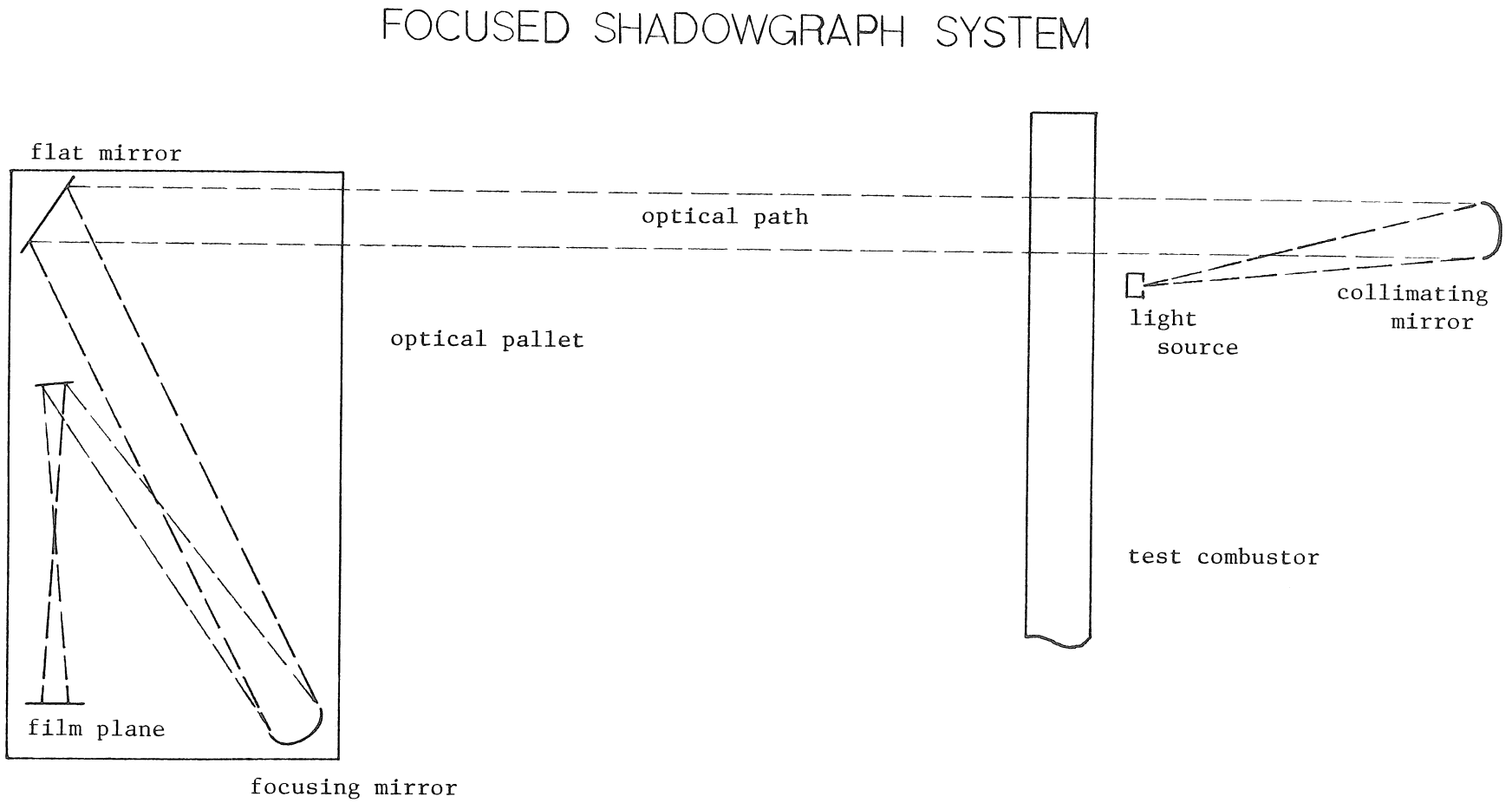

Figure 2.4 Flow Visualization Technique

CHAPTER 3

ONE-DIMENSIONAL ACOUSTIC ANALYSIS

3.1 Acoustic Modeling of the Experimental Combustor Apparatus

An acoustic analysis of the entire combustor apparatus is required in order to interpret the measured data from the combustor test. If the possible acoustic modes of the system are known, then the frequency analysis of the experimental data would become more valuable, or in other words, the spectrum could be divided into acoustic frequencies and other non-acoustic signals to aid in evaluation of the experimental results.

The experimental apparatus shown in Figure 2.2 is broken into four segments for modeling purposes. A sketch of the model geometry is shown in Figure 3.1. Section 3 represents the large volume plenum chamber and section 2 denotes the inlet region. An inductance section labeled A is used to model the flameholder. It is followed by a temperature rise in the gas as it enters the combustor which is designated as section 1. The flow in all regions of the apparatus was assumed one-dimensional and the fluctuations are presumed to be acoustic for the purpose of this analysis.

The conservation of mass and momentum describing the flow in the combustor apparatus are of the following form:

$$\frac{\partial \rho}{\partial t} + \rho \frac{\partial u}{\partial x} + u \frac{\partial \rho}{\partial x} = 0$$

$$\rho \frac{\partial u}{\partial t} + \rho u \frac{\partial u}{\partial x} = - \frac{\partial p}{\partial x} \quad .$$

Because the disturbances are assumed acoustic, the fluid can be described by isentropic relationships. Hence, the previous equations may be linearized to the following form:

$$\frac{\partial p}{\partial t} + \gamma p_o \frac{\partial u}{\partial x} + u_o \frac{\partial p}{\partial x} = 0$$

$$\rho_o \frac{\partial u}{\partial t} + \rho_o u_o \frac{\partial u}{\partial x} = - \frac{\partial p}{\partial x} \quad .$$

Here each property of the fluid is described by the sum of an undisturbed steady value and a perturbation value.

$$\rho = \rho_o + \rho$$

$$p = p_o + p$$

$$u = u_o + u$$

This set of partial differential equations, describing the fluid motion, can be reduced to a set of ordinary differential equations as functions of x only, if a solution is selected with a periodic time dependence such as

$$p = p(x,t) = p(x)\ e^{-i\Omega t}$$

$$u = u(x,t) = u(x)\ e^{-i\Omega t} \quad .$$

The resulting set of ordinary differential equations is

$$\gamma p_o \frac{du}{dx} - i\Omega p + u_o \frac{dp}{dx} = 0$$

$$\rho_o u_o \frac{du}{dx} - i\Omega \rho_o u = - \frac{dp}{dx} \quad .$$

The solution for the pressure and velocity fluctuations, p and u, may be found by alternately solving for one in terms of the other to obtain:

$$p(x) = P^{+} e^{i \frac{k}{1+M_o} x} + P^{-} e^{-i \frac{k}{1-M_o} x}$$

$$u(x) = \frac{1}{\rho_o a_o} \left[P^{+} e^{i \frac{k}{1+M_o} x} - P^{-} e^{-i \frac{k}{1-M_o} x} \right]$$

with M_o = local Mach number = $\frac{u_o}{a_o}$

k = wave number = $\frac{\Omega}{a_o} = \frac{\omega + i\alpha}{a_o}$

P^{+}, and P^{-} are complex coefficients computed from the boundary and matching conditions.

These solutions may also be expressed in the form

$$p(x) = \left[P^{+} e^{iKx} + P^{-} e^{-iKx} \right] e^{-iM_o Kx}$$

$$u(x) = \frac{1}{\rho_o a_o} \left[P^{+} e^{iKx} - P^{-} e^{-iKx} \right] e^{-iM_o Kx}$$

with $K = \frac{k}{1-M_o^2}$.

The solutions obtained for p and u are valid in all regions of the apparatus. For example, in region 3 the pressure may be described as

$$p_3(x) = \left[P_3^{+} e^{iK_3 x} + P_3^{-} e^{-iK_3 x} \right] e^{-iM_3 K_3 x}$$

for $-LP \leqq x \leqq -LI$.

The contraction between the plenum chamber and inlet, sections 2 and 3, is short compared to the wavelength of the disturbances. Consequently, this interface may be assumed acoustically compact and the matching conditions which must be met are continuity of pressure and continuity of mass flow across the abrupt area change.

$$p_3(-LI) = p_2(-LI)$$

$$\rho_3 A_3 u_3(-LI) = \rho_2 A_2 u_2(-LI)$$

Similarly, the temperature jump at the interface between region A and region 1 requires continuity of pressure and continuity of volume flow.

$$p_A(0) = p_1(0)$$

$$A_A u_A(0) = A_1 u_1(0)$$

To simplify the computations, flow through the inductance section may be determined by considering this region acoustically compact, also. This assumption is valid because the length of the inductance is 7.62 cm.; a small distance compared to the wavelength of the disturbance. Therefore, the density variation across the inductance is negligible and may be assumed constant. Thus, the conservation of mass equation reduces to a velocity match.

$$u_2(0) = u_A(0) \ .$$

Furthermore, the pressure drop across the inductance may be computed utilizing the momentum equation:

$$[\ p_2(0) - p_A(0)\ ]\ A_e = \frac{d}{dt}(\ m_e u_e)\ .$$

The boundary conditions at the ends of the combustor apparatus are the final constraints required to solve the problem. These conditions specify the phase relationship between the left traveling wave and right traveling wave at each of the two boundaries. At the entrance of the apparatus, the relationship is

$$P_3^- e^{iK_3LP} = \beta_p\ P_3^+ e^{-iK_3LP}$$

with β_p = complex reflection coefficient at the plenum chamber entrance.

The corresponding condition at the burner exit is

$$P_1^+ e^{iK_1LC} = \beta_e\ P_1^- e^{-iK_1LC}$$

with β_e = complex reflection coefficient at the combustor exit.

The acoustic resonant modes of the system may be determined from this set of matching and boundary conditions. In addition, the acoustic

velocity and pressure in each section are described by the wave equation, so that the pressure and velocity distribution within the entire system can be computed with the appropriate matching conditions between the segments.

3.2 Computer Solution Technique

The equations derived from the matching conditions between the component segments and the boundary constraints in the previous section are listed in a final form in the appendix. Solving for the system resonant modes requires solving this set of 8 equations containing 9 unknown parameters. One way to solve the problem is to eliminate 8 of the variables in favor of a single variable. In this case, the complex frequency is chosen as the favored variable, and the resulting equation containing only the complex frequency is solved by an iterative technique. The roots of this equation, or the eigenvalues, are the normal acoustic modes inside the combustor apparatus. The remaining pressure coefficients, i.e., the remaining 8 unknown parameters, may be determined by choosing a value for one of the coefficients and computing the remaining coefficients based upon this selection.

Since reduction of the experimental data yields a time-average estimate of the relative pressure magnitude in a narrow frequency bandwidth for different test conditions, the choice of the pressure coefficient at a certain frequency need not be entirely arbitrary. For example, experimental pressure measurements, obtained during test of the combustor, can be used as pressure coefficient inputs. An

experimentally determined pressure amplitude, from a specific measurement location, is used as the basis for computing the values of the acoustic pressure and velocity fluctuations throughout the entire apparatus. The real portion of $p(x)$, the pressure at some location within the apparatus, is scaled such that the value of the real portion of the pressure at the dump plane, Real $\{p(0)\}$, is equal to the measured pressure spectrum amplitude at x equals zero. The same scale value is also employed during computation of the velocity distribution. Hence, the computation of the acoustic velocity fluctuation, based upon the experimental pressure measurements, yields results which have physical significance.

COMBUSTOR APPARATUS ACOUSTIC MODEL

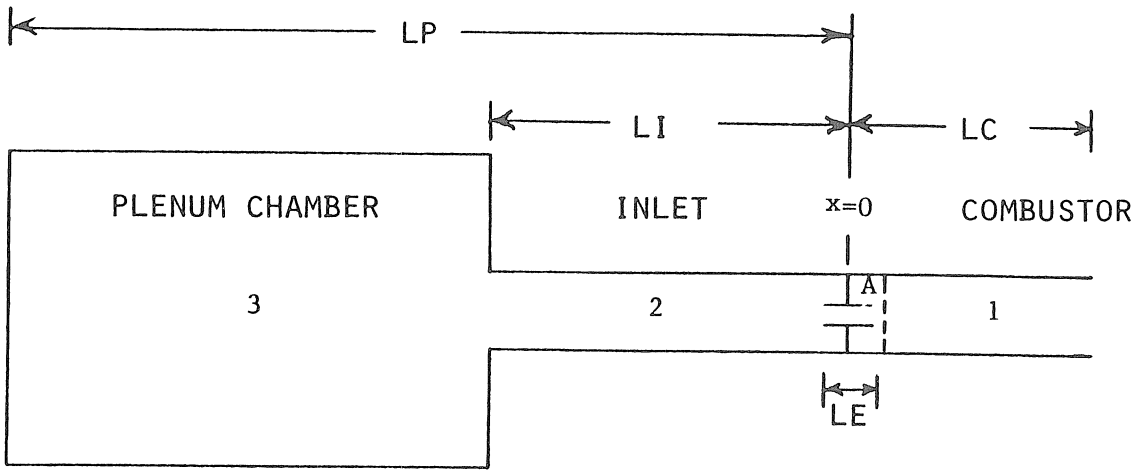

ENTRANCE BOUNDARY CONDITION,
$\beta_p = (1,0)$

EXIT BOUNDARY CONDITION,
$\beta_e = (-1,0)$

<u>AREA CHANGE</u>

continuity of pressure
$$P_3 = P_2$$
continuity of mass flow
$$\rho_3 u_3 A_3 = \rho_2 u_2 A_2$$

<u>INDUCTANCE</u>

conservation of momentum
$$\Delta p\, A_e = \frac{d}{dt}(m_e u_e)$$
continuity of mass
$$u_2 = u_A$$

<u>TEMPERATURE RISE</u>

continuity of pressure
$$P_A = P_1$$
continuity of volume flow
$$A_1 u_1 = A_A u_A$$

Figure 3.1 Theoretical Acoustic Model

CHAPTER 4

RESULTS

4.1 Acoustic Model Results

The acoustic model is formulated to predict the resonant frequencies of the various combustor apparatus configurations. Subsequent calculation of the acoustic pressure and velocity distributions, within the system at these resonant frequencies, is made with the aid of experimental pressure data. These pressure data, obtained at the flameholder ($x/LC = 0$), are employed to compute the pressure and velocity perturbations in the remainder of the apparatus. The experimental investigation of the combustor covers various geometries and inlet flow parameters; therefore, the acoustic model is employed to determine the acoustic properties of the apparatus for several of these situations.

The plenum chamber length, one geometric variable of the combustor apparatus, is changed to create three distinct apparatus geometries (Figure 4.1). The length variations change the resonant modes of the system and illustrate the influence of system acoustics upon the pressure and velocity fields. During the experimental study of the apparatus, the mean flow velocity at the dump plane is varied from 22 to 70 m/sec. These velocities are small compared to the cold gas acoustic velocity, i.e., only about 6 percent, and were found to have a negligible influence upon the computed pressure and velocity distributions. Therefore, a constant mean flow velocity, in the combustor, equal to 30 m/sec is employed as the mean flow speed when the

computer model is used to compute these distributions at the various experimental operating conditions.

Analytical results are calculated for 6 of the operating conditions. A typical computation, employing the acoustic computer model for the normal modes, generates an output of the form illustrated in Figure 4.2. The calculation shows the computed frequencies with the boundary conditions and geometry used in the computation. Table 4.1 lists the computed frequencies of interest below 600 hertz for the 3 geometric configurations. Pressure amplitudes, obtained from the experimental data records, are employed to calculate the acoustic pressure and velocity elsewhere inside the apparatus. The major frequency components for these computations are plotted (Figures 4.3 to 4.14) to illustrate the distribution of the acoustic pressure and velocity within the apparatus under the 6 different experimental situations.

4.2 Experimental Results

For each of the three geometric configurations, the research combustor is operated under 4 inlet flow velocities and various fuel-air ratios. The four entrance velocities, referred to as the dump plane velocities, are standardized at 22, 40, 50, and 70 m/sec. The dump plane velocity is the mass averaged velocity of the combustible mixture flowing through the narrow region above the flameholder as the gas enters the combustor. The normalized fuel-air ratio, or equivalence

ratio, is varied for each dump plane velocity to determine the effects of stoichiometry changes upon the combustion process. In addition, measurements of the localized heat release rate via the light radiation are obtained at 3 locations (x/LC = 0.094, 0.188, and 0.344) inside the combustor for a variety of test conditions and geometries.

Numerous measurements are required to survey the three combustor apparatus geometries at all the various flow conditions. Consequently, the data are presented with minimal explanation in the following results, sections 4.2.1 and 4.2.2. Detailed discussion of the results and implications of data will be presented in the discussion sections of Chapter 5.

In an attempt to make the presentation of the numerous data records clear, the table on the next page lists the experimental test conditions under which the apparatus was operated. Pressure and flame emission results are presented for each of the operating conditions illustrated in the table. To avoid confusion, data from all the operating conditions are presented in a group for a specific geometrical configuration. For example, all the pressure and light emission data obtained using the configuration I apparatus are presented together. Then, data from another configuration are presented in another group. The table summarized the test conditions for each of the geometric configurations.

EXPERIMENTAL OPERATING CONDITIONS

GEOMETRIC CONFIGURATION	DUMP PLANE VELOCITY (m/sec)	EQUIVALENCE RATIO
I	22	0.65, 1.0, 1.28
	40	1.0
	50	1.0
	70	1.0
I + steel wool	22	1.0 *
	40	1.0
	50	1.0 *
	70	1.0
II	22	0.74, 1.0
	40	1.0 *
	50	1.0
	70	1.0
III	22	1.0
	40	1.0
	70	1.0

* = no flame emission data presented

4.2.1 Pressure and Radiation Measurements

During investigation of the configuration I geometry, both static and fluctuating pressure measurements are obtained along with flame emission measurements. The static pressure results are shown in Figures 4.15 and 4.16. The results obtained for the fluctuating pressure inside the combustor are shown in Figures 4.17 to 4.22 as Power Spectral Density plots. The corresponding light intensity results to these test

conditions follow in Figures 4.23 to 4.40. The frequency, in hertz, is plotted as the abscissa for all spectral plots. The ordinate in both the pressure and intensity results is the positive square root of the sum of the squared real and imaginary portions calculated by the FFT algorithm. These values represent the Fourier coefficients and are utilized as inputs for the theoretical model.

In subsequent testing of the configuration I geometry, an acoustic damping material, steel wool, is inserted into the upstream plenum chamber to attenuate the resonance of this segment of the apparatus. The measured pressure spectra obtained under various experimental conditions are shown in Figures 4.41 to 4.44. Radiation observations for the acoustically damped system are presented for the 40 m/sec and 70 m/sec dump plane velocities (Figures 4.45 to 4.50). The light intensity measurements of the 40 m/sec case are representative of the two remaining velocities (22 and 50 m/sec) as can be seen by examining the similarity between the pressure spectrum plots for these velocities. The 22 and 50 m/sec tests are omitted because the inclusion of these cases adds no insight into the problem and are thus deleted for the sake of brevity.

During examination of the acoustically undamped configuration I apparatus, simultaneous measurements are made of the oscillating pressure and light emission. The results obtained at the three radiation observation positions are illustrated in Figures 4.51 and 4.52 for the 22 m/sec and 40 m/sec test cases, when the equivalence ratio is set equal to 1. The pressure signal is low-pass filtered so the low frequency oscillation is highlighted. Filtering the pressure interjected a time delay; therefore, the pressure signals are time

shifted by the filter phase shift so the pressure and intensity are presented with coordinate time scales. The pressure in all cases is the pressure measured at the dump plane, whereas the light intensity measurements are measured at three positions. Data obtained with the configuration I geometry are presented in the greatest detail for purposes of the following discussion. The remaining two configurations are presented in an abbreviated form to illustrate the important results.

The pressure spectra (Figures 4.53 to 4.56) and the light intensity spectra (Figures 4.57 to 4.68) from the configuration II apparatus with no damping material are presented to illustrate the influence of changing the acoustic properties of the apparatus. Notice that the 40 m/sec test data are not included because the results are very similar to the lowest speed measurements at 22 m/sec.

Only two test conditions are presented for the configuration III apparatus. The pressure and light intensity spectra (Figures 4.69 to 4.80) are presented for two dump plane velocities, 40 and 70 m/sec.

4.2.2 Flow Visualization Results

Short time exposure, spark shadowgraph records are used for preliminary examination of the reacting flow field within the combustor. The two basic types of flow fields are shown in Figure 4.81. The upper photograph illustrates the stable combustion process in which a shear layer forms behind the rearward facing step flameholder. Below, in the lower photo, a solitary vortex dominates the flow field when an acoustic resonant mode of the system is highly excited.

A composite of prints made from the high-speed motion pictures are shown in Figures 4.82 to 4.85. The sinusoidal curve at the left-hand portion of the photo illustrates the fluctuating pressure at the frequency of vortex shedding. The sinusoidal oscillation represents the pressure fluctuation created by the resonance of the excited acoustic mode at the dump plane, i.e., at the rear edge of the flameholder. The vortex evolution is shown with respect to this period of oscillation at the right of the photo. Figures 4.82 and 4.83 illustrate the vortex formation at two dump plane velocities, 22 and 40 m/sec, under stoichiometric conditions with the configuration I geometry. At both velocities, the period of vortex formation is 5.3 msec. Changing the fuel-air ratio eliminates the large vortex and the upper photograph of Figure 4.86 shows the flow field under lean conditions (an equivalence ratio of 0.70), while the middle photograph of Figure 4.86 illustrates the flow field under rich conditions (an equivalence ratio of 1.28). At stoichiometric mixture ratios, increasing the dump plane velocity also eliminates the solitary vortex as shown in the lower photograph of Figure 4.86. As the system acoustics is changed by shortening the

plenum chamber length to the configuration II geometry, the vortex formation appears similar, but the period of formation has decreased to 1.9 msec (Figure 4.84). Under off-stoichiometric conditions at this velocity, 50 m/sec, stable burning occurs within the combustion chamber. However, at the lower velocities, such as 22 and 40 m/sec, the normal shear layer is present during stoichiometric operation, but a large vortex is observed during lean operation as shown in Figure 4.85. These vortices form at 2.2 msec intervals and accompany strong pressure oscillations.

Details of the movement of the large vortex structure are determined from a frame by frame evaluation of the high speed movies. As the vortex evolves, two particular points are important to watch. Movement of the inner and outer fronts (Figure 4.91) shed insight upon the movement of the vortex, and the velocity of these fronts are plotted in Figures 4.87 to 4.90. The lower portion of these figures show the velocity of the inner and outer fronts as a function of time. The sinusoidal pressure of the excited mode, measured at the dump plane, is shown above the velocity curves. In Figures 4.87 and 4.88, the front velocities are plotted for the test conducted using the configuration I apparatus and a stoichiometric fuel-air ratio. Figure 4.87 shows the movement of the fronts when the dump plane velocity is 22 m/sec, while Figure 4.88 illustrates the effect of the change in dump plane velocity from 22 to 40 m/sec. Varying the acoustic conditions of the apparatus, by changing the system geometry to configuration II, produced front velocities as shown in Figure 4.89 where the dump plane velocity is 50 m/sec. Decreasing the fuel-air ratio and velocity to 40 m/sec and an equivalence ratio of 0.74 produced front movements as shown in Figure

4.90.

The relationship between the location of the vortex and the radiation measurements is shown in Figure 4.92. The vortex evolution over one cycle is illustrated on the left-hand portion of the figure. A sketch of the pressure at the dump plane and the light emitted at three locations within the combustor are shown to the right. The white vertical lines drawn on top of the photographs illustrate the location at which the measurements are recorded. Figure 4.92 illustrates the configuration I measurements and flow field conditions at a flow speed of 22 m/sec and an equivalence ratio of 1.0.

GEOMETRIC CONFIGURATION	DUMP PLANE VELOCITY (m/sec)	PHI	COMPUTED FREQUENCIES (under 600 Hz.)
I	22	1.0	180, 229, 385, 470, 590 (c = 750 m/sec)
	70	1.0	180, 229, 385, 470, 590 (c = 750 m/sec)
II	22	0.74	206, 305, 438, 518 (c = 675 m/sec)
	50	1.0	209, 306, 468, 532 (c = 750 m/sec)
	70	1.0	209, 306, 468, 532 (c = 750 m/sec)
III	22	1.0	211, 398, 446, 531 (c = 675 m/sec)
	40	1.0	214, 400, 477, 542 (c = 750 m/sec)
	70	1.0	214, 400, 477, 542 (c = 750 m/sec)

Table 4.1 Summary of Computer Results

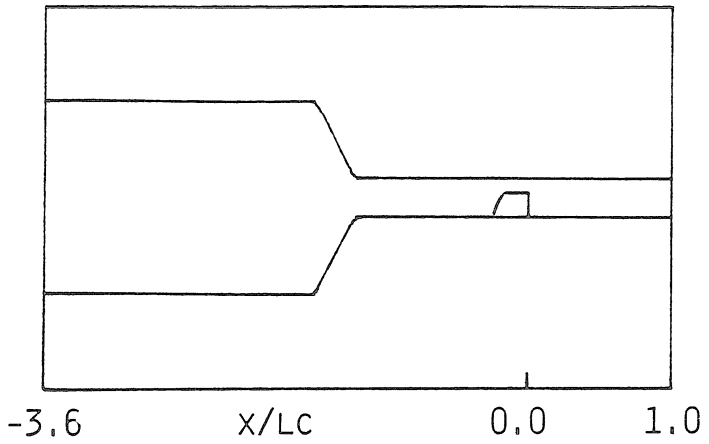

CONFIGURATION I

86 cm plenum chamber
56 cm inlet section
7.6 cm inductance
40 cm combustor

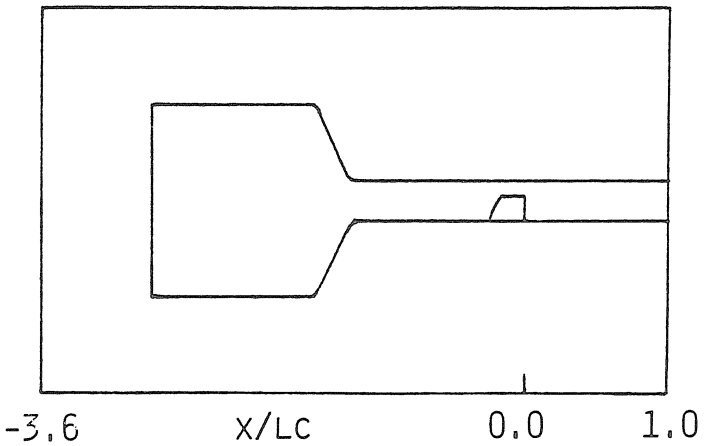

CONFIGURATION II

56 cm plenum chamber
56 cm inlet section
7.6 cm inductance
40 cm combustor

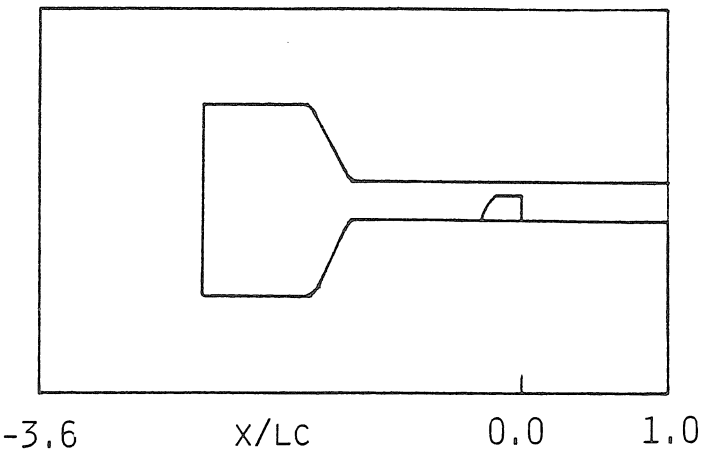

CONFIGURATION III

41 cm plenum chamber
56 cm inlet section
7.6 cm inductance
40 cm combustor

Figure 4.1 Geometrical Configurations of the Combustor Apparatus

```
THE ROOTS RETURNED HAD A PROBLEM WITHCONVERGENCE
IN    16  ITERATIONS
THE COMPLEX FREQUENCY 16 IS       (
THE COMPLEX FREQUENCY  1 IS       (      18.940704346,       -0.000002459)     HZ
THIS ROOT WAS FOUND IN        7   ITERATIONS
THE COMPLEX FREQUENCY  2 IS       (     180.095642090,        0.000002416)     HZ
THIS ROOT WAS FOUND IN        8   ITERATIONS
THE COMPLEX FREQUENCY  3 IS       (     228.585174561,        0.000004988)     HZ
THIS ROOT WAS FOUND IN        7   ITERATIONS
THE COMPLEX FREQUENCY  4 IS       (     385.344329834,       -0.000001738)     HZ
THIS ROOT WAS FOUND IN       10   ITERATIONS
THE COMPLEX FREQUENCY  5 IS       (     470.202239990,        0.000004352)     HZ
THIS ROOT WAS FOUND IN       12   ITERATIONS
THE COMPLEX FREQUENCY  6 IS       (     533.316833496,       -0.000004365)     HZ
THIS ROOT WAS FOUND IN       11   ITERATIONS
THE COMPLEX FREQUENCY  7 IS       (     589.738586426,       -0.000000294)     HZ
THIS ROOT WAS FOUND IN       10   ITERATIONS
THE COMPLEX FREQUENCY  8 IS       (     830.337036133,        2.662309408)     HZ
THIS ROOT WAS FOUND IN       17   ITERATIONS
THE COMPLEX FREQUENCY  9 IS       (    1499.938964844,      -16.320249557)     HZ
THIS ROOT WAS FOUND IN       17   ITERATIONS


THE COMPLEX PLENUM REFLECTANCE IS                    ( 1.00000,  0.00000)
THE COMPLEX EXIT REFLECTANCE IS                      (-1.00000,  0.00000)


THE INLET DUCT GAMMA IS                                 1.4000
THE COMBUSTOR GAMMA IS                                  1.3000


THE INLET TO PLENUM AREA RATIO IS                       0.1061
THE INDUCTANCE AREA RATIO (>1) IS                       4.0000


THE LENGTH OF THE INLET IS                              1.7292     (FT)
THE LENGTH OF THE COMBUSTOR IS                          1.3333
THE LENGTH OF INDUCTANCE IS                             0.2500
THE LENGTH OF THE PLENUM IS                             2.8333


THE COMBUSTOR SONIC VELOCITY IS                      2460.0000     (FT/SEC)
THE INLET DUCT SONIC VELOCITY IS                     1100.0000
THE PLENUM SONIC VELOCITY IS                         1100.0000


THE COMBUSTOR STATIC PRESSURE IS                       14.7000     (PSI)
THE INLET STATIC PRESSURE IS                           14.7000
THE PLENUM STATIC PRESSURE IS                          14.7000


THE COMBUSTOR MACH NUMBER IS                            0.0407
THE INLET DUCT MACH NUMBER IS                           0.0227
THE PLENUM MACH NUMBER IS                               0.0023


THE COMBUSTOR STATIC TEMPERATURE IS                  2712.3379     ('R)
THE INLET STATIC TEMPERATURE IS                       503.5867
THE PLENUM STATIC TEMPERATURE IS                      503.5867
```

Figure 4.2 Analytical Computations of Acoustic Modes

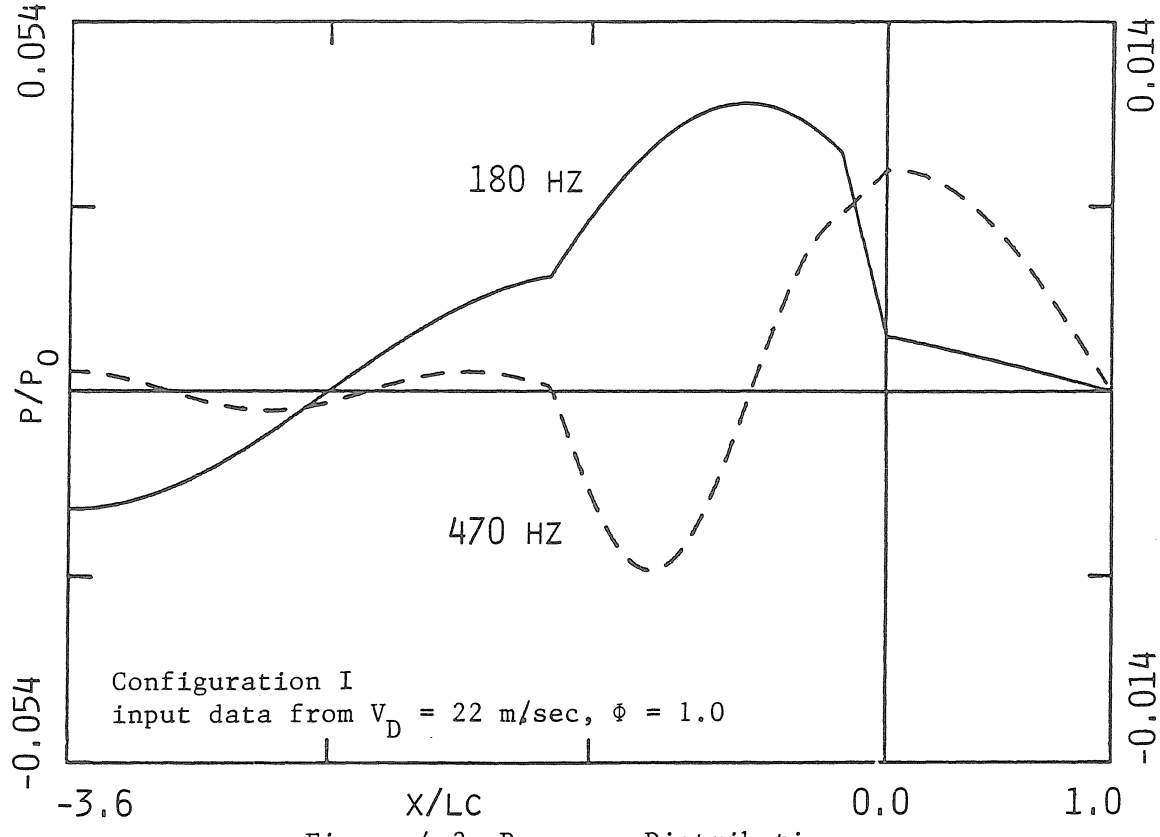

Figure 4.3 Pressure Distribution

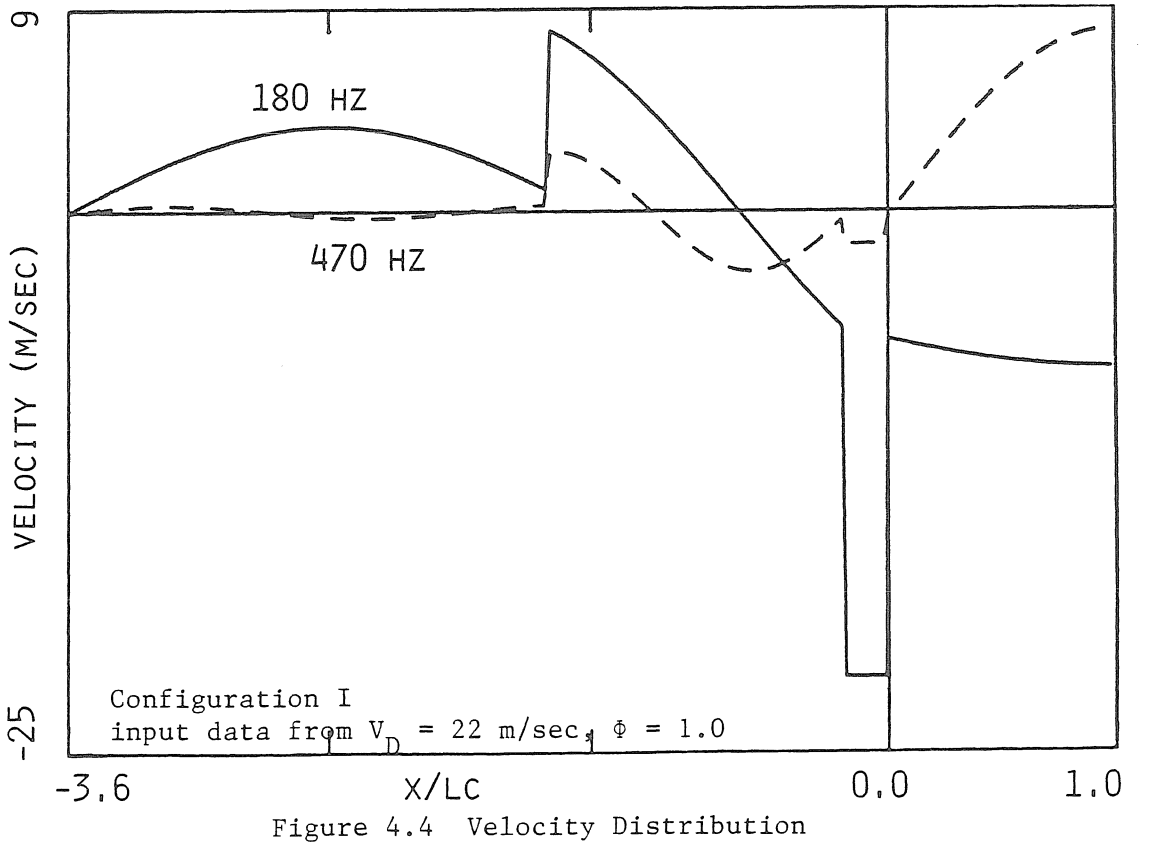

Figure 4.4 Velocity Distribution

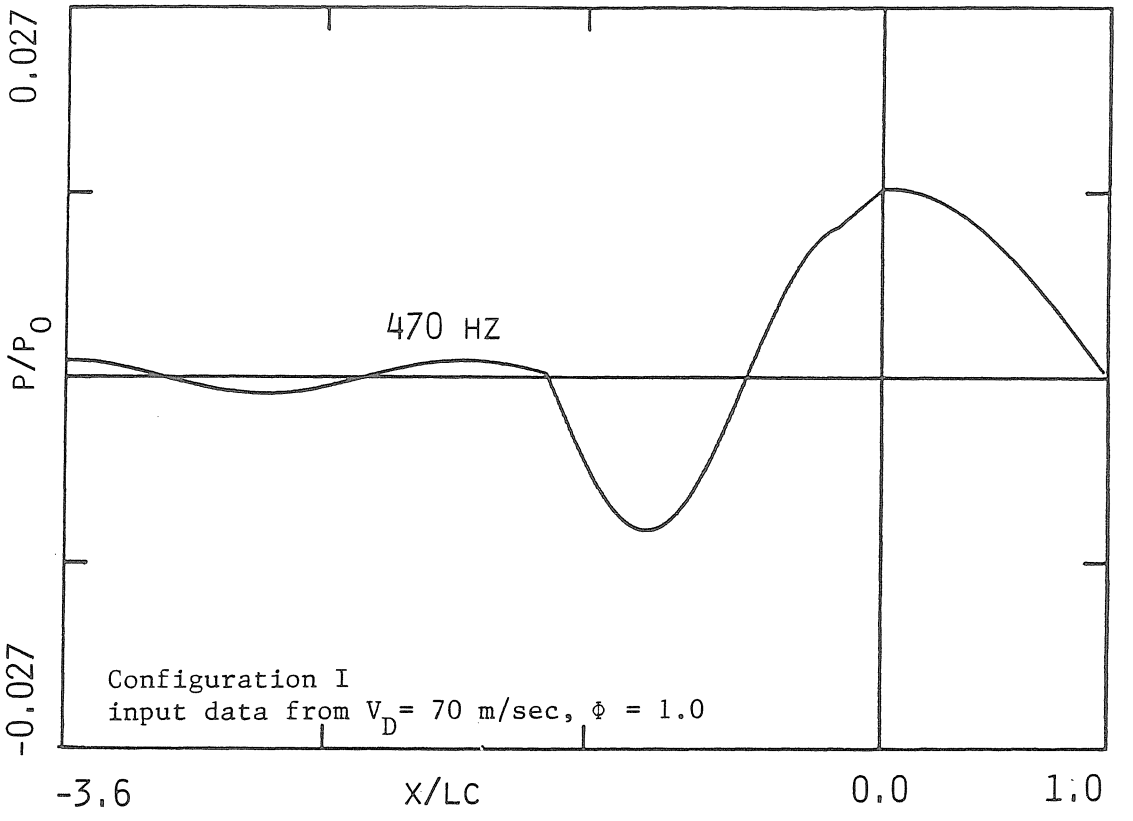

Figure 4.5 Pressure Distribution

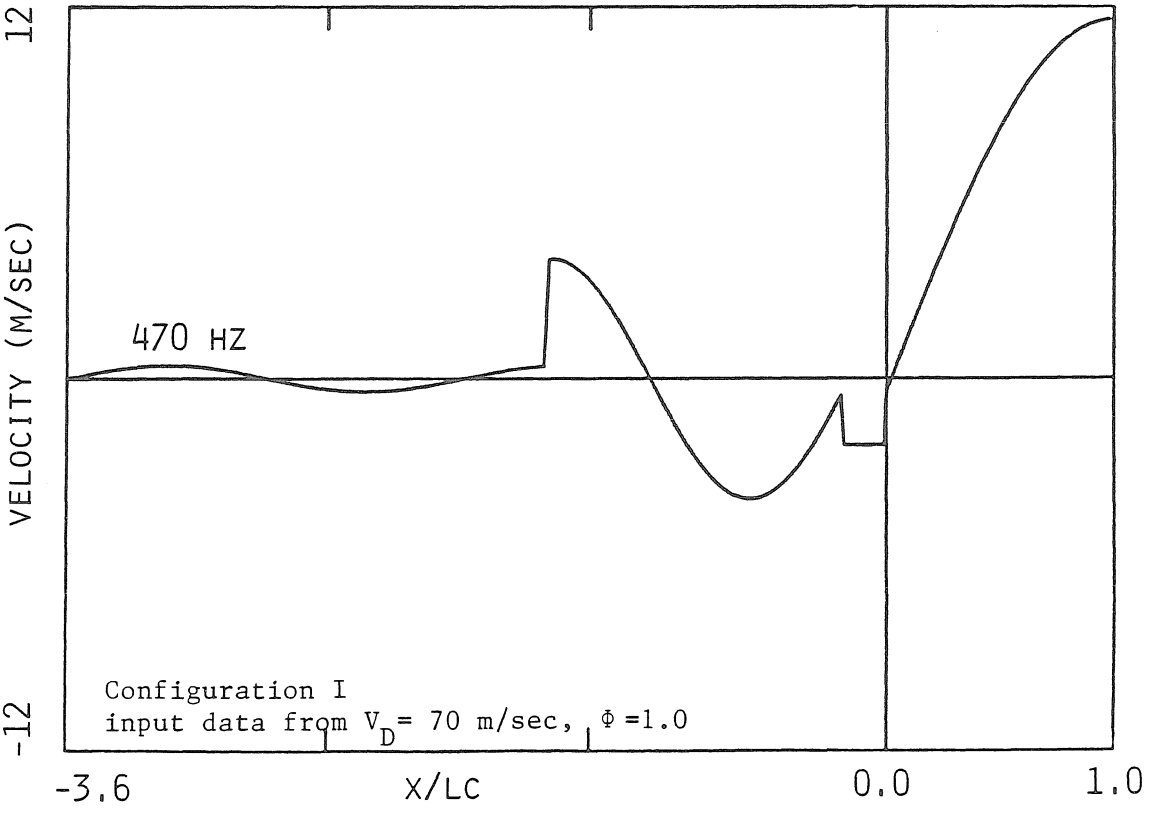

Figure 4.6 Velocity Distribution

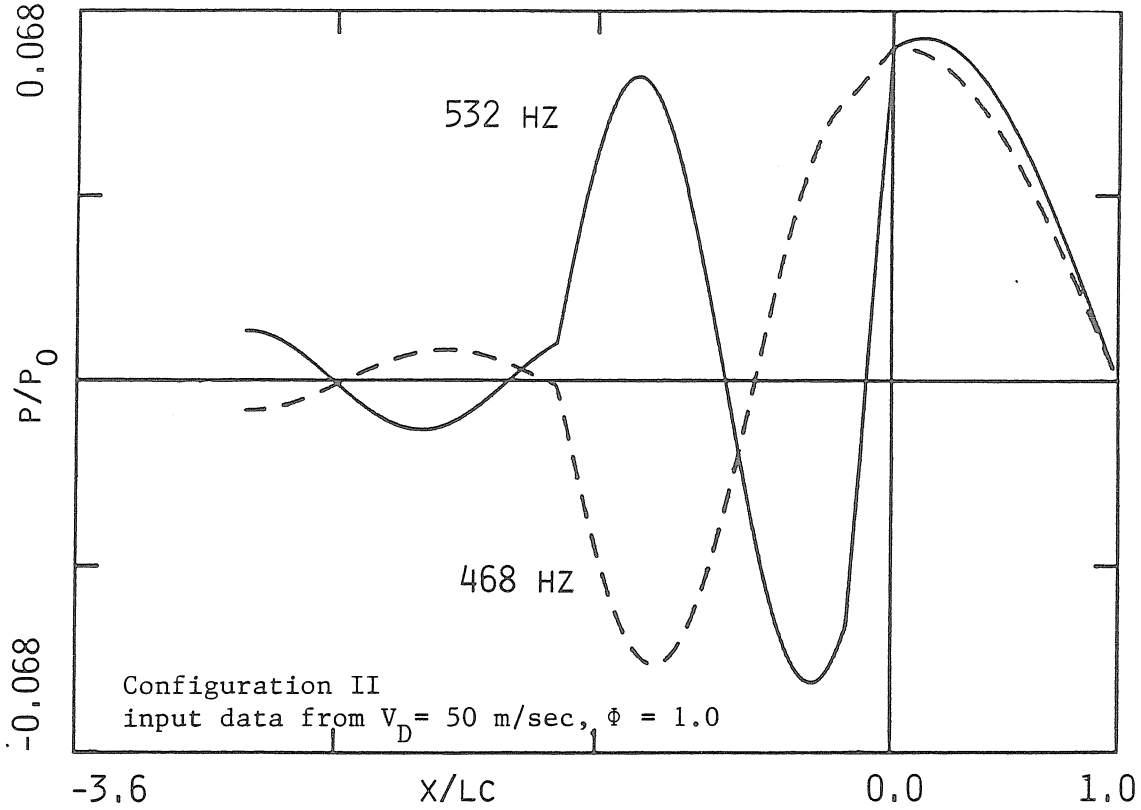

Figure 4.7 Pressure Distribution

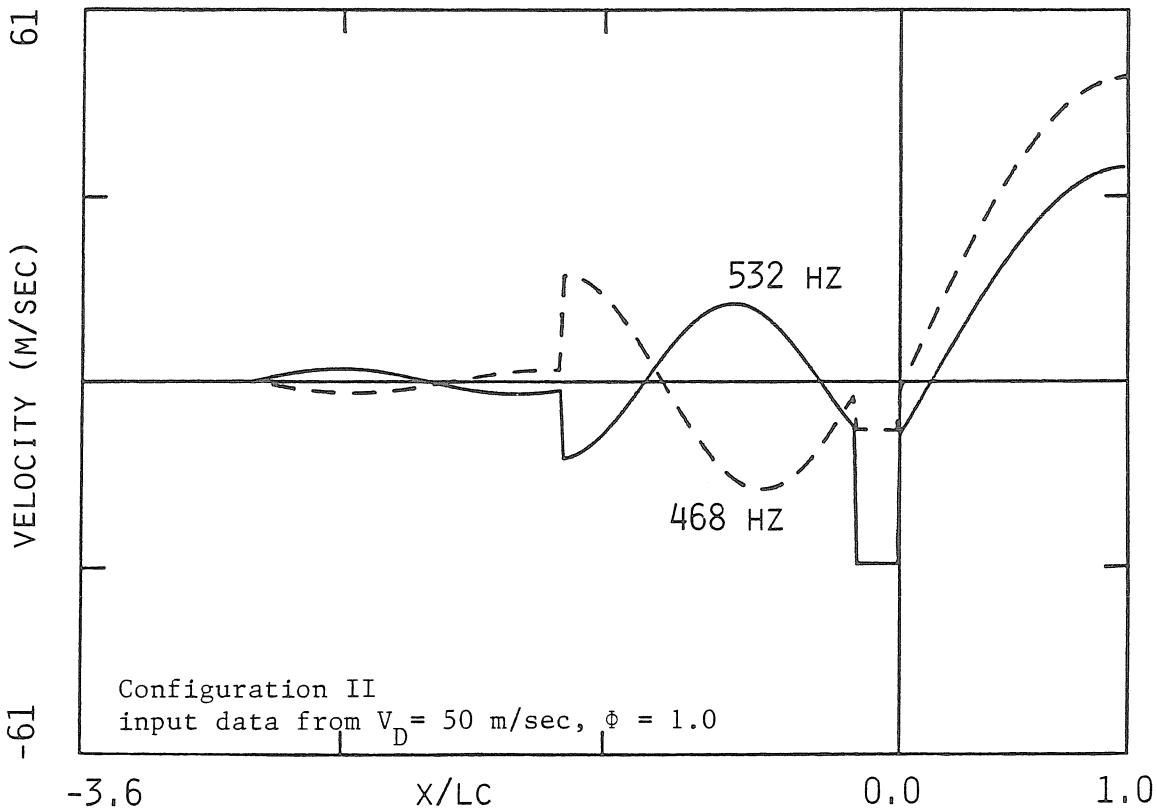

Figure 4.8 Velocity Distribution

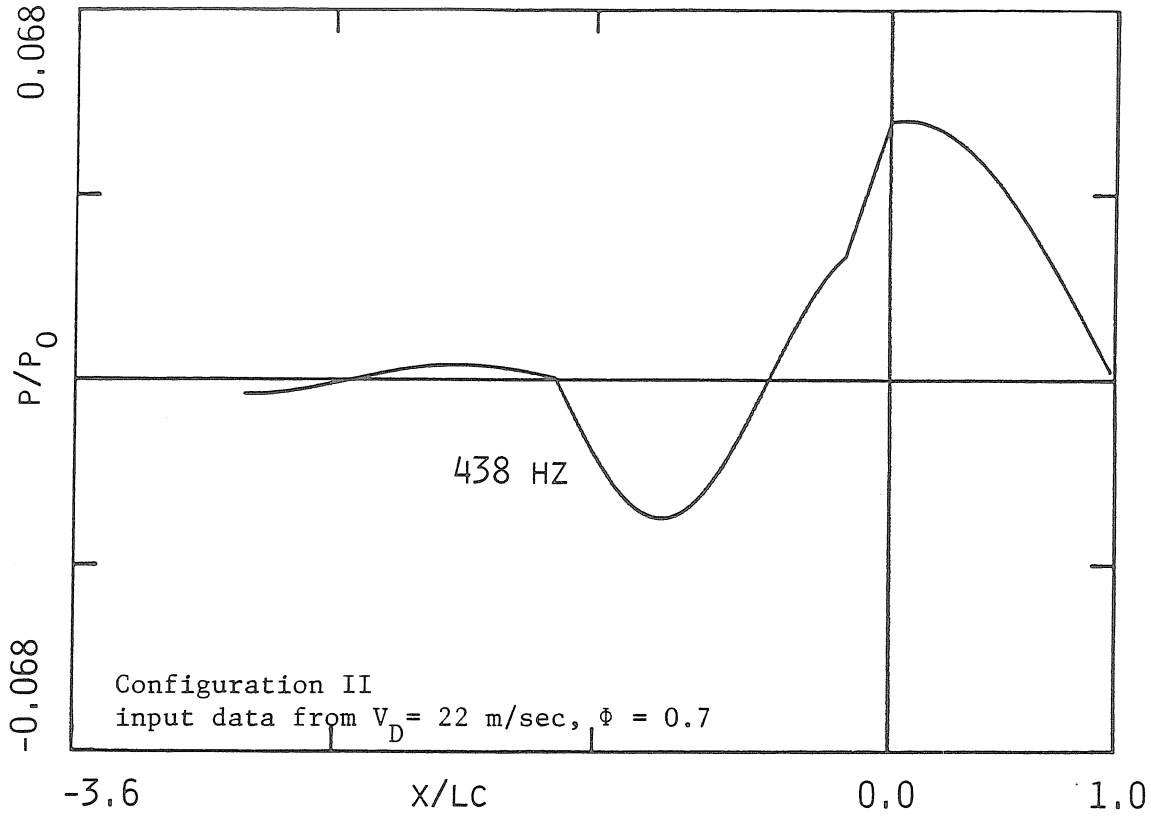

Figure 4.9 Pressure Distribution

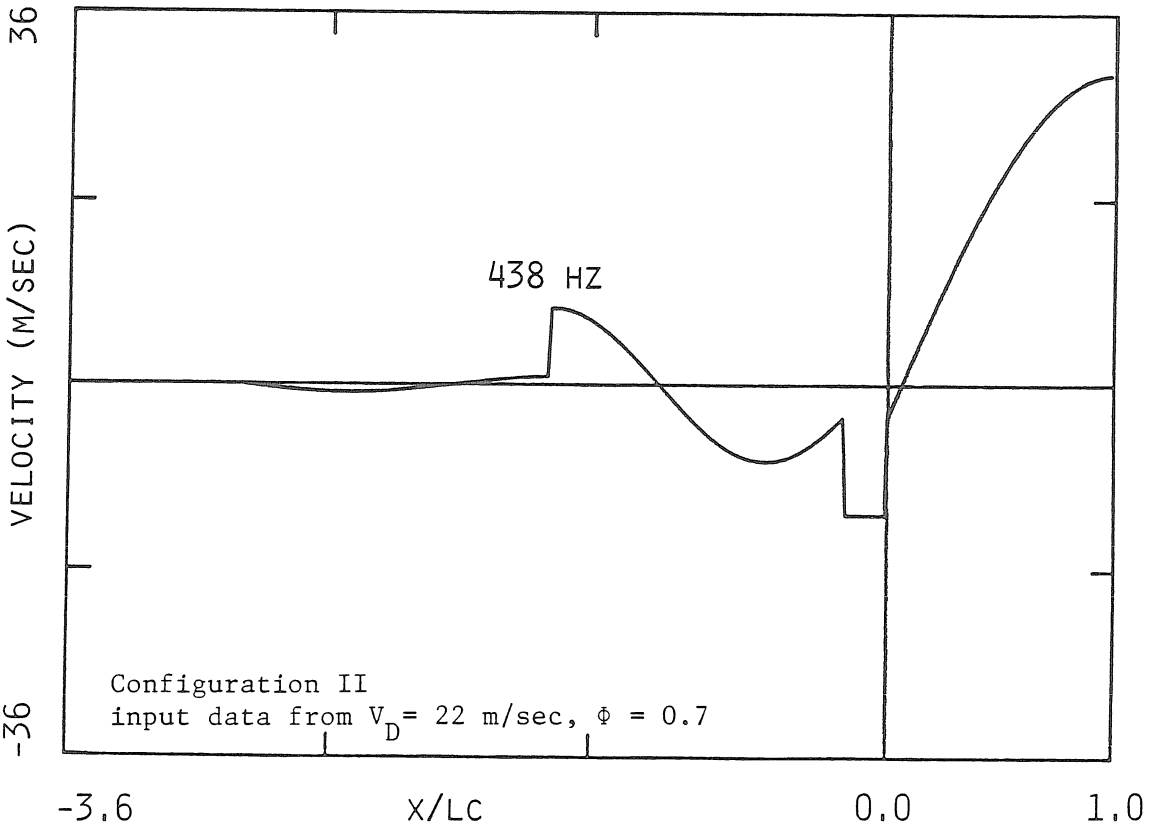

Figure 4.10 Velocity Distribution

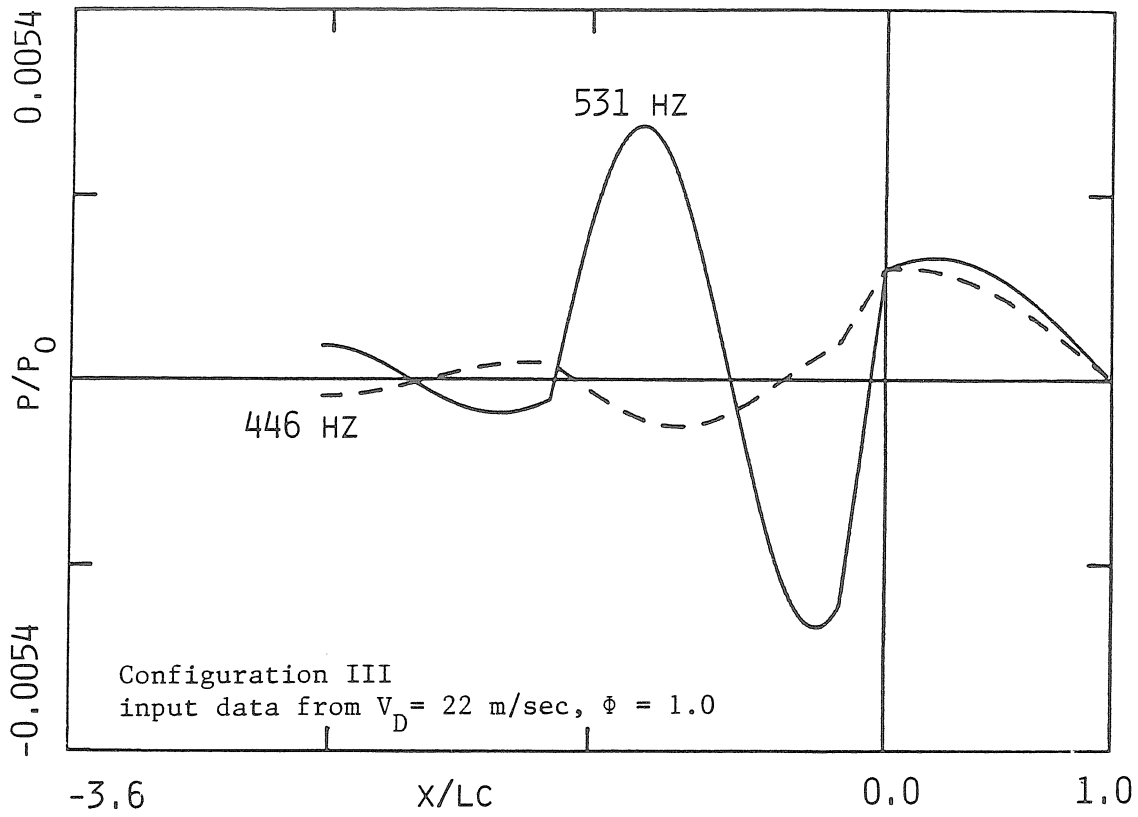

Figure 4.11 Pressure Distribution

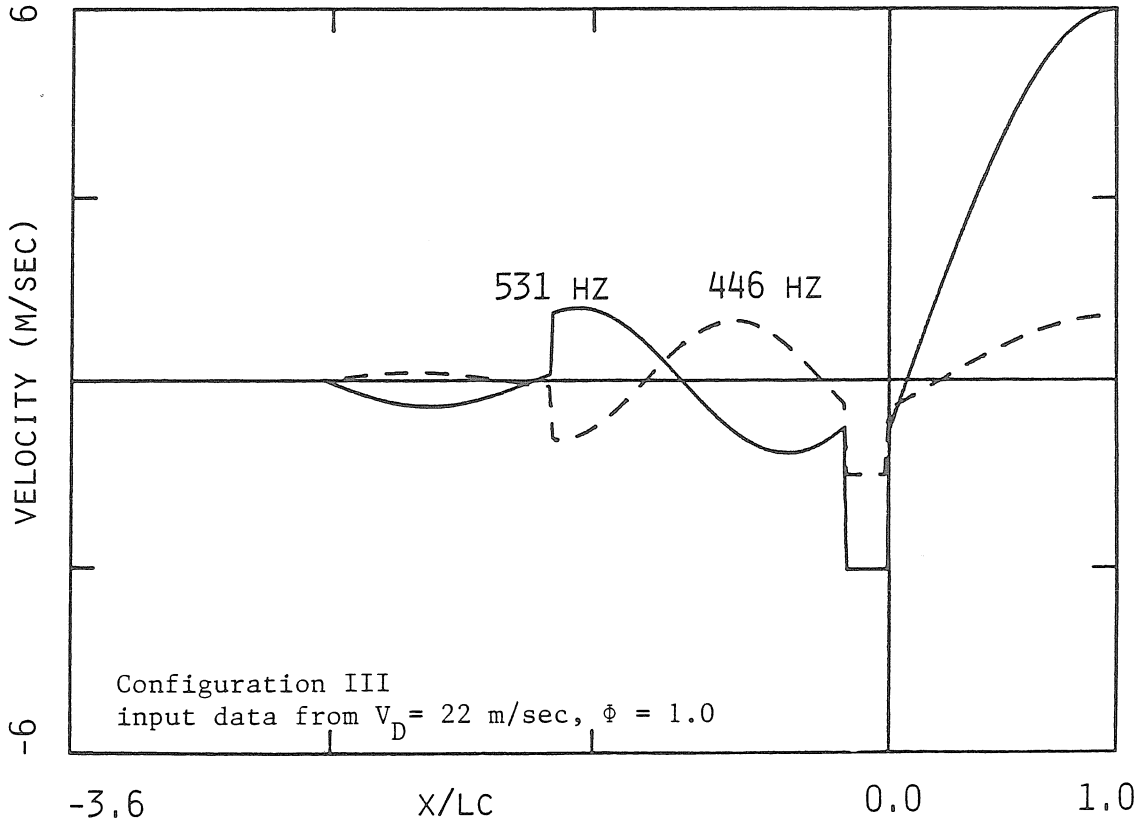

Figure 4.12 Velocity Distribition

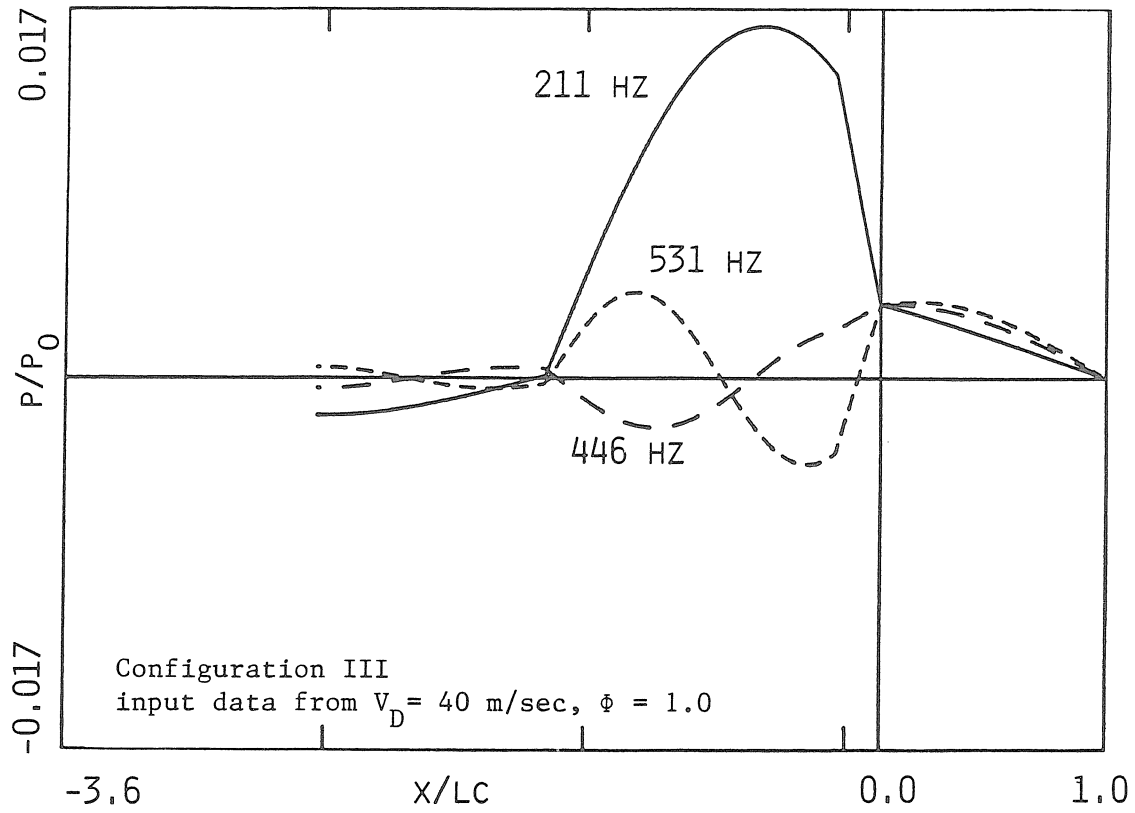

Figure 4.13 Pressure Distribution

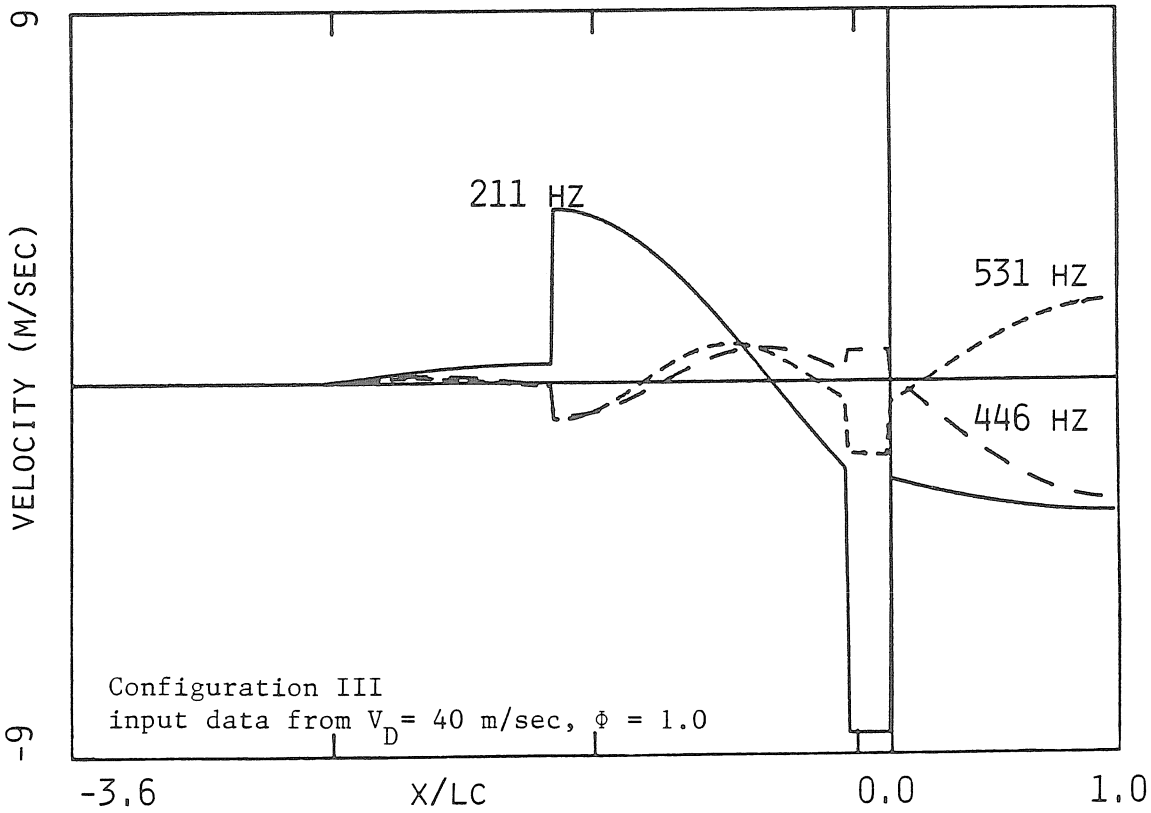

Figure 4.14 Velocity Distribution

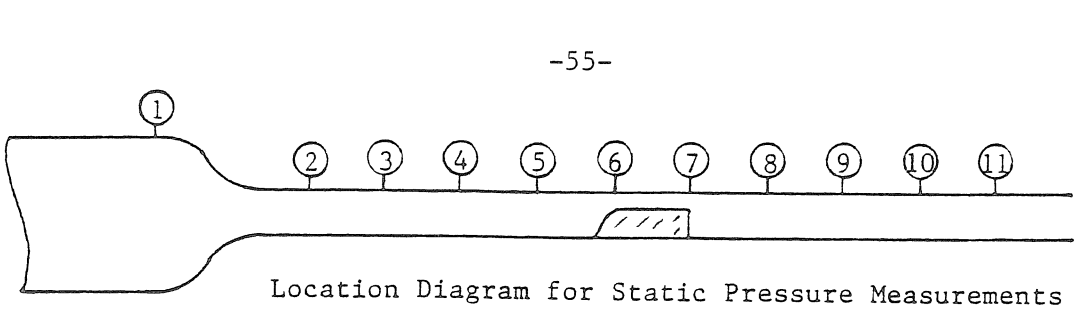

Location Diagram for Static Pressure Measurements

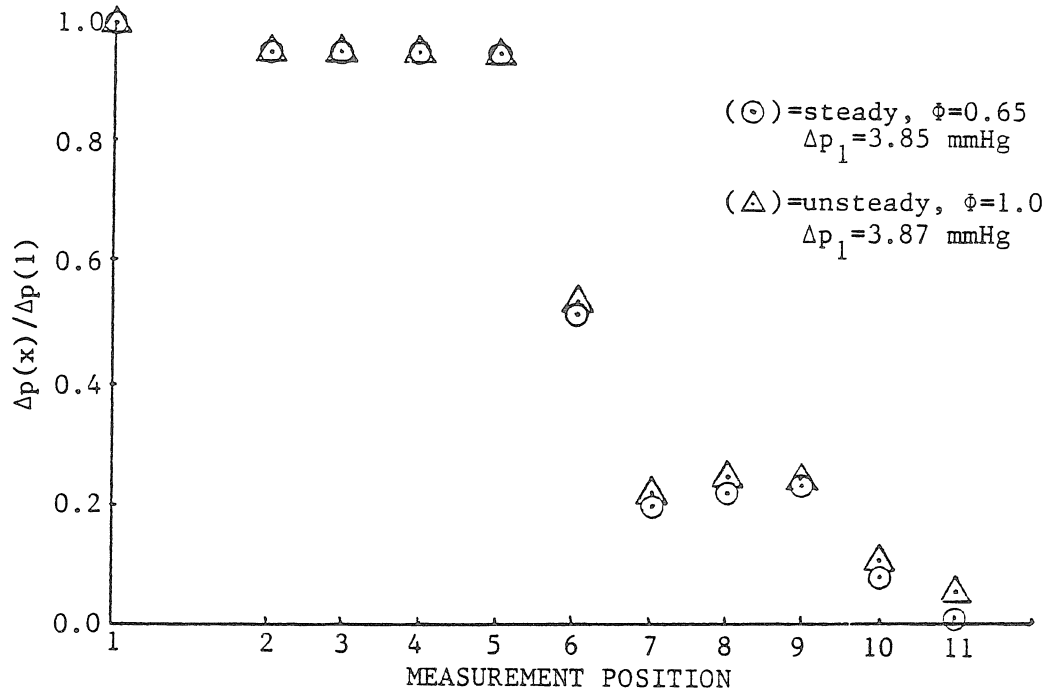

Figure 4.15 Low Speed (22 m/sec) Static Pressure Measurements

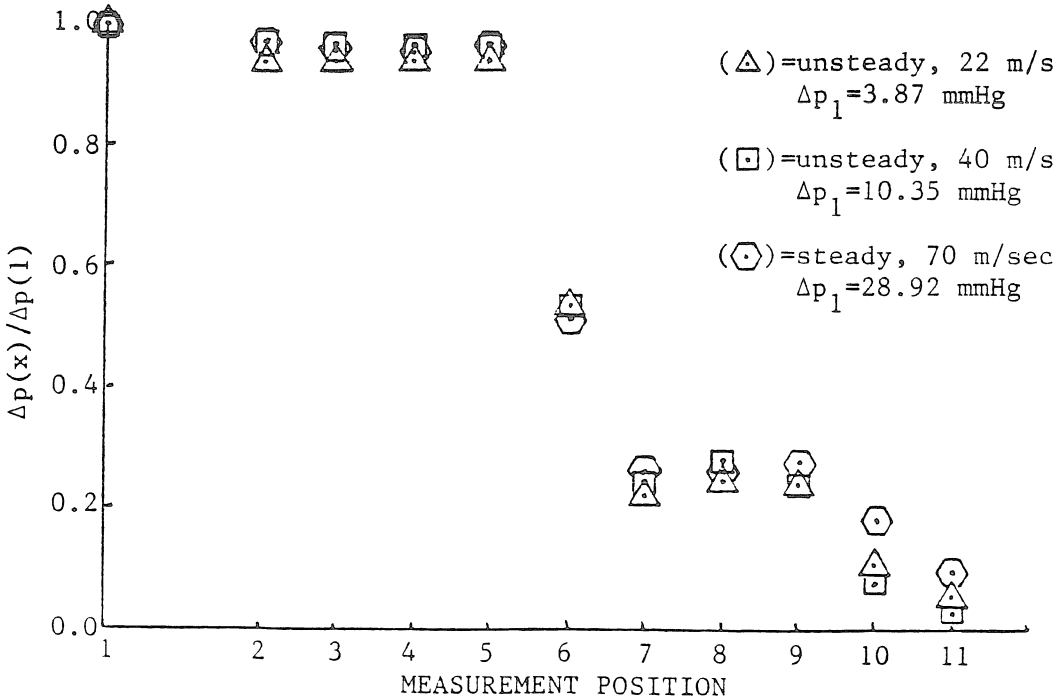

Figure 4.16 Static Pressure Measurements at Φ = 1.0

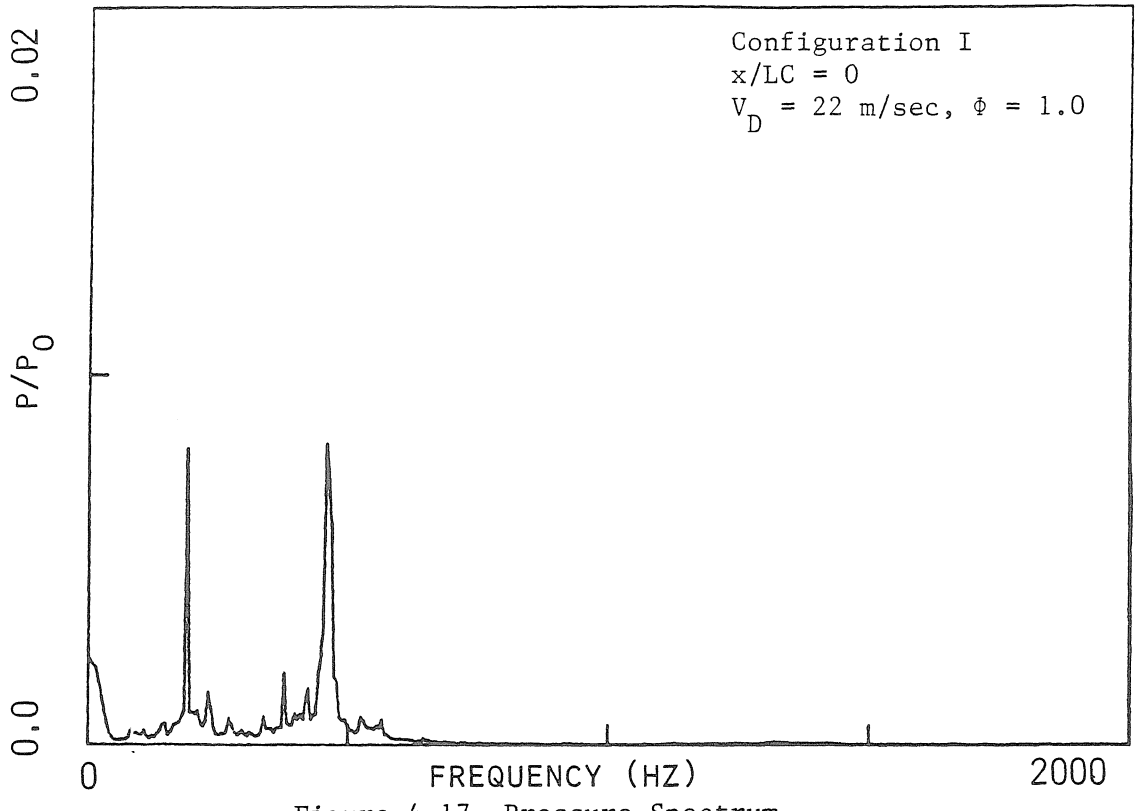

Figure 4.17 Pressure Spectrum

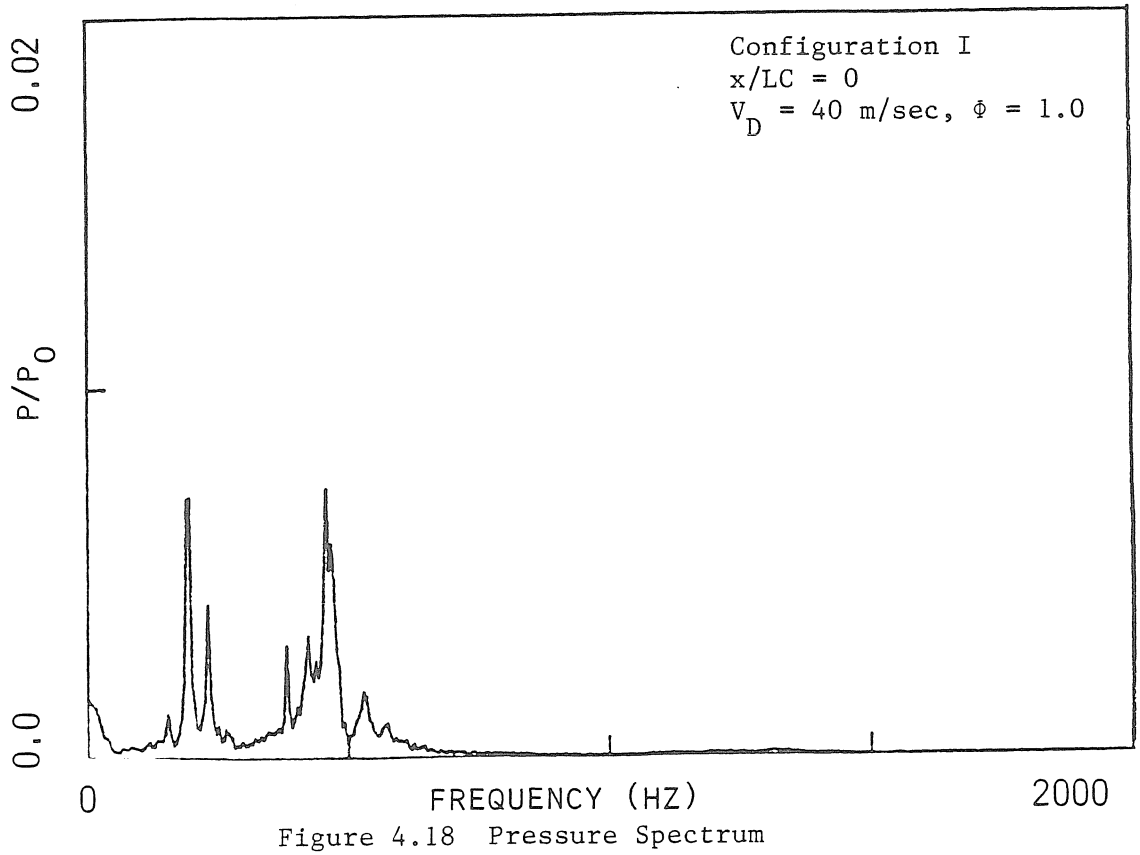

Figure 4.18 Pressure Spectrum

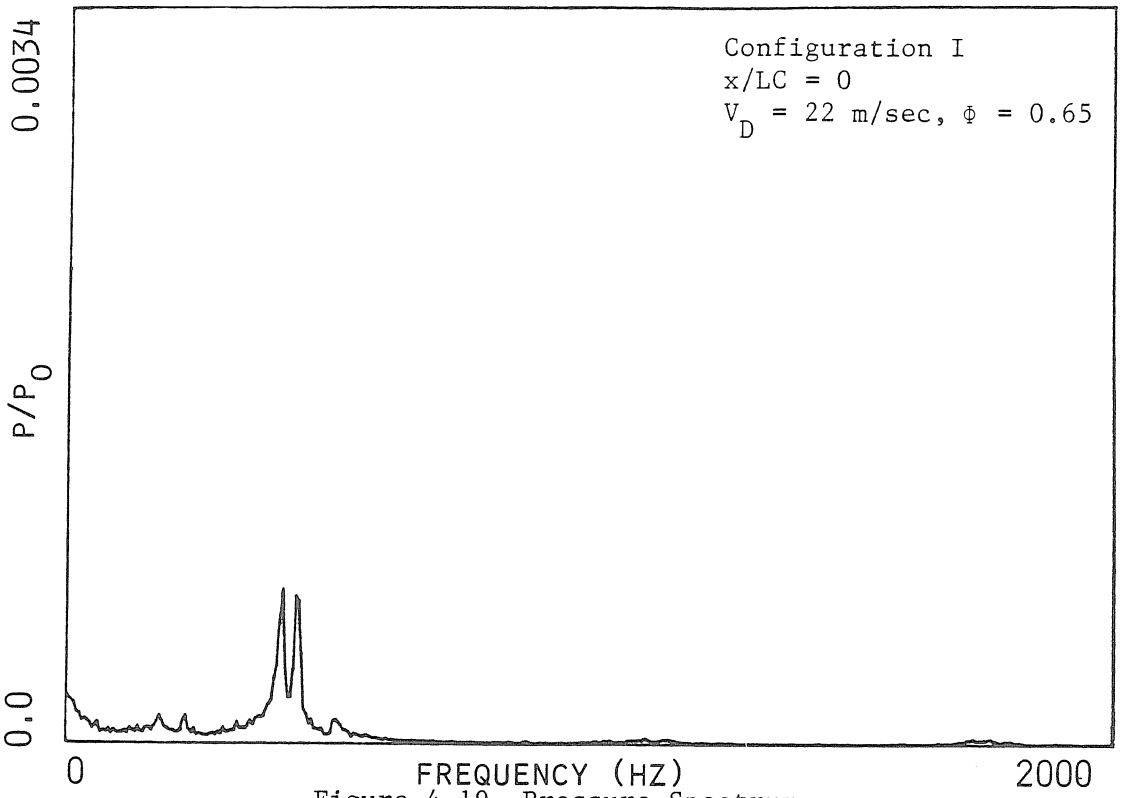

Figure 4.19 Pressure Spectrum

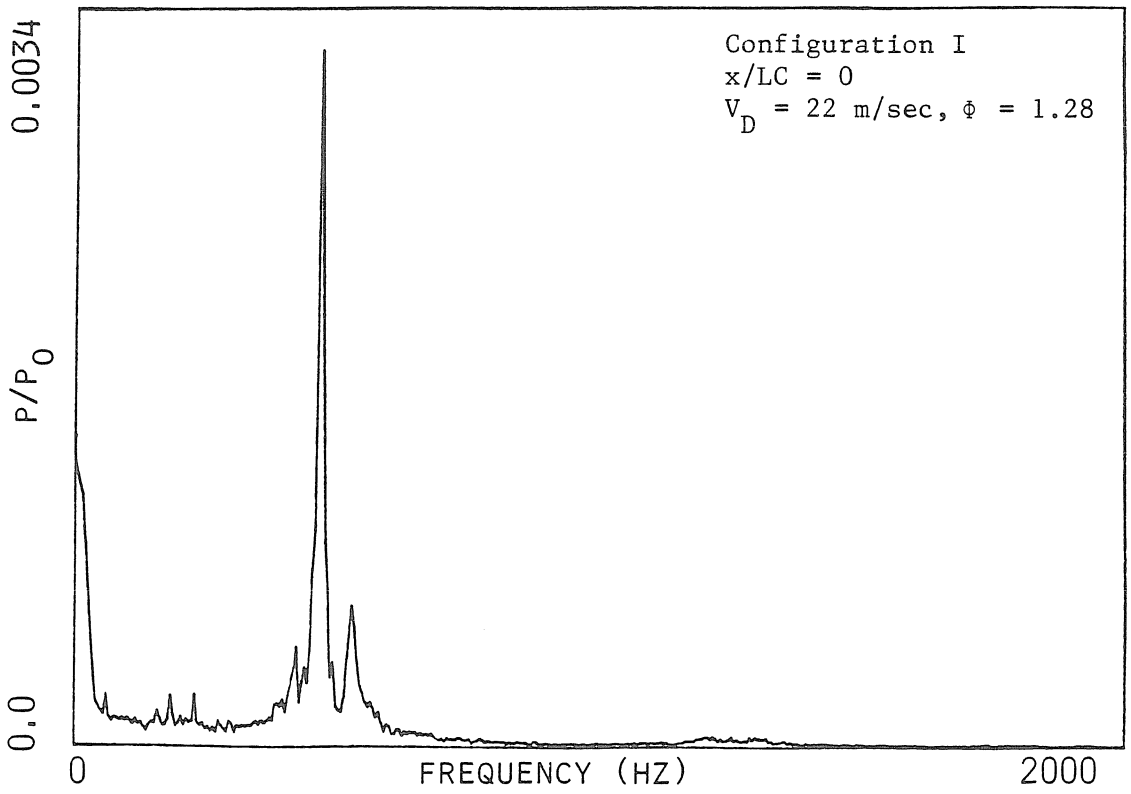

Figure 4.20 Pressure Spectrum

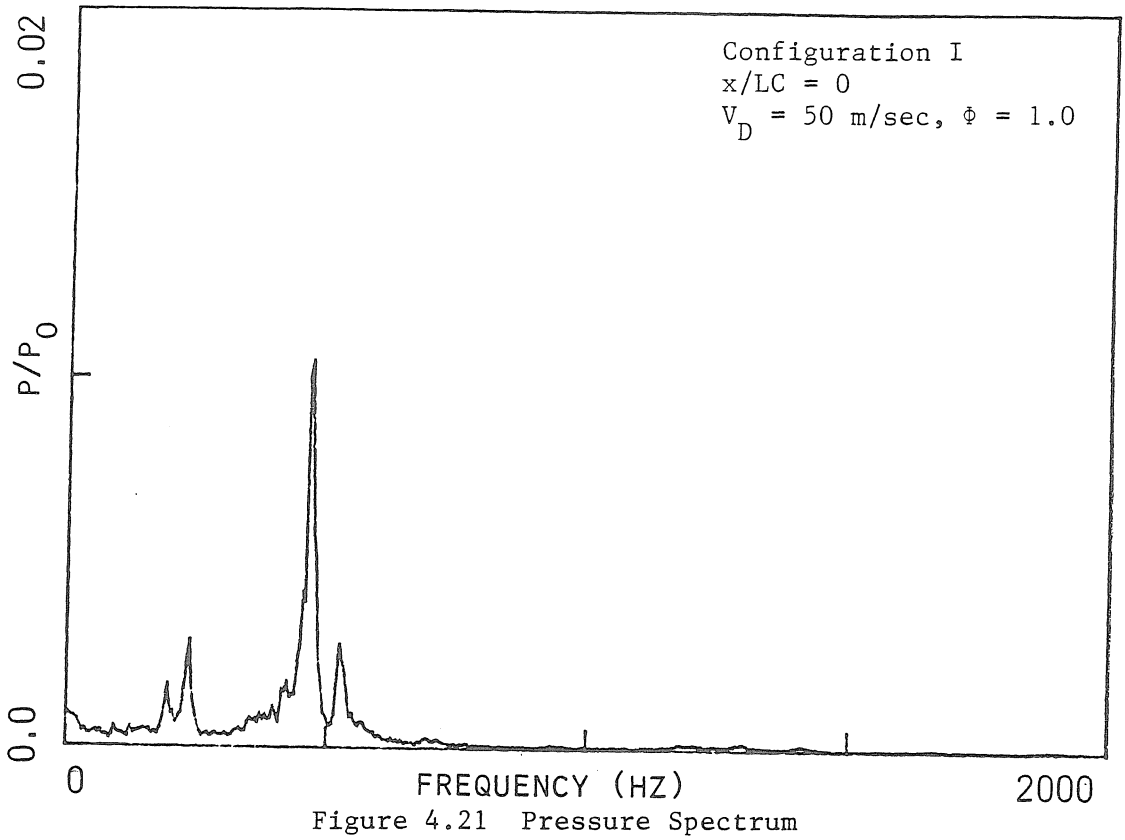

Figure 4.21 Pressure Spectrum

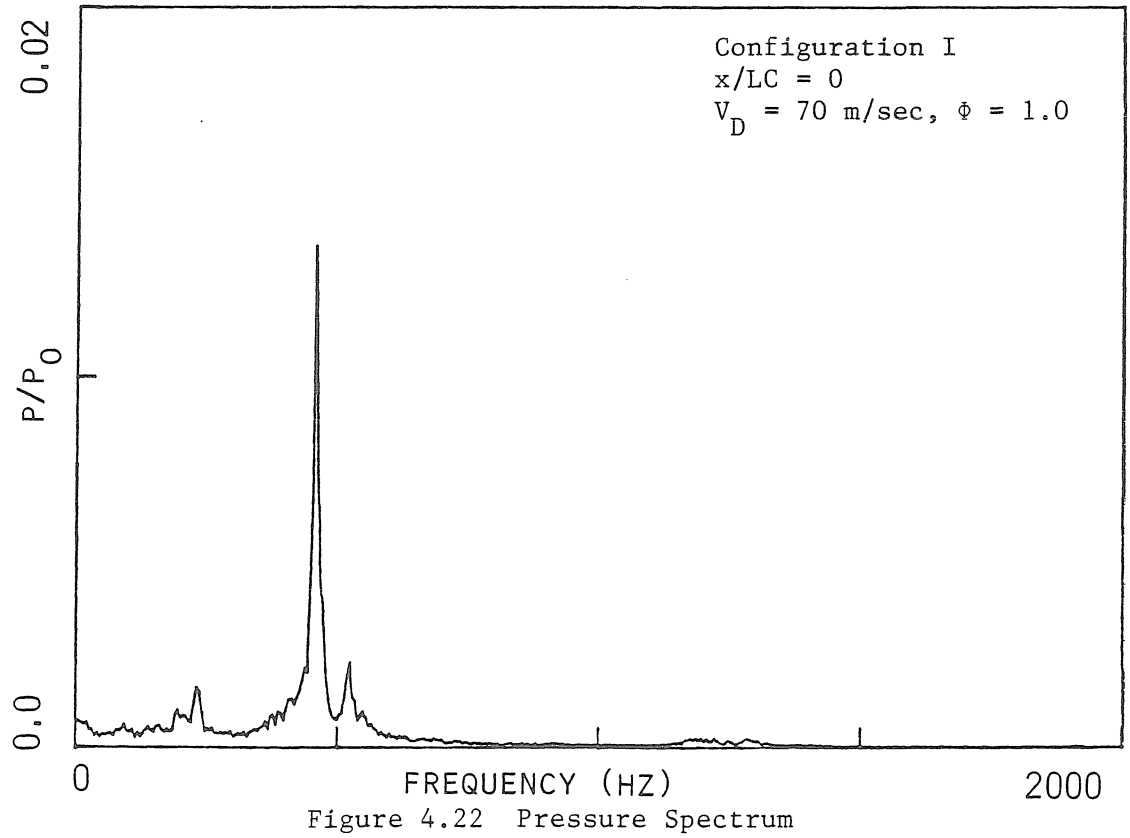

Figure 4.22 Pressure Spectrum

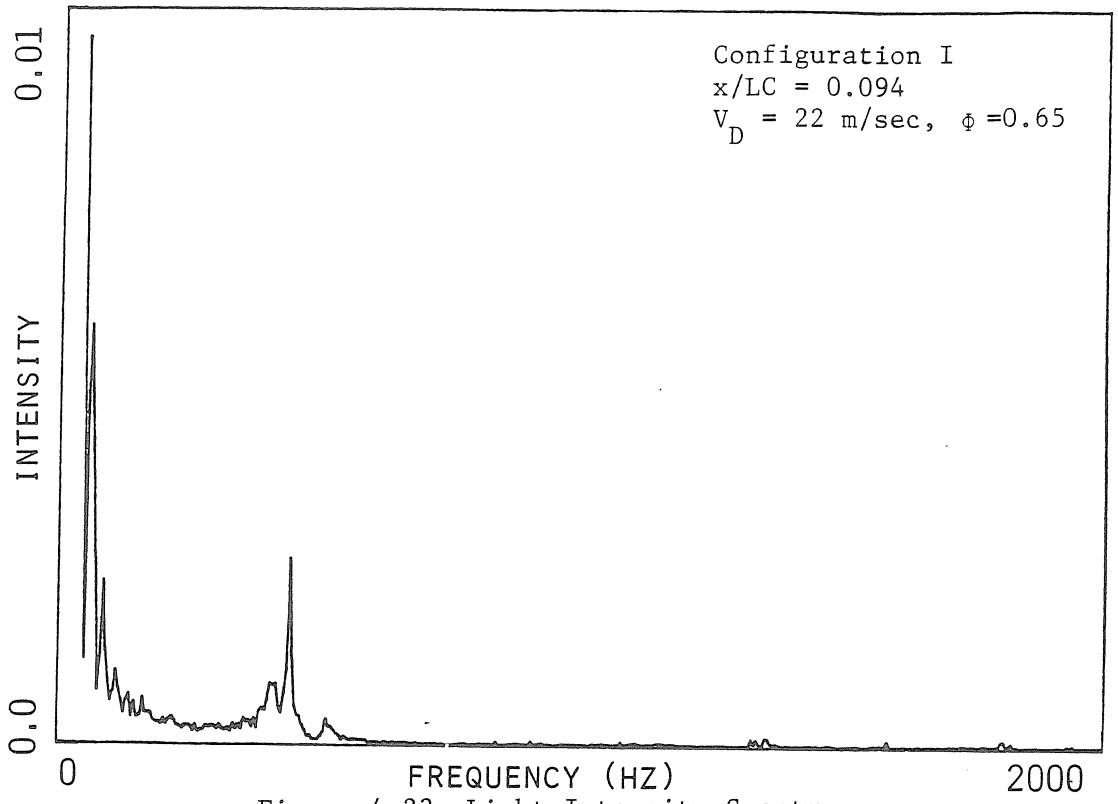

Figure 4.23 Light Intensity Spectrum

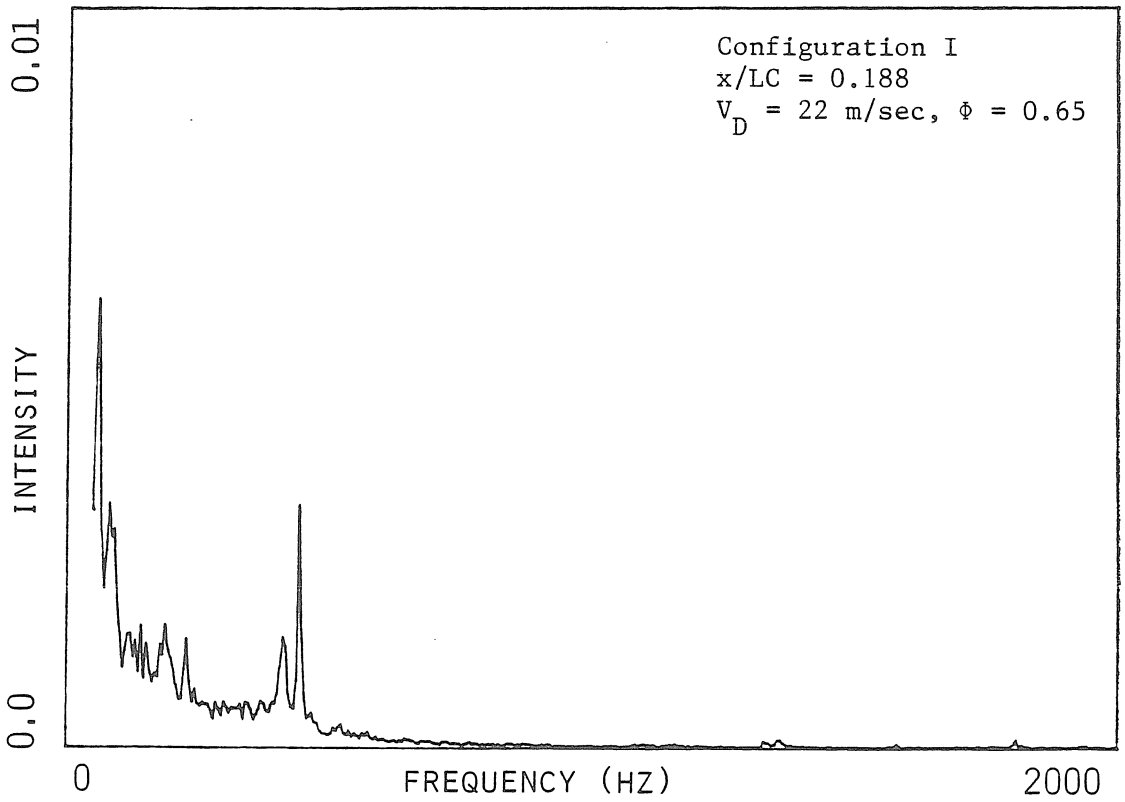

Figure 4.24 Light Intensity Spectrum

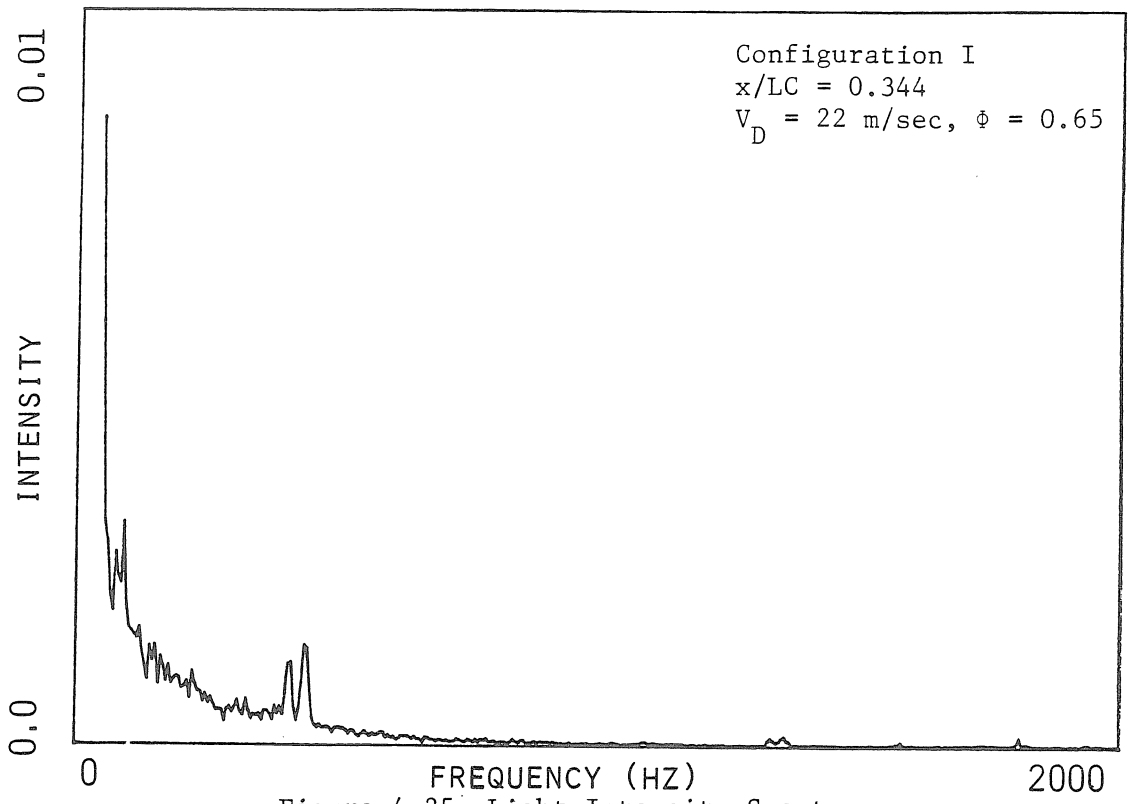

Figure 4.25 Light Intensity Spectrum

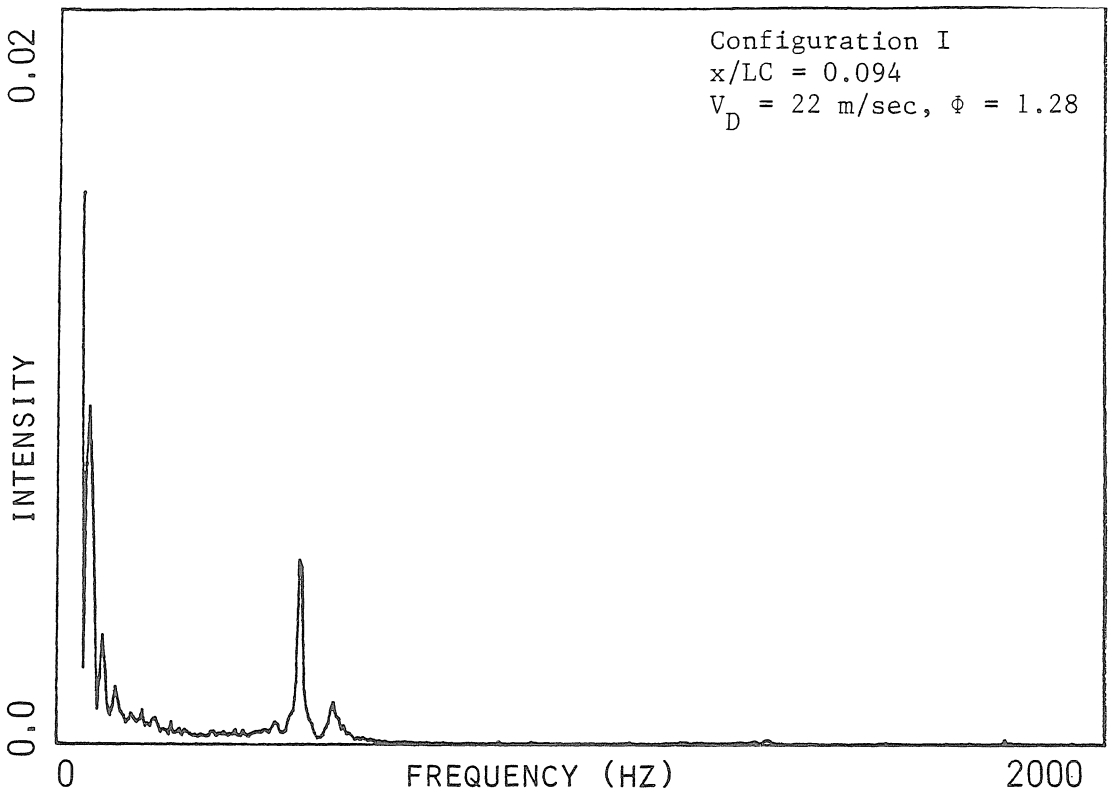

Figure 4.26 Light Intensity Spectrum

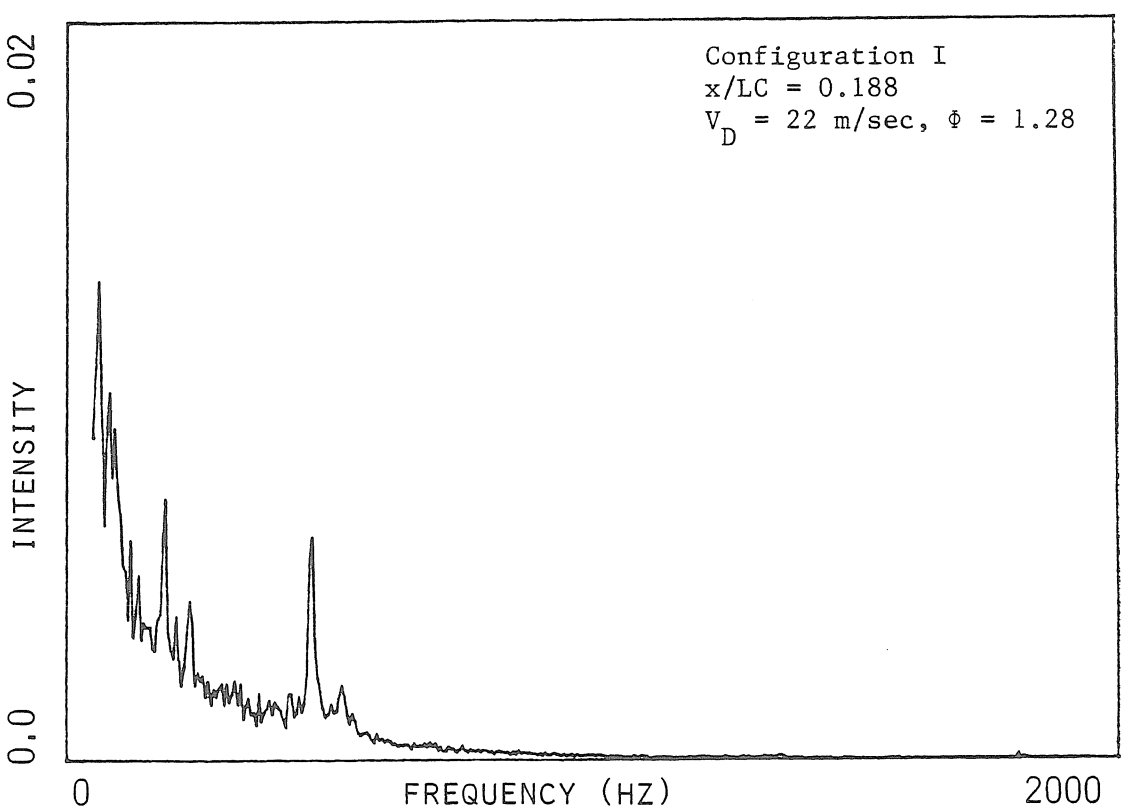

Figure 4.27 Light Intensity Spectrum

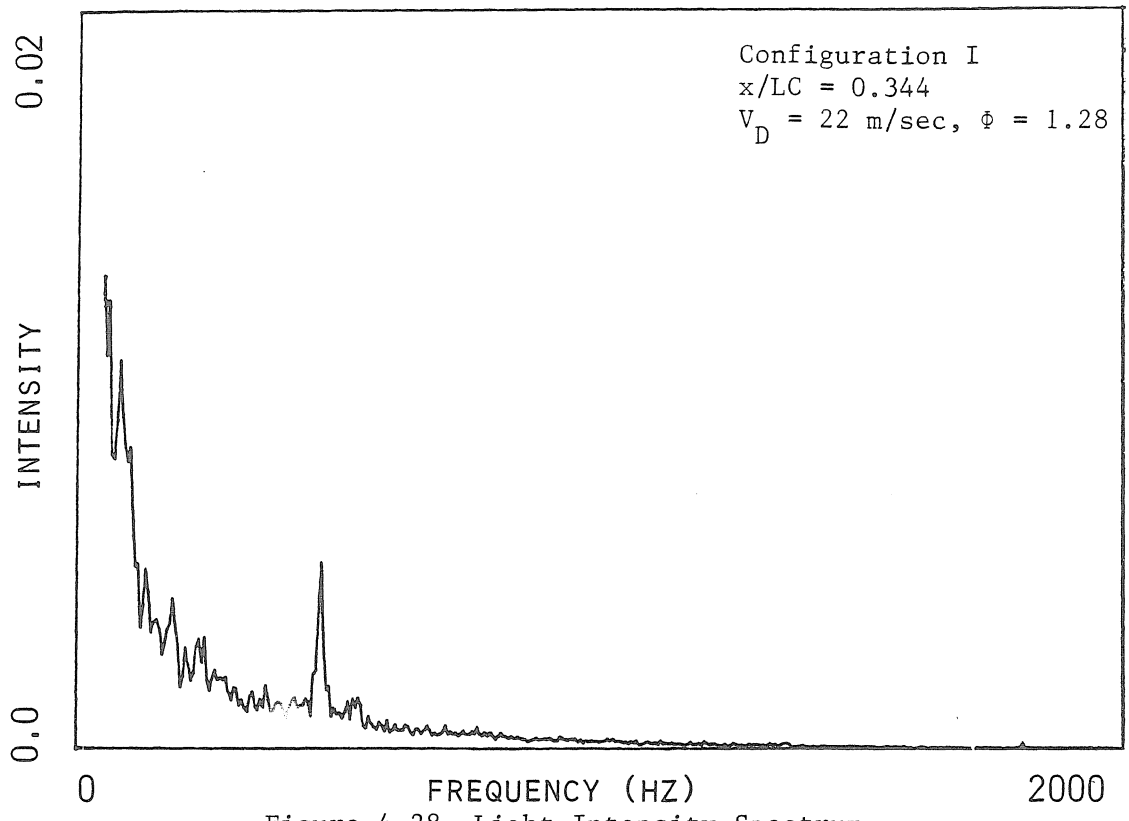

Figure 4.28 Light Intensity Spectrum

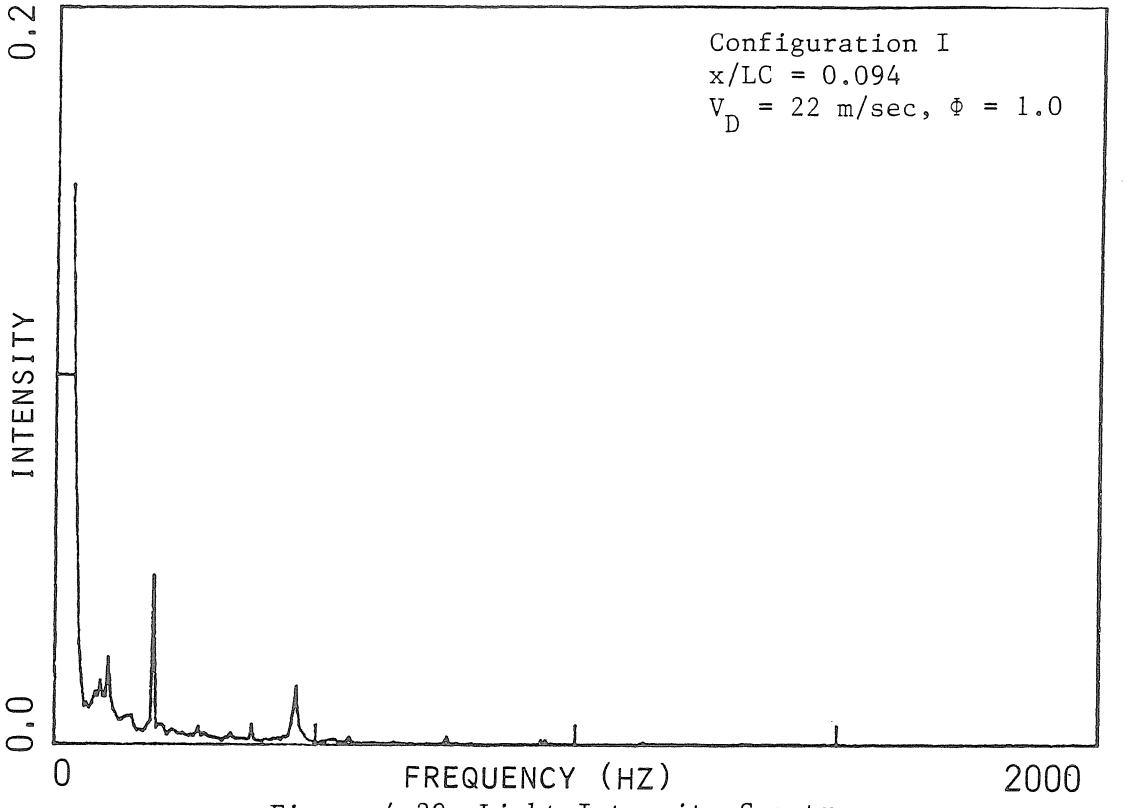

Figure 4.29 Light Intensity Spectrum

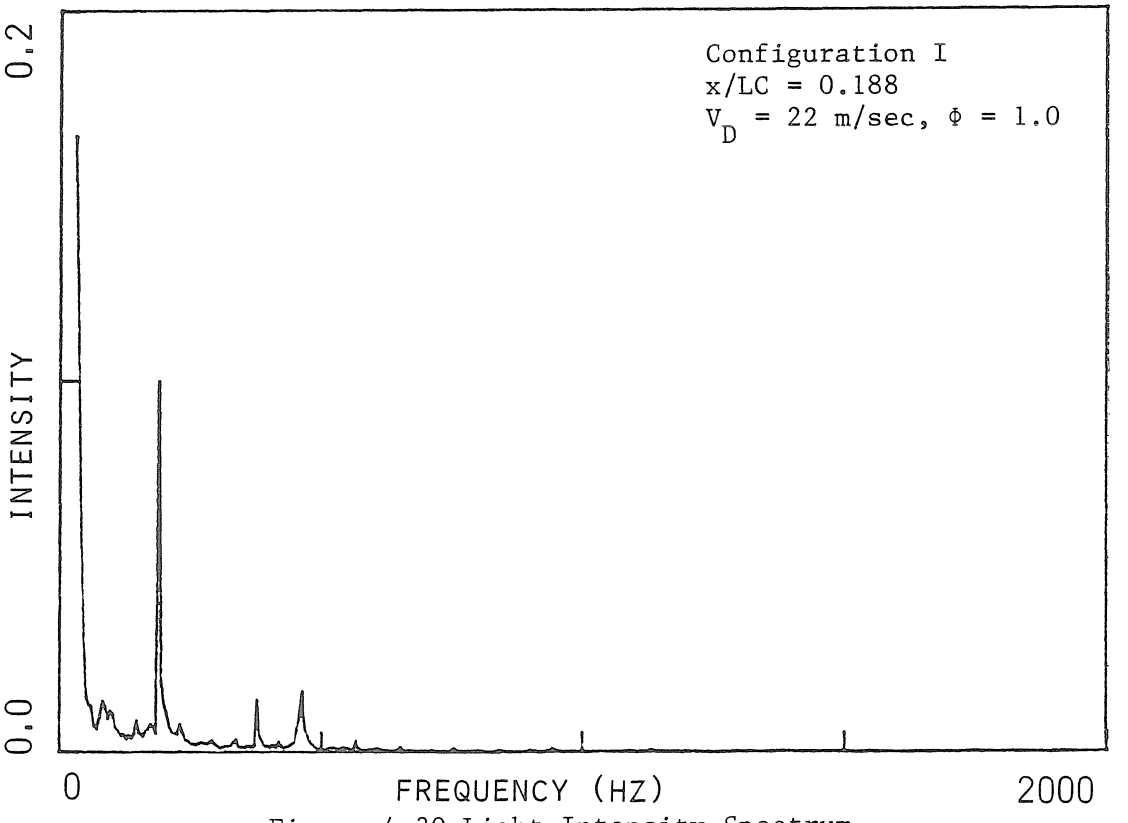

Figure 4.30 Light Intensity Spectrum

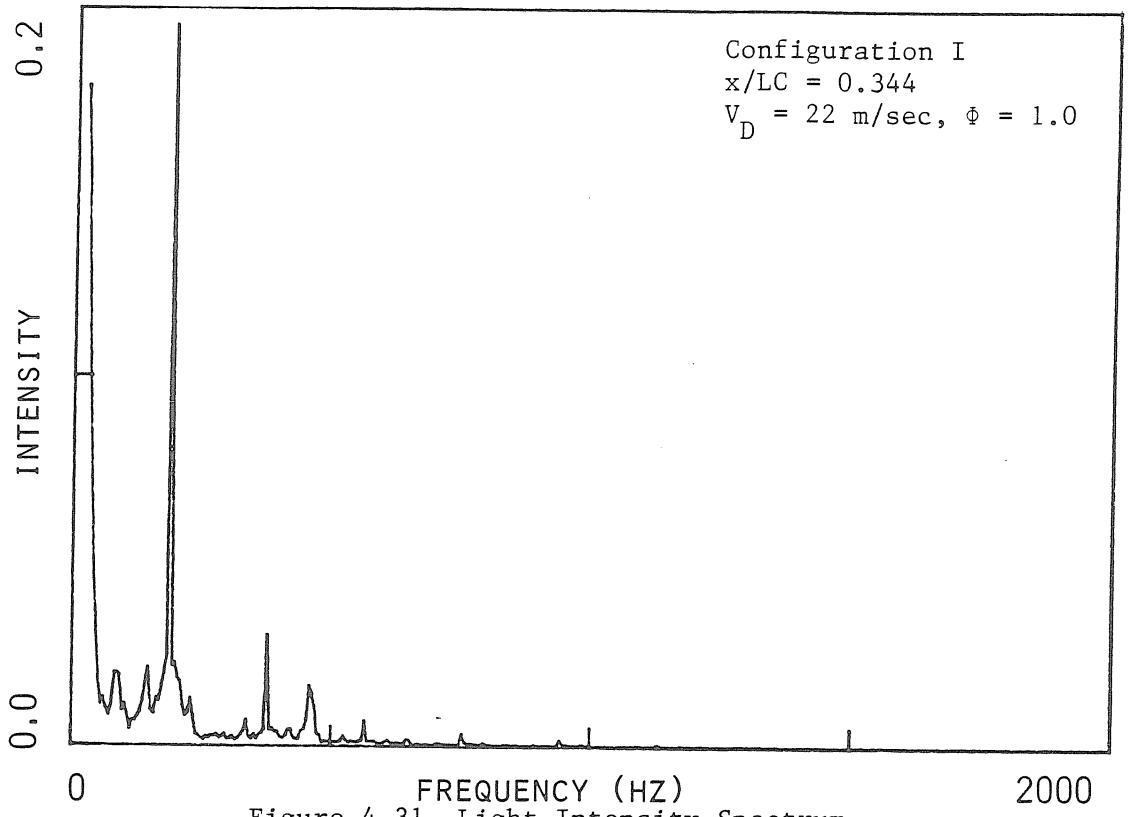

Figure 4.31 Light Intensity Spectrum

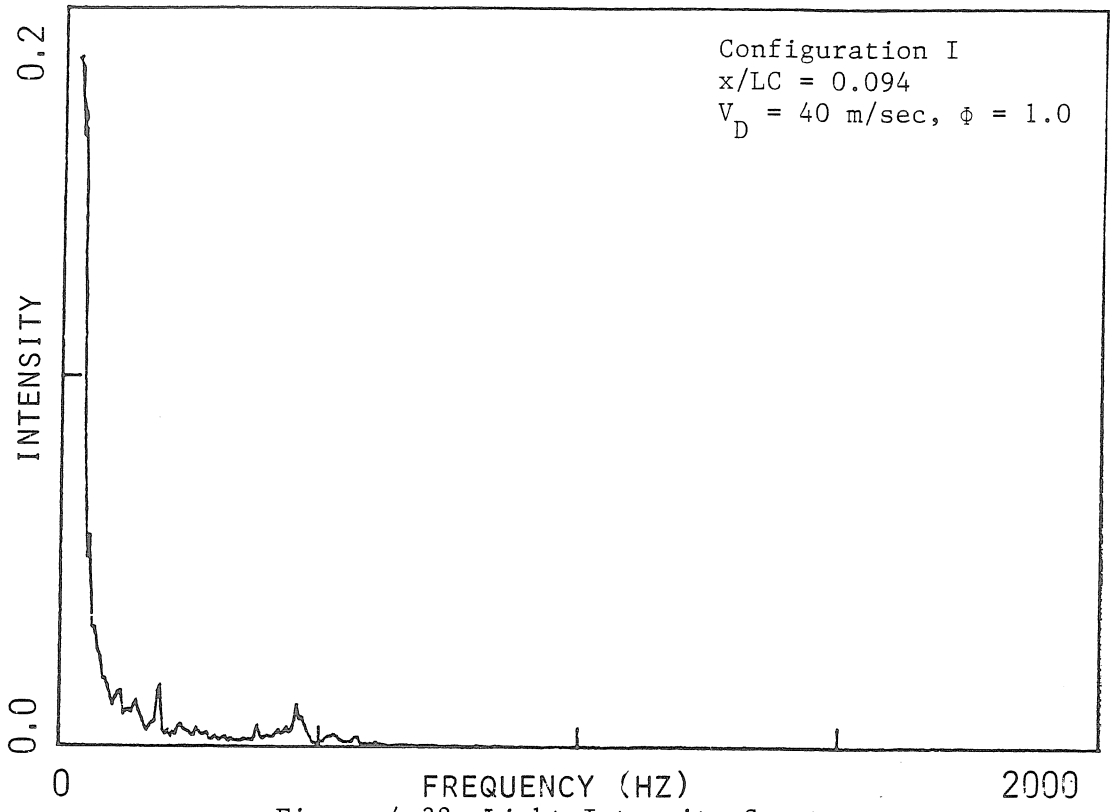

Figure 4.32 Light Intensity Spectrum

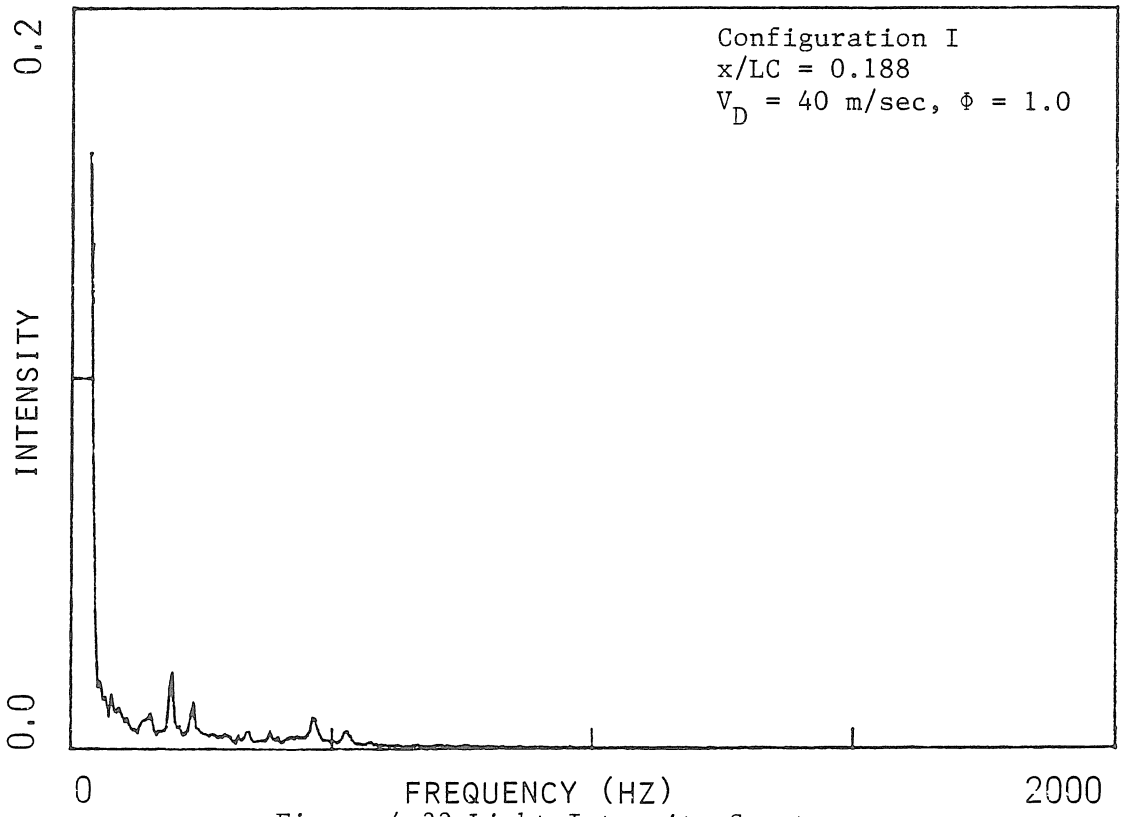

Figure 4.33 Light Intensity Spectrum

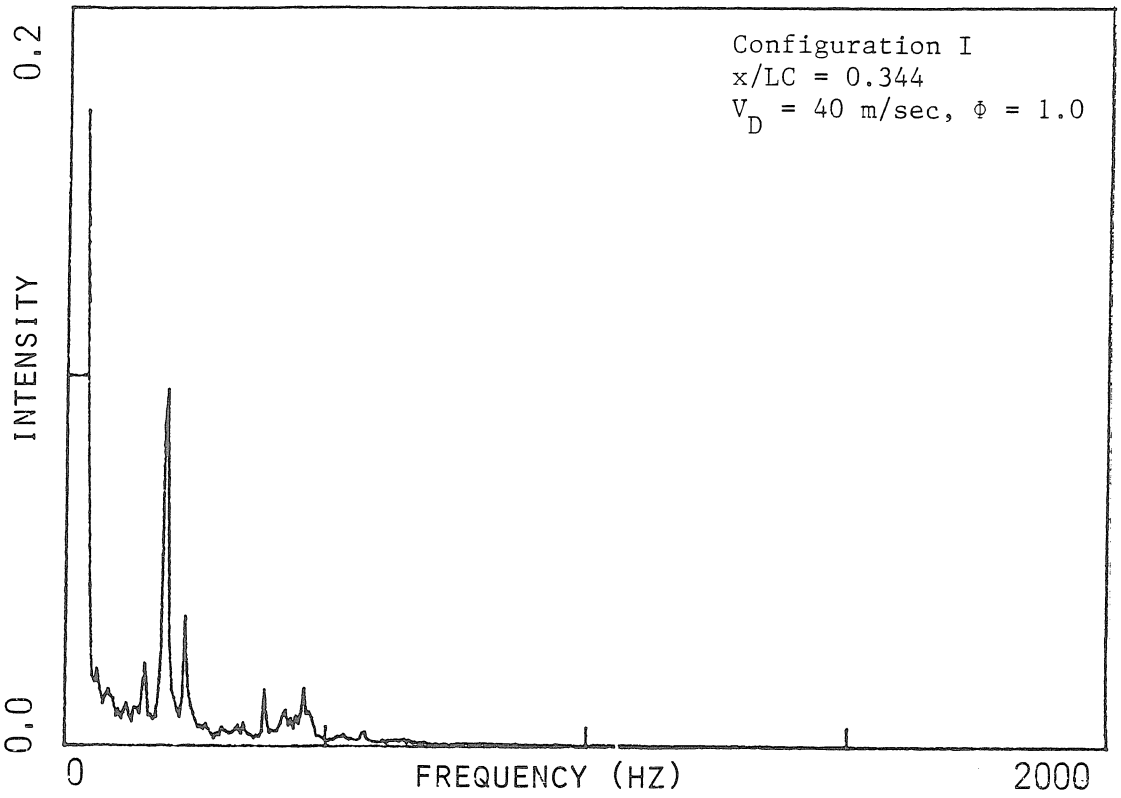

Figure 4.34 Light Intensity Spectrum

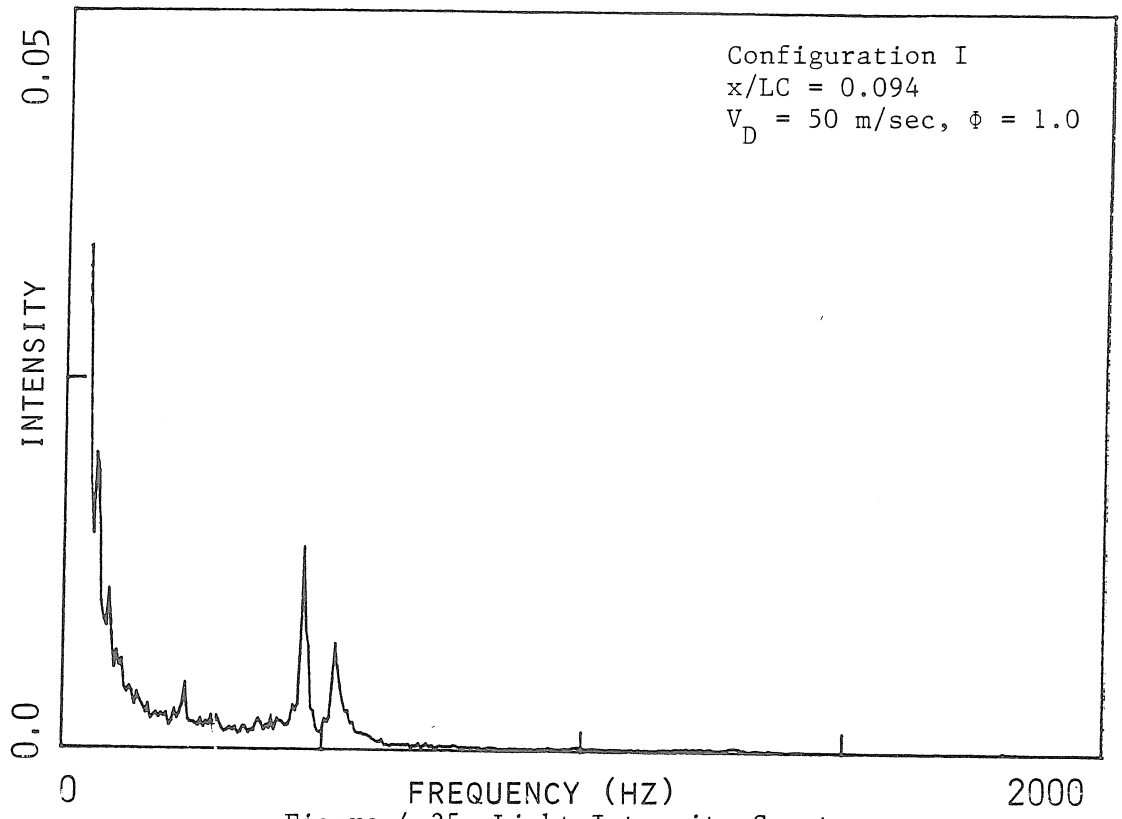

Figure 4.35 Light Intensity Spectrum

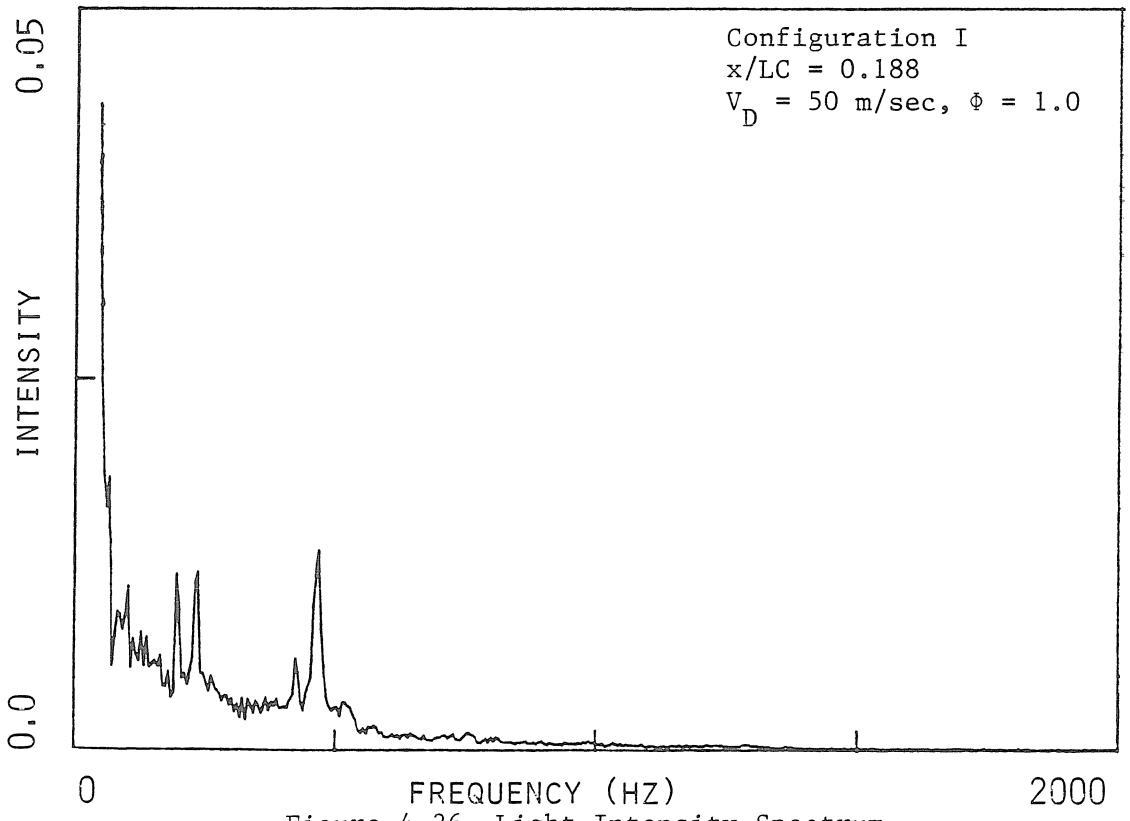

Figure 4.36 Light Intensity Spectrum

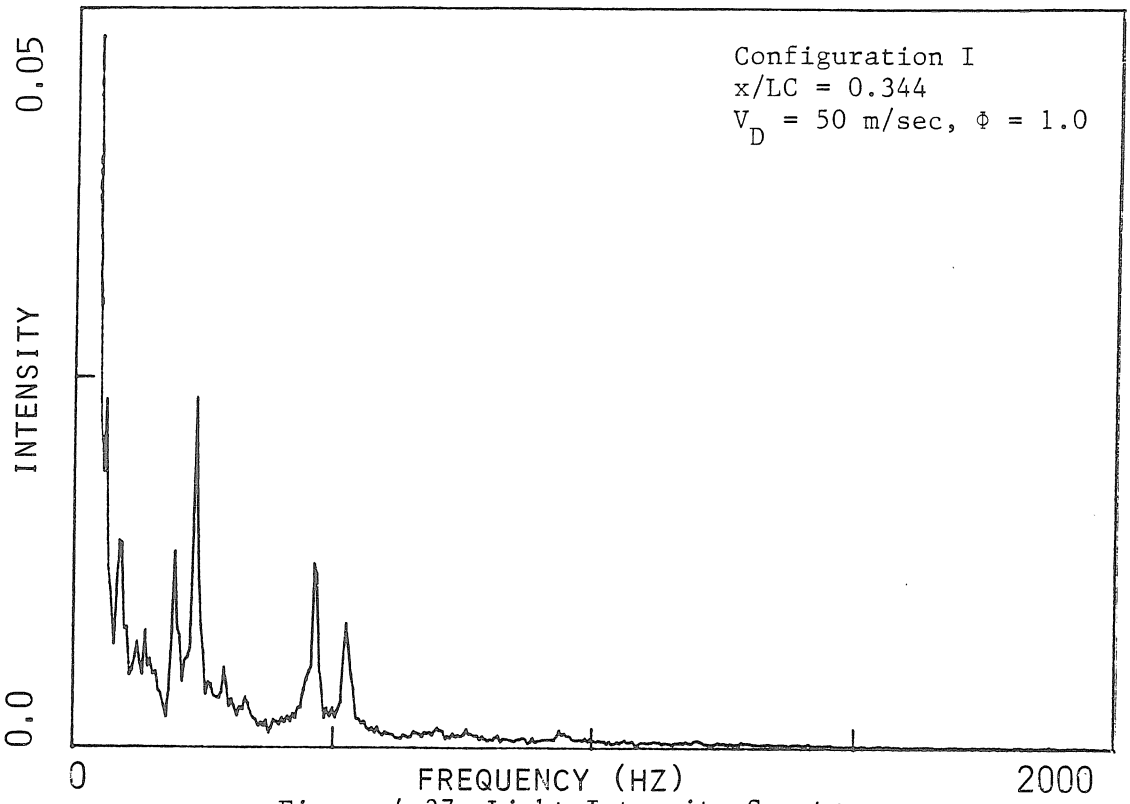

Figure 4.37 Light Intensity Spectrum

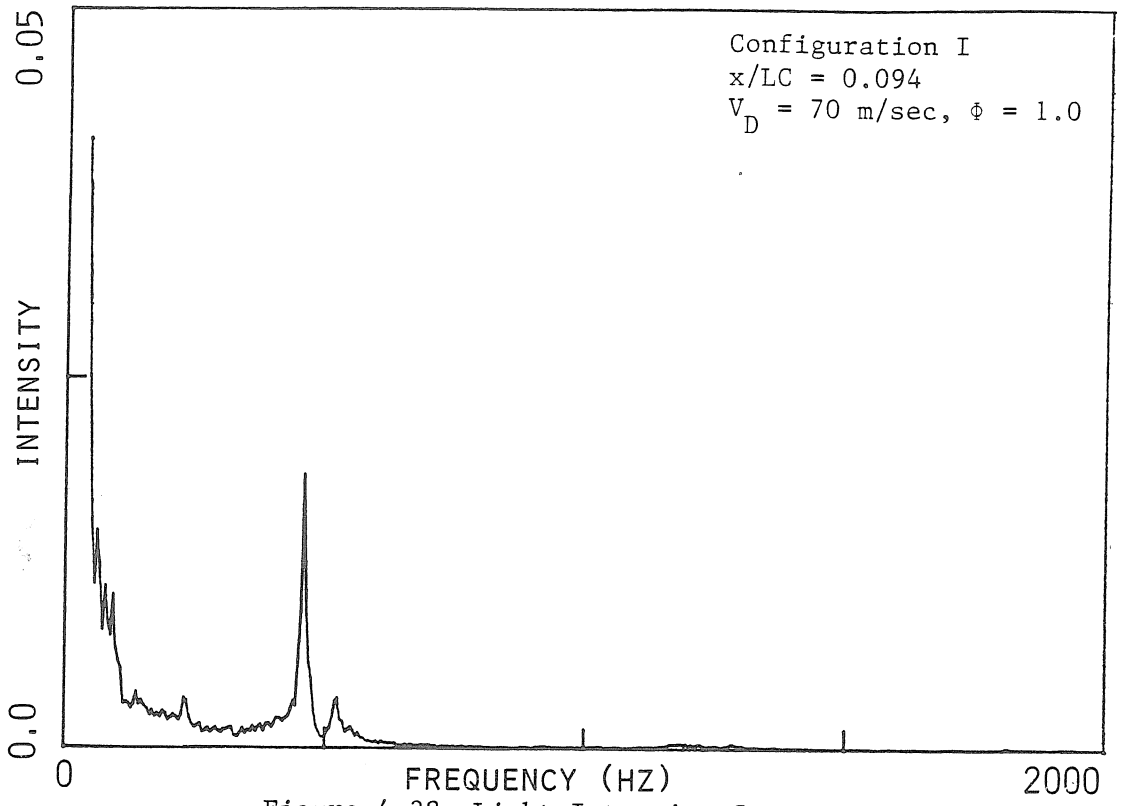

Figure 4.38 Light Intensity Spectrum

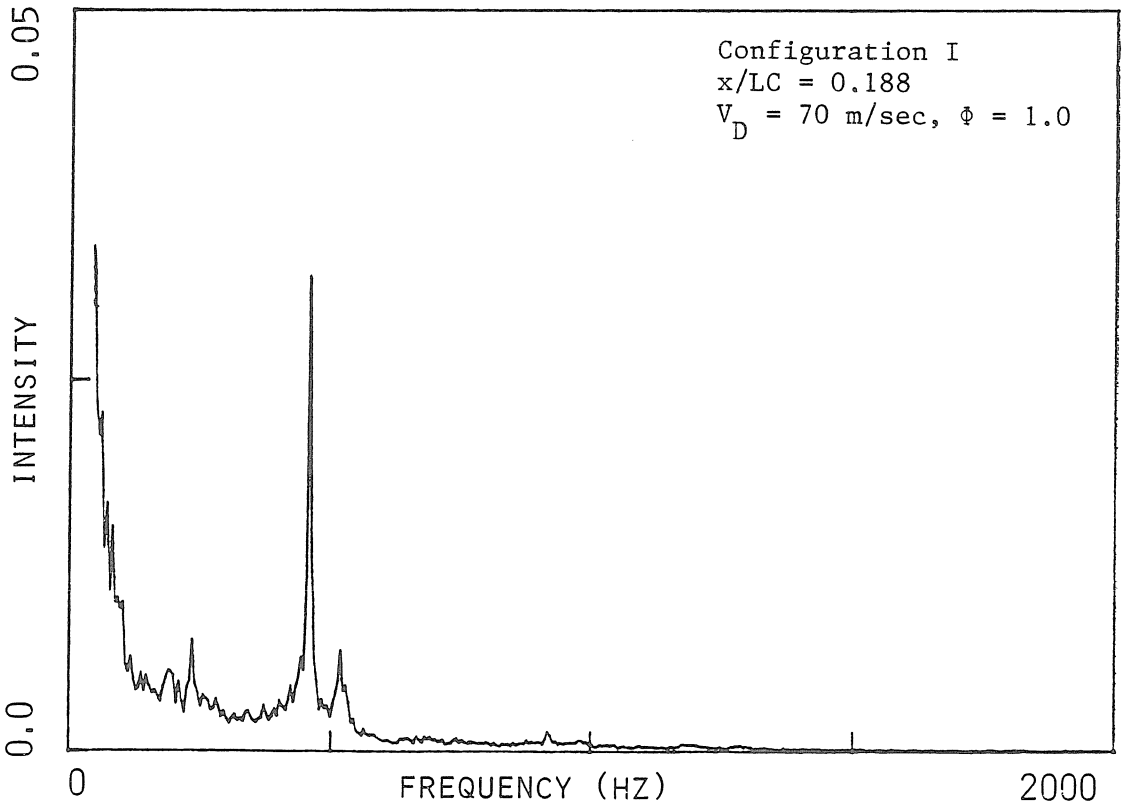

Figure 4.39 Light Intensity Spectrum

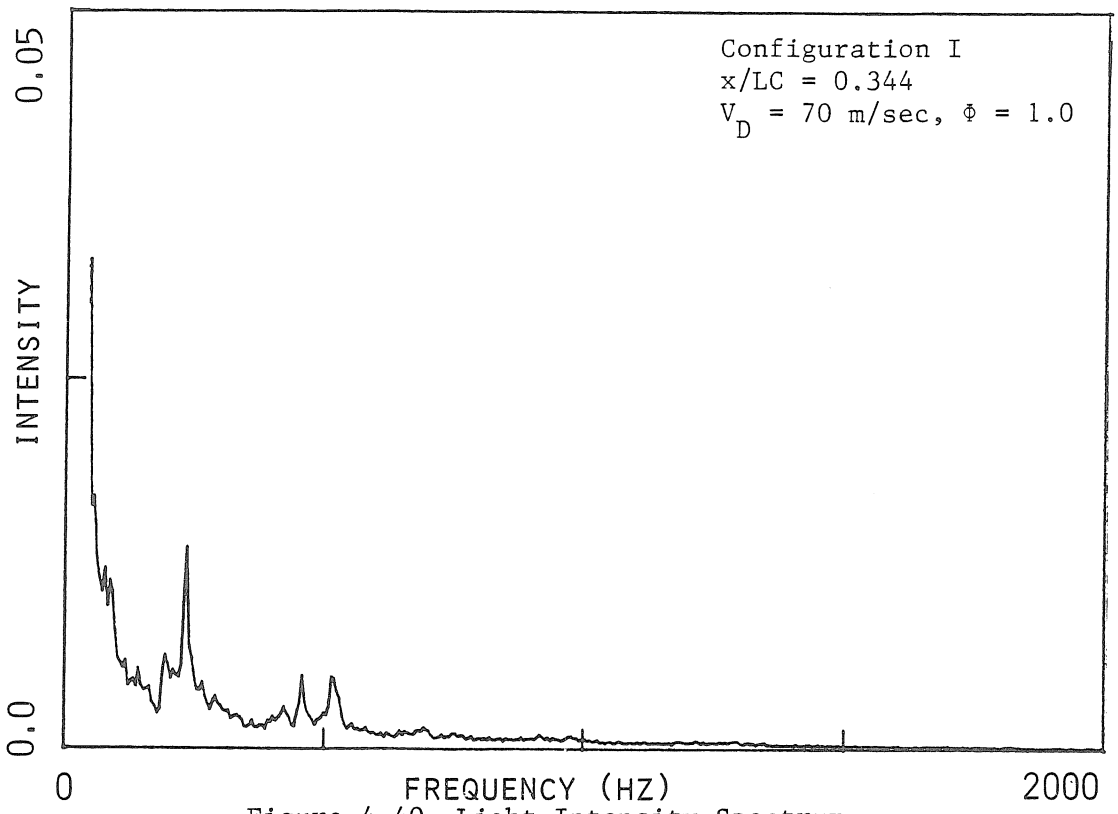

Figure 4.40 Light Intensity Spectrum

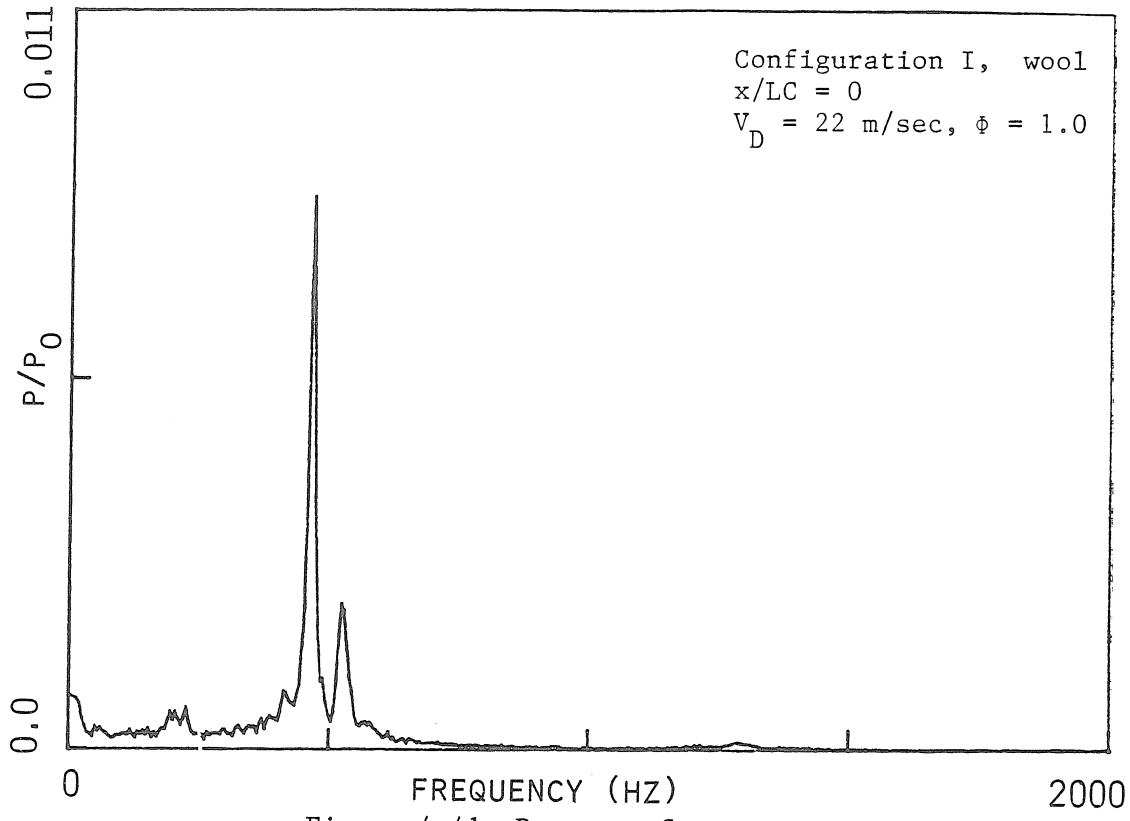

Figure 4.41 Pressure Spectrum

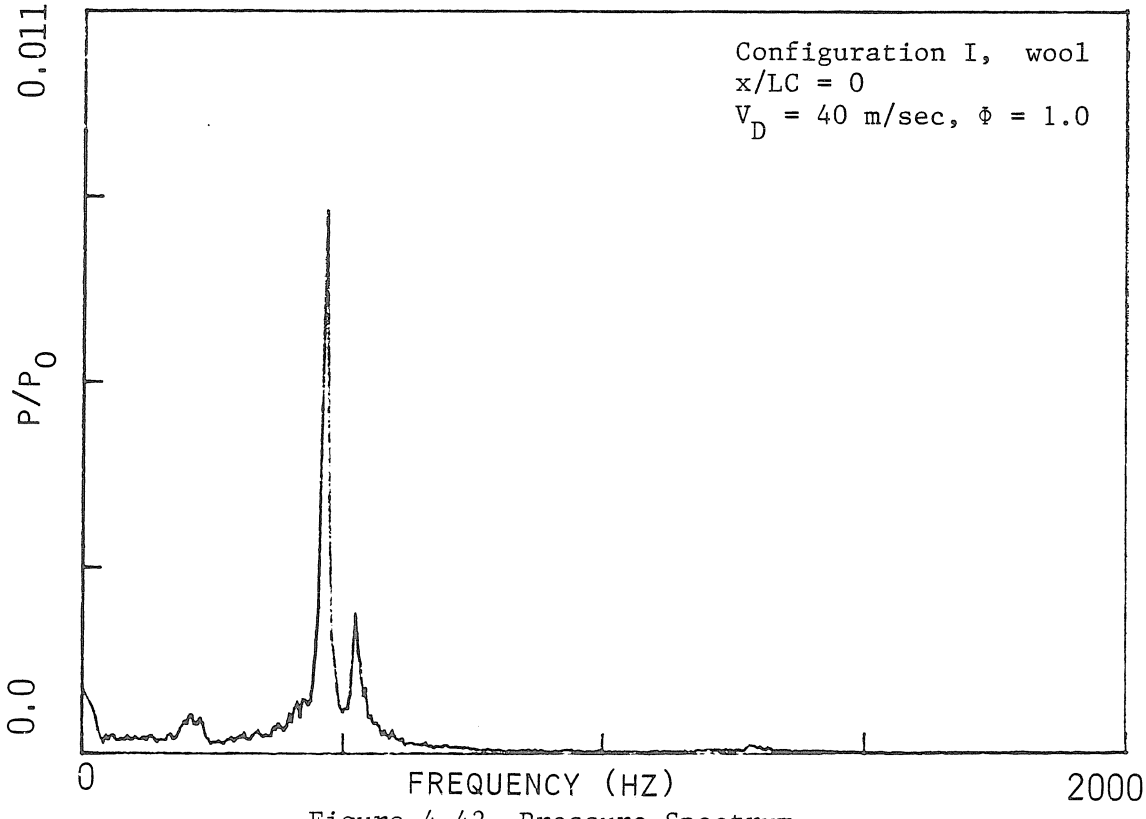

Figure 4.42 Pressure Spectrum

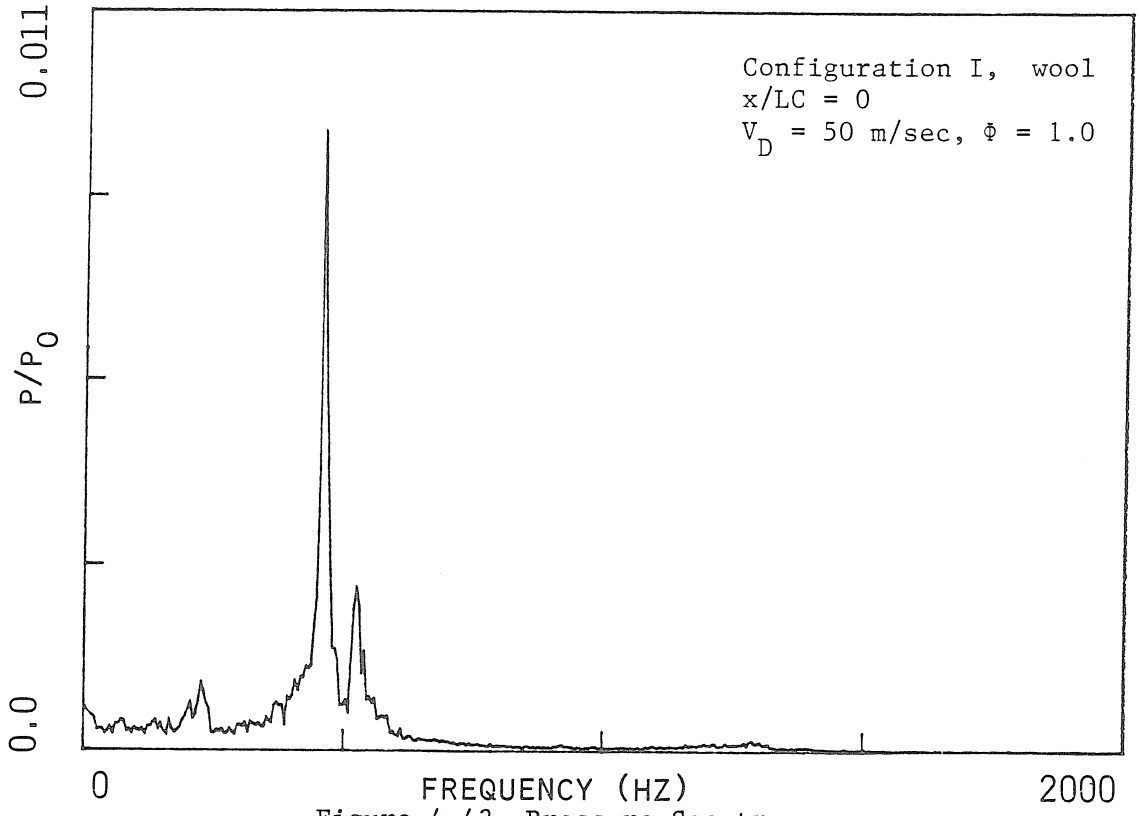

Figure 4.43 Pressure Spectrum

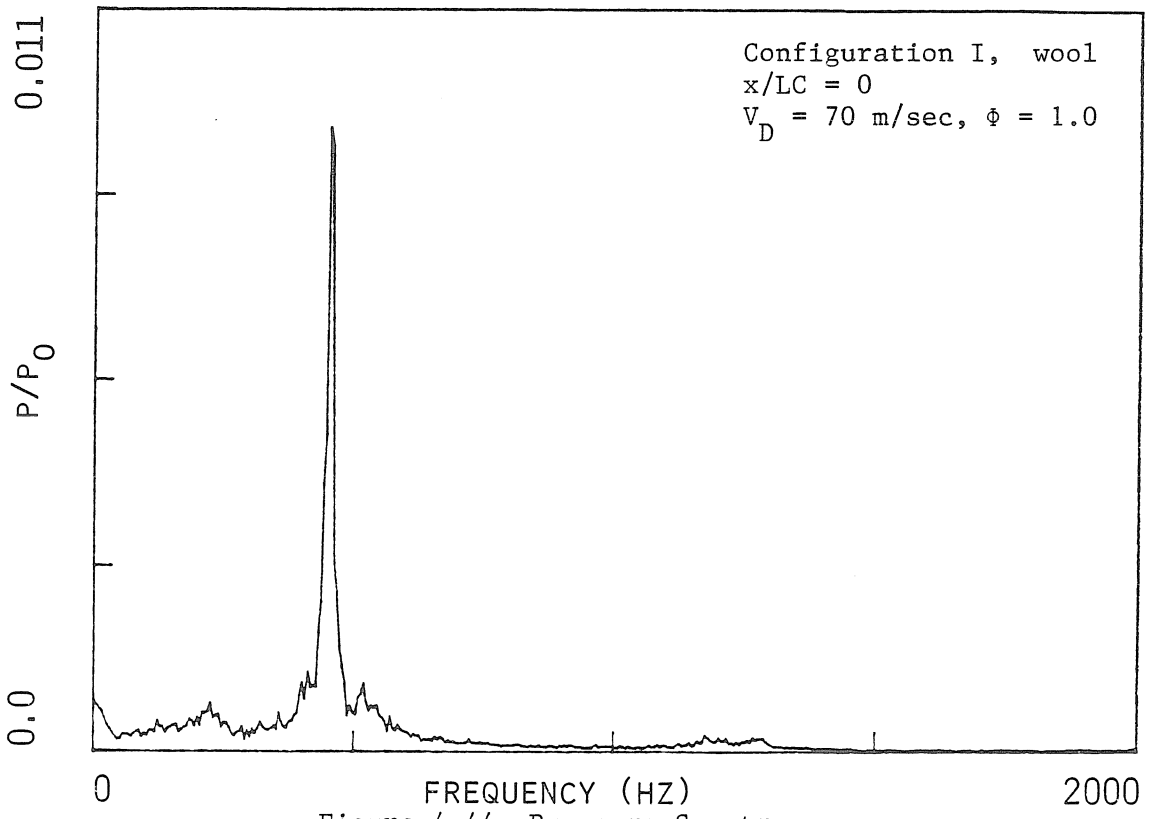

Figure 4.44 Pressure Spectrum

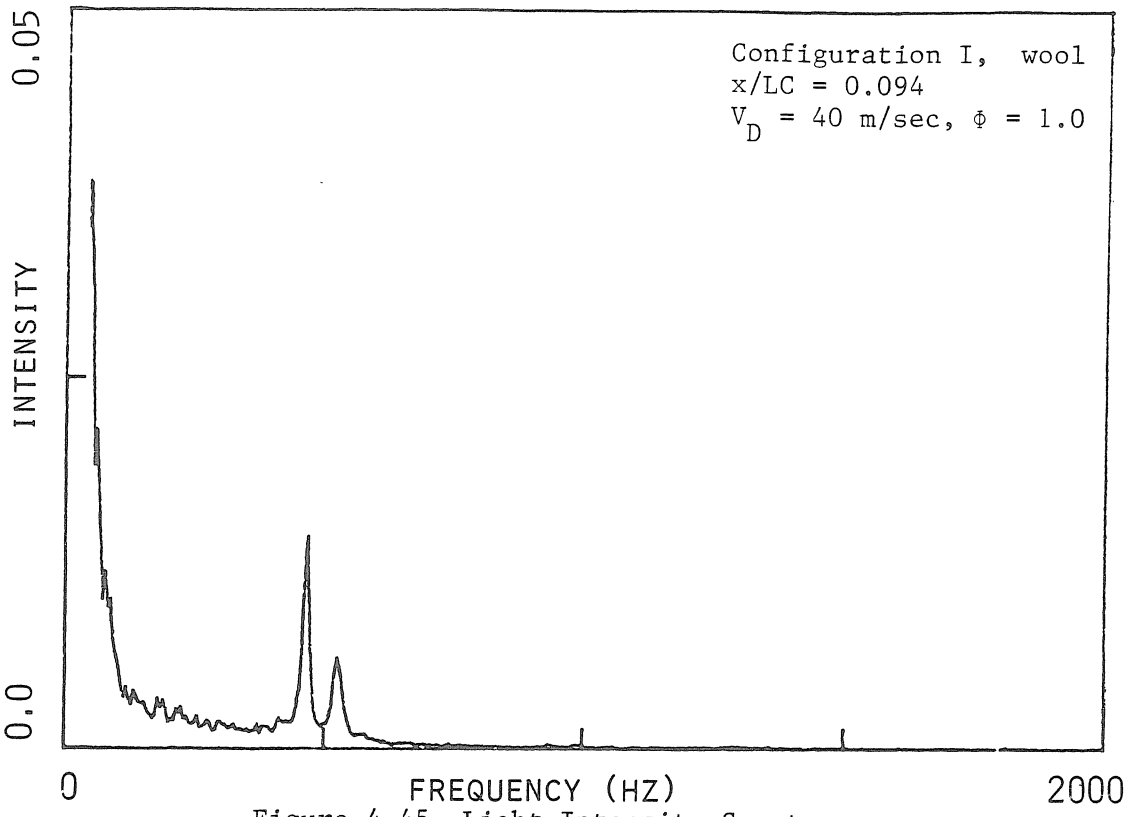

Figure 4.45 Light Intensity Spectrum

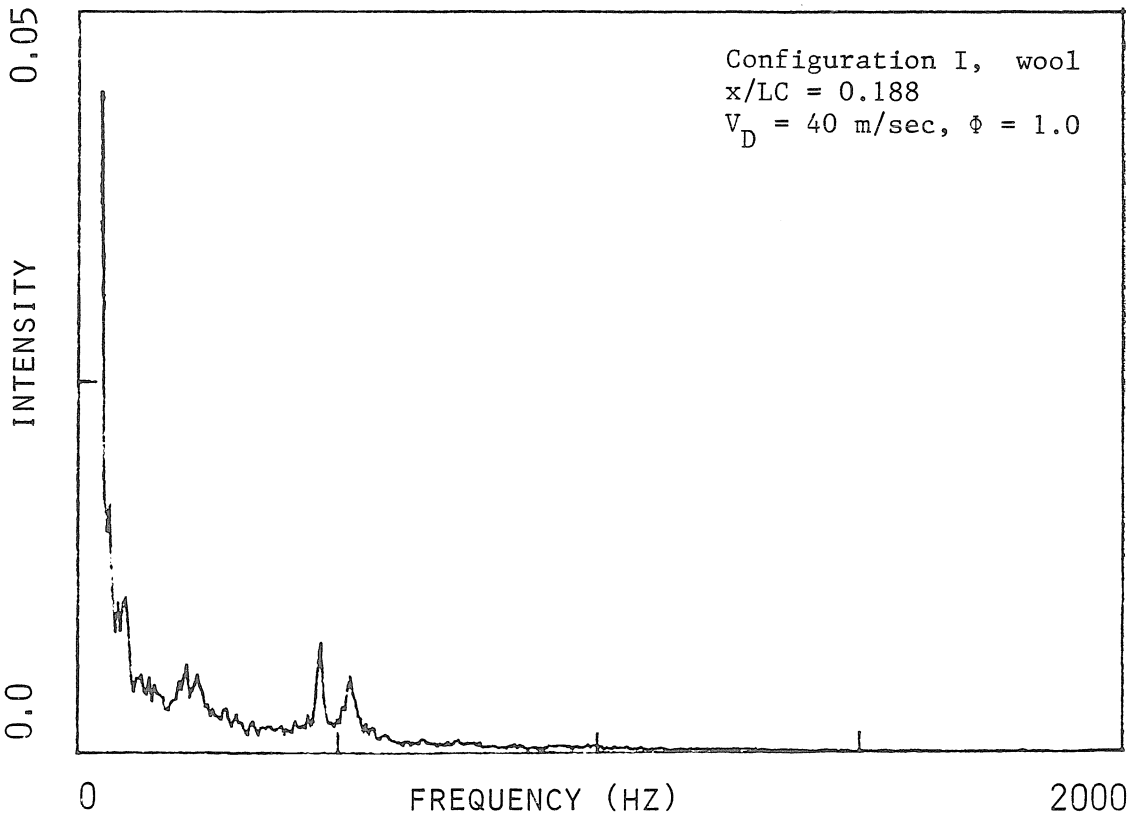

Figure 4.46 Light Intensity Spectrum

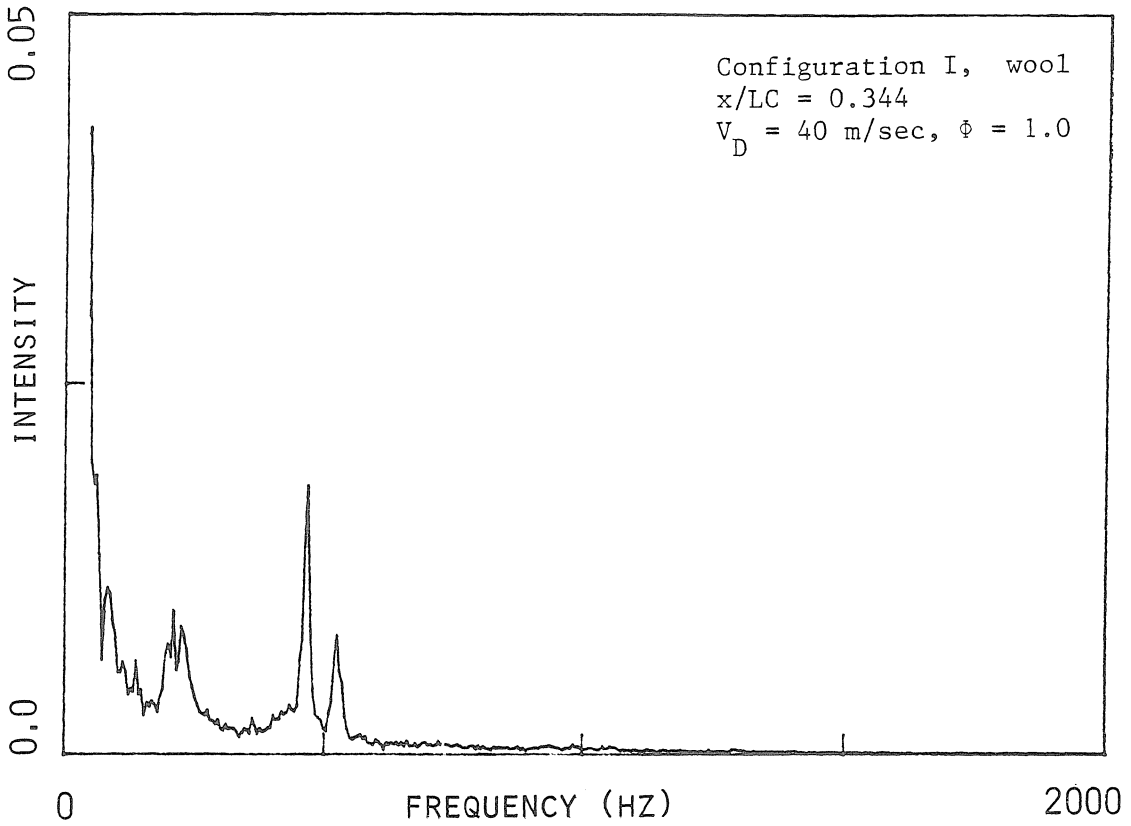

Figure 4.47 Light Intensity Spectrum

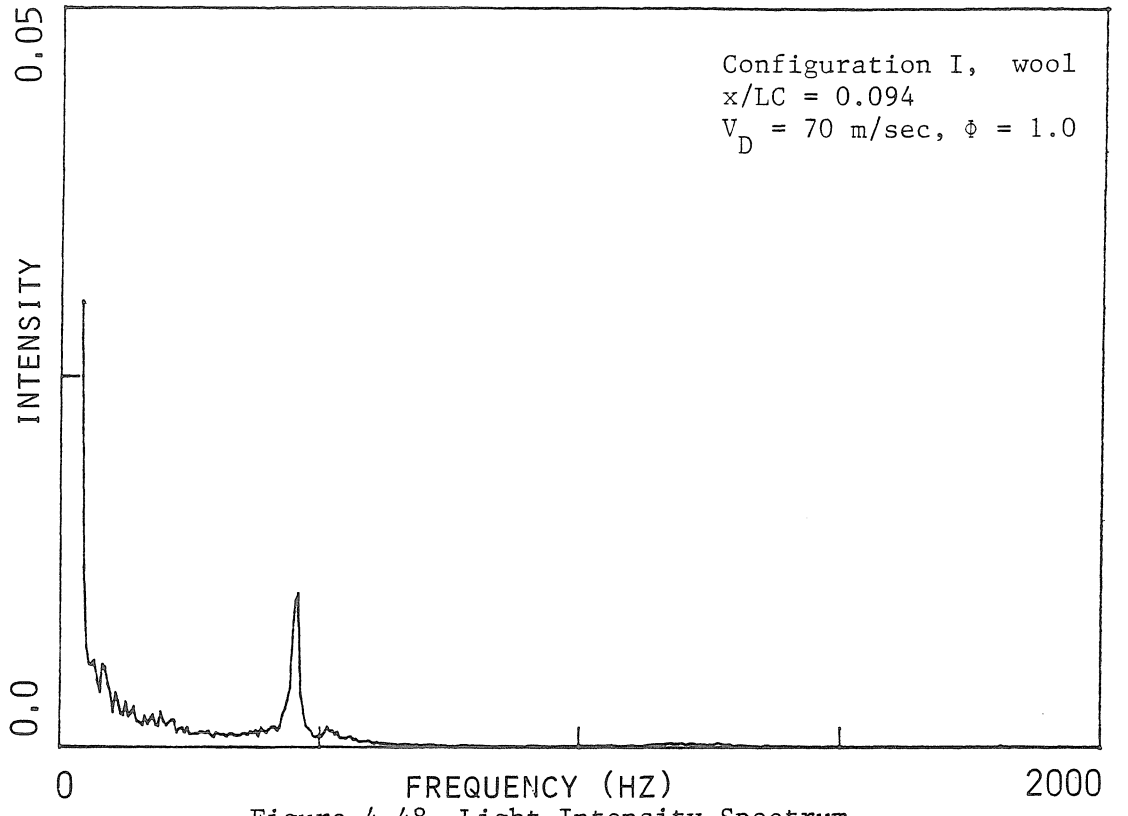

Figure 4.48 Light Intensity Spectrum

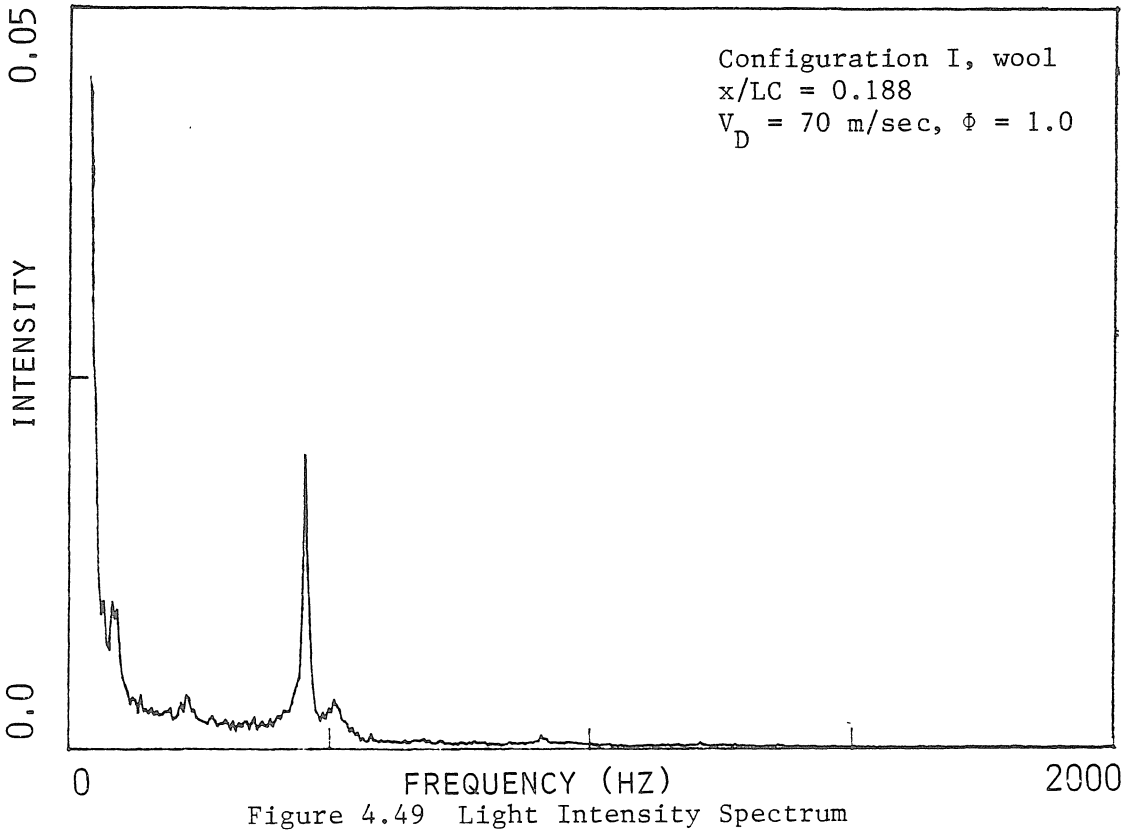

Figure 4.49 Light Intensity Spectrum

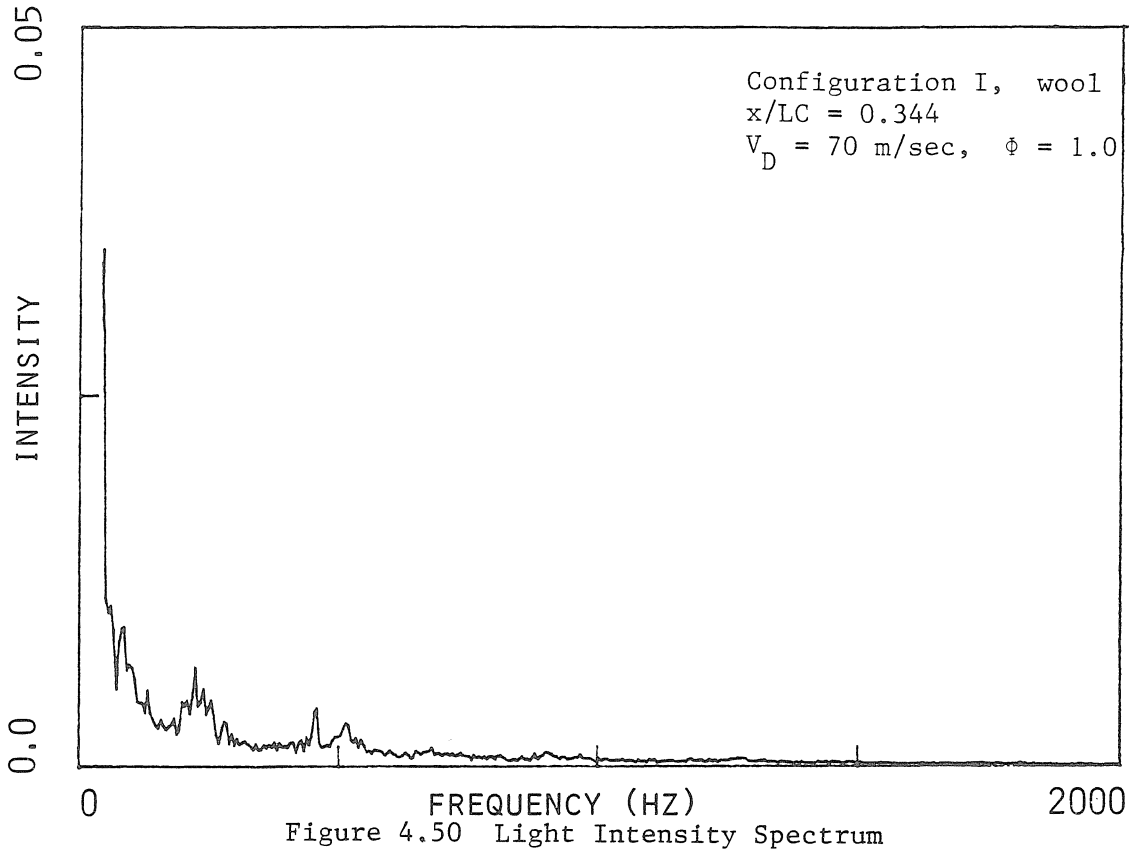

Figure 4.50 Light Intensity Spectrum

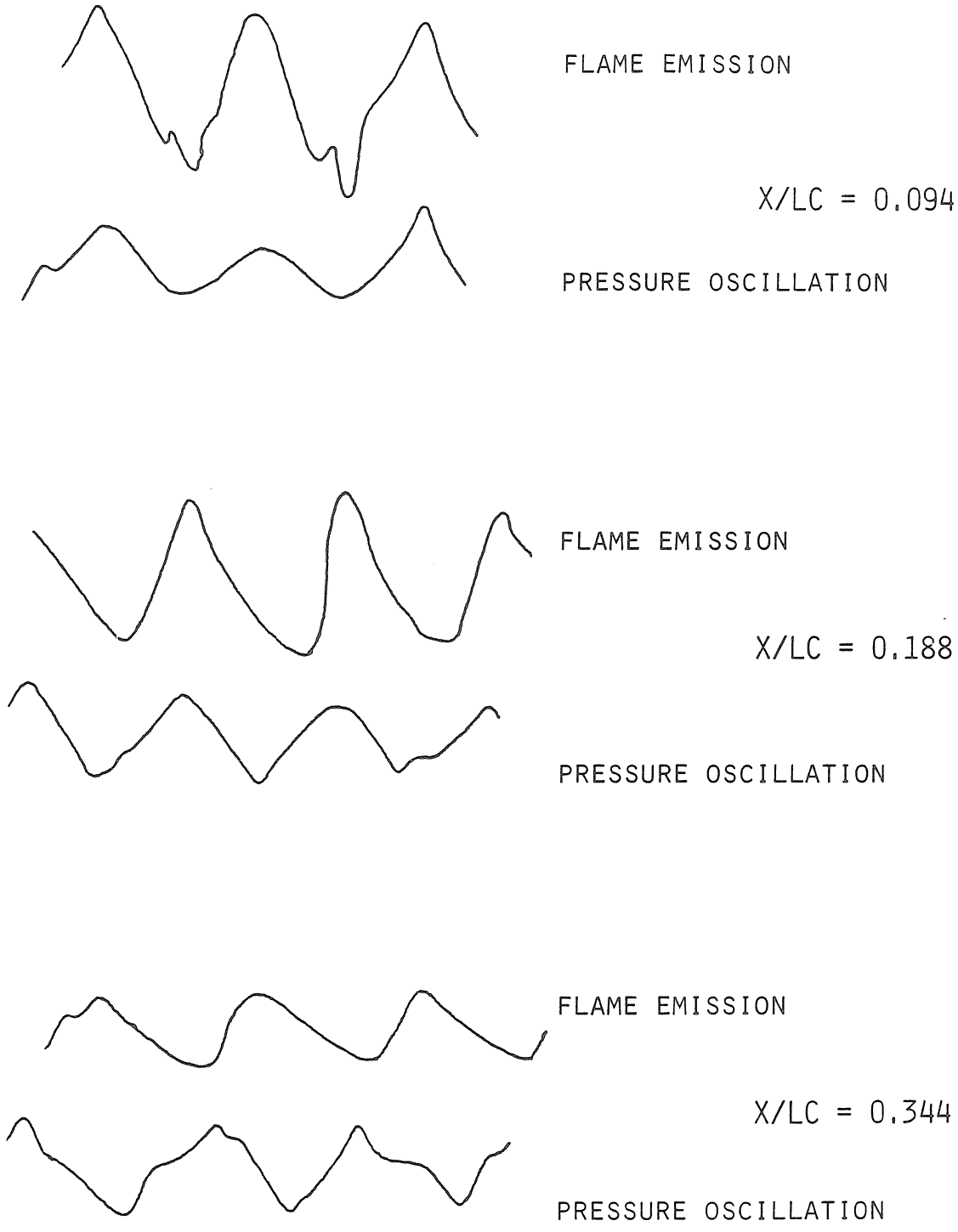

Figure 4.51 Simultaneous Pressure and Emission Measurements

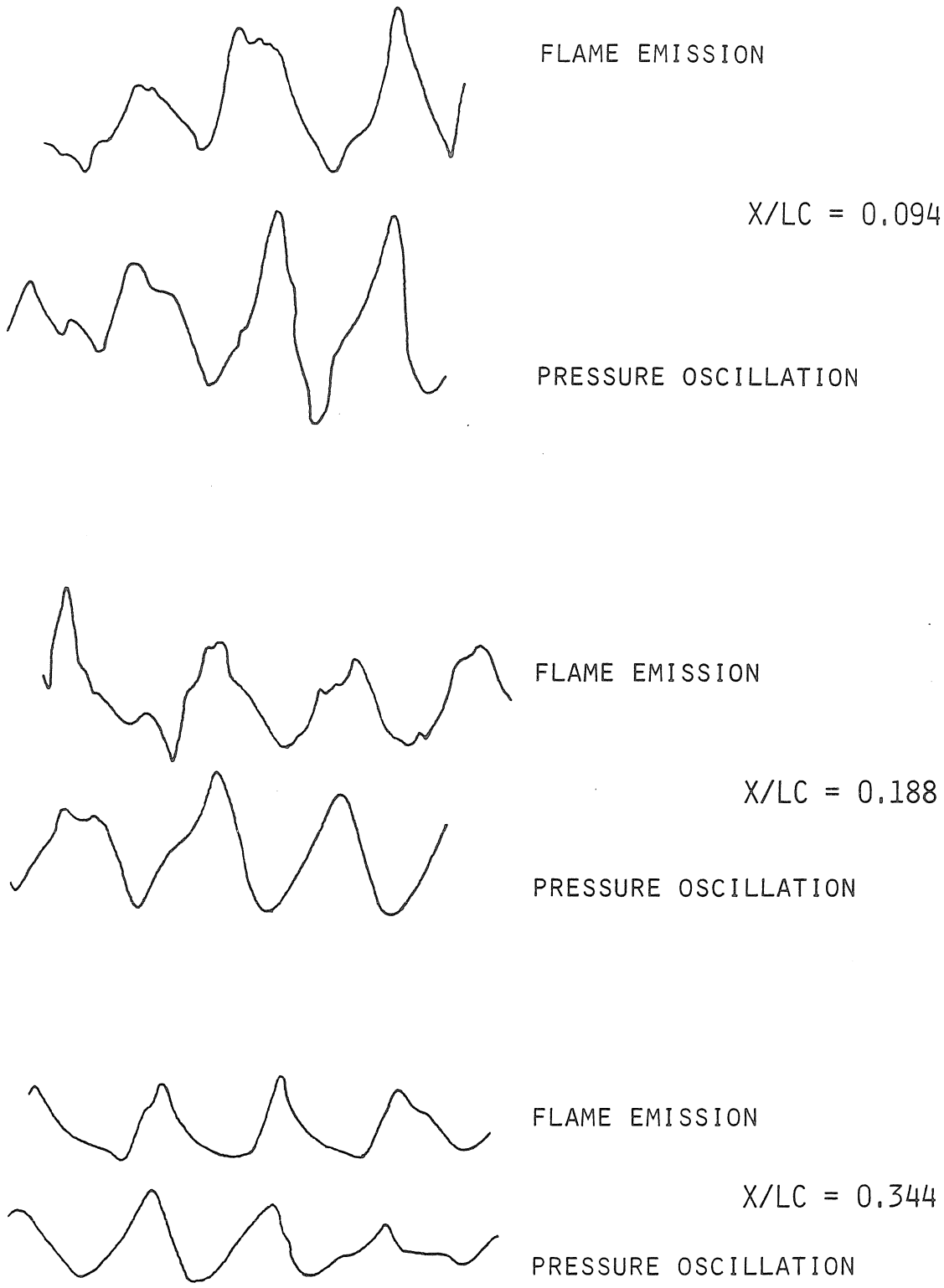

Figure 4.52 Simultaneous Pressure and Emission Measurements

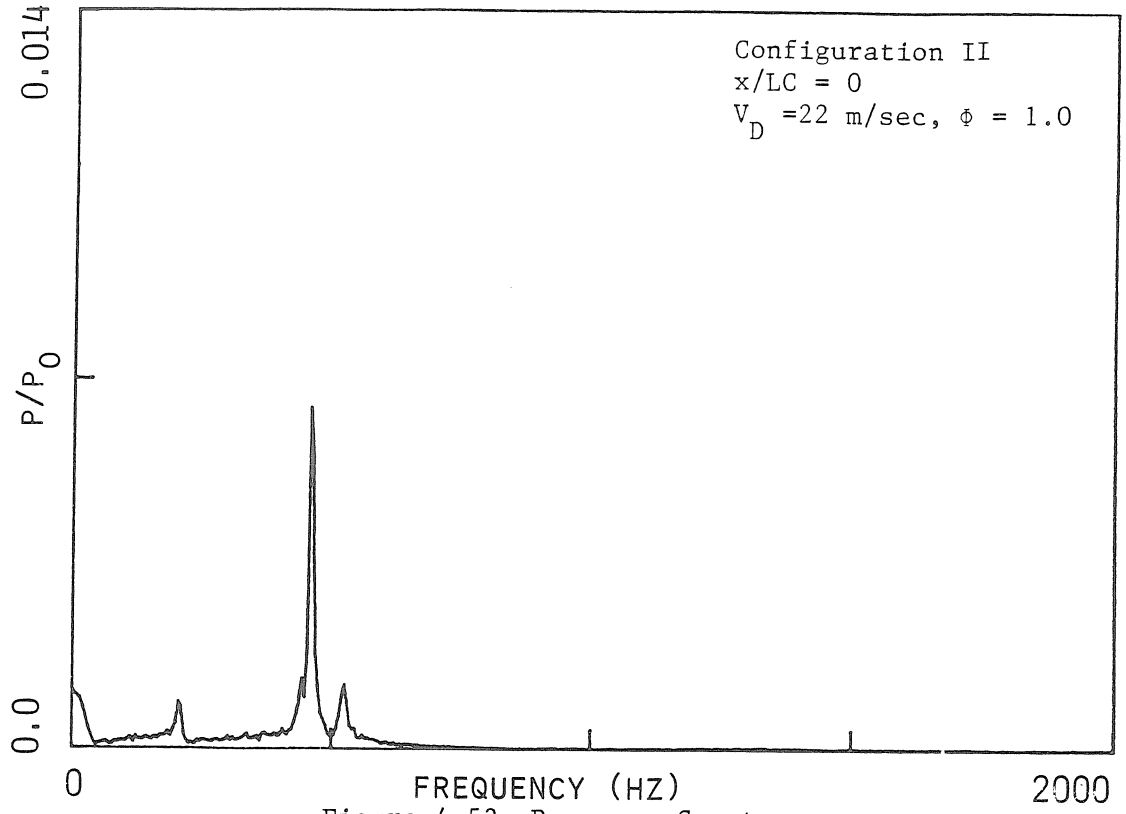

Figure 4.53 Pressure Spectrum

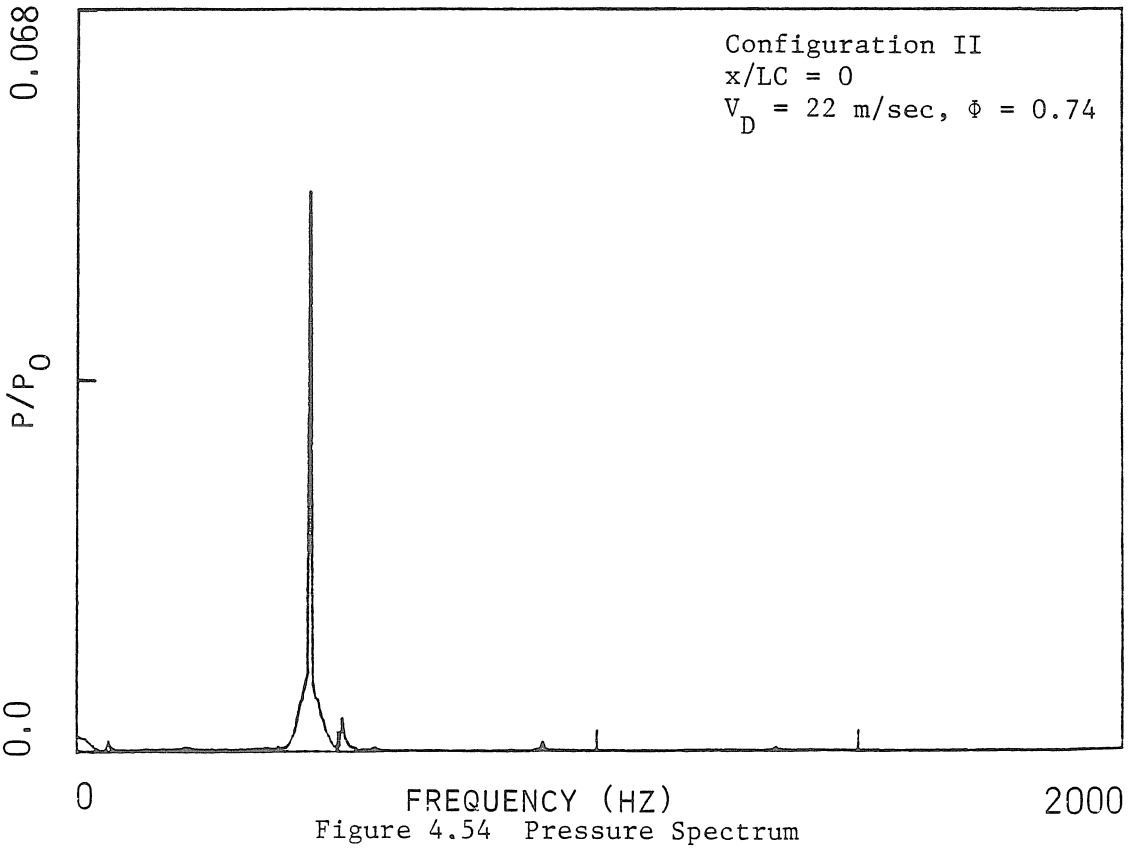

Figure 4.54 Pressure Spectrum

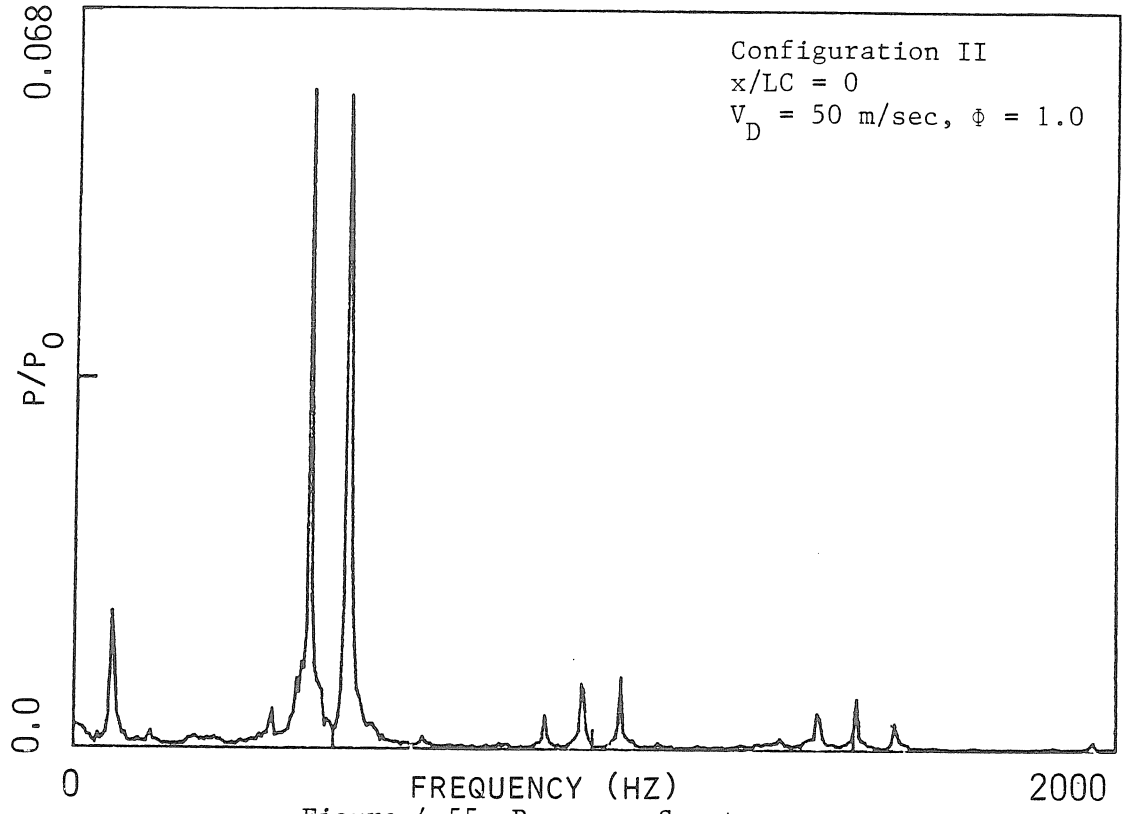

Figure 4.55 Pressure Spectrum

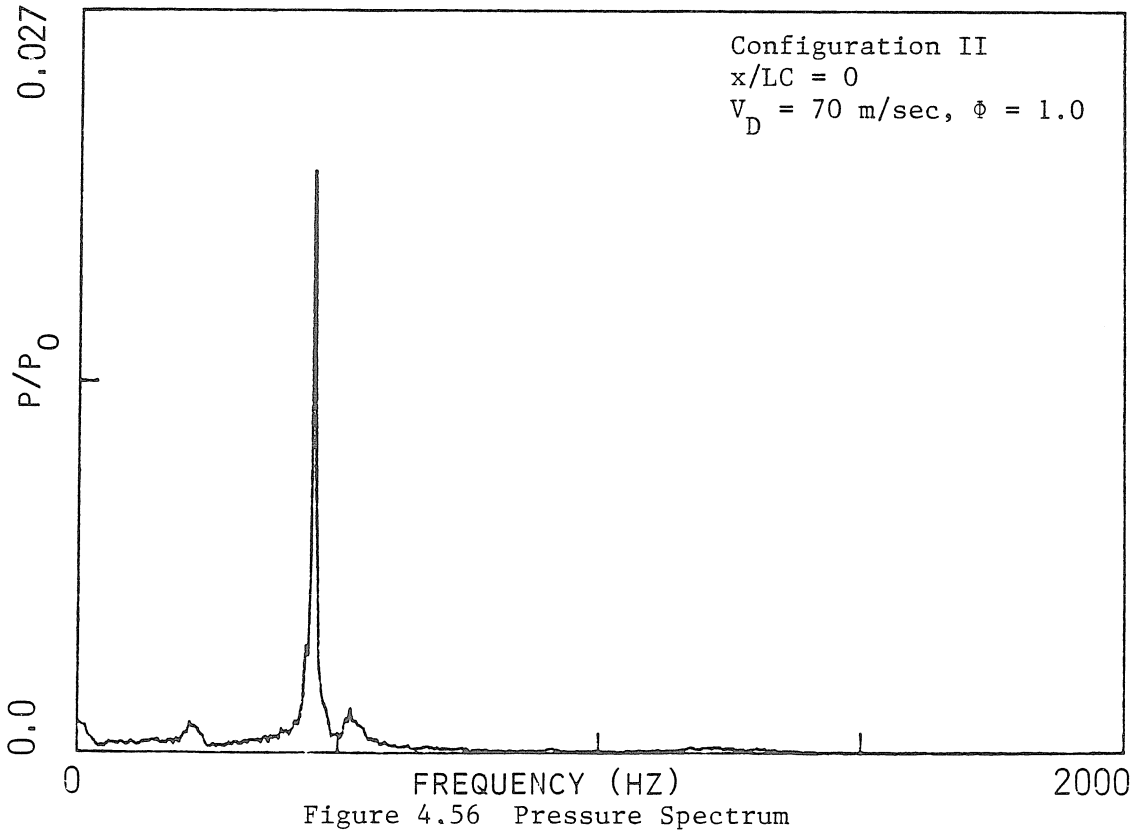

Figure 4.56 Pressure Spectrum

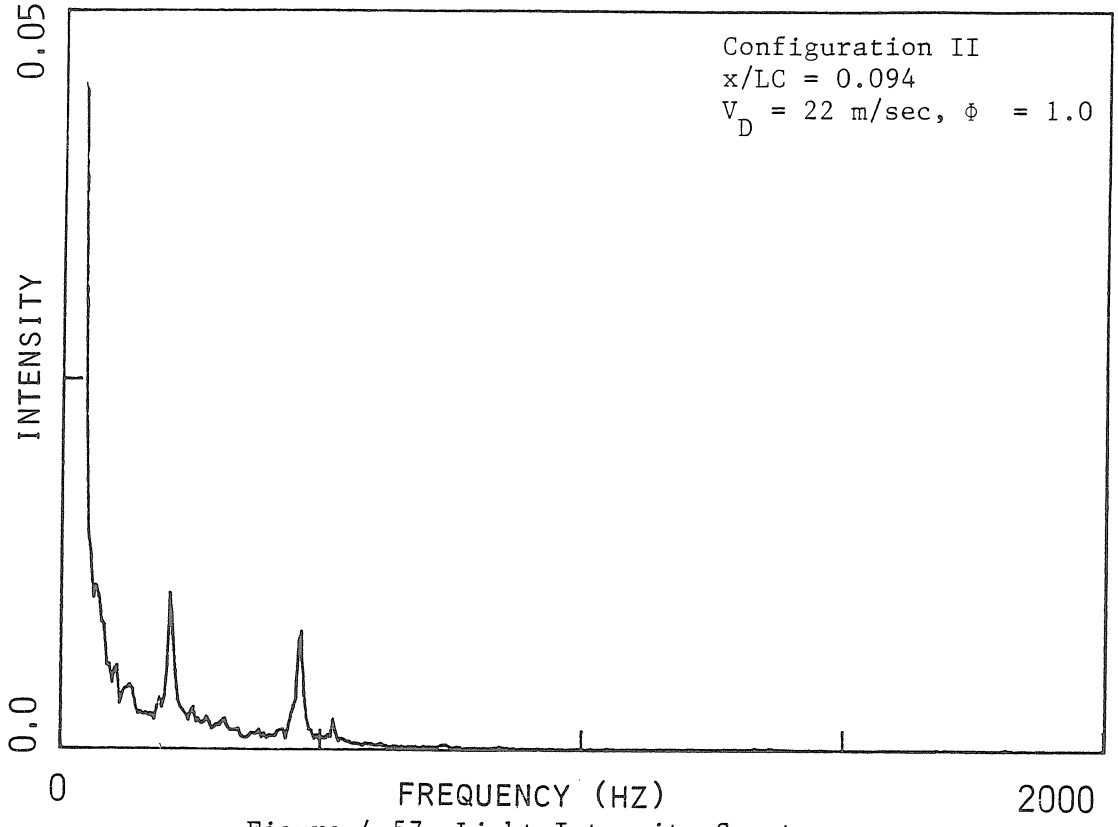

Figure 4.57 Light Intensity Spectrum

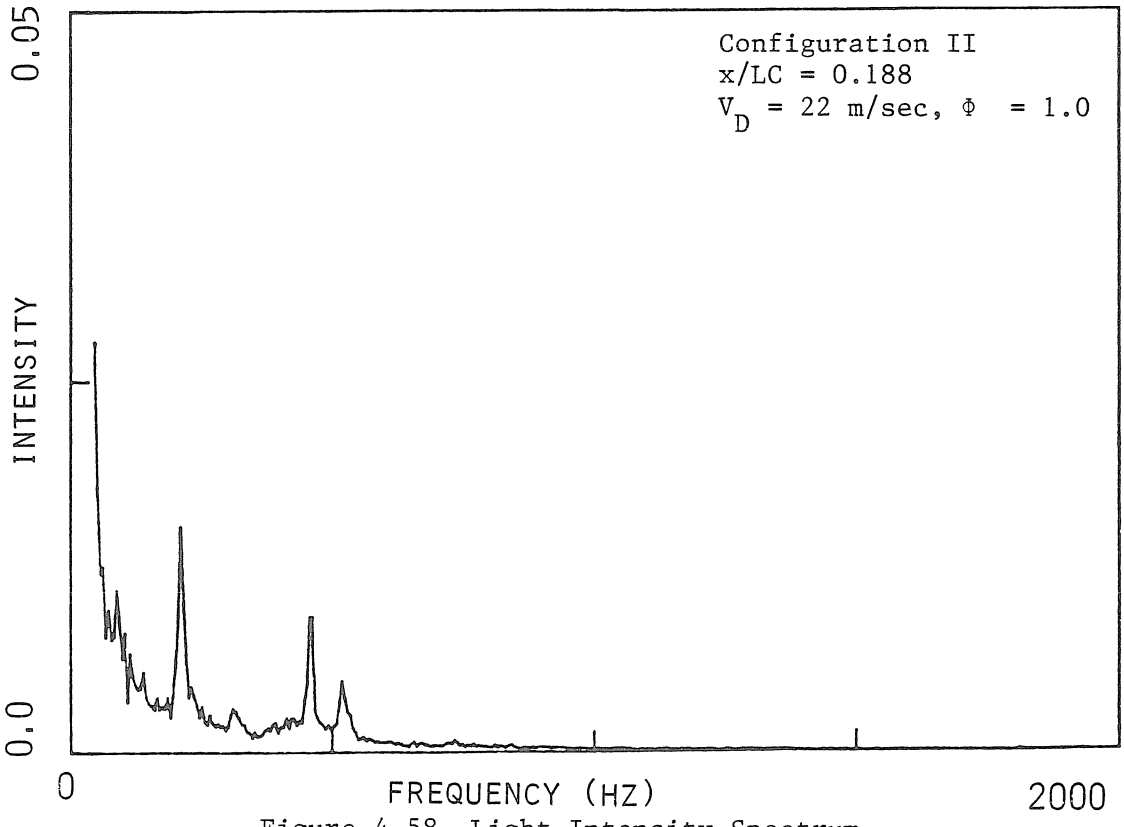

Figure 4.58 Light Intensity Spectrum

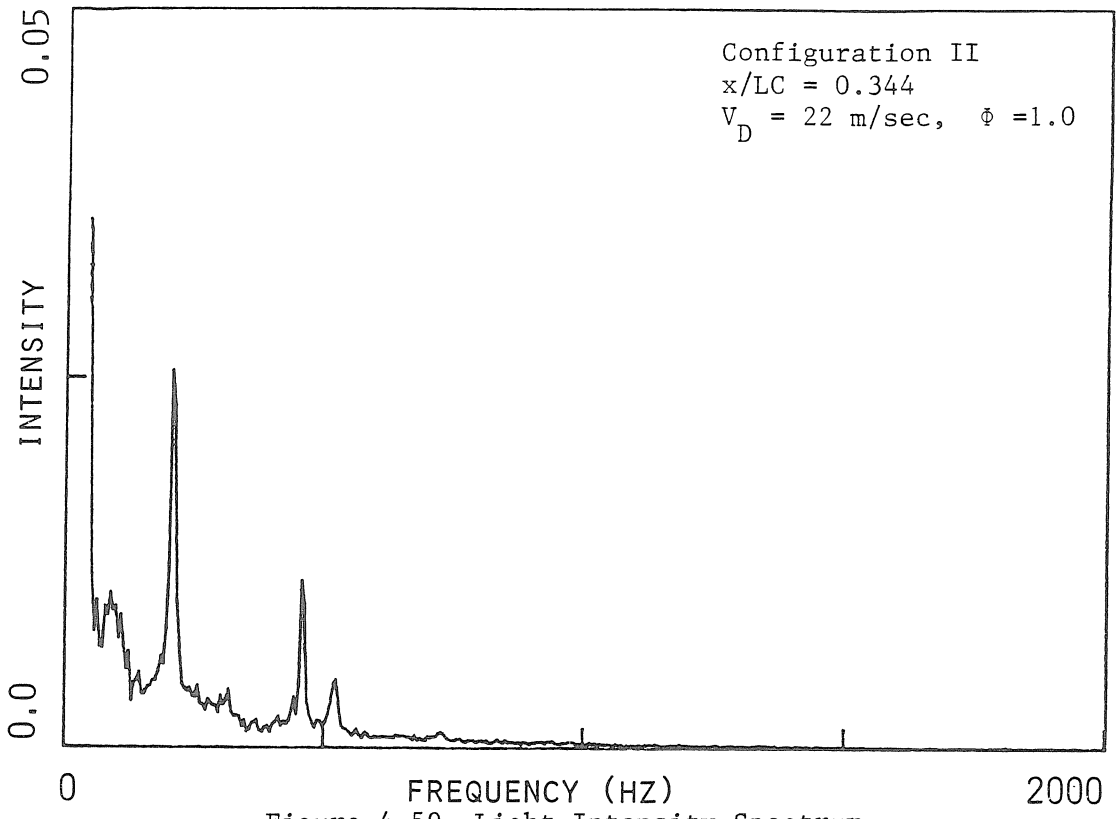

Figure 4.59 Light Intensity Spectrum

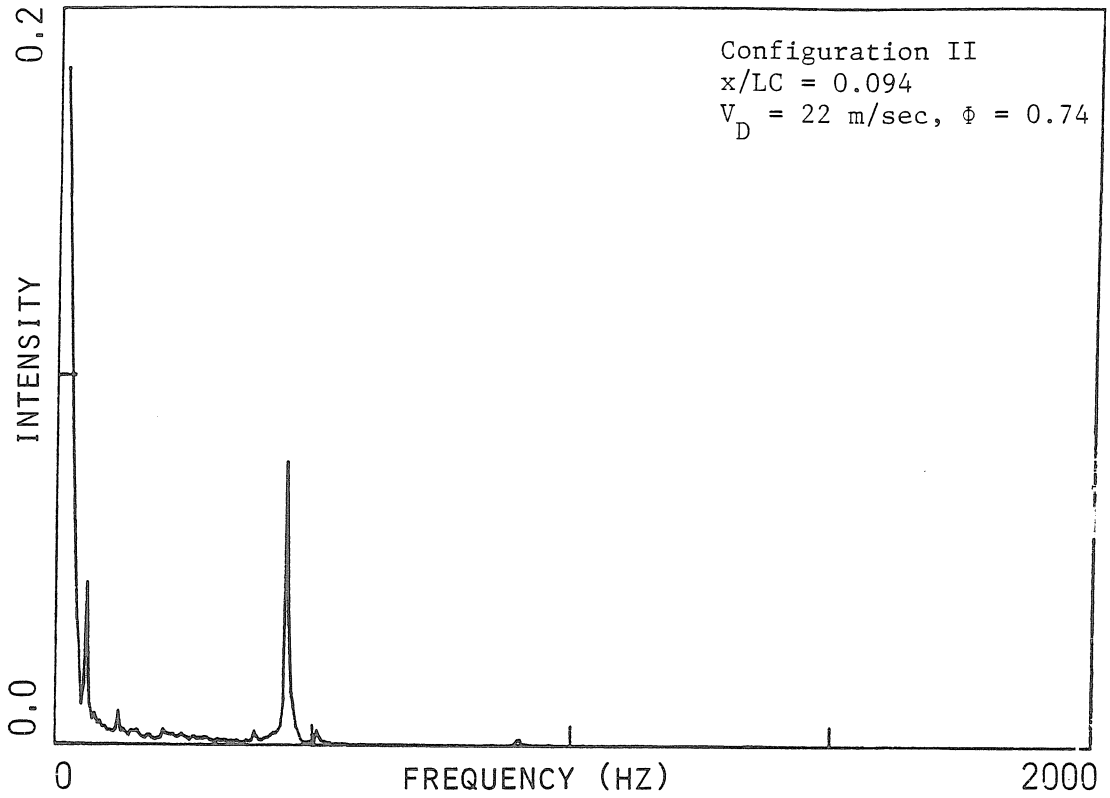

Figure 4.60 Light Intensity Spectrum

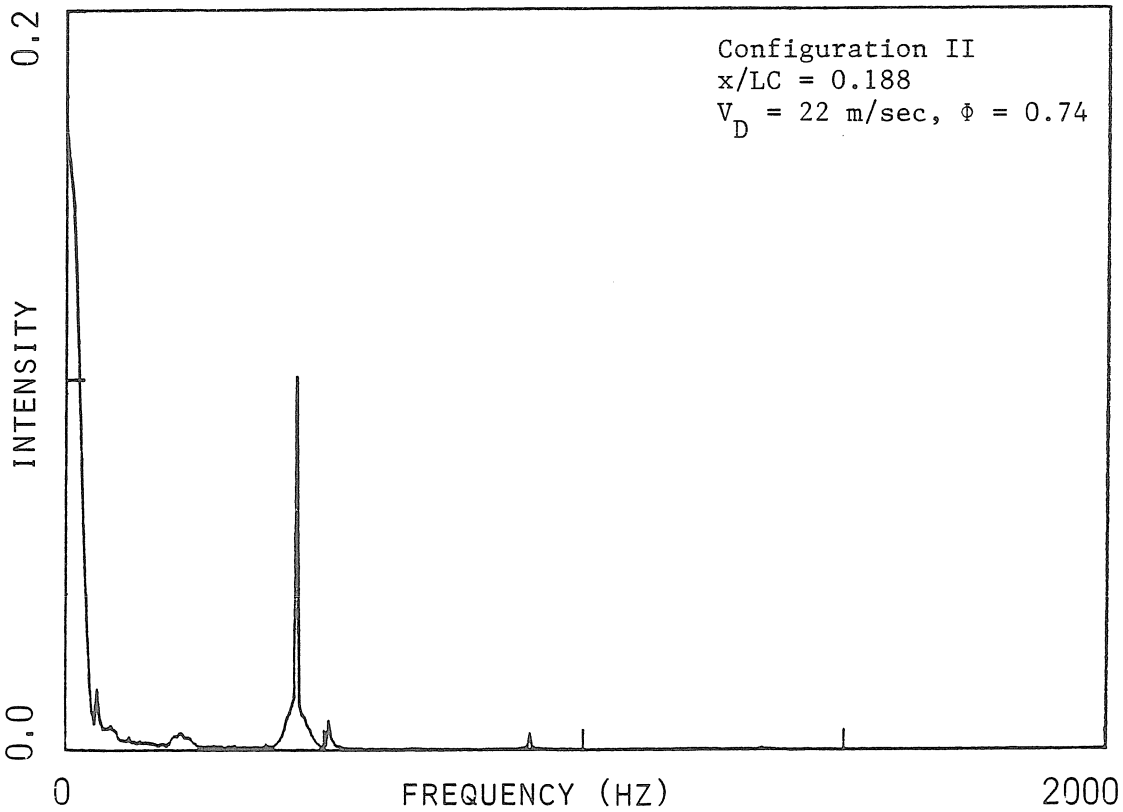

Figure 4.61 Light Intensity Spectrum

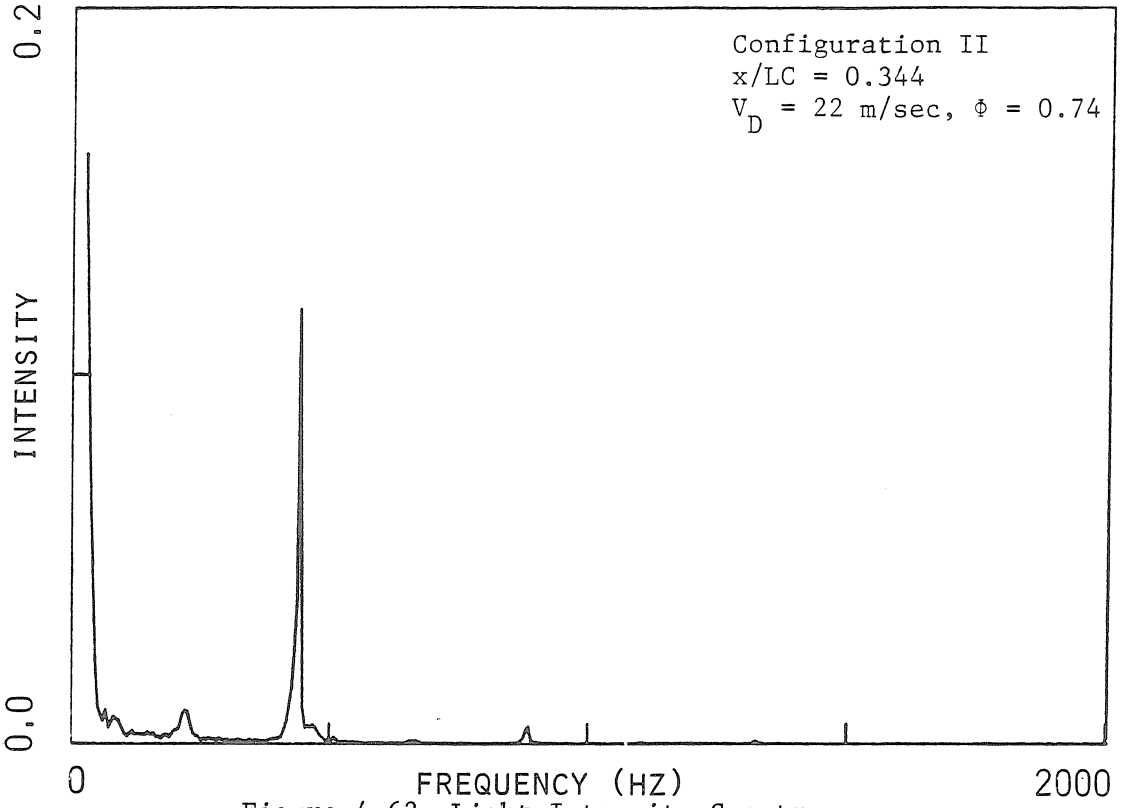

Figure 4.62 Light Intensity Spectrum

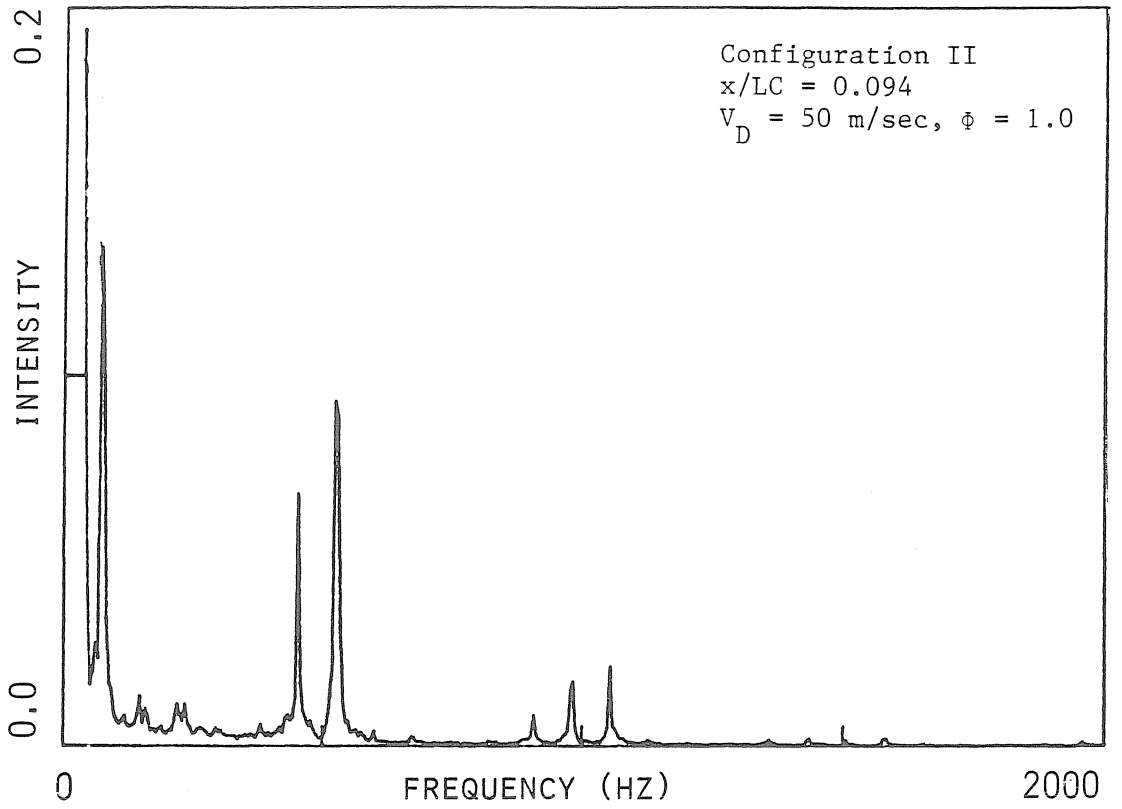

Figure 4.63 Light Intensity Spectrum

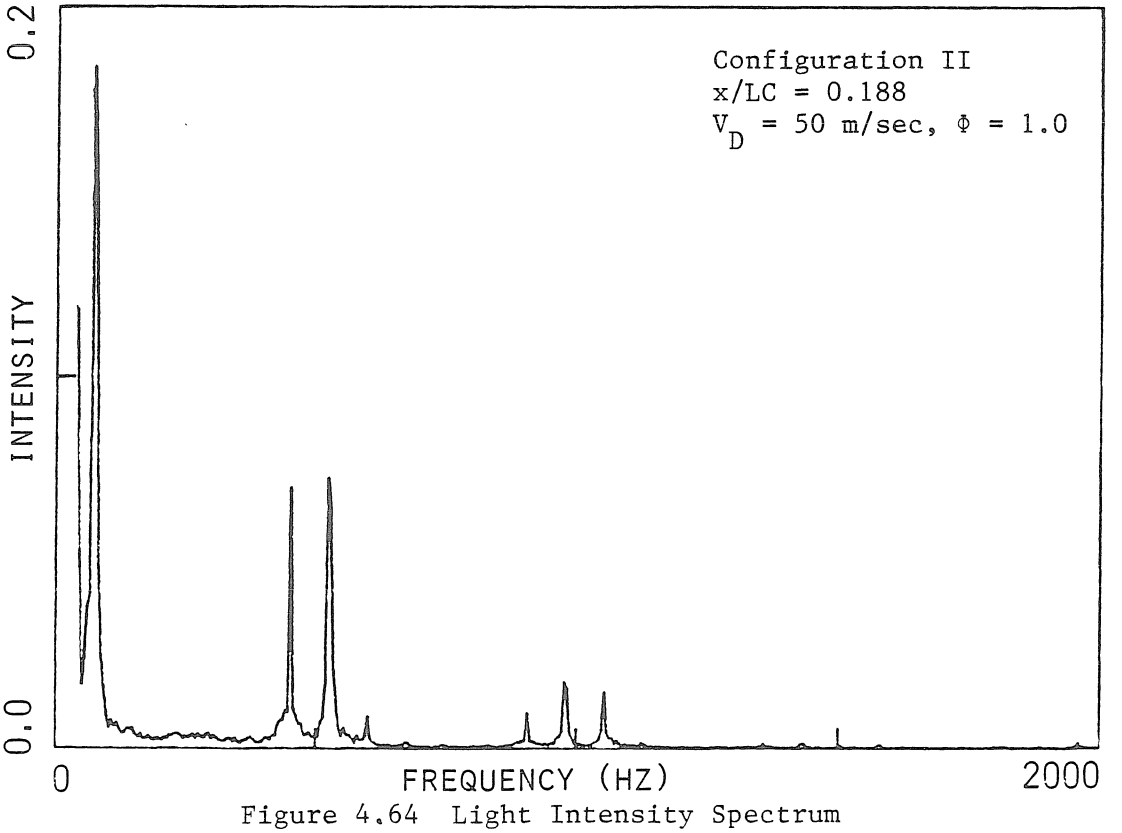

Figure 4.64 Light Intensity Spectrum

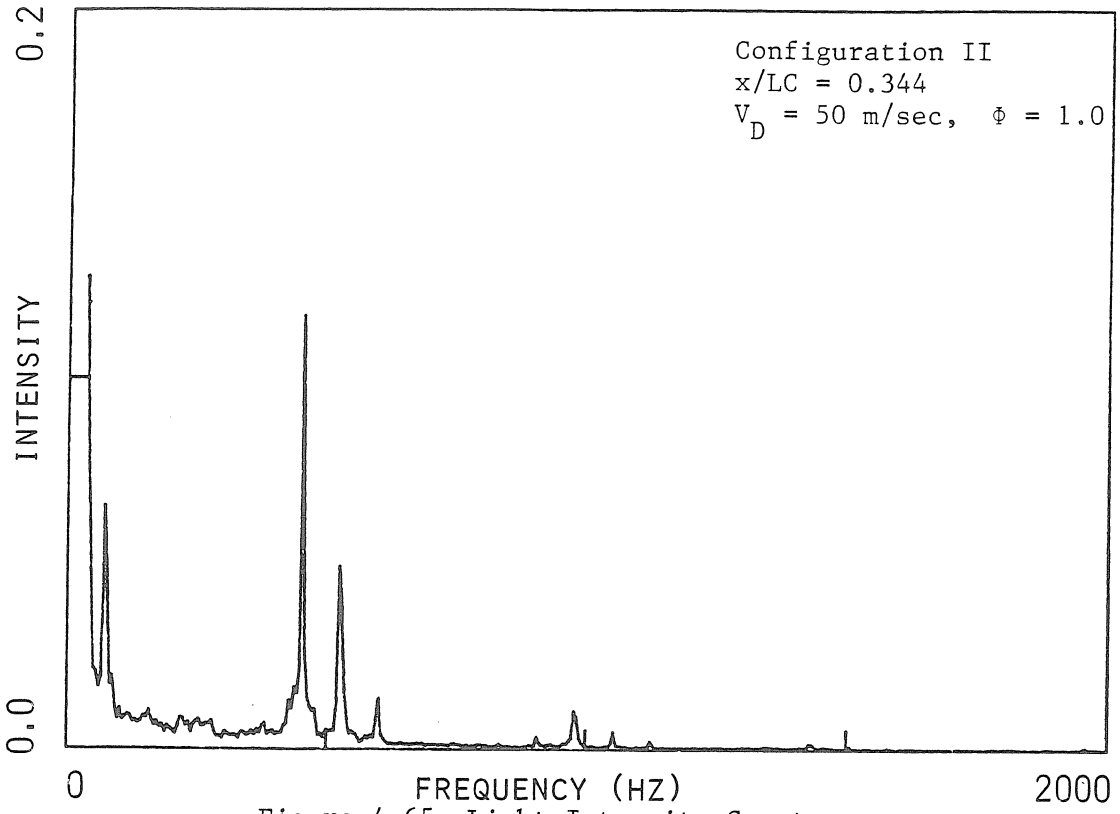

Figure 4.65 Light Intensity Spectrum

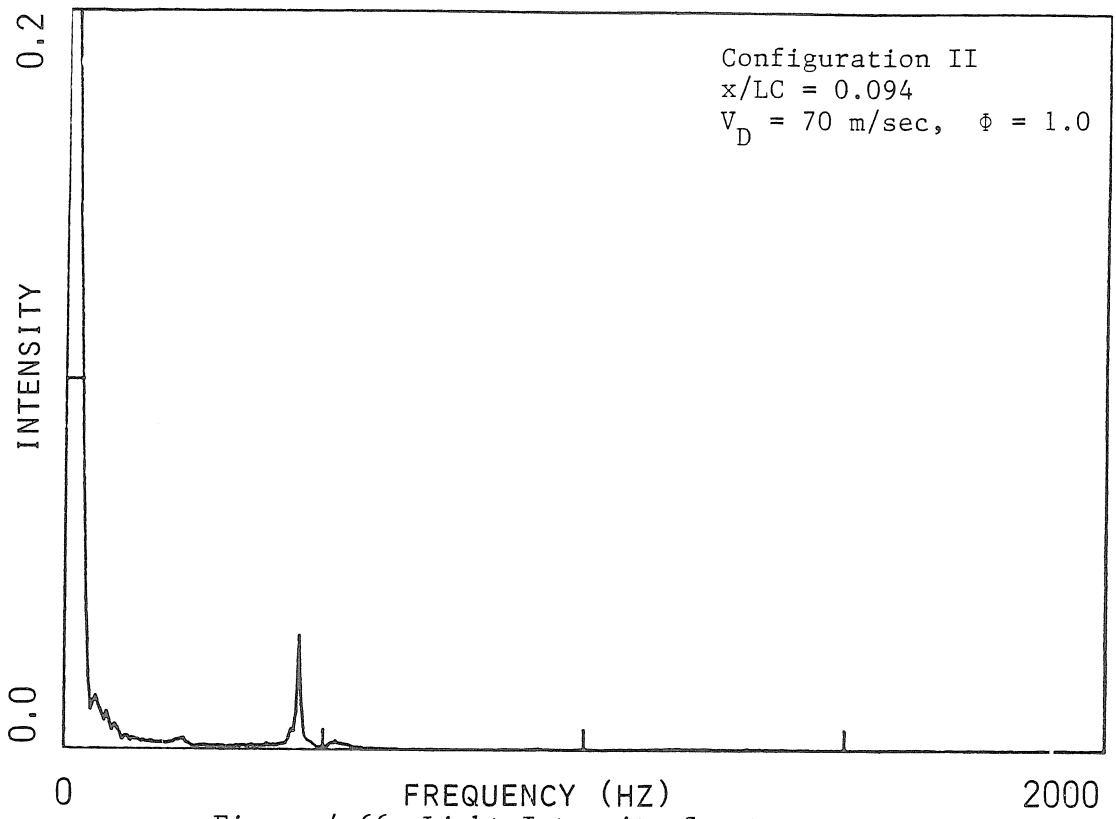

Figure 4.66 Light Intensity Spectrum

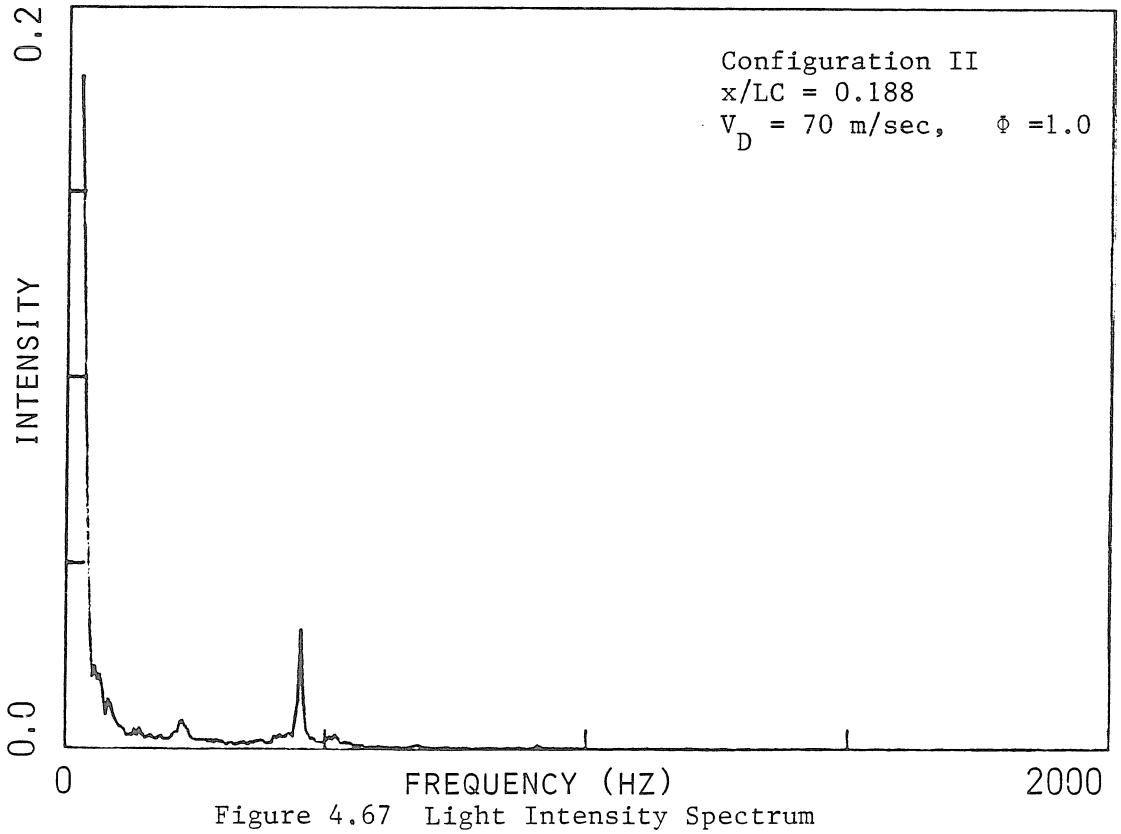

Figure 4.67 Light Intensity Spectrum

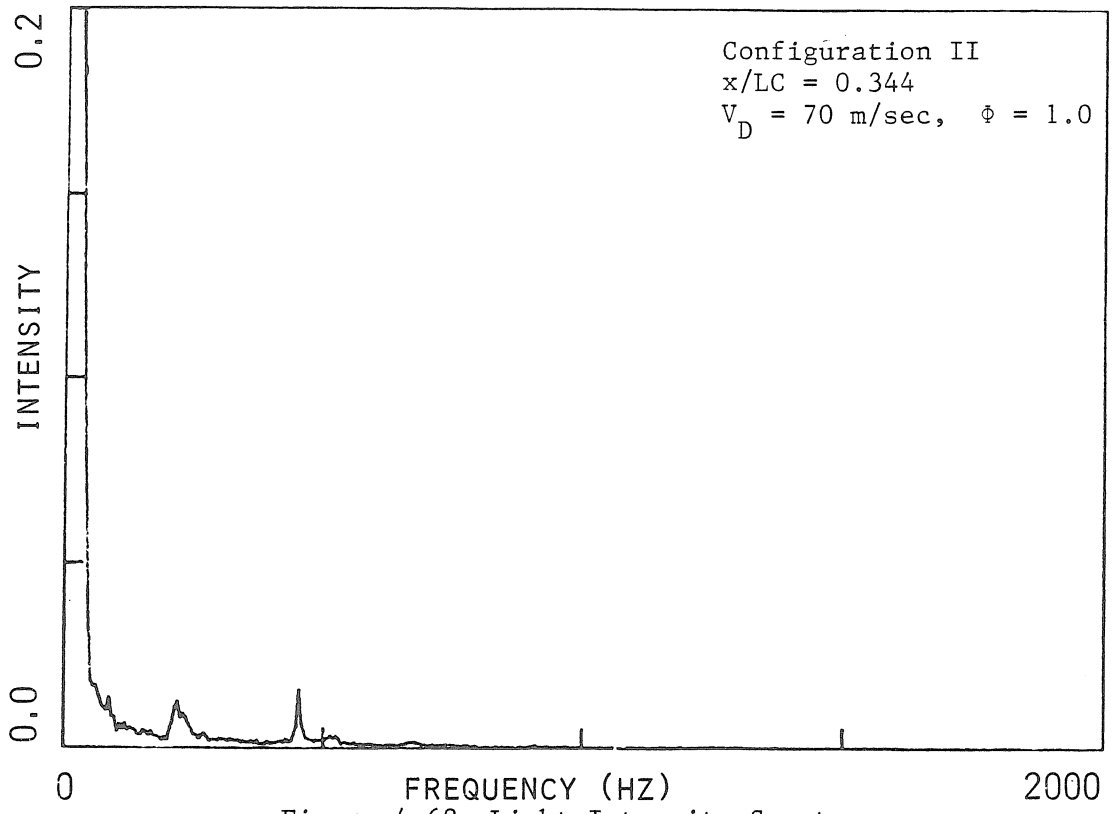

Figure 4.68 Light Intensity Spectrum

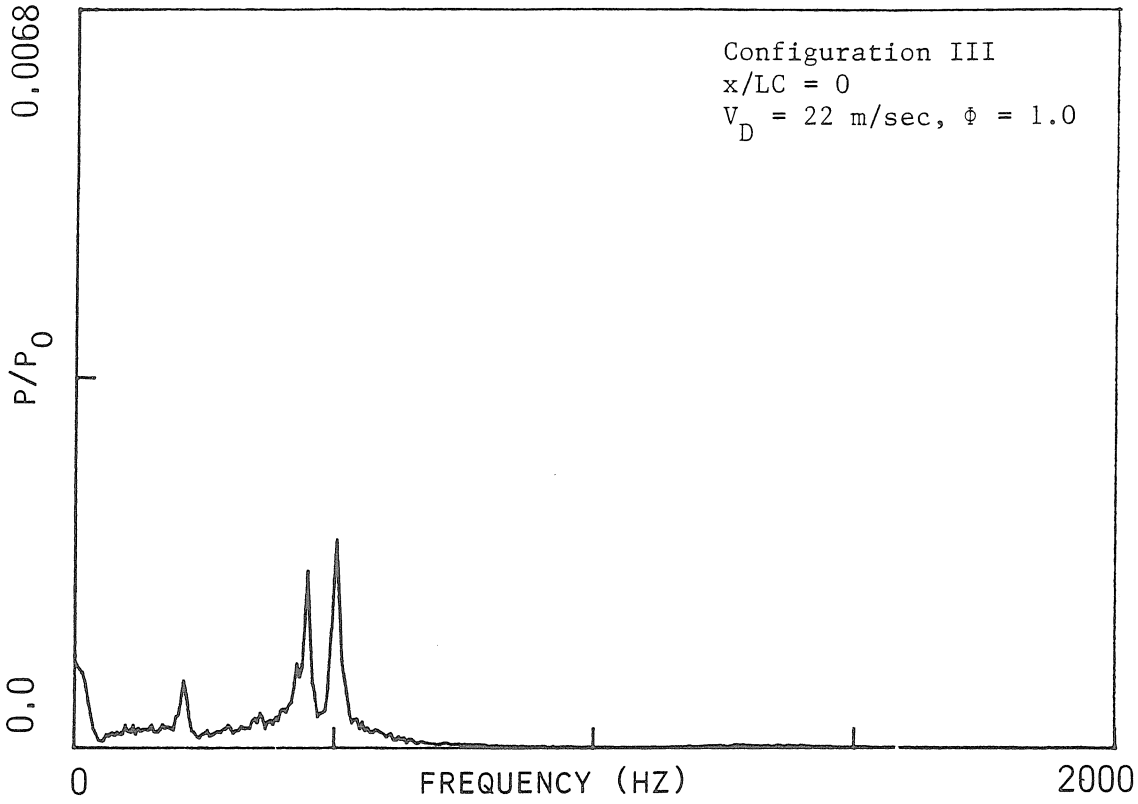

Figure 4.69 Pressure Spectrum

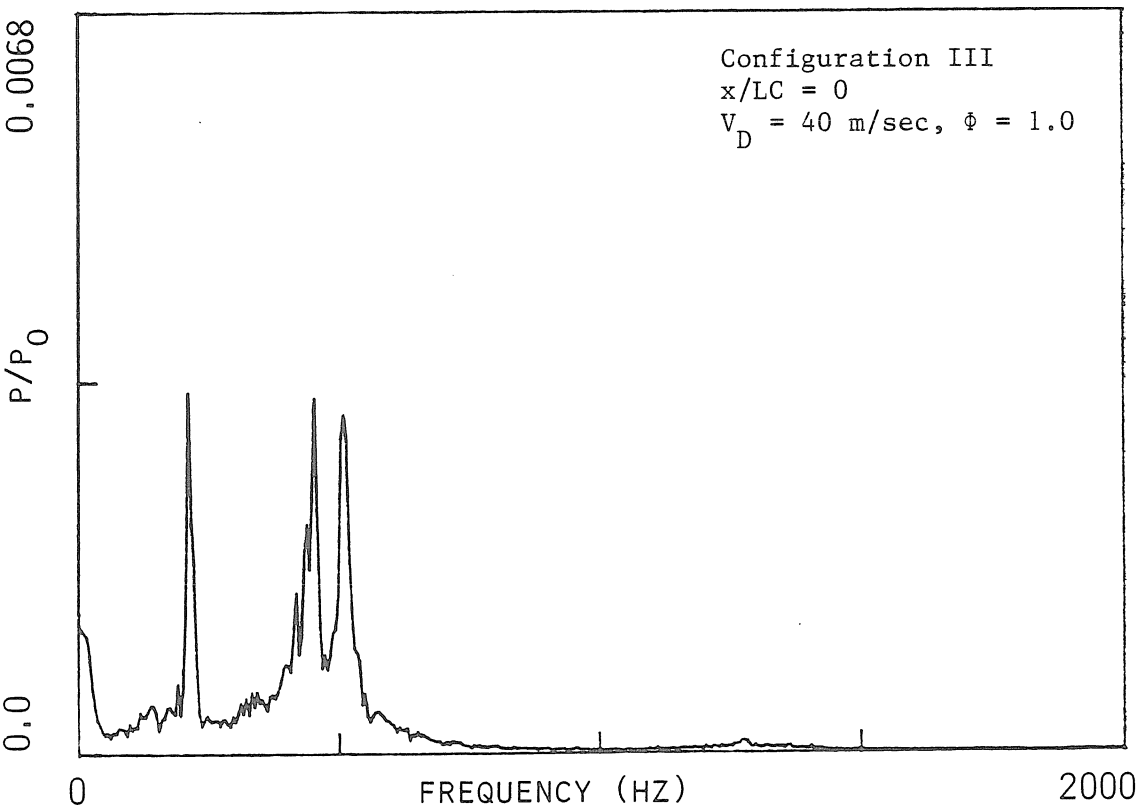

Figure 4.70 Pressure Spectrum

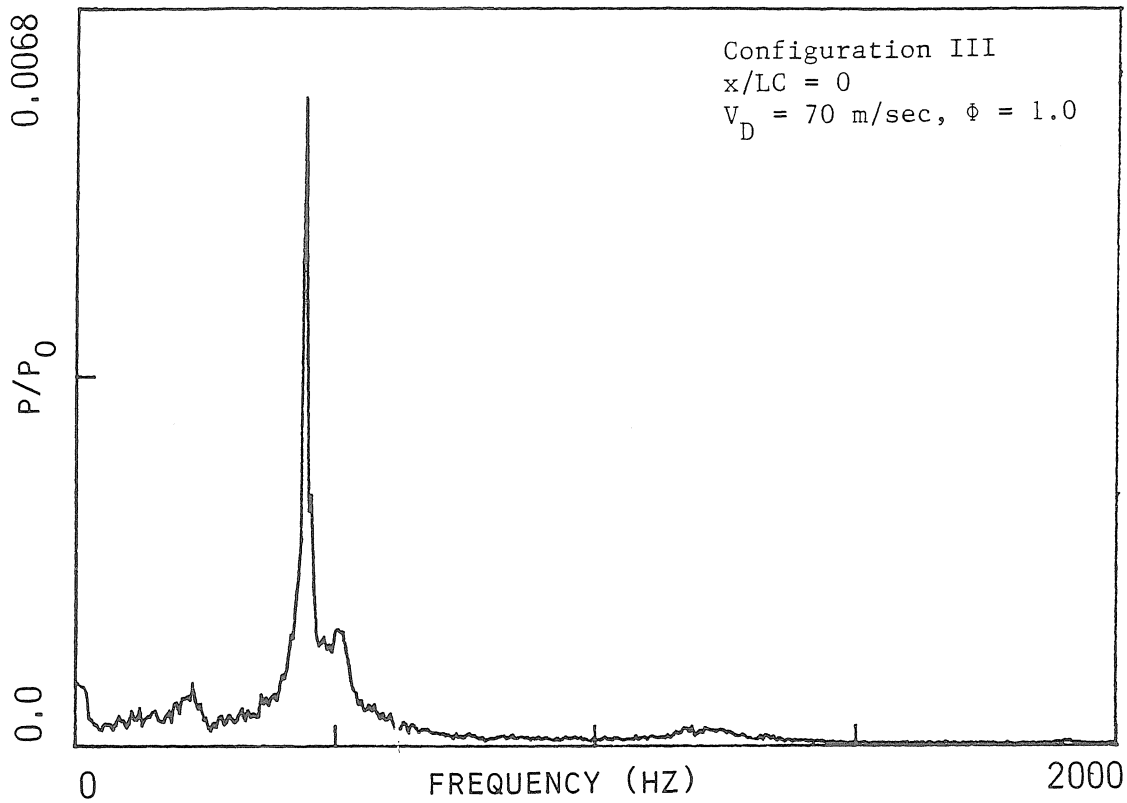

Figure 4.71 Pressure Spectrum

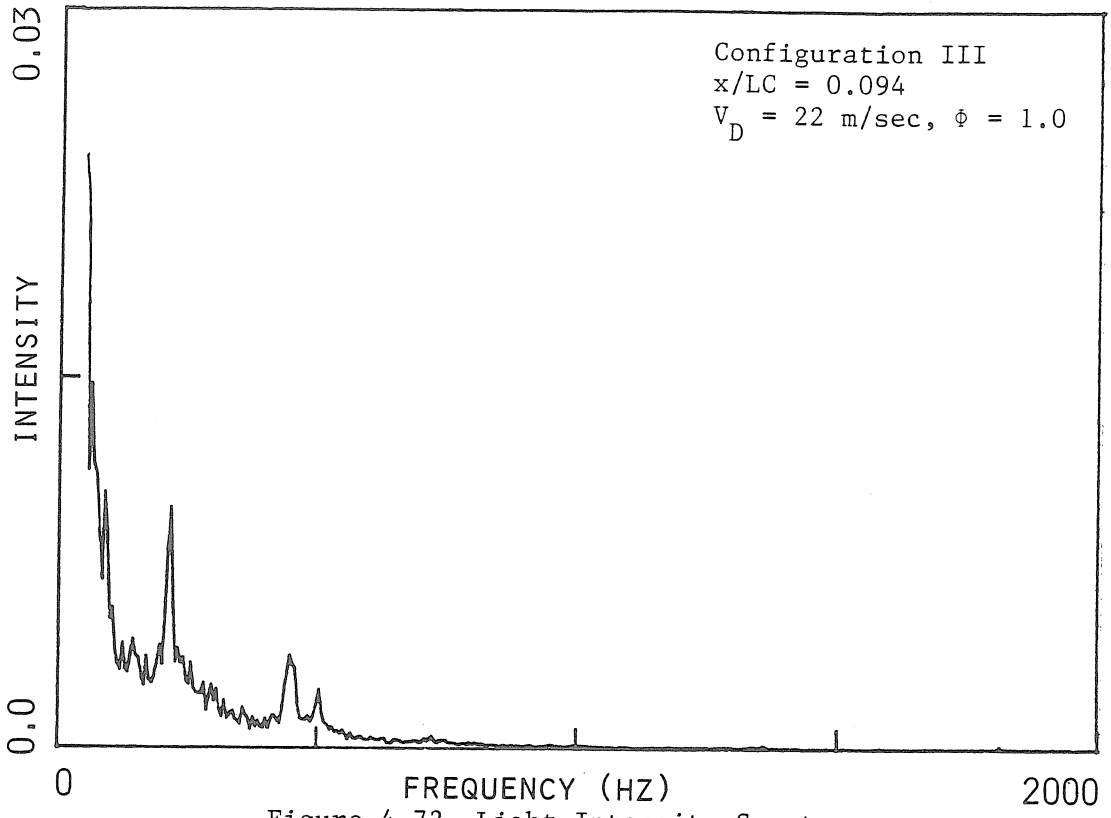

Figure 4.72 Light Intensity Spectrum

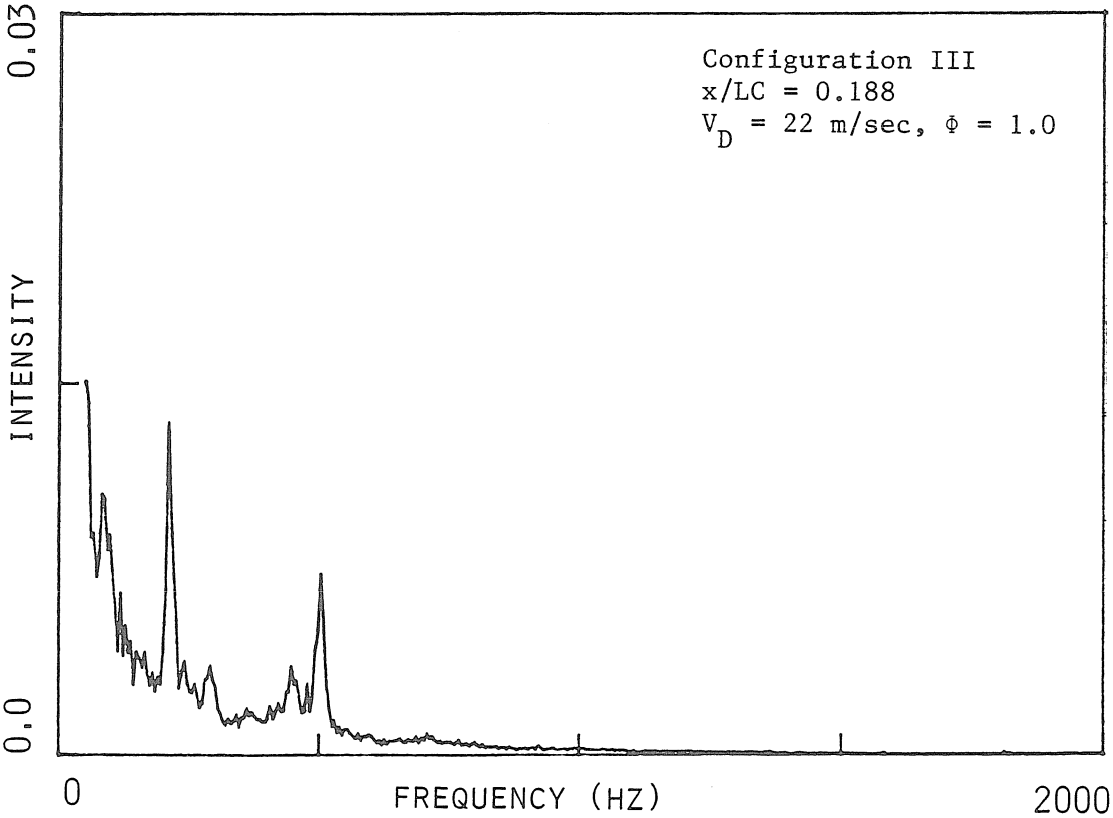

Figure 4.73 Light Intensity Spectrum

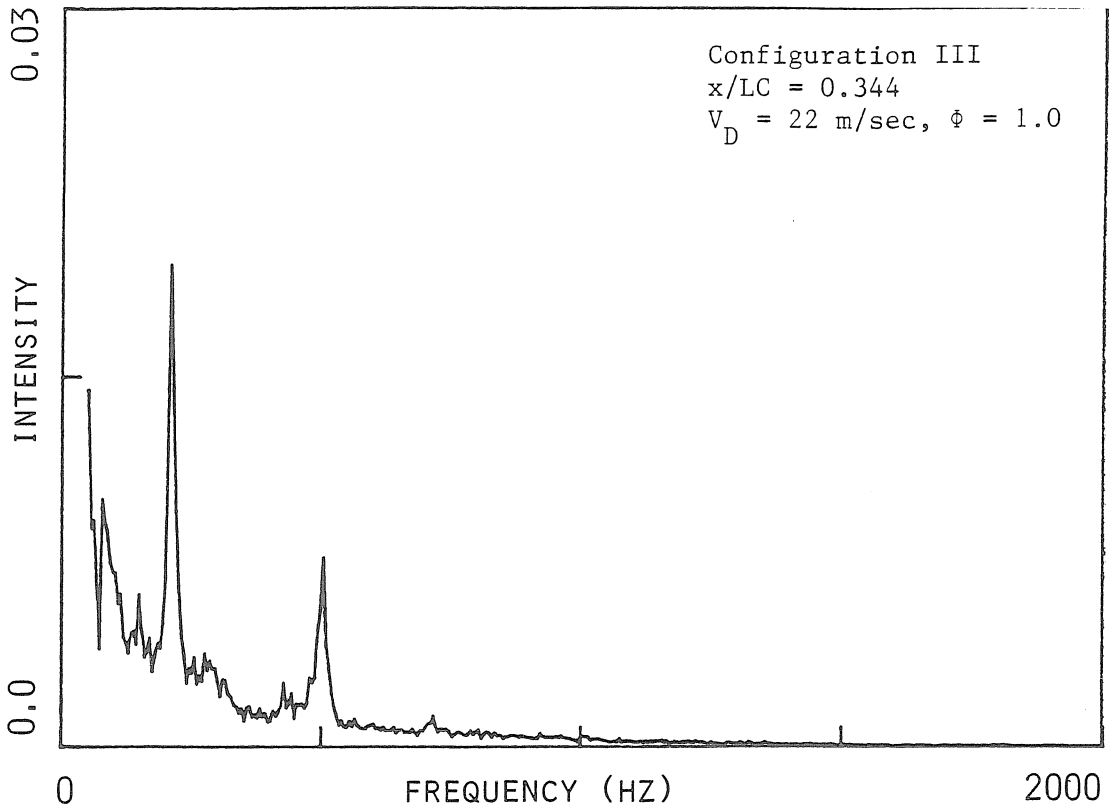

Figure 4.74 Light Intensity Spectrum

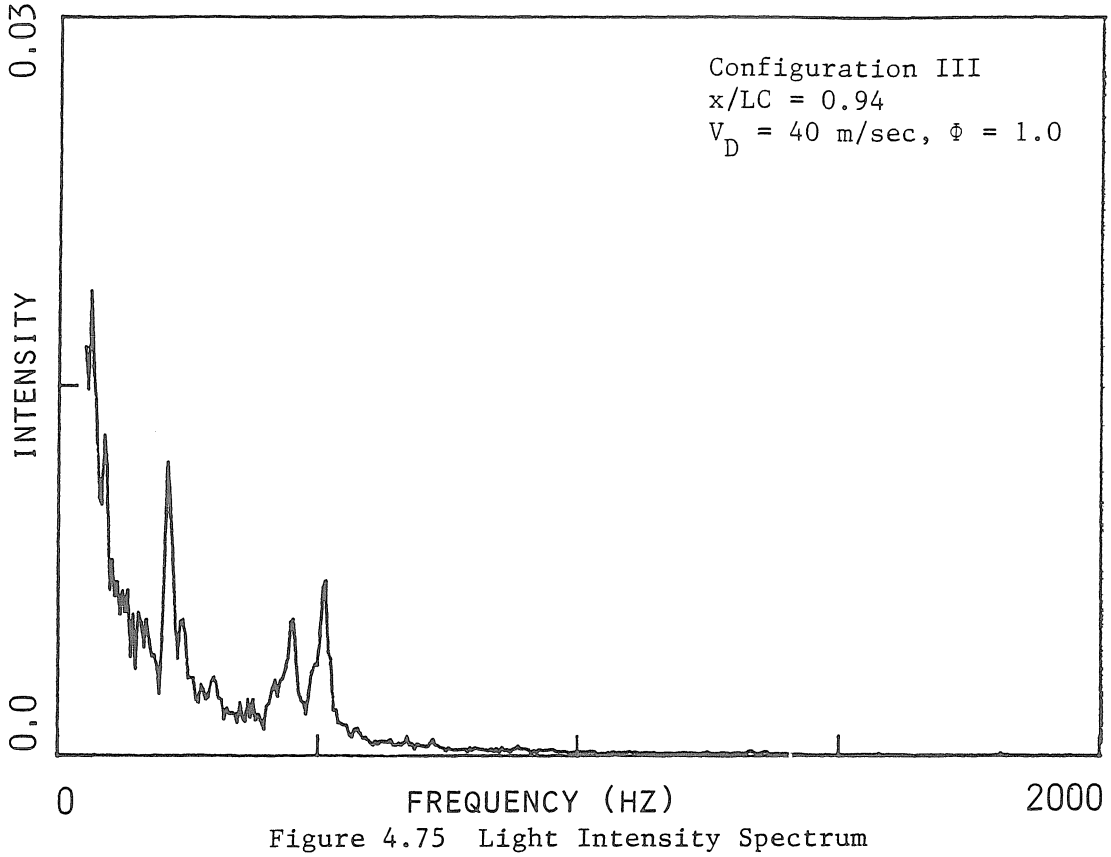

Figure 4.75 Light Intensity Spectrum

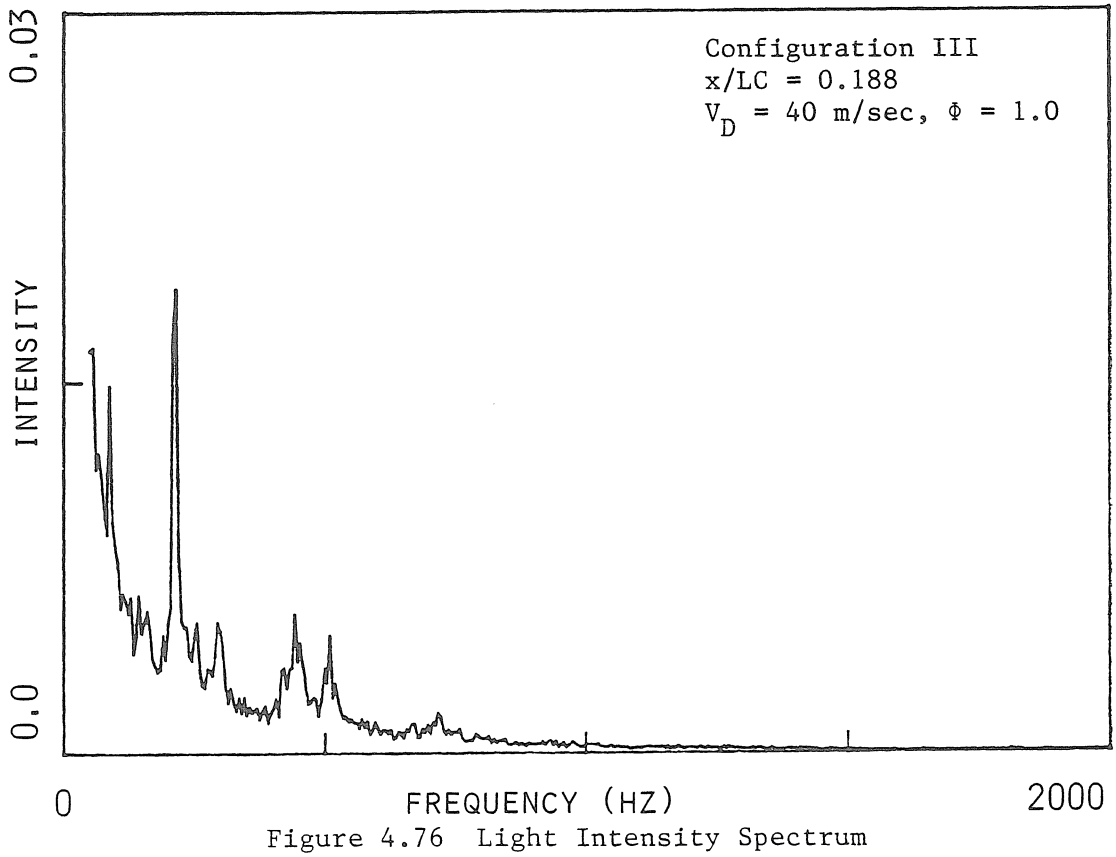

Figure 4.76 Light Intensity Spectrum

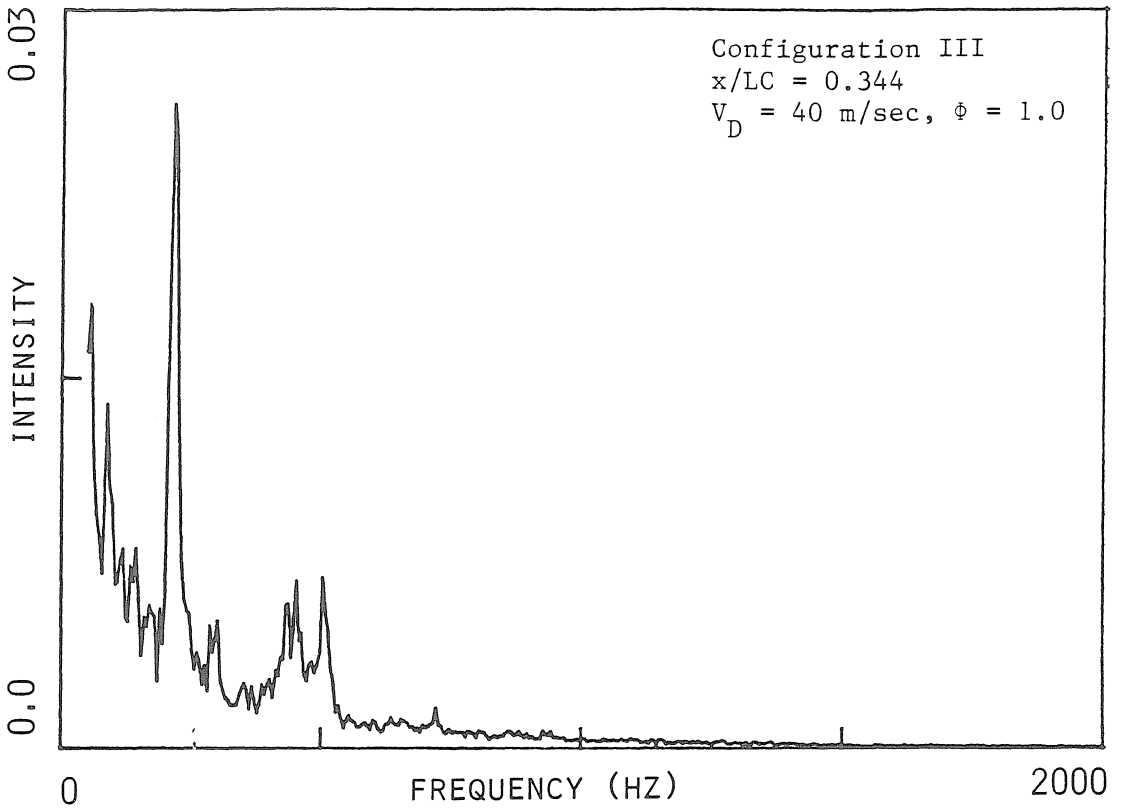

Figure 4.77 Light Intensity Spectrum

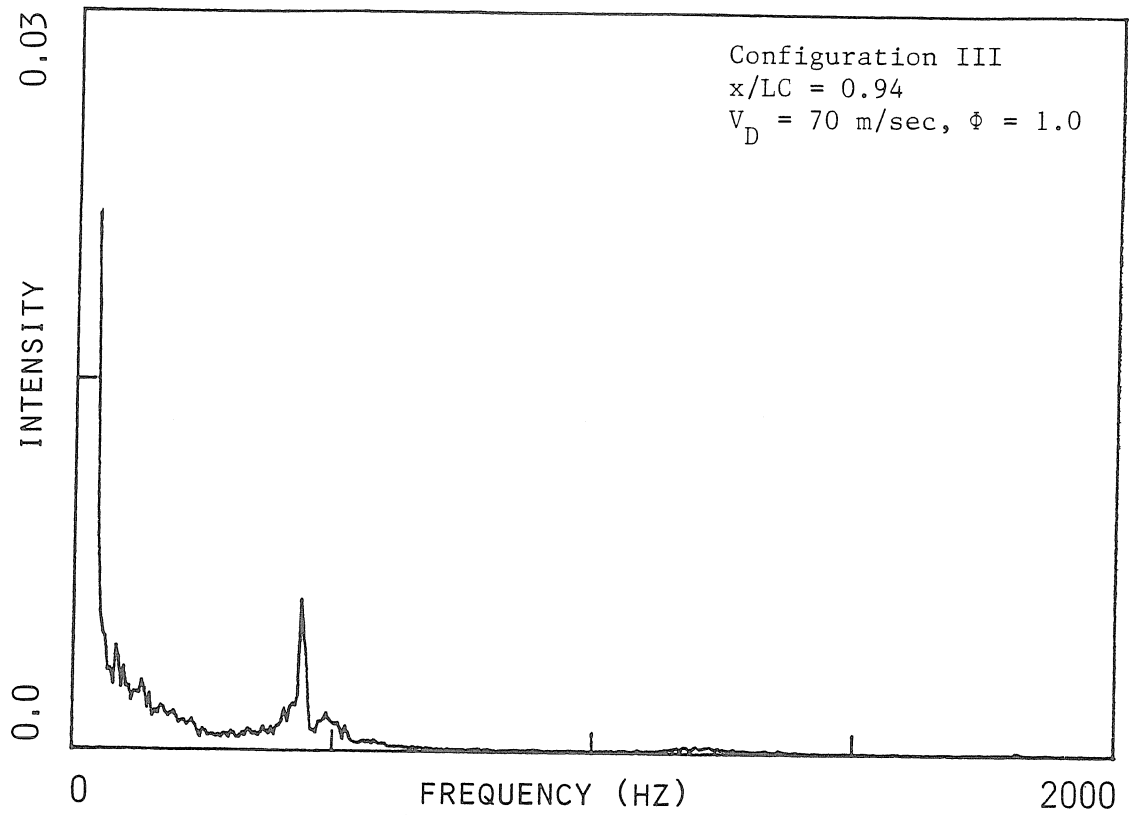

Figure 4.78 Light Intensity Spectrum

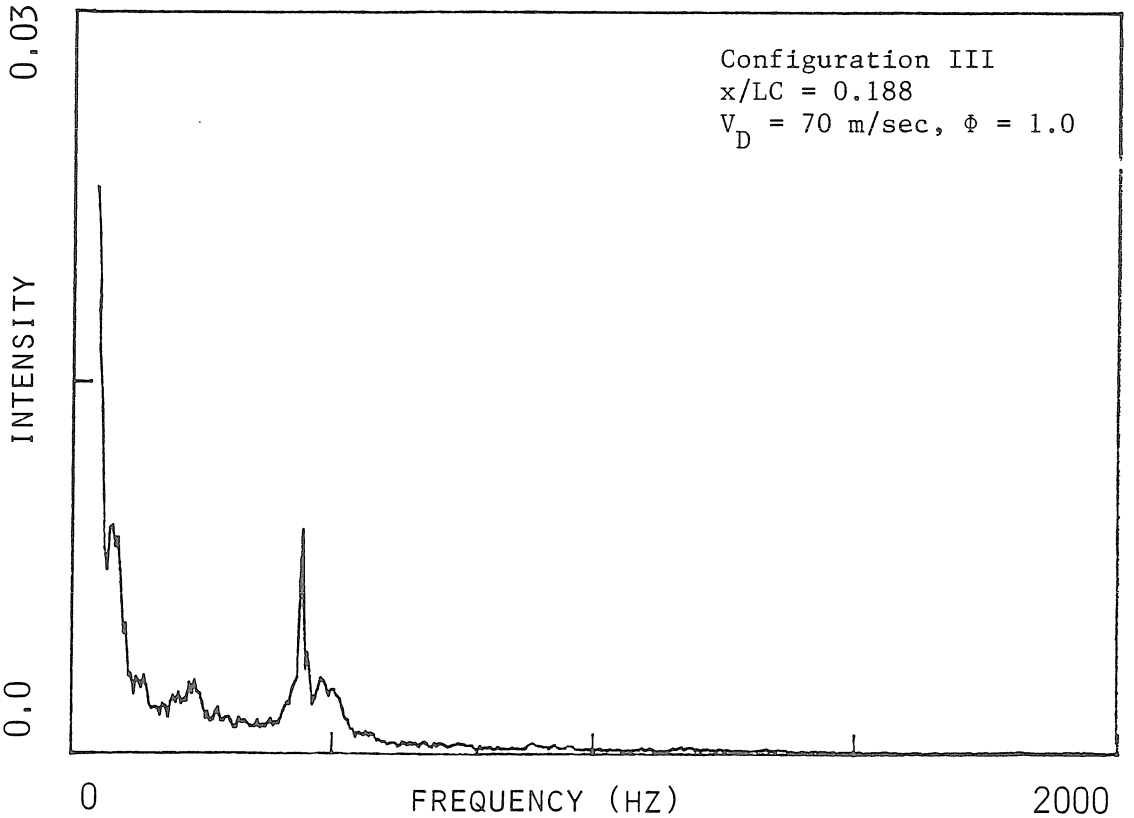

Figure 4.79 Light Intensity Spectrum

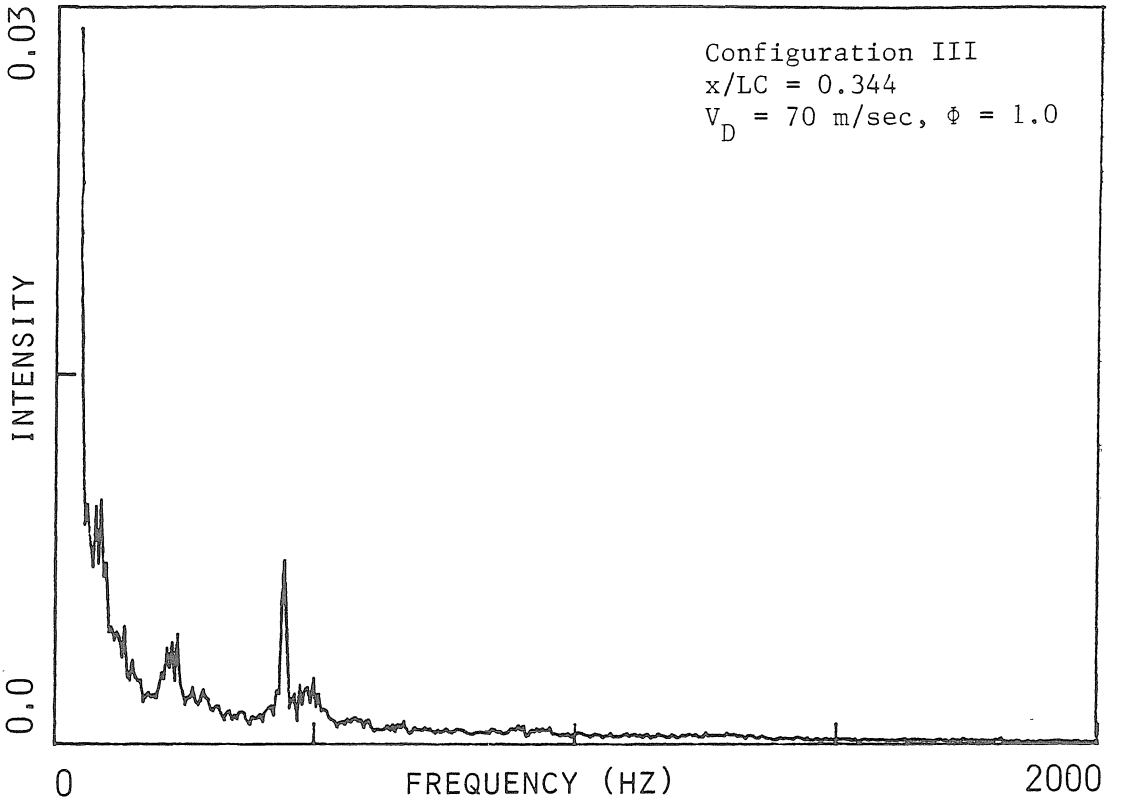

Figure 4.80 Light Intensity Spectrum

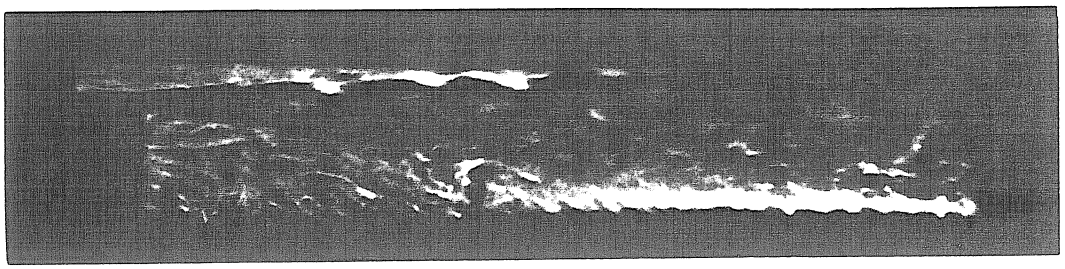

STABLE FLOW

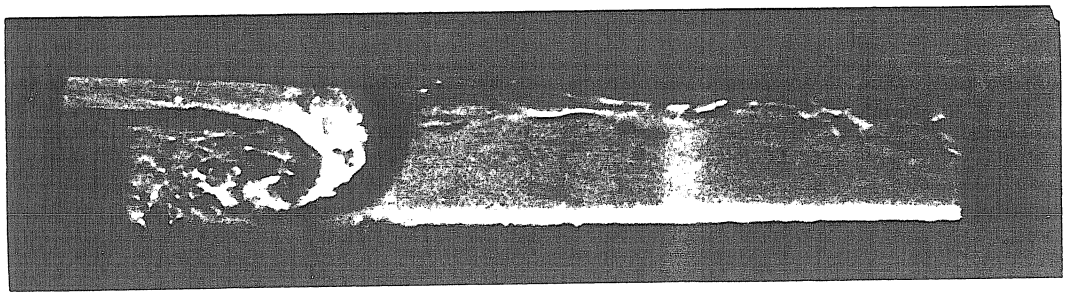

UNSTABLE FLOW

Figure 4.81 Flow Field Classifications

VORTEX EVOLUTION

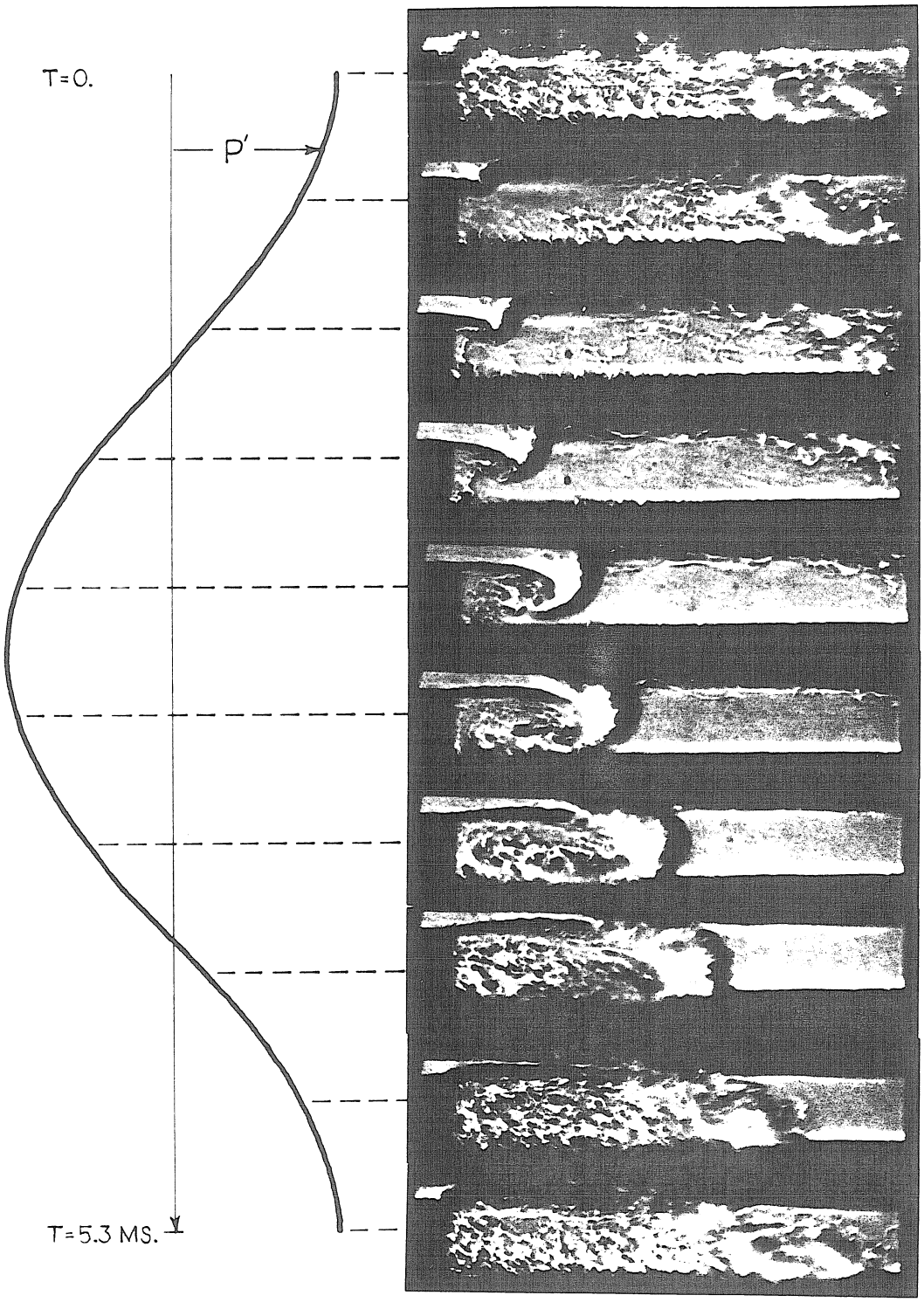

Figure 4.82 Vortex Formation at $V_D = 22$ m/sec, $\Phi = 1.0$

VORTEX EVOLUTION

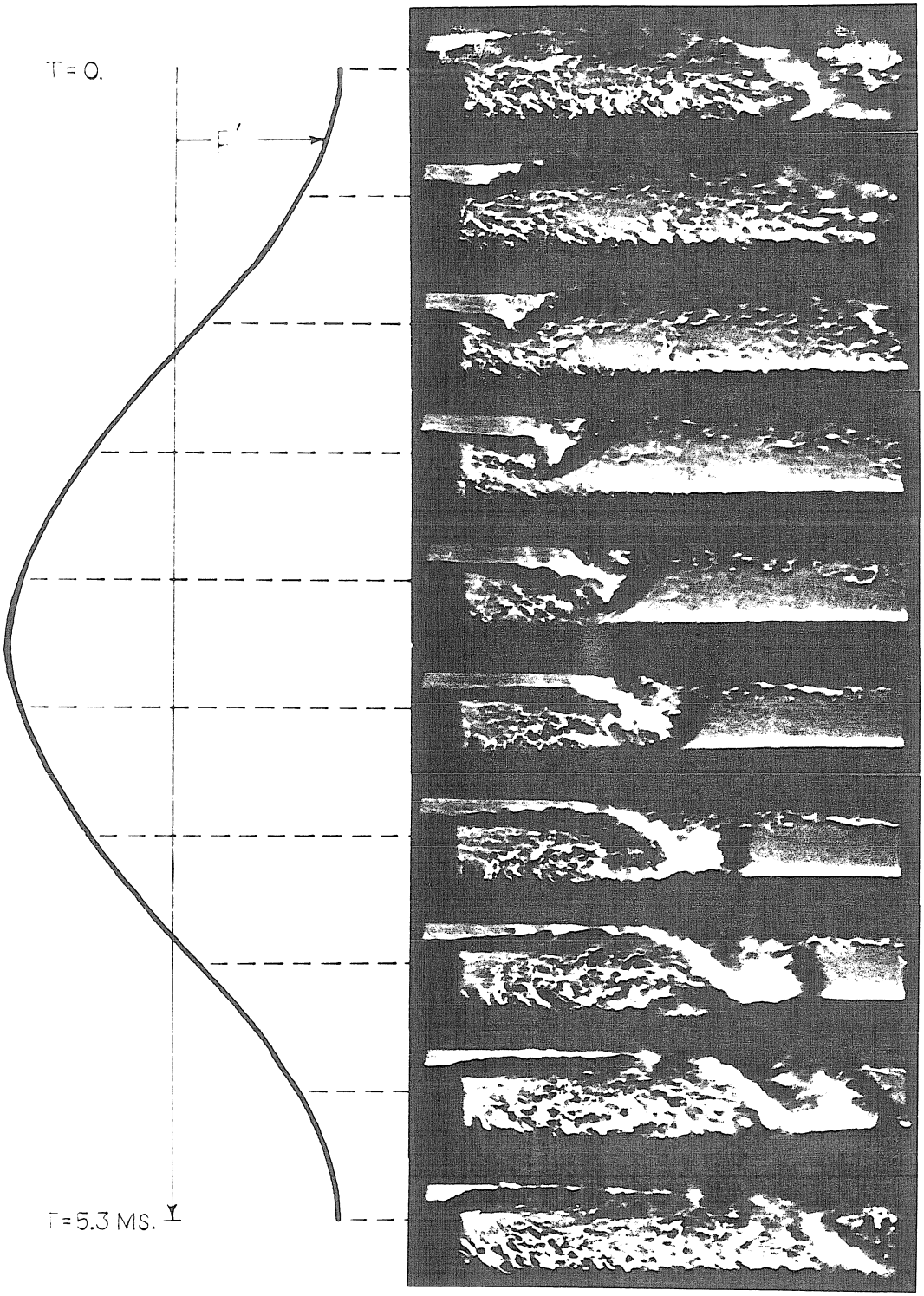

Figure 4.83 Vortex Formation at $V_D = 40$ m/sec, $\Phi = 1.0$

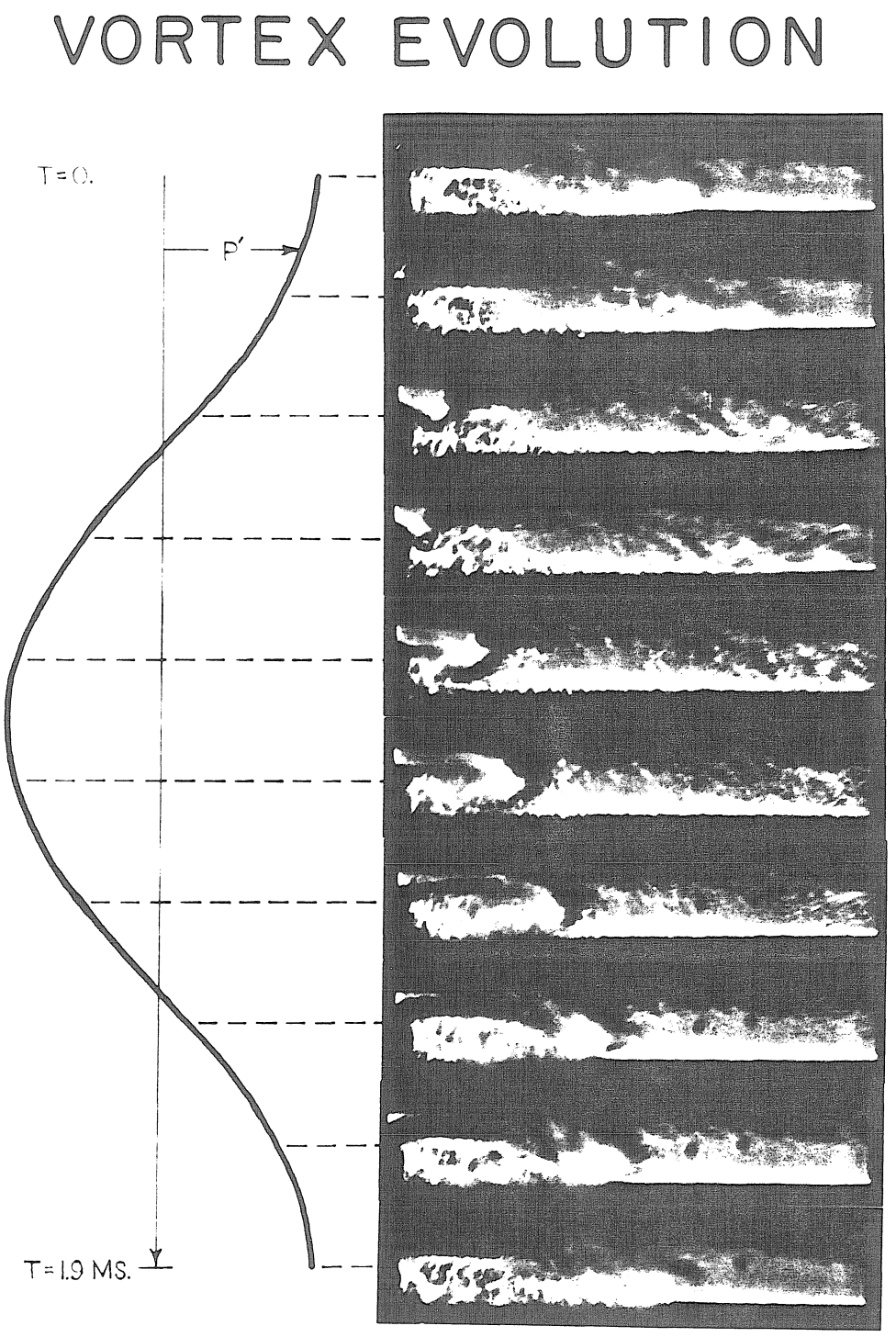

Figure 4.84 Vortex Formation at $V_D = 50$ m/sec, $\Phi = 1.0$

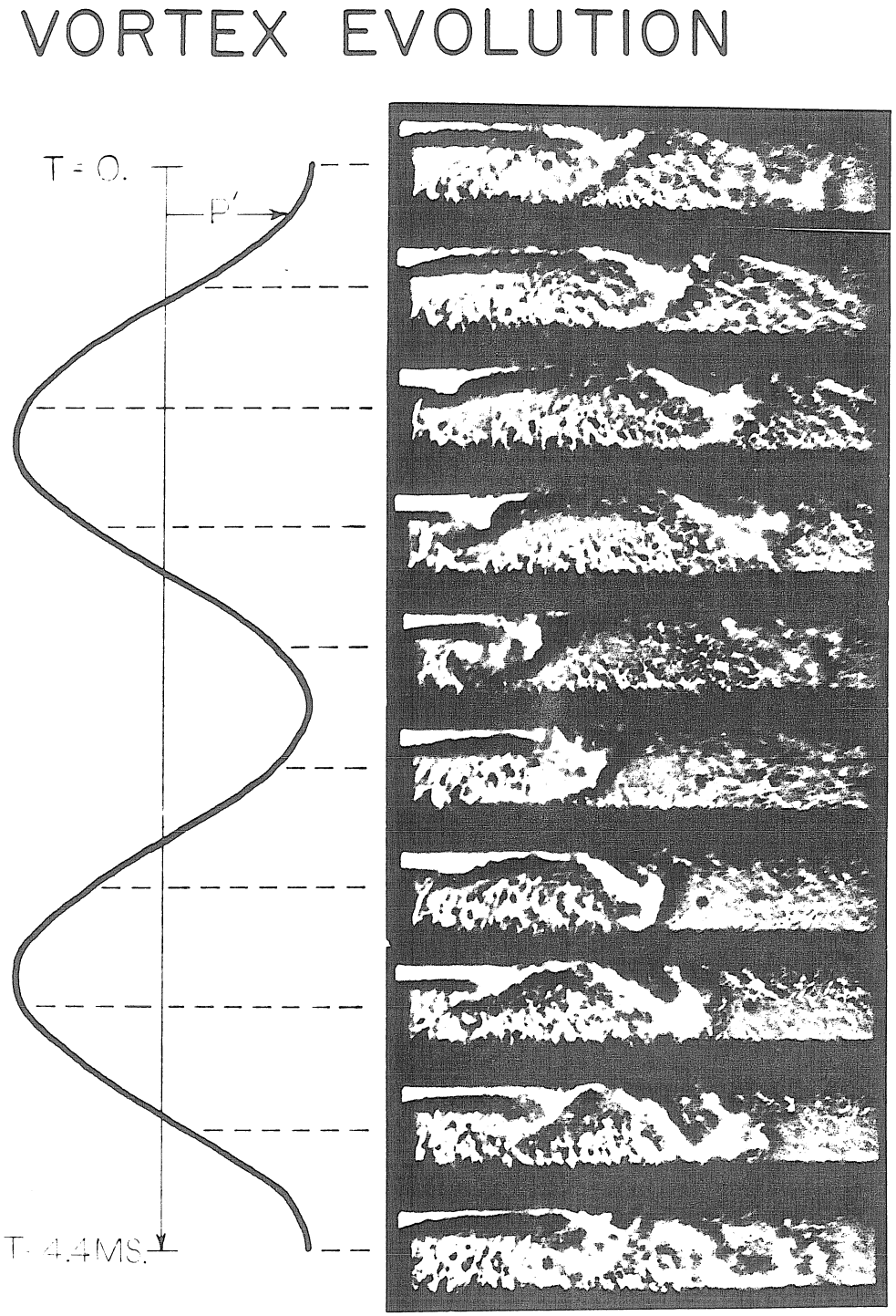

Figure 4.85 Vortex Formation at $V_D = 40$ m/sec, $\Phi = 0.74$

STABLE FLOW FIELDS

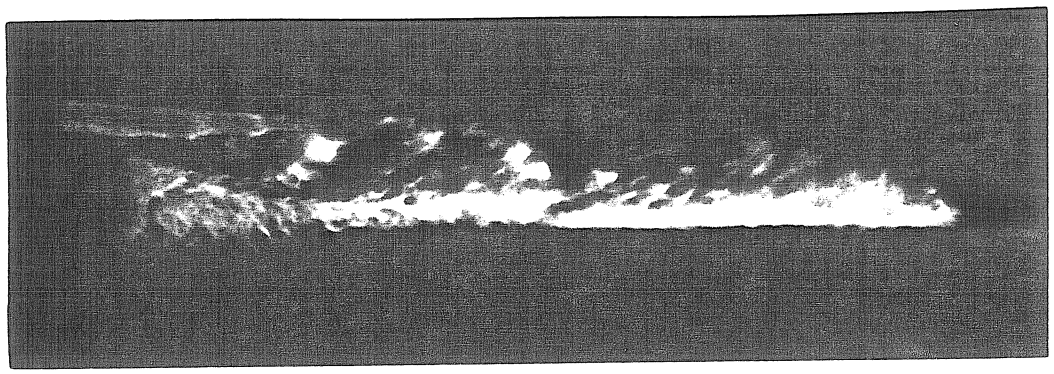

22 m/sec, Φ=0.65

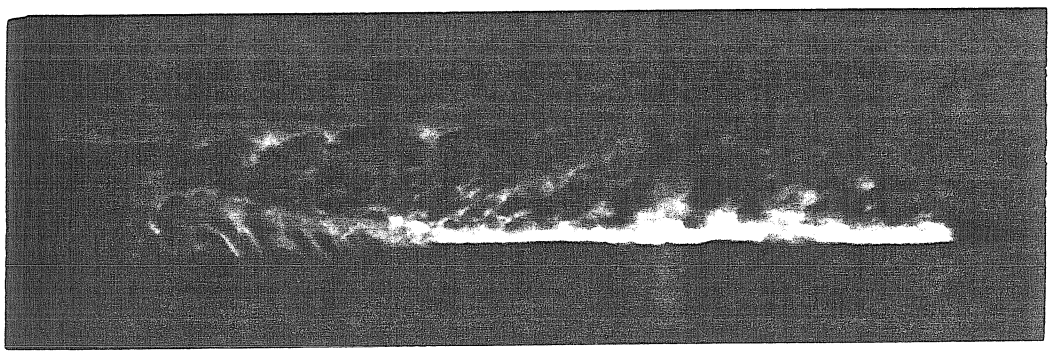

22 m/sec, Φ=1.28

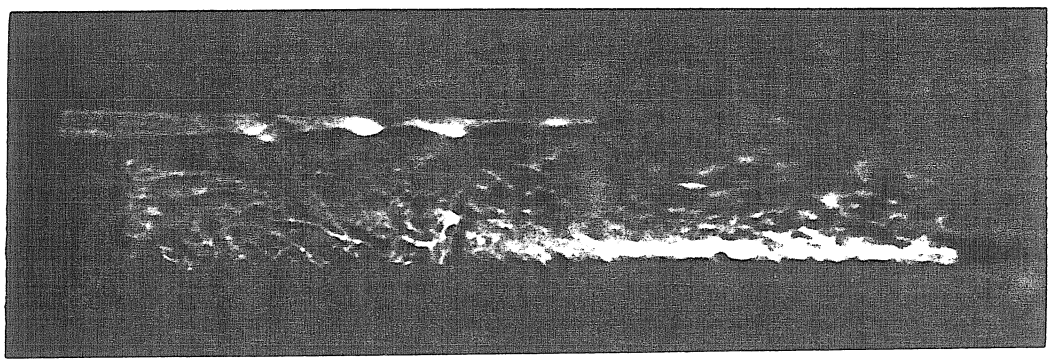

70 m/sec, Φ=1.0

Figure 4.86 Shear Layer Formation

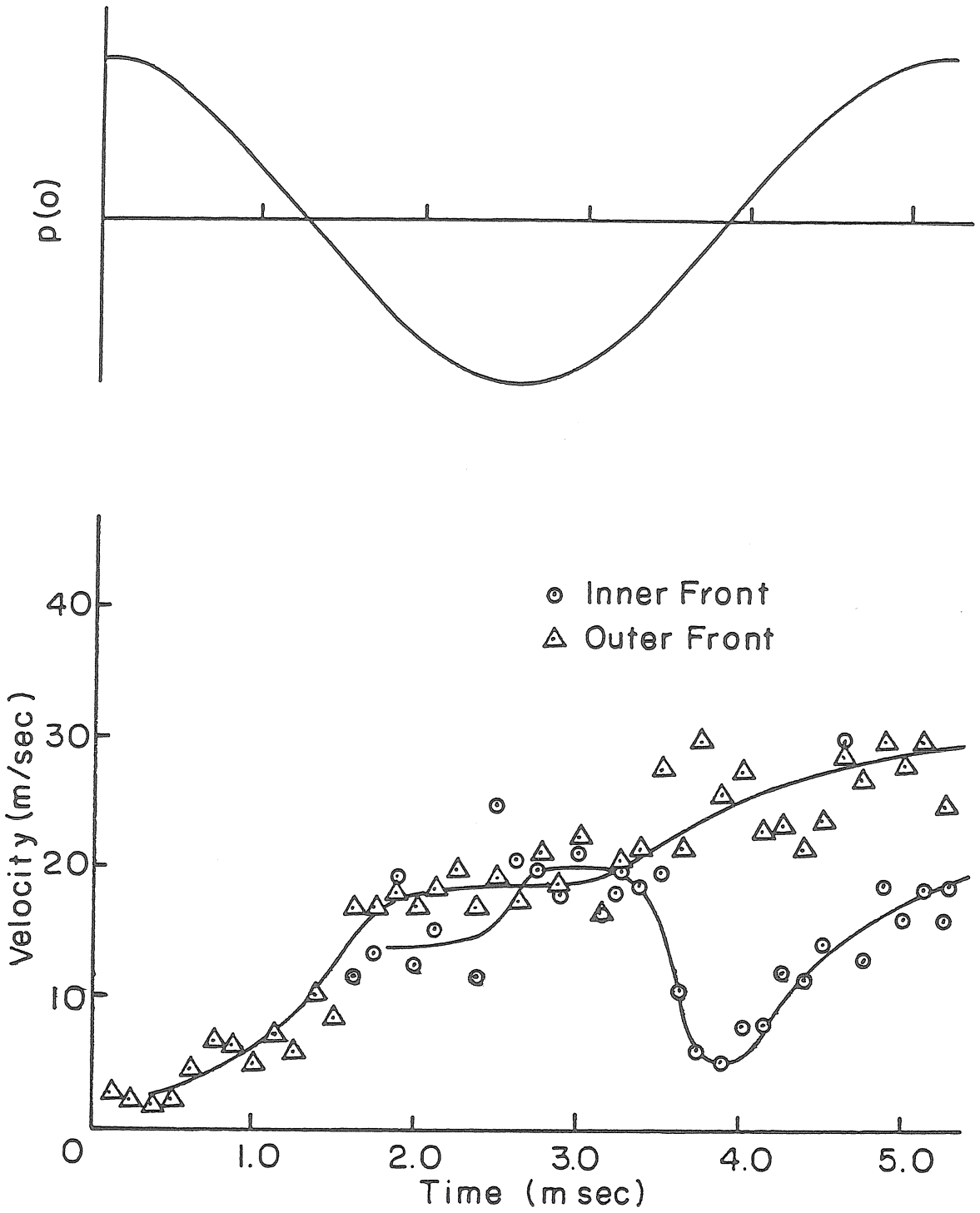

Figure 4.87 Velocity Diagram for V_D = 22 m/sec, Φ = 1.0, configuration I.

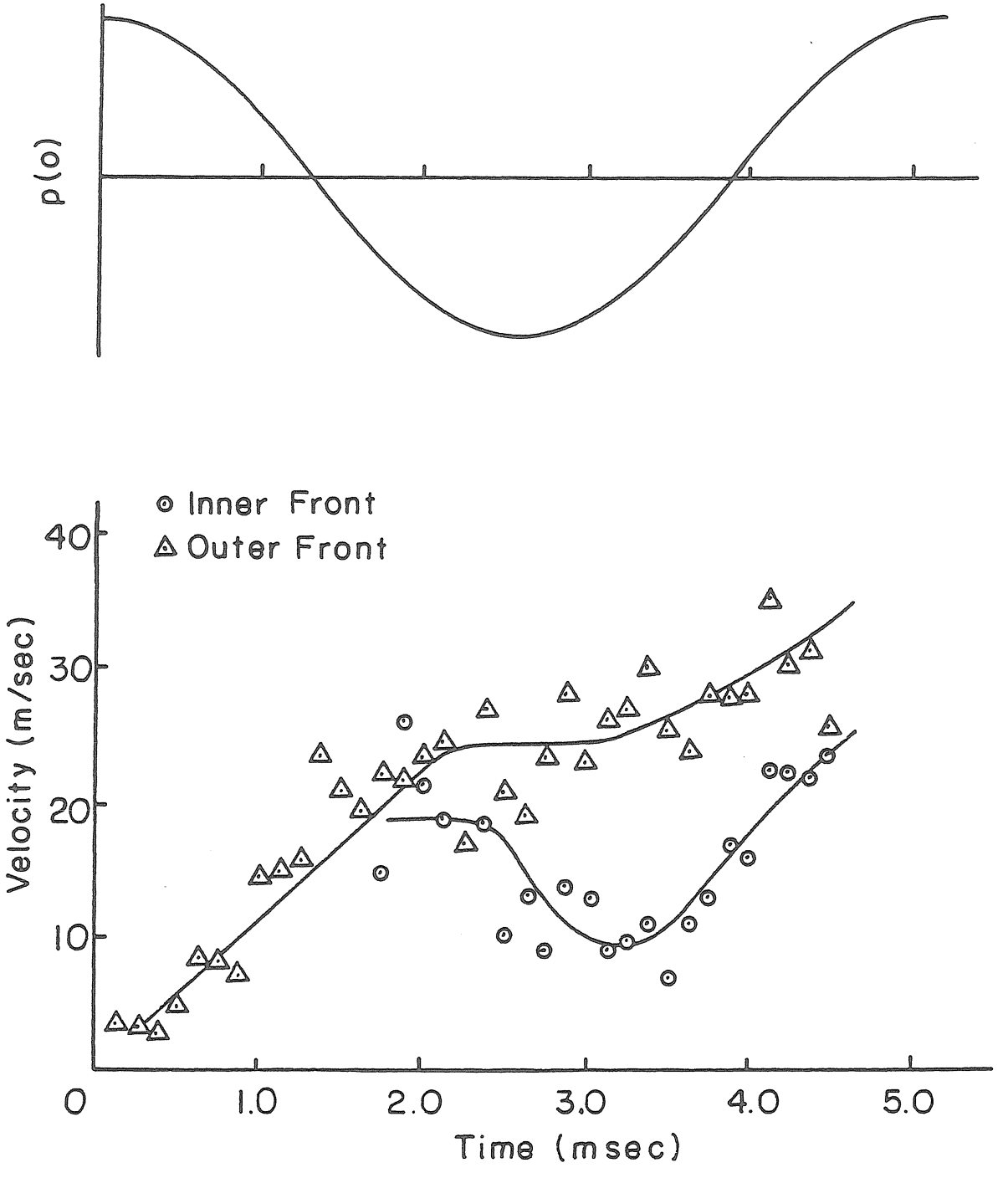

Figure 4.88 Velocity Diagram for V_D = 40 m/sec, Φ = 1.0, configuration I.

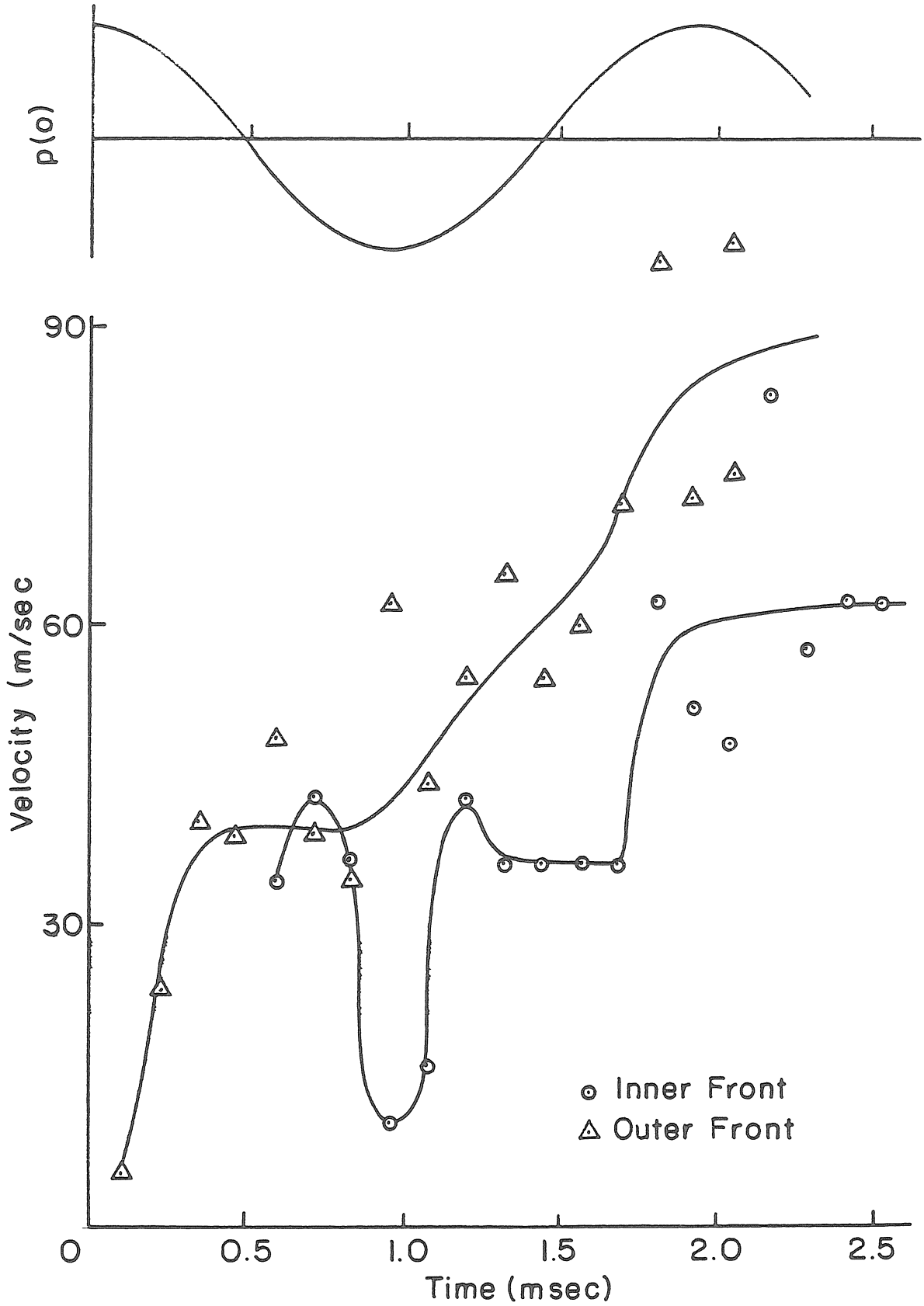

Figure 4.89 Velocity Diagram for V_D = 50 m/sec, Φ = 1.0, configuration II.

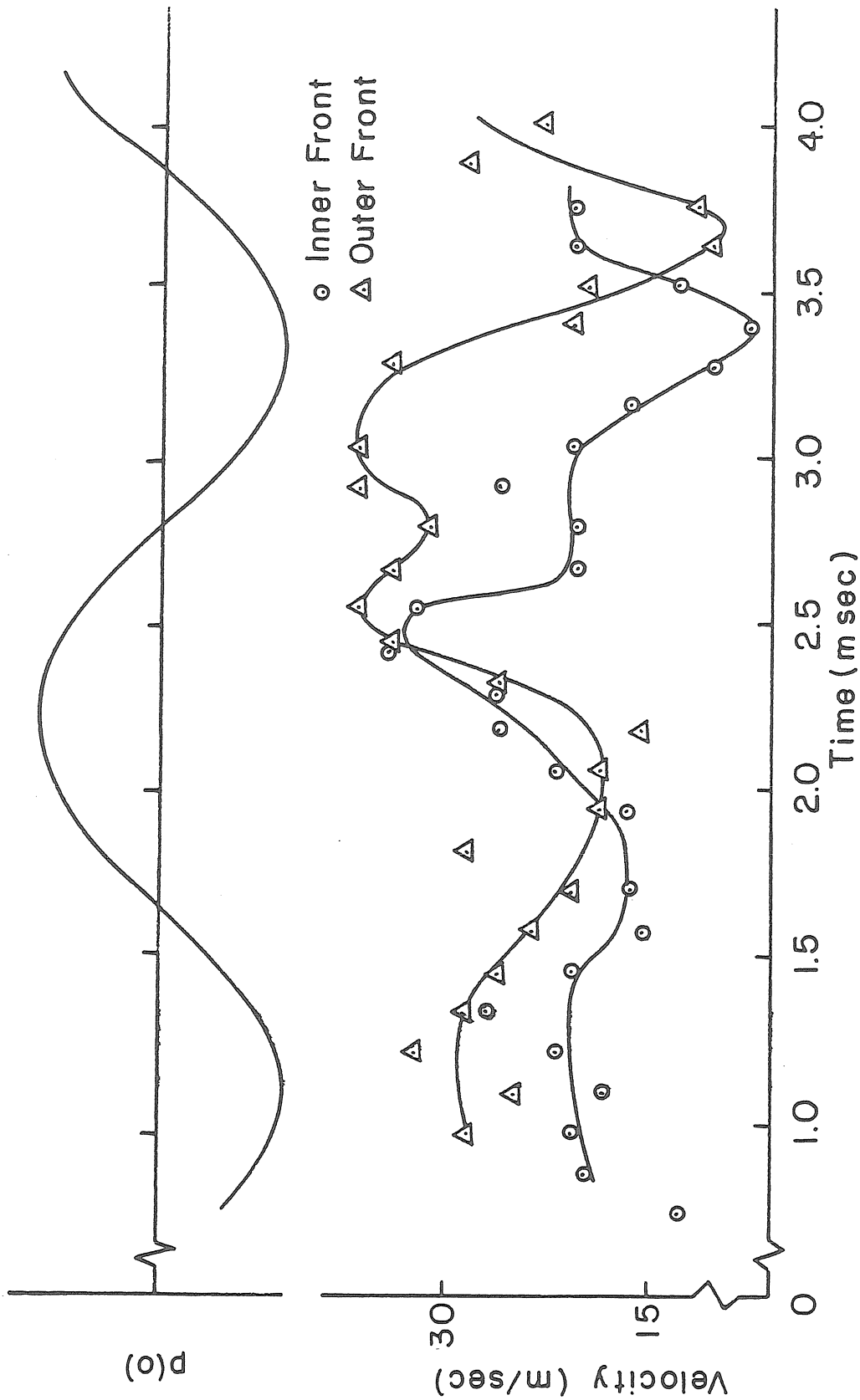

Figure 4.90 Velocity Diagram for V_D = 40 m/sec, Φ = 0.74, configuration II.

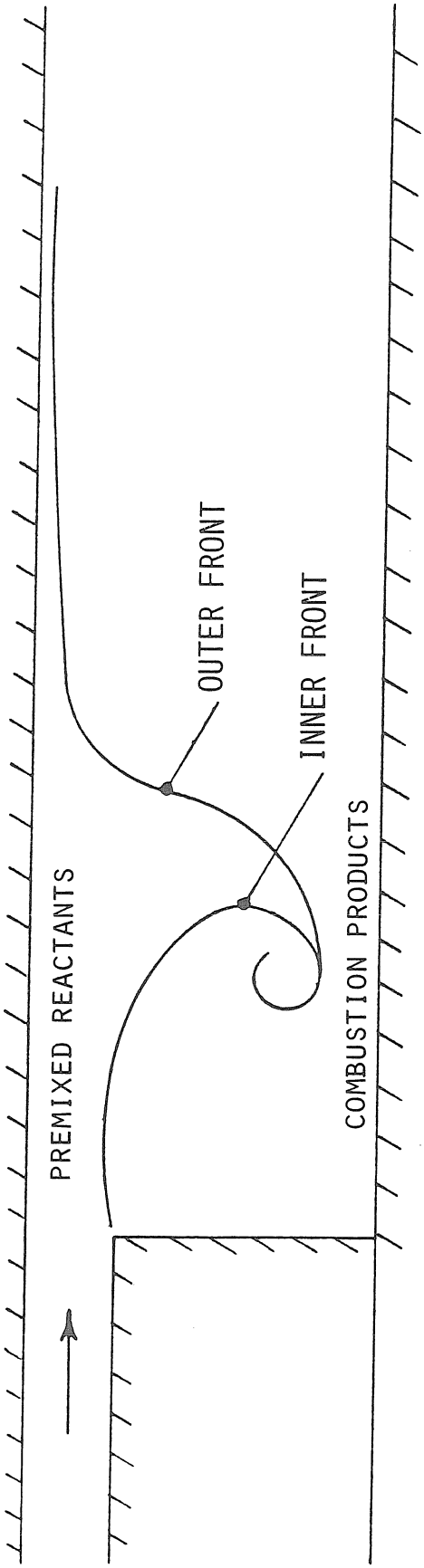

Figure 4.91 Definition of Flame Fronts

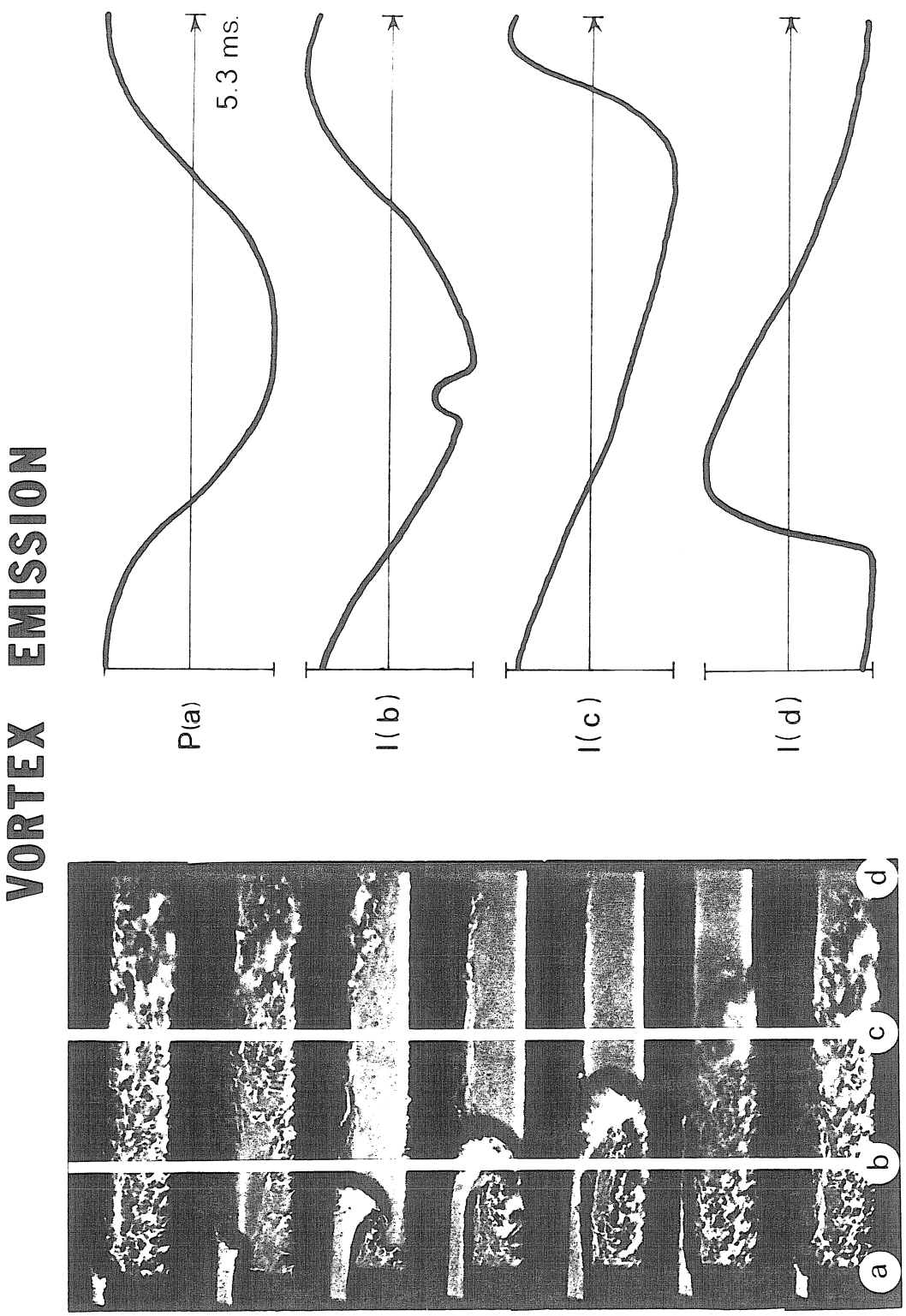

Figure 4.92 Flame Emission from Vortex formed at $V_D = 22$ m/sec , $\Phi = 1.0$

CHAPTER 5

DISCUSSION OF RESULTS

5.1 Comparison of Analytical and Experimental Results

The pressure oscillations observed inside the combustor apparatus appear to be produced by excitation of the acoustic resonant modes of the apparatus. Therefore, I am going to begin the discussion by comparing the analytical and experimental results to show that the one-dimensional, linearized approach gives an excellent prediction of resonant frequencies. Furthermore, the analytically predicted velocity fluctuations, based upon experimentally measured pressures, seem to agree with the flow visualization results. The experimental results suggest that the complex two-dimensional flow field can be modeled with a relatively simple one-dimensional analysis to get an idea of the streamwise flow field perturbations which lead to combustion instabilities.

Calculations of the acoustic frequencies, from the model describing the combustor apparatus, requires geometric, boundary, and acoustic velocity, or temperature information. The geometry depends solely upon the physical construction of the system; consequently, no assumptions are required to qualify any of the input parameters; however, some assumptions are required to define the boundary conditions and temperature field. These items are discussed next before comparing analytical and experimental results.

The boundary constraints at the entrance to the plenum chamber and exit of the burner are fairly easy to interpret. At the entrance, the

area of the combustible mixture supply line is a small fraction of the plenum chamber cross sectional area - only about 6 percent. An acoustic pressure disturbance traveling upstream from the combustor toward this boundary would essentially see a solid wall. The assumption of total in-phase reflectance is appropriate for this condition. At the burner exit, the opposite is true. An acoustic pressure disturbance traveling downstream toward the exit would encounter little resistance at the exit plane of the combustor. Thus, a boundary condition is used in which total inverse phase reflection occurs.

Under these boundary constraints, the acoustic pressure and velocity characteristics are well defined at either end of the apparatus. At the entrance, the solid boundary requires the pressure to be at its maximum point or at an antinode. Since no flow can penetrate the solid wall, the acoustic velocity must, of course, be zero. However, at the burner exit, the velocity fluctuations are maximized and the pressure fluctuations are zero. The final variable of interest, gas temperature, is treated in a somewhat more arbitrary manner.

The gas temperature is simple to determine upstream of the flameholder. The prevaporized, premixed combustible mixture in this region is at room temperature. The reaction rate at this temperature is extremely small and can only create a negligible temperature rise. Thus, assuming a constant temperature is very reasonable in this region of the apparatus.

The gas is also assumed to be at constant temperature inside the combustor. Given the geometry of the flame, this is a reasonable assumption for calculation purposes, but the magnitude of this temperature is difficult to determine. Details of the local temperature

at each longitudinal position could be installed into the model, but the incorporation of such details would be very cumbersome. After all, the temperature at a specific location would change under almost every operating condition. Furthermore, the determination of such detailed information would be very difficult. Consequently, describing the entire complex combustor region with a simple, single, average temperature is very attractive and is a logical way to proceed.

Take, for example, the heat addition process during stable operation of the combustor apparatus in which a mixing layer forms downstream of the flameholder. Inside the combustion chamber, the reactants pass through a flame zone distributed throughout the length of the burner. So, the temperature, averaged across the cross section, rises along the entire length as the combustible mixture is consumed. The combustor is not entirely filled with hot combustion products, either. Unburnt cold reactants occupy about 15% of the volume inside the chamber, and thus the gas temperature could not be equal to the adiabatic flame temperature. Furthermore, there is no assurance that all the reactants which enter the flame zone are consumed and, thus, the temperature of the reacting gases will not reach the adiabatic flame temperature. Finally, the gas temperature is reduced further because of heat transfer to the water cooled combustor walls. These three factors make the determination of the temperature inside the burner difficult a priori, and the incorporation of such complex details in the model would not be beneficial.

The adiabatic flame temperature can be used as a starting point for estimation of the mean temperature inside the combustion chamber. Obviously, the adiabatic flame temperature is too high, and not the

correct value for the mean temperature of the gas inside the combustor. However, results from the experiments can be used in conjunction with this estimate to determine the overall mean temperature inside the combustor. The length and condition at each end of the combustor chamber fixes the wavelength of the resonant mode in that section. For example, the flameholder at the entrance to the combustor occupies 75 percent of the cross-sectional area. As an estimate, this boundary may be considered similar to a solid wall. The exit, as discussed before, may be considered open. Given the constraints imposed by these two boundary conditions, the resonant mode must conform to a one-quarter wavelength sinusoidal distribution, with the maximum pressure occurring at the flameholder. With the length and mode shape well defined, the resonant frequency may be estimated, given a mean average temperature inside the combustor. Because of the potential temperature losses, a mean temperature, 25% less than the adiabatic flame temperature, is used as an initial guess for the gas temperature inside the burner. Results from the experiments indicate a major frequency occurs near this estimate of the resonant frequency. Thus, a very good estimate of the average combustor temperature may be determined, given the experimentally measured frequency result.

All the normal mode computations are made using the same mean combustor temperature except when the fuel-air ratio is changed. Under off-stoichiometric conditions a slightly lower temperature is employed. Acoustic disturbances travel at the rate of 750 m/sec when the average gas temperature inside the combustor is 1510 Kelvin. The speed of sound in the combustor is decreased to 675 m/sec during off-stoichiometric operating conditions. Using these estimates of the gas temperature, the

model can be employed to predict the resonant modes of the system. With experimental pressure measurements, the pressure and velocity distributions within the apparatus can also be determined.

The pressure measurements (Figure 4.17) obtained during testing the configuration I geometry, under stoichiometric conditions at the lowest dump plane velocity, show two major frequency components present inside the combustor. The 457 hertz component corresponds to the system mode sensitive to the combustion chamber conditions, i.e., the one-quarter wavelength normal mode inside the combustor. The 188 hertz component is the system mode which is influenced by the conditions within the plenum chamber located upstream of the combustor. As discussed earlier, the entrance to the plenum chamber appears like a solid wall boundary. At the exit of the plenum, the cross-sectional area changes abruptly, in the acoustic sense, by a factor of 10. This acoustically compact contraction reflects an acoustic pressure disturbance approaching it as if it were a solid wall. Under these boundary conditions in which each end is effectively closed, the plenum chamber resonance occurs near 188 hertz. This mode corresponds to a one-half wavelength pressure distribution inside the chamber with pressure maximums located at either end.

The spectrum, Figure 4.17, also reveals several frequencies of smaller magnitudes. Notice the small components at 231 and 377 hertz. These frequencies are also predicted by the analytical model to be acoustic resonant modes of the system. At each resonant frequency, the pressure oscillation magnitude is determined by the amount of energy supplied to that particular mode by the heat addition process. For this geometry, the 188 and 457 hertz resonances are the preferred modes of

the apparatus in that these frequencies dominate the pressure spectrum. However, note that the normal mode computation can not predict a preferred mode. The model is only capable of computing the characteristics roots (resonant modes) of the characteristic equation describing the combustor apparatus. The table below lists the characteristic roots calculated by the acoustic model along with the experimentally measured frequencies of the pressure oscillations. The measured values are quite close to the computed values. Evidently, the assumptions employed to generate the analytical model are sound, enabling accurate calculation of the resonant acoustic modes of the combustor apparatus.

computed frequencies	measured frequencies
180 Hz.	188 Hz.
229 Hz.	231 Hz.
385 Hz.	377 Hz.
470 Hz.	457 Hz.
533 Hz.	535 Hz.

The magnitudes of the spectral components, shown on the pressure spectrum under discussion (Figure 4.17), are essentially the Fourier coefficients. These pressure results, measured at the dump plane, are used to compute the pressure distribution throughout the rest of the apparatus. In addition, the fluctuating velocity field is computed based upon this measured pressure value. Overall, the acoustic pressures and velocities can be computed anywhere within the apparatus given a single, experimental pressure input value for that resonant frequency. For example, the pressure distribution (Figure 4.3), computed from the 22 m/sec test, illustrates the computation of the pressure distribution inside the apparatus for the two major resonant

modes. The resonance at 180 hertz, which is influenced by the length of the plenum chamber, and the system resonance sensitive to the combustion chamber, at 470 hertz, are shown to illustrate their effect upon the mean flow field. Notice that the amplitude scales, against which the pressures are plotted, differ for the two components in this case. The scale for the 180 hertz component is shown on the left of the diagram, whereas the 470 hertz scale is marked on the right-hand side. At the dump plane, $x/LC = 0$, the pressure magnitude of the two components are identical even though their magnitudes at this location appear much different in the plot. The difference is simply due to the factor of 4 scaling between the two when the results are plotted on the figure. Sufficient pressure measurements were taken to verify the pressure distribution in the combustor region; however, the upstream distribution could only be monitored at two locations. Nevertheless, the magnitude of the pressure at all measurement locations compare favorably, i.e., within plus or minus ten percent of the model predicted magnitudes.

Notice the pressure drop across the inductance section in the figure. One advantage of employing the compact assumption for this element is the elimination of the need to calculate the detailed distribution of pressure through the inductance area above the flameholder. In the figure, the pressure change is shown to be linear. The linear distribution is shown to illustrate the pressure change across this region, not the actual distribution.

The model is derived for two basic purposes: first, to predict the normal acoustic modes of the apparatus, and, second, to predict the velocity fluctuations as a result of this pressure field. The velocity distribution, calculated from the 22 m/sec pressure field is presented

in Figure 4.4 and shows the large velocity fluctuations imposed upon the mean flow by the 180 hertz disturbance. At the flameholder, the velocity fluctuation created by the 180 hertz resonance is quite large at 21 m/sec. The measured pressure spectrums for the 22 and 40 m/sec test conditions are similar for this configuration (Figures 4.17 and 4.18), and, consequently, the result in Figures 4.3 and 4.4 are representative of the analytical computation for both flow speeds.

Notice, for these dump plane speeds, the velocity fluctuation created by the 180 hertz disturbance at the flameholder is a major fraction of the mean flow speed; 95 percent of the mean flow speed for the 22 m/sec dump plane velocity, and 53 percent of the mean flow velocity for the 40 m/sec case. On the other hand, the 470 hertz velocity fluctuation is a small fraction of the mean flow speed; only 7 percent, for the lower 22 m/sec flow speed.

As the flow speed is increased to 50 or 70 m/sec, the experimental results (Figures 4.21 and 4.22) show that the 188 hertz pressure component becomes much smaller than the 457 hertz component. Figures 4.5 and 4.6 are plotted from the model results based upon the pressure spectrum obtained during the 70 m/sec testing. The result of the computation for the 70 m/sec velocity distribution indicates that only a small velocity fluctuation is created at the flameholder from the 470 hertz pressure component. The velocity fluctuation is only 3.2 percent of the mean flow velocity at the flameholder or dump plane.

Examination of the movement of the flame front in the region near the flameholder, as shown in the flow visualization collages of Figures 4.82 and 4.83, also suggest that large velocity fluctuations occur during the 22 and 40 m/sec experiments. The upstream motion of the

initial portion of the flame front in the photographs indicate that the velocity fluctuation has a large negative value when the pressure is a maximum. In other words, the flow is retarded at the entrance to the combustor when the pressure at the flameholder reaches a maximum. This is consistent with the model results (Figures 4.3 and 4.4). When the pressure at the dump plane, x/LC = 0, is a maximum, the velocity fluctuation for the 180 hertz component is negative, reducing the flow velocity entering the combustor at this time. For example, in the 22 m/sec case, the photographs show the flow is slowed almost to a stop, implying that the velocity fluctuation must be of approximately the same magnitude as the mass-averaged dump plane velocity. Using the experimental pressure results, the analytical model predicts a velocity fluctuation of 21 m/sec, nearly equivalent to the mean dump plane velocity of 22 m/sec.

As the fuel-air ratio is changed, the 188 hertz pressure fluctuation disappears. Stabilizing the flame under lean conditions produces two comparatively small pressure oscillations at 414 and 446 hertz as shown in the experimental results of Figure 4.19. The 446 hertz signal is the system mode associated with the combustion chamber. The frequency of this particular mode decreases because the fuel-lean operating condition lowers the overall mean temperature inside the burner. The frequency of the oscillation is proportional to the local acoustic velocity, and thus to the square root of the temperature. Therefore, a 36 percent change in equivalence ratio, from stoichiometric to .64, lowers the temperature by 10 percent, reducing the resonant frequency to 446 hertz.

Operating the combustor under fuel-rich conditions also eliminates

the 188 hertz pressure signal (Figure 4.20). Again one dominant frequency, the 468 hertz system mode associated with the combustor, is present when the equivalence ratio is increased to 1.28. The magnitude of the dominant pressure oscillation during fuel-rich conditions is smaller than stoichiometric operation, yet the overall mean temperature inside the burner appears to be nearly the same since the frequency remains the same. However, the magnitude of the oscillation under fuel-rich conditions is much larger than the oscillations generater during fuel-lean operation.

The system resonance which is sensitive to the plenum chamber conditions can also be eliminated under all operating conditions if an acoustic damping material is placed inside the plenum chamber. For example, the experimental pressure results (Figures 4.41 to 4.44) indicate only one frequency, the combustor normal mode, generated when the steel wool fills a major portion of the plenum chamber volume. The viscous damping produced from the steel wool attenuates the velocity fluctuation in the plenum chamber or resonant section. Under these conditions, the magnitudes of the pressure oscillations are nearly constant at all the dump plane velocities (22, 40, 50, 70 m/sec) during stoichiometric operation of the combustor. Changing the mean flow speed by a factor of 3.25 does not influence the frequency or magnitude of the pressure oscillation. The frequency should be essentially constant, barring no temperature changes, if the oscillations are acoustic. Consequently, the fact that the frequency is constant is no surprise. However, the magnitude of the fluctuation depends upon the amount of energy supplied to the acoustic field by the combustion processes. It is surprising that the pressure oscillations arising from the heat

released during chemical reaction is independent of the mean flow speed.

When the apparatus geometry is changed by shortening the length of the plenum chamber, i.e., by moving the entrance boundary condition closer to the combustor, different acoustic modes are produced. For example, when the plenum chamber is shortened to the configuration II geometry, operation of the combustor at 22 m/sec under stoichiometric conditions produces nothing but essentially the 457 hertz resonant mode sensitive to the conditions within the combustor as shown in Figure 4.53. Small pressure oscillations at 208 and 524 hertz are present, but the dominant fluctuations occur at 457 hertz. Under this gas speed and mixture ratio, no other acoustic modes besides the combustor mode seem to be appreciably excited.

As the equivalence ratio is decreased to 0.74, keeping the dump plane velocity constant at 22 m/sec, the magnitude of the combustor pressure oscillation changes drastically (Figure 4.54). Instead of the magnitude of the Fourier pressure coefficients decreasing, as in the configuration I geometry, the magnitude of the normal mode influenced by the combustor increases markedly in this 56 centimeter plenum chamber length configuration. The ratio of the fluctuating pressure to the average static pressure changes from about 0.63 percent, at stoichiometric conditions, to a rather large magnitude of 5.2 percent. The decrease in frequency to 449 hertz was expected because the temperature of the combustor is lowered in response to the fuel-lean conditions, but the 8.25 times greater pressure fluctuation was quite surprising.

The oscillations generated under the previous geometry I conditions are large in the acoustic sense; however, these oscillations, at 449

hertz, are quite large. The ratio of the peak-to-peak pressure oscillation to the atmospheric pressure is slightly greater than 10 percent of the local static pressure with this geometry operating at 22 m/sec and an equivalence ratio of 0.74. The analytical model assumes linear acoustic behavior. Beranek (1954) suggests that the acoustic approximation, used in the reduction of the equations of motion, hold for sound pressure levels below 110 db (reference 0.0002 microbar). This sound pressure level corresponds to a ratio of disturbance pressure to ambient pressure of about 6.25E-11. Obviously, the strong pressure oscillations encountered here are huge in the acoustic sense. The oscillations are over 10E+10 times greater.

The strong pressure oscillations, creating losses or nonlinearities in the system, are ignored in the theory utilized for the modeling. Frequency computation is not strongly influenced by the nonlinear behavior of the system (Nayfeh and Mook, 1979). Therefore, calculations of the frequencies should be accurate. However, calculations of the pressure and velocity distribution may become inaccurate as they are computed far from the position of the experimental input value. Losses due to flow separation and other nonlinear behavior affect the results upstream in the plenum chamber. Nevertheless, expectations are that the computations near the flameholder should be nearly correct. The velocity fluctuation produced by the pressure oscillation at this point is important in determining the nature of the flow field inside the combustor. Thus, the model should provide insight into the magnitude of the velocity fluctuation at the flameholder, using the experimental pressure input in spite of the ignored nonlinearities.

Computation of the acoustic modes of the apparatus are listed below for the geometry II configuration:

measured frequencies	computed frequencies	
217 Hz.	206 Hz.	
--	305 Hz.	for c=675 m/sec,
449 Hz.	438 Hz.	equivalence
507 Hz.	518 Hz.	ratio of 0.74

measured frequencies	computed frequencies	
71 Hz	--	
203 Hz	209 Hz.	
--	306 Hz.	for c=750 m/sec,
457 Hz	468 Hz.	equivalence
522 Hz	532 Hz.	ratio of 1.0

The first listing corresponds to the case in which the dump plane velocity was set at 22 m/sec and the equivalence ratio was 0.74. Figure 4.54 shows that, during the test, the mode sensitive to conditions within the combustor is clearly the dominant oscillation. Using the pressure measured at the flameholder, Figure 4.10 illustrates that the velocity fluctuation, computed in the region above the flameholder, is 13 m/sec. This fluctuation is clearly a major fraction of the mean flow velocity. In fact, the fluctuating velocity is 58 percent of the mean flow velocity in the vicinity of the flameholder. Such a fluctuation creates a large perturbation in the mean flow. The flow visualization records (Figure 4.85) do indicate that this is indeed the case, as large vortices are formed when the mean flow speed is 40 m/sec and the equivalence ratio is 0.74.

The second listing above is computed from measured pressure input values obtained when the dump plane velocity is increased to 50 m/sec under the same geometric conditions (configuration II) and

stoichiometric mixture ratio. As the experimental pressure measurements show (Figure 4.55), the combustor generates very large pressure fluctuations concentrated at 457 and 527 hertz. Both components have nearly identical magnitudes measured to be 0.0605 of an atmosphere. The magnitude of these pressure oscillations are nearly an order of magnitude larger than the pressure fluctuations encountered with the configuration I geometry under identical flow conditions. Using the experimental pressure data in the acoustic model, the relative influence of the two strong oscillations upon the velocity fluctuation at the flameholder can be examined (Figure 4.8).

The 468 hertz oscillation produces a relatively small velocity perturbation of only 7.3 m/sec. This disturbance is only 15 percent of the mean flow velocity. On the other hand, the 532 hertz disturbance generates a 30 m/sec or 60 percent perturbation of the mean flow. Thus, the major contribution to the velocity fluctuation at the flameholder under these circumstances is created by the 527 hertz disturbance, a computed system resonant mode.

The shadowgraph records, obtained during the 50 m/sec testing (Figure 4.84), show that the gas entering the combustor is nearly stopped. Consequently, the velocity fluctuation must be on the order of the mean flow velocity of 50 m/sec. The calculated fluctuations are substantially less than this. One explanation for the discrepancy could be based upon the large pressure oscillations which introduce nonlinearities that are ignored in the formulation of the acoustic model. Even though the computed magnitude of the fluctuation appears slightly inaccurate, this calculated value is nevertheless large, indicating the 527 hertz system mode greatly affects the mean flow

field.

Increasing the dump plane velocity to 70 m/sec under the geometry II constraints produces pressure oscillation of similar magnitude and frequency as the configuration I geometry at the same speed. Figure 4.56 shows the pressure spectral decomposition of data obtained from the stoichiometric, 70 m/sec operation of the apparatus. The major frequency component is the system resonant mode attributed to the combustion chamber, namely, 457 hertz, the same as in the configuration I case. The magnitude, however, is 55 percent larger for the configuration II test. Nevertheless, the shape of the velocity distribution for the combustor resonant mode is similar to the one computed for the configuration I case (Figure 4.5 and 4.6). Even though the pressure magnitude used to compute the velocity fluctuation is somewhat larger, the relative influence of the velocity fluctuation upon the mean flow field at the flameholder is representative of the velocity distribution presented in Figure 4.6. The velocity fluctuation is small compared to the mean flow velocity and the effect upon the flow field is still negligible.

In both listings of the calculated resonant frequencies on page 121 for the configuration II geometry, notice that a 305 or 306 hertz system resonance frequency is predicted by the acoustic model. Yet, no pressure oscillations are measured near this frequency in either experimental case. The 305 hertz frequency is the characteristic system resonance mode of the shortened plenum chamber. Evidently very little energy is supplied to this mode, and the other system modes dominate the pressure field. Also, notice that the value of the two lowest frequencies in the listings are essentially unchanged as the speed of

sound increases in the combustor. However, the higher frequencies, 468 and 532 hertz, are influenced substantially by the temperature change inside the burner. These two system modes appear sensitive to conditions present inside the combustion chamber.

The plenum chamber is shortened to slightly less than one-half its original length for the final group of experiments. Testing with the configuration III geometry revealed no extremely large pressure oscillations at any of the combustor apparatus operating conditions. Assuming the speed of sound inside the combustor is 675 m/sec, the acoustic model computations of the system resonant frequencies are listed below beside the experimentally measured pressure oscillation frequencies.

measured frequencies	computed frequencies	
208 Hz.	211 Hz.	
--	398 Hz.	c=675 m/sec,
451 Hz.	446 Hz.	equivalence
506 Hz.	531 Hz.	of 1.0

Measurements (Figures 4.69 and 4.70) of the pressure oscillations inside the combustor during the lower speed testing indicate three dominant pressure disturbance frequencies. Oscillations at 208, 451, and 506 hertz are present in the burner under stoichiometric conditions at dump plane velocities of 22 and 40 m/sec.

The magnitude of the 451 and 506 hertz components, as shown by the Fourier coefficients, are almost the same when the dump plane velocity is 22 m/sec (Figure 4.69). The pressure fluctuation is about 0.17 percent of the average static pressure for both frequency components measured at the dump plane, x/LC = 0. The 208 hertz component is,

however, only one-third of this magnitude. Figure 4.11 shows the pressure distribution calculated from the experimental pressure results. The experimentally determined pressure magnitudes from the spectral plots are used to scale the pressure distribution at one of the model predicted modes, 446 or 531 hertz. The largest pressure fluctuation occurs in the inlet region at a frequency of 531 hertz. The set of curves directly below this one, Figure 4.12, shows the computation of the velocity field using the same experimentally determined input values. The largest contribution to the velocity fluctuation at the flameholder is from the 531 hertz oscillation, also. However, the calculated velocity fluctuation at this frequency is 3 m/sec, small with respect to the 22 m/sec mass average velocity through this region.

As the flow speed is increased to 40 m/sec, the experimental results, Figure 4.70, show that the same three frequencies are generated. However, the magnitudes of the oscillations are greater. As before in the 22 m/sec test, the pressure at the two higher frequencies, 451 and 506 hertz, have equal magnitudes at the measurement location, although the magnitudes of the pressure fluctuations have just about doubled. For these two components, the fluctuating pressure oscillation is now about 0.34 percent of the static pressure at x/LC = 0. The major difference, appearing in the pressure spectrum between the two operating conditions, is the much larger excitation of the 208 hertz resonance at the 40 m/sec dump plane velocity. In fact, the fluctuation of the 208 hertz oscillation is the same magnitude as the other two oscillations at the flameholder. Calculation of the pressure distribution, inside the apparatus using the experimentally determined pressure coefficients as the scaling parameter, is shown in Figure 4.13. Large pressure

oscillations are created by the low frequency disturbance. In fact, the velocity fluctuation at the flameholder is almost totally due to the 211 hertz oscillation as is illustrated in Figure 4.14. The velocity perturbation for the 211 hertz oscillations at the flameholder is 8.5 m/sec. This fluctuation is not large compared to the local mean flow velocity of 40 m/sec. The fluctuation is 21 percent of the mean flow, but the flow visualization indicates this perturbation is not large enough to produce a major distortion of the mean flow field.

Figure 4.71 shows the experimentally measured pressure field at the dump plane, x/LC = 0, as the flow speed is increased to 70 m/sec. The geometry and stoichiometry are the same as discussed in the last four paragraphs. One dominant pressure oscillation at 451 hertz is generated under these conditions. As in all the other cases presented at 70 m/sec, the velocity perturbations to the mean flow field are negligible. No major disturbance of the kinematic flow field occurs because the magnitude of the pressure coefficient under the geometry III conditions is smaller than any of the other cased discussed.

Overall, the oscillating pressure disturbances measured inside the combustor appear to be solely acoustic in nature. The energy available through heat released during combustion is supplied to the naturally available acoustic modes of the system. A relatively simple one-dimensional acoustic model is capable of computing the acoustic resonant modes of the apparatus quite accurately. All the computed frequencies are within 5 percent of the measured pressure oscillations associated with combustion-driven acoustic fluctuations. Furthermore, calculations of the pressure and velocity distributions inside the apparatus may be obtained from a single experimentally determined pressure input. These

calculations appear to represent accurately the pressure induced velocity fluctuations in the combustor apparatus when the pressure oscillations are small. However, if the oscillations become large, i.e., over ten percent of the local static pressure, the agreement is not as good. The error may arise from flow losses which introduce nonlinearities not incorporated into the acoustic model. Nonlinearities affect most strongly the computation of the pressure and velocity distributions inside the combustion apparatus, and do not have a major influence upon the computation of the resonant frequencies. The worst deviation was noticed in the velocity field computation for the 50 m/sec, geometry II situation where the computed fluctuation at the flameholder was 30 m/sec. Flow visualization results indicate the fluctuation to be on the order of the mean flow speed, 50 m/sec: an error of 40 percent. However, the analytical computations appear close for the remainder of the situations examined, and even in the poor agreement situation, the predicted streamwise velocity fluctuation is still large, implying the acoustic field is a major influence.

5.2 Kinematic Flow Field

During the experimental investigation of the combustor apparatus, two distinctly different kinematic flow fields were found to exist inside the combustion chamber. One flow field, as found in the steady burning case, is characterized by the formation of a mixing layer immediately downstream of the flame holder. The combustible mixture enters the burner continuously, and the flame is stabilized by the hot

recirculating combustion products trapped below the mixing layer as discussed by Zukoski and Marble (1956). The flame then begins to fill the remainder of the burner as it propagates into the unconsumed combustible mixture.

In sharp contrast, the unsteady burning case is characterized by a nonsteady reactant flow into the burner. Hence, individual pockets of reacting gas are convected downstream through the combustion chamber. Consequently, the two flow fields are quite different. Instead of a continuous mixing and burning of the reactants throughout the entire length of the burner, as in the stable operation, regions of burning gases are swept through the burner separated by totally burnt products during unstable operation. These burning regions are the remainder of vortices formed at an acoustic resonant frequency of the system which creates large velocity fluctuations in the vicinity of the flameholder. All the experimental data suggest that the unsteady burning within these vortical structures is the fundamental mechanism which sustains the large velocity fluctuations, and is the key to the instability mechanism.

The type of flow field created inside the combustor depends upon several parameters, namely, the flow velocity, the fuel-air ratio, and the geometry. The geometrical configuration determines the possible acoustic resonant modes which may be excited within the apparatus, while the relative magnitude of the acoustic velocity perturbation upon the mean flow field depends strongly on the flow velocity of the gases entering the combustor. Additionally, the stoichiometry controls the physical consumption rate of the reactants by the combustion process and the amount of energy released. A summary of the flow fields,

encountered during the testing of the apparatus, is presented in Table 5.1. The table lists the flow fields observed for a specific geometry at a certain test condition. The table provides a quick reference of the flow situation at various test conditions and is helpful to avoid confusion between the experiments discussed in the following sections.

5.2.1 Steady Flow Field

The steady flow field is somewhat similar to the flow fields found behind other bluff body flameholders. Flame stabilization is achieved because the region behind the unstreamlined flameholder consists mainly of hot combustion products which act as a continuous ignition source for the incoming combustible gas mixture, Zukoski and Marble (1956). The premixed combustible mixture is entrained into the mixing layer from one side and the hot combustion products from the other. As the mixture temperature rises, rapid chemical reaction between the reactants, or burning, occurs. For the combination of reactants in this study, a blue flame indicates the location of the rapid reaction. Once the flame is established in the mixing layer, the recirculation zone is supplied with hot products required to insure continuous ignition of the mixture entrained into the mixing layer. After the flame is anchored, it spreads into the remainder of the reactants at an angle dependent upon the local turbulent burning velocity. The key to flame stabilization in these systems is the unstreamlined, bluff-body flameholder which created a high temperature wake region behind it. A streamlined body which forms no wake will not anchor or stabilize a flame.

In reacting systems, the wake region behind the bluff body is much

different than the wake formed behind unstreamlined bodies in isothermal flows where the typical vortex street forms. The 1949 examination by Williams, Hottel, and Scurlock revealed a very smooth mixing layer formed at either edge of the body instead of vortical structures which are shed alternately from either edge as in isothermal flows. They suggested that vortex formation was suppressed because the heat released during combustion causes the viscosity of the gas to change. Consequently, they proposed that the local Reynolds number is decreased sufficiently to eliminate the vortex formation.

In the current investigation, flames are stabilized by hot combustion products present in the wake formed downstream of a rearward facing step. The recirculating wake region is, however, one-half the wake width of a typical bluff body flameholder placed in the center of the oncoming flow. The lower wall effectively splits the entire flow field in half so that it resembles only the upper half of the standard bluff-body flow field.

On the surface, one major difference between the ordinary bluff-body flame stabilization and the rearward facing step flame stabilization is the presence of distinct vortical structures inside the mixing layer separating the recirculating hot products from the incoming fresh reactants. No vortical structures were found in the bluff body stabilized flames of Zukoski (1954), but their existence may have been masked by the flow visualization technique. The vortices within the mixing layer of the current study are similar in nature to the ones discovered in the nonreacting free shear layer discussed in Brown and Roshko (1974). The vortices are coherent in that an identifiable vortex structure is formed and is transported throughout the layer. Ganji and

Sawyer (1980) were the first to report the existence of clear coherent structures in a reacting flow field. In their work, the flame is anchored by a rearward facing step flameholder similar to the one employed in the current investigation. Mixing layers are characteristic of stable combustion as defined in the current work, and steady combustion occurs at many of the experimental test conditions (Table 5.1). Even though the main emphasis of this thesis concentrates on the unsteady combustion phenomena, some aspects of the steady flow are worth consideration, and I would like to present them here.

The steady flow field can be broken into two main segments: first, the vortex dominated mixing layer near the flameholder which stabilizes the flame, and second, the propagating flame region that occupies the remainder of the combustor. Combustion takes place inside the mixing layer as the fresh reactants are heated by the combustion products entrained in the vortical structures. Consequently, the characteristic blue flame, associated with burning premixed, prevaporized methane and air, is visible in various portion of the shear layer.

The shear layer grows and impinges against the lower combustor wall. The impingement location is characterized by the reattachment length or the point at which no flow reversal occurs. Pitz (1981) measured the mean flow field reattachment length to be 4.3 to 5.3 step heights downstream for a reacting flow field. This reattachment length was a function of the mean flow velocity. At a low velocity of 9 m/sec, he found the length to be 4.3 step heights downstream of the step, and increased to 5.3 step heights at 22 m/sec. This length is somewhat shorter than the 8 step heights that exist in standard bluff-body flows (Oates, 1978). Using the Pitz results as a guideline, the shear layer

occupies roughly 25 percent of the initial combustor length.

The remaining 75 percent of the combustor length consists of a propagating flame zone. The reacting zone begins at the interface between the flame front propagating into the unburnt combustible mixture and terminates at the lower combustor wall. The blue flame in this zone indicates that chemical reaction occurs across the entire height of the zone and not just at the interface of the unburnt combustible mixture.

Steady flow fields, or flow fields possessing mixing layers, could be produced at any one of the four standard flow velocities depending upon the fuel-air ratio selected. The dump plane velocity is used in this report to describe the various flow field conditions. However, turbulent mixing layers are generally described by the Reynolds number based upon the momentum thickness of the boundary layer at the formation of the free mixing layer, and not the mean flow velocity. Consequently, for comparison purposes, the following table lists the Reynolds number and momentum thickness for the experimental flow velocities. The momentum thickness is calculated assuming laminar flow along the flat surface of the flameholder as the mixture enters the combustor. Remember, the gas accelerates as it enters the region above the flameholder because the area changes by a factor of four. Whatever boundary layer which existed upstream is thinned markedly; therefore, the boundary layer thickness is assumed negligible at the upstream edge of the flameholder and develops laminarly from this point till it reaches the combustor, assuming that the velocity in the region above the flameholder is constant. The flameholder is 7.6 cm long, and the momentum thickness computations below are based on this length.

Dump plane velocity (m/sec)	Reynolds Number Re_1	Momentum thickness (θ ; cm)	Reynolds Number Re_θ
22	115,600	.0158	2560
40	210,200	.0116	3490
50	262,800	.0102	3970
70	367,900	.0087	4640

The location of the rapid chemical reaction, or burning, occurs within different portions of the mixing layer depending upon the fuel-air ratio of the combustible mixture. Figure 4.86 shows the mixing layer formed under three different conditions. The upper two photographs are shadowgraph images of the mixing layer when the dump plane velocity is 22 m/sec. The top photograph is taken at an equivalence ratio of 0.65, and the middle photograph is taken at rich conditions, or an equivalence ratio equal to 1.28. The lowest photograph in this figure illustrates the flow field at a stoichiometric mixture ratio and an entrance velocity of 70 m/sec. Notice that the general character of the mixing layers in all three photographs appears similar. Vortical structures are present in the layer under all the operating conditions. However, photographs of the visual flame show that the region of burning is not the same for all of these situations.

Figure 5.1 illustrates the location of the visible flame within the mixing layer. At the low-speed lean conditions, visible flame is observed in the lower portions of the mixing layer, while at low-speed rich and high-speed stoichiometric conditions, the visible flame spans the entire mixing layer. Consequently, chemical factors seem to control

the location of reaction as well as the quantity of heat released.

First, the amount of heat released depends on the mixture ratio which ultimately determines the temperature of the combustion products. Since the high temperature products act as the ignition source, the product temperature plays a role in the flame stabilization. The equilibrium temperature for stoichiometrically mixed reactants is approximately 2260 Kelvin [Jones (1984)], and does not change much at an equivalence ratio of 1.28 where the temperature is down about 6 percent to 2130 Kelvin. In contrast, at an equivalence ratio of 0.65, the equilibrium temperature is down 23 percent to 1750 Kelvin. The data suggest that when the temperature is high, as in the stoichiometric or fuel rich cases, the mixing zone is of sufficiently high temperature to sustain burning throughout the whole width of the layer. However when the product temperature is lowered, only the lower portion of the mixing layer is sufficiently hot to initiate rapid combustion. Consequently, the visible flame does not span the entire shear layer.

The flame emission measurements reinforce the notion that the heat release rate is larger for the stoichiometric and fuel-rich mixing layers. Figures 4.38 through 4.40 show the fluctuating light intensity data (heat release rate) corresponding to the flow field pictured in the bottom photograph of Figure 4.86, namely, the case of stoichiometrically mixed reactants entering the combustor at a dump plane velocity of 70 m/sec. Figures 4.38 and 4.39 show the light intensity fluctuations at locations within the region of shear layer development. The dominant fluctuating component of the heat release rate at 468 hertz increases in magnitude from an emission amplitude of 0.003, at x/LC = 0.094, to an amplitude of 0.019 at x/LC = 0.188. The constant emission from the

flame, or the steady measurements, indicate that the light emission grows from 0.02 to 0.14 at the two observation points.

During fuel-rich operation at an equivalence ratio of 1.28, Figures 4.26 and 4.27 show the same dominant fluctuating heat release rates with emission magnitudes of 0.007 at both observation locations, x/LC = 0.094 and 0.188. The steady measurements show that the light emission increases from 0.02 at x/LC = 0.094 to 0.07 at x/LC = 0.188. In both the steady and fluctuating heat release rate measurements during fuel-rich conditions, the magnitude of the heat released is less than at stoichiometric conditions, indicating that the combustion process is less intense and the temperature lower; nevertheless, the photographic evidence indicates that reaction occurs across the entire mixing layer.

At fuel-lean conditions, an equivalence ratio of 0.65, the emission from the flame is substantially lower, suggesting that the region of rapid chemical reaction may be smaller. Figures 4.23 and 4.24 show the spectral emission from the flame at x/LC = 0.094 and 0.188, respectively. The fluctuating component of heat release rate occurs at 442 hertz with an emission amplitude of about 0.003 at both measurement locations. The steady measurements indicate roughly equal magnitudes of 0.07 at both locations, also. For all measurements at x/LC = 0.094, the amplitude of flame emission observed during fuel-lean operation is at least one-half the amplitude observed during fuel-rich or stoichiometric operation. These results tend to suggest that the area of flame emission during fuel-lean operation is less than stoichiometric or fuel-rich operation, and reinforce quantitatively the observation that the visible flame occupies only a portion of the mixing layer during fuel-lean conditions.

As mentioned earlier, the interpretation of the intensity of the chemi-luminescence from the flame in this study, assumes that the intensity fluctuations are proportional to the magnitude of the heat release rate. The flame radiation is measured locally by a photomultiplier tube apparatus. The photomultiplier apparatus is not calibrated, so the magnitude of the results can not be directly related to the quantity of heat released. However, a comparison between different measurement locations or different experimental conditions can be made from the relative values of the emission amplitudes.

The fuel-air ratio effects the time required for complete combustion as well as the equilibrium temperature. Therefore, the region of rapid combustion, or visible flame, may depend upon the chemical time. If the chemical time is small compared to the fluid mechanic time of mixing, then the combustion is prompt and heat is liberated locally. On the other hand, if the chemical time is of the same order as the fluid mechanic time, then the reaction will not be complete until the gas has passed through the mixing layer.

For the current work, the picture of the time required for complete combustion, or the chemical reaction time, is based upon the work of Zukoski as described in Oates (1978). In this approach, the characteristic chemical time is experimentally determined from detailed flame blow-off studies. The advantage of this approach is that, once the chemical time has been evaluated experimentally, then the results are valid for any flameholder configuration as long as the operational limits are within the same range of chemical parameters. In the experiments to determine the chemical time, the flame is stabilized behind a right circular cylinder with its axis placed perpendicular to

the incoming flow. The flow field behind the cylinder consists of a nearly stagnant recirculating region composed of mostly burnt products, with a reacting mixing layer bordering each edge of the recirculation zone. The important parameter for this approach is a dimensionless parameter evaluated at the flame blow off:

$$\frac{Vt}{L_e} = \beta_c$$

where: V = average gas velocity in the mixing layer
t = residence time of gas in the layer
L_e = length of the recirculation zone
β_c = particular value of parameters at flame blow off.

If the turbulent mixing layer is assumed self-similar, then the expression can be rewritten as:

$$\frac{Vt}{L_e} = \left(\frac{V}{V_c} \frac{L}{L_e} \right)\left(\frac{V_c t}{L} \right) = \beta_c$$

where: L = maximum length of recirculation zone
V_c = unburnt cold gas velocity at edge of mixing layer

with $\frac{V}{V_c}$ and $\frac{L}{L_e}$ being constants for self similar layers.

Thus, at flame blow off, all constants may be combined to yield

$$\frac{V_c t}{L} = \text{constant}$$

By defining τ_c, the chemical time, as $\frac{L}{V_c}$, then at flame blow off

$$\frac{V_c \tau_c}{L} = 1.$$

So, the fluid dynamic properties are separated from the chemical properties in this approach. Dependence upon chemical properties is contained within the chemical time, and the fluid mechanic dependence in L/V_c ,which is determined from the experimental observations at flame blow off. Their experimental results indicate that the chemical time is nearly independent of the size and shape of the flameholder, but does

depend upon the fuel type and fuel-air ratio.

The chemical time is a very strong function of fuel-air ratio for a specific fuel type. For the heavy hydrocarbon fuel used in the Zukoski and Marble experiments, the minimum chemical time occurred near stoichiometric mixture ratios (an equivalence ratio of 1.05), and increased rapidly as the fuel fraction was increased or decreased. The chemical time at an equivalence ratio of 1 was about .28 msec and increased to over 2 msec for an equivalence ratio of 0.6. As the fuel fraction was increased to an equivalence ratio of 1.4, the chemical time increased to .6 msec. Consequently, changing the fuel fraction can markedly change the time required to consume the combustible mixture.

In the current study, methane is used as the fuel for the reaction. The molecular weight of methane is 16, or about 6.25 times less than the heavy hydrocarbon fuel used for the chemical time determination. Consequently, the detailed nature of the chemical time dependence upon fuel-air ratio may change slightly. The shape of the curve may change somewhat and the minimum chemical time will occur just to the lean side of stoichiometric (Zukoski, 1954). Nevertheless, the chemical times determined by Zukoski for the heavy hydrocarbon fuel are similar for methane, and act as a guideline to assess the impact of mixture ratio.

Using the aforementioned values for chemical time, and an estimate of the vortical structure propagation time within the mixing layer, the chemical time is short compared to a simple-minded estimate of the fluid mechanic time. For example, consider the propagation of a vortical structure within the mixing layer. The average speed of a structure in the low-speed layer, i.e., the top photograph of Figure 4.86, is roughly 11 m/sec. The speed of the combustible mixture above the layer is

nearly the entrance, or dump plane velocity of 22 m/sec, and the recirculation region below the layer is stagnant and very low velocity; therefore, the average is approximately 11 m/sec. The layer grows till it spans the height of the duct which is 2.54 centimeters high. If the structure is basically cylindrical, then the time required for the structure to convect the one diameter, or 2.54 cm, is about 9 msec. This fluid mechanic convection time is greater than the largest chemical time of 2 msec at an equivalence ratio of 0.60, and the combustion is thus prompt. The reactants are quickly consumed when entrained into the vortical structures when they are sufficiently high temperature to react. Consequently, the temperature of the recirculation zone appears to be the major factor for determining the location of the visible flame within the layer.

Not only is the location of the visible flame different for various operating conditions, but the growth rate of the mixing layer is different for each situation presented in Figure 4.86. Four factors may influence the growth rate of the reacting, reattaching mixing layer: (1), the axial pressure gradient; (2), periodic forcing of the mixing layer; (3), the initial condition of the boundary layer at formation of the free mixing layer; and (4), the heat release within the layer. The data suggest that neither the axial pressure gradient nor forcing is a primary factor in the layer growth. The condition of the boundary layer and heat release may contribute, but the relative importance was not able to be determined by results of this study. The following discussion will introduce the manner in which layer growth is determined and will present some discussion about the four items that may affect the growth of the mixing layer.

In Figure 4.86, the layer growth rates in each of the three pictures are different. The layer growth is determined in the fashion outlined by Brown and Roshko (1974). In their experiments, the growth of a two-dimensional shear layer is described by a linear relationship. For the current experiments, the reattaching shear layer in the early stages of development is very similar in structure to the free shear layer studied by Brown and Roshko. During early development, the mixing layer is not aware that the lower wall boundary exists, and the influence of the wall is negligible. Consequently, the reacting, reattaching layer closely resembles the free shear layer, and the same type of analysis is used to determine the growth rate.

The growth of the layer is determined experimentally from the relationship:

$$\delta' = \frac{d\delta}{dx} = \frac{\delta}{x-x_o}$$

with: δ' = visual growth rate of the layer

δ = experimental width of the layer measured 5.1 cm downstream of the flameholder

x_o = point of intersection of the tangent line drawn along the border of the layer.

Brown and Roshko found that the layer growth is a function of the velocity ratio and density ratio across the layer. For the case in which a free shear layer exists between fluids of identical density, and the velocity of the fluid on the lower side of the layer is equal to zero, the shear layer grows at a rate of 0.38. If the density of the lower side is 7 times larger than the density on the upper side of the layer, the layer growth rate increases by one-third for the same velocity ratio. If, however, the density ratio is reversed, the lower

side density becoming 1/7 as large as the upper side density, the spreading rate is reduced by 26 percent.

In the reacting, reattaching shear layer under investigation, the velocity on the lower side of the layer is not identically zero. The flow behind the flameholder, on the lower side of the layer, is, in fact, recirculating. Fluid is swept into the recirculating region from the mixing layer at the reattachment point. This provides material for growth of the layer. Even though the velocity of the fluid on the lower side of the layer is not constant and varies along the length of the layer, the flow velocity is small because this is a stagnant region. Thus, for comparison of growth rates between nonreacting and reacting layers, the velocity on the lower side of the layer may be assumed negligible.

The recirculation zone consists mainly of burnt products. The composition measurements of Williams, Hottel, and Scurlock (1949) indicated that the zone is made up of at least 90 percent products. So, a density ratio across the reacting layer of approximately 1/7 would be appropriate to assume. Overall, it appears as if the reacting, reattaching shear layer, examined in the current experiments, is governed by almost the same parameters as the free shear layer, studied by Brown and Roshko, whose growth rate was determined to be 0.28, and forms a base for comparison between the reacting layer and nonreacting layer.

Analysis of the shadowgraph records is presented in the following table. The growth rates are listed with the experimental operating conditions.

growth rate	operating condition	
0.37 0.30 0.18	22 m/sec, =0.70 22 m/sec, =1.28 70 m/sec, =1.0	configuration I
0.14	70 m/sec, =1.0	configuration I + steel wool

The off-stoichiometric conditions produce layers with larger growth rates than reported by Brown and Roshko for the nonreacting, free shear layer under similar conditions. In contrast, the stoichiometric operation produces growth rates less than the free shear layer counterpart. Obviously, the combustion, or one of the other 3 factors, plays a role in determining the growth rate of the reacting layer. As the layer evolves, it grows by entraining fresh reactants from the upper portion of the layer and hot burnt combustion products from the lower side of the layer. The data suggest that the manner in which the reactants are entrained and consumed affects the overall layer growth rate.

Brown and Roshko (1974) compiled data from several experimenters on the behavior of mixing layers. For isothermal layers with no density gradient, the agreement between experimental measurements for growth of the vorticity thickness as plotted against a velocity parameter, which is the ratio between the velocity difference and the mean average velocity across the layer, is good for experiments with both streams having non-zero flow velocities. However, rather large deviations between experimenters occur when one stream is stagnant. The measurements vary from a minimum vorticity thickness growth rate of

0.147 to a maximum of 0.219, a variation of about 50 percent from minimum to maximum. Therefore, considerable deviation exists in the published data, and the Brown and Roshko data are the ones chosen to be a baseline for the current work.

Pitz (1981) measured the reacting, reattaching layer's vorticity growth rate using laser-Doppler velocimeter measurements based upon the average layer properties. Under lean operating conditions similar to the ones in the current study, he found the layer grew 60 percent faster than the nonreacting counterpart, while, in the current study, the lean reacting layer grows about one-third faster than the nonreacting layer. Sizeable differences exist between these two experiments and perhaps the layer growth when the velocity of one stream is zero is apparatus sensitive as mentioned in Ho and Huerre (1984).

One of the factors mentioned earlier which does not appear to affect the growth rate of the mixing layer is the axial pressure gradient imposed upon the layer. The pressure gradient affects the growth of the mixing layer because the flow field consists of cold reactants above the mixing layer, and hot gases within the layer and in the recirculation zone. When a pressure gradient is imposed upon this stratified flow field, the lighter hot gases either accelerate or decelerate relative to the cool gases, depending upon the nature of the gradient. If a negative gradient is imposed, then the hot fluid will accelerate faster than the cool fluid. The mixing layer contains hot gases, so the fluid in the layer would tend to accelerate more quickly than the cool fluid above the layer. Thus, the layer tends to thin out and the growth rate decreases as the density of the gas within the layer becomes smaller. The opposite trend, or greater layer growth, occurs if

an adverse pressure gradient is applied.

The pressure distribution measured inside the apparatus is plotted in Figures 4.15 and 4.16. The pressure is normalized by the pressure measured at the first measurement location which is a measurement of the static pressure in the plenum chamber. Velocities in the plenum chamber are small, less than 2 m/sec, so that the local static pressure is almost the total pressure. The gas accelerates and the pressure falls as the reactants enter the inlet. The pressure in the inlet remains constant (stations 2 to 5) because the inlet area is constant. The flow again accelerates as it passes over the flameholder (stations 6 and 7). The pressure increases slightly from stations 7 through 9 before falling to atmospheric pressure at the burner exit.

The distance between measurement stations 7 and 9 is 16.3 centimeters, just about the reattachment length. So, the shear layer forms behind the rearward facing step flameholder in a region in which the pressure is nearly constant. In fact, for all test conditions, the pressure rises slightly as the flow expands to fill the combustor, the same type of pressure recovery observed in diffusers. The expected effect of the pressure rise, i.e., a positive pressure gradient, upon the flow field would be to increase the growth rate of the mixing layer. However, the flow visualization records show the opposite trend. For example, Figure 4.15 shows a measured pressure rise of 0.06 mmHg for the fuel-lean, 22 m/sec, stable burning situation, and Figure 4.16, an 0.66 mmHg pressure rise at stoichiometric, 70 m/sec operation. These experimental pressure data clearly suggest the layer formed at 70 m/sec should grow faster than the layer created at 22 m/sec. Yet, analysis of the shadowgraph photos reveals that the layer does not grow more

rapidly. In fact, the mixing layer formed under high-speed conditions grows at about one-half the rate of the low-speed layer. Clearly, the effect of the pressure gradient is negligible and some other factor governs the overall spreading rate of the mixing layer.

The heat released within the layer may also affect the layer growth rate, and, in fact, with the inlet velocity held constant, greater heat addition seems to reduce the growth rate of the mixing layer. For example, two different visual growth rates occur at the same dump plane velocity of 22 m/sec, namely, a growth rate of 0.37 at an equivalence ratio of 0.70 and a growth rate of 0.30 for an equivalence ratio of 1.28. The layer growth decreases by about 25 percent when the heat release within the layer is larger (Figures 4.23, 4.24 and 4.26, 4.27). The data reveal that increased heat release inhibits the growth of the layer and suggest that the heat released within the layer may modify the entrainment process of fluid into the layer.

If one assumes the entrainment process is independent of the quantity of heat released, then a larger heat release would lead to a greater growth rate. After all, the amount of fluid entrained into the mixing layer would be fixed for a certain velocity ratio across the layer. During combustion, heat is liberated and the fluid expands. Greater heat release would imply greater expansion and the layer would grow faster. The measurements contradict this argument, which indicates the entrainment process may be altered by the quantity of heat released.

Recently, much work is being done to attempt to determine the effects of periodic forcing on the growth rate of free mixing layers. In essence the growth of the mixing layer can be controlled under certain conditions by perturbing the free stream flow. The growth of

the free mixing layer has been found to depend upon the velocity ratio across the layer, the Reynolds number at the origin, the forcing frequency, and the forcing level as explained in Ho and Huang (1982). The vortical structures are created by the Kelvin-Helmholtz instability mechanism, and linear stability theory has been shown by Michalke (1964 and 1965) to describe the initial growth and development of the layer before the first vortex roll-up. In Michalke's calculations, the growth rate is a function of the Strouhal number with the peak amplification occurring near a Strouhal number, based upon momentum thickness, of 0.032. Michalke and Freymuth (1966) verified experimentally that the natural instability frequency of the mixing layer does indeed occur at this Strouhal number, and thus, forms a basis for calculation of the natural instability frequency of mixing layers.

The relationship between the periodic disturbance and the natural frequency of the mixing layer plays a major role in the growth of the layer. Ho and Huang (1982) have shown that the initial vortex formation frequency corresponds to the natural frequency or a subharmonic of the forcing frequency that is closest to but less than the natural instability frequency of the mixing layer. The periodic forcing of the mixing layer tends to create layers in which the vortical structures roll up and pair at specific downstream locations, with this roll-up position sensitive to the frequency of excitation; Ho and Huang (1982). The vortex roll-up location is, however, not very sensitive to the amplitude of forcing as described in Michalke and Freymuth (1966). Consequently, modulating the growth of the layer is most effectively accomplished by varying the frequency of excitation and not the forcing amplitude.

The natural frequency of the low-speed, 22 m/sec mixing layer is 2510 hertz based upon a Strouhal number of 0.032. This frequency is much higher than the major pressure oscillation at 468 hertz present in the combustor (Figures 4.19 and 4.20). Hence, the major velocity fluctuation imposed upon the flow occurs at 468 hertz, a nonsubharmonic of 2510 hertz. Of course, in a reacting flow field, an economical measurement of the streamwise velocity fluctuation is impractical, and the velocity fluctuation must be inferred from the acoustic calculations. Fortunately, all the major pressure oscillations are acoustic in nature and this technique is sufficient to compute the major velocity fluctuations.

However, small pressure oscillations do occur at 420 hertz for both low-speed, 22 m/sec, off-stoichiometric operating conditions (Figures 4.19 and 4.20). This frequency is the fifth subharmonic of the natural frequency, 2510 hertz. Consequently, pressure oscillations at 420 hertz may be produced by some sort of subharmonic excitation of the mixing layer. The origin of such excitation is unknown, but the level of forcing is much less than the level of forcing at 468 hertz, and thus the data suggest that the major mixing layer forcing at 468 hertz has little effect upon the layer growth.

At the higher dump plane velocity of 70 m/sec, the natural frequency of the mixing layer is very high, namely, about 14,337 hertz. This frequency is at least an order of magnitude greater than any measurable pressure oscillations; therefore, the chances for subharmonic excitation appears slim.

The state of the boundary layer at the rear edge of the flameholder is somewhat unclear at 70 m/sec, and hence, its influence upon the layer

growth. The layer growth rates for the 70 m/sec cases are close to the same value at 0.18 and 0.14, but nevertheless far greater than the ones measured at 22 m/sec. As mentioned in Ho and Huerre (1984), the condition of the boundary layer upon the layer growth rate is somewhat controversial; however, the general trend seems to be that turbulent boundary layers decrease the initial spreading rate of the mixing layer. The Reynolds number for the 70 m/sec flow velocity is definitely in the transition region at the rear edge of the flameholder. If the free stream turbulence is high, as well might be in this experiment, then the boundary layer may be turbulent and the decreased layer growth may be due, in part, to this.

From the rather limited data obtained during stable combustion in which a mixing layer forms downstream of the flameholder, the mixing layer growth rate appears to be primarily affected by the heat released within the mixing layer, and the initial condition of the boundary layer at the formation of the mixing layer. As mentioned, a systematic investigation was not implemented, but limited results tend to show these two factors are important. The axial pressure gradient and forcing appear to have smaller influences upon the growth rate of the mixing layer under these circumstances.

5.2.2 Large Vortex Formation

Under certain experimental conditions, the typical flow field described in 5.2.1 is drastically altered as shown in Figure 4.86. Instead of a steady flow of reactants entering the combustion chamber, the combustible mixture surges into the burner periodically. In the current study, this condition is referred to as a condition of combustion instability. Combustion instabilities are produced when a pressure oscillation, created by an acoustic resonance of the system, generates appreciable velocity fluctuations in the vicinity of the flameholder. The steady flow field, which is characterized by the two-dimensional reattaching mixing layer formed downstream of the flameholder, is destroyed by the presence of the large velocity fluctuations. In fact, when the instability exists, large vortices are formed near the flameholder with the same frequency as the large velocity fluctuations.

Figure 4.82 is a good example for illustration of the flow field conditions during instability. The sinusoidal curve, shown on the left-hand side of the figure, represents the pressure fluctuation for the component whose period coincides with the formation cycle of the vortex. This pressure oscillation is the fluctuation measured at the downstream edge of the flameholder during evolution of the vortex.

The photographs on the right hand side of the figure are prints obtained from the high-speed cinematography. The collage of photos illustrates sequentially the time resolved history of the vortex. Each photo shown is about every sixth frame of the recorded shadowgraph movies. Dashed lines are drawn between the sinusoidal pressure

oscillation and the flow field photographs to illustrate the elapsed time along with the flow field condition at this point in time during the cycle.

Consider the uppermost photograph as the beginning point in the vortex formation. Generation of the vortex is triggered by the sudden increase in velocity at the rear edge of the flameholder which accompanies the local fall in pressure. As the pressure decreases, the vortex grows, moves downstream, and approaches the lower wall. Notice the third photograph from the top. The dark line, originating from the rear edge of the flameholder and then bending sharply upwards and extending along the upper wall, is the reaction front. All the gas below the front is basically burnt hot combustion products. The gas entering the combustor at the upper left corner above the dark line is the fresh combustible mixture. The surge of reactants entering the combustor, due to the large velocity fluctuation, is partially entrained into the forming vortex along with the hot combustion products as the vortex grows and is convected downstream. As the vortex grows, a region of unburnt gas intrudes between the downstream face of the vortex and the burnt material farther downstream as shown in the fifth photograph from the top of Figure 4.82. The unburnt gas in this region has a large velocity component directed downward toward the lower combustor wall.

The vortex growth is such that it reaches the lower wall at a time approximately equal to three-quarters of the pressure oscillation period (picture 8). The vortex and region of unburnt reactants impinge against the combustor wall with an appreciable downward velocity, and the shadowgraph records indicate that vigorous mixing occurs between the hot products and the remaining unburnt reactants. Large turbulence,

generated by the wall interaction, increases the reaction rate locally. Consequently, the remaining reactants are consumed rapidly, producing a volumetric expansion of the region. At the same time, the pressure is rising at the rear edge of the flameholder. The volumetric expansion occurs in unison with the pressure rise and thus helps to sustain the pressure oscillation by further inhibiting flow into the combustion chamber.

The pressure at the downstream edge of the flameholder continues to rise as the remaining reactants are consumed. In fact, the pressure rise illustrated in Figure 4.82 appears to be of the same order as the dynamic pressure of the mean flow at the flameholder, causing the flow to reverse itself and propagate upstream for a brief period. After reaching a maximum, the pressure begins to decrease again and the instability phenomenon is repeated as a new vortex is created by the surge of fresh reactants into the combustor. The vortex formation occurs periodically at the frequency of the pressure oscillation which produces a large velocity fluctuation at the rear edge of the flameholder.

For the vortex evolution just discussed (Figure 4.82), the mean flow velocity is 22 m/sec and the reactants are mixed in a stoichiometric ratio. Analysis of the high-speed shadowgraph movies indicate that the large vortices are formed periodically every 5.3 milliseconds. The acoustic model predicts that the system resonant frequency sensitive to the large volume plenum chamber located upstream is 188 hertz with the configuration I geometrical constraints. Consequently, the data suggest that this resonance is driven by the energy released during vortex burning which produces the large velocity

fluctuations at the rear edge of the flameholder. The subsequent large velocity fluctuation generates a new vortex structure whose burning will reinforce the system resonance and form yet another vortex. Under these conditions the vortices are formed periodically at the resonant frequency sensitive to conditions in the plenum chamber.

Figures 4.82 and 4.83 show the effect of mean flow speed upon the instability. In both figures, the geometry (configuration I) and the fuel-air ratio (an equivalence ratio of 1.0) are identical. The velocity of the mean flow is the only variable. In Figure 4.82 the dump plane velocity is 22 m/sec, while the velocity is 40 m/sec in Figure 4.83. The shadowgraph movies reveal a large vortex structure which evolves in a very similar manner to the one formed when the velocity was 22 m/sec. In both cases, a large vortex forms periodically at 188 hertz, the system resonance associated with the plenum chamber. However, the flame-front curvature, immediately downstream of the flameholder, is different for the two velocities at the time of maximum disturbance pressure. Figure 4.82, the low velocity 22 m/sec case, shows a large flame-front curvature as the flame propagates upstream above the flameholder. As the flow velocity is increased to 40 m/sec, only a modest bowing of the flame front is observed (Figure 4.83).

At the dump plane, the pressure measurements and flow visualization both indicate that the incoming flow is severely retarded under the 22 m/sec instability velocity fluctuations, and less so at 40 m/sec. The following table shows the relationship between the normalized pressure fluctuation, i.e., the Fourier coefficient from the pressure spectra at 188 hertz, and the dynamic pressure of the gas entering the combustion chamber.

Dump Plane Velocity	Pressure Fluctuation / Static Pressure	Dynamic Pressure / Static Pressure
22 m/sec	0.0082	0.0028
40 m/sec	0.0072	0.0092

As the velocity is increased to 40 m/sec, the flow entering the combustor is not totally halted as seen in the first photograph of Figure 4.83. Instead, some fluid passes over the upper side of the flame surface as the vortex forms. However, in either case, the formation rate of the large vortex structure remains constant at 188 hertz, and a large 188 hertz component is found in both pressure spectra (Figures 4.17 and 4.18), having about the same amplitude.

Since the magnitude of the pressure oscillations for both flow speeds are similar, the analytical prediction of the acoustic velocity field, using the 22 m/sec experimental data, is an adequate description of the 40 m/sec acoustic velocity fluctuations. In this analysis, the maximum computed velocity fluctuation at the flameholder is 21 m/sec, which further reinforces the visual observations that the gas velocity entering the combustor is negligible at the point of maximum pressure for the 22 m/sec instability.

As mentioned earlier, the shadowgraph records indicate that the rate of vortex formation remains constant as the flow speed is increased from 22 to 40 m/sec. This would imply that the vortex formation rate is not determined by the mean flow velocity and, consequently, is not a Strouhal type shedding phenomena. Rather instead, the vortex shedding is governed by the acoustic excitation of the whole combustor apparatus.

If Figures 4.82 and 4.83 are compared further, it is apparent that

the propagation of the vortical structure is not greatly affected by the mean flow velocity, either. Consider the low-speed, 22 m/sec situation of Figure 4.82. The vortex reaches the lower wall after about 3.5 milliseconds and has traveled approximately 8 centimeters downstream. As the mean flow speed is increased 80 percent to 40 m/sec, Figure 4.83 indicates that the vortex formed under these conditions has only propagated about 20 percent farther downstream than the vortex formed at 22 m/sec.

In addition, the pressure spectra for both these velocities (Figures 4.17 and 4.18) indicate that the amplitude of the pressure oscillations are about the same for both test situations, 22 and 40 m/sec. Subsequently, the velocity fluctuation at the 188 hertz disturbance frequency is approximately the same for both cases. Thus, the data suggest that the propagation of the vortex appears to be primarily governed by the magnitude of the fluctuating velocity component and not the mean flow velocity.

So, the generation of the combustion instability, i.e., the creation of the large vortex structures, appears to depend mainly upon the relative magnitude of the velocity fluctuation, the ratio of fluctuating velocity to mean velocity. If the velocity perturbation is of sufficient magnitude to form a large vortical structure, then the propagation of the vortex seems to be controlled by the actual amplitude of the velocity fluctuation.

In order to study the above supposition, the geometry of the apparatus is changed so that a different set of acoustic system modes can be excited. Figure 4.84 shows prints made from the high-speed flow visualization of the configuration II apparatus. The dump plane

velocity for the flow field illustrated in this figure is 50 m/sec and the equivalence ratio is unity. Therefore, under these conditions, the geometry of the system is different from the two instability cases presented earlier, but the stoichiometry which governs the chemical reaction rate is the same, and the flow speed is somewhat larger. Analysis of the time resolved flow field, using the high-speed motion pictures, indicates that the vortex formation occurs at 520 hertz under these experimental conditions. The photographs in the figure are not as clear as the ones obtained for the 188 hertz vortex formation because of the higher gas speeds, but these show that the evolution of the vortex formed at 520 hertz resembles that of the vortices formed at 188 hertz.

For example, Figure 4.84 shows that the vortex forms, grows, and reaches the lower wall in about three-quarters of the cycle of the pressure oscillation, creating the 520 hertz disturbance. This is the same as the vortices formed at 188 hertz (Figure 4.82). Vortex interaction with the lower wall occurs in the seventh picture from the top of Figure 4.84, the same point as the two previously discussed cases (Figures 4.82 and 4.83). Yet, the elapsed time is much less because the shedding frequency has increased. During 520 hertz shedding, the vortex reaches the wall in about 1.26 milliseconds. Since the time required for the vortex to propagate downstream and reach the lower wall is much less, the magnitude of the velocity fluctuation at the rear edge of the flameholder must be much larger than the velocity fluctuation required to form vortices at 188 hertz.

The data indicate that this is indeed the case. The high-speed flow visualization (the uppermost photograph of Figure 4.84) shows that the flame front is nearly vertical at the rear edge of the flameholder

when the fluctuating pressure is near a maximum. This implies the fluctuating velocity is on the order of the mean flow velocity of 50 m/sec. In addition, the amplitude of the pressure oscillation, at the vortex shedding frequency of 520 hertz, is over seven times larger than the oscillations encountered during 188 hertz vortex formation. Figure 4.17 shows the amplitude of the 188 hertz pressure oscillation to be 0.0082, while Figure 4.55 shows the amplitude of the 520 hertz oscillation to be 0.0605. So, the fluctuating velocity at the frequency of vortex formation is much larger, 50 m/sec, for the 520 hertz vortex shedding, than the velocity fluctuation of 22 m/sec observed during 188 hertz shedding.

Two of the vortex formation cases presented thus far are very similar, namely, the 520 hertz, 50 m/sec case and the 188 hertz, 22 m/sec case. In both situations, large vortical structures form at the rear edge of the flameholder at the frequency of the large velocity fluctuations. In addition, the velocity fluctuations in the vicinity of the flameholder are of the same order as the mean flow velocity, and these large amplitudes severely retard the incoming flow (Figures 4.82 and 4.84). Notice that the ratio of the vortex formation frequencies, 520 and 188 hertz, is just about 2.7. If the magnitudes of the velocity fluctuations are assumed to be 50 and 22 m/sec, then the ratio between the 520 hertz velocity fluctuation and the 188 hertz velocity fluctuation is approximately 2.3. The velocity fluctuation ratio, 2.3, is nearly the ratio between the vortex formation frequencies, 2.7. Consequently, for similar flow fields, the data suggest that the velocity fluctuations increase proportionally with the vortex formation frequency so that higher frequency instabilities require larger velocity

fluctuations. This result implies that any number of system resonant modes may be excited to produce combustion instabilities depending upon the geometry of the system.

For a stoichiometric reactant mixture ratio, the large vortex, produced by the sizeable velocity fluctuation, grows and reaches the lower wall of the combustor within the cycle of formation. The convection speed for this type of vortex evolution depends upon the magnitude of the velocity fluctuation. However, if the time required for the chemical reaction is altered, then the burning within the vortices will change so that the characteristics of the vortex evolution will be affected. The presentation of the next case illustrates the effect of changing the chemical time delay.

Figure 4.85 shows the flow field generated by the configuration II apparatus during off-stoichiometric conditions. The vortex formation, illustrated in this figure, occurs when the equivalence ratio is 0.7 and the dump plane velocity 40 m/sec. Analysis of the shadowgraph movies indicate the vortices form at 449 hertz, a system resonant frequency sensitive to conditions within the combustion chamber. The vortex evolution, however, is much different under these fuel-lean conditions because of the relatively small velocity fluctuations at the rear edge of the flameholder. Since vortices are shed at 449 hertz, the pressure oscillation required to produce a sizeable velocity perturbation must be large. Indeed, the pressure oscillations are substantial. Figure 4.54 shows the peak-to-peak magnitude of the pressure oscillation to be 10 percent of the local static pressure. However, the velocity fluctuations at the rear edge of the flameholder are much smaller than would be expected if the velocity fluctuations

scale with the vortex formation frequency. In fact, the computation of the velocity fluctuation, using the acoustic model and the experimental data, indicates a fluctuation magnitude of 13 m/sec at the flameholder. Hence, the acoustic fluctuating velocity is about one-third of the mean velocity and the perturbance introduced by the acoustic resonance is relatively small compared to the previous situations where the disturbance was approximately equal to the mean flow. Consequently, the vortex evolution is quite different than any one of the other combustion instability cases.

Since the velocity fluctuation is relatively small, the expectation is that the propagation velocity of the vortex structure would be less than that found in the examples discussed above and, in fact, this is the case. The shadowgraph records (Figure 4.85) show that, for this 449 hertz instability, a vortex formed at the point of maximum pressure does not reach the lower combustor wall within the cycle of formation as in all the previously discussed cases. Instead, the vortex does not impinge against the wall until well into the next cycle after another vortex has been shed from the rear edge of the flameholder.

The mean flow speed in this situation with vortices formed at 449 hertz is 40 m/sec, not radically different from the 520 hertz shedding case in which the velocity was 50 m/sec. Yet, the frequency of vortex shedding has changed from 520 hertz to 449 hertz by changing the fuel-air ratio of the reactant mixture. Remember before, shedding at 188 hertz could be established with flow velocities differing by 80 percent (22 to 40 m/sec), and the vortex shedding frequency seemed insensitive to the mean flow speed. But, the mixture ratio was held constant in that situation so that the evolution of the vortex was similar for both

velocities. Now, the stoichiometry has been changed, leading to two different possible excitation frequencies, 520 or 449 hertz. Thus, the instability frequency is sensitive to the fuel-air ratio. At the lean fuel mixtures, it appears that the actual instability mechanism is altered, producing vortices whose evolution and characteristics are different than anticipated by the previous test results.

The vortices which are formed at 188 hertz and 520 hertz are similar because the vortex structures form, grow, and reach the lower wall at approximately the same point in the formation cycle for both frequencies. Consequently, the velocity perturbation required for the 520 hertz vortex shedding needed to be larger than the perturbation required for the 188 hertz vortex shedding. Furthermore, the magnitude of the velocity fluctuations increased by a scaling factor directly proportional with the frequency increase. However, evolution of the 449 hertz vortex is quite different. A combustion instability still exists in that large vortical structures are formed behind the flameholder (Figure 4.85). However, during 449 hertz vortex formation, the velocity fluctuation at the rear edge of the flameholder is relatively small, 33 percent of the mean flow speed. Consequently, the vortex propagation speed is substantially less than the propagation velocity of the vortices shed at 520 hertz, even though the frequency of shedding has only decreased 12 percent. The entire shedding phenomenon is altered by changing the fuel-air ratio, because the time required to complete the chemical reaction process is a strong function of the fuel-air ratio, as discussed in section 5.2.1. If the mechanism sustaining the 188 or 520 hertz instabilities depends upon a prompt release of energy when the vortex and unburnt reactants impinge against the lower combustor wall,

then a change in mixture ratio would inhibit rapid combustion and the prompt release of energy. Thus, the chemical time enters the problem in a dramatic fashion.

The chemical time delay is small at stoichiometric mixture ratios. As Zukoski discusses in Oates (1978), the chemical time is on the order of 0.2 milliseconds for a typical stoichiometric hydrocarbon-air flame. This chemical time value is only about 10 percent of the oscillation period for the 520 hertz vortex shedding. Thus, the time required for reaction is small compared to the period of oscillation, and the combustion is prompt in the sense that it is small with respect to the vortex formation time. In contrast, the chemical time for an equivalence ratio of 0.7 is just about an order of magnitude greater, or about 2 milliseconds. Now, the chemical reaction time is of the same order as the vortex formation period and the combustion is not prompt because the reaction is not completed within the cycle of vortex formation. Consequently, the chemical time delay influences the matter in which the heat is released during the combustion process, altering the energy feedback, which, in turn, affects the mechanism controlling the instability, and the resulting vortices are generated at a different rate in a different fashion.

The chemical time delay is a strong function of mixture ratio. Furthermore, the time delay can be significantly different for different fuel types. For example, the chemical time for hydrogen is roughly ten times smaller than for a hydrocarbon fuel. Consequently, the possibility of exciting any number of the system resonance frequencies exists, depending upon the fuel type chosen and the mixture ratio selected.

I would now like to turn to a discussion of the data concerning the heat release fluctuations. During combustion instability, the heat released at a specific location within the combustion chamber is quite different than during stable burning because the burning within and around the large vortex structure alters the heat addition process. The light emission measurements show a very strong component of the heat release rate, much larger than ones encountered during stable burning, at the frequency of vortex shedding. The light emission from the flame is measured at the same three locations used during stable combustion: x/LC = 0.094, 0.188, and 0.344. These measurements shed insight on the manner in which heat is released. Since this is a key to the mechanism which sustains the combustion instability, the flame emission measurements for each instability case is discussed in some detail in the following paragraphs.

The first case of interest is the 188 hertz vortex shedding case sustained with the configuration I apparatus and 22 m/sec dump plane velocity under stoichiometric mixture ratio. Figures 4.29 to 4.31 show the frequency resolved light radiation measurements for the three locations. At all positions, the dominant mode of heat addition is at the system resonance of 188 hertz associated with the plenum chamber. The Fourier coefficients from the light intensity spectrums show the quantity of heat released, at 188 hertz for the position x/LC =0.094, is three times larger than the amount of heat released at 457 hertz, the system mode sensitive to the combustion chamber conditions. As the vortex grows and is convected downstream, the proportional amount of heat released at 188 hertz increases. At x/LC = 0.344, the ratio of heat released at 188 hertz to heat released at 457 hertz is over 12

times greater. So, the data suggest that a large fluctuation occurs in the heat release rate at 188 hertz, which is produced by the burning process of the vortex.

The magnitude of the resultant pressure oscillations for this test condition (Figure 4.17) shows that two primary oscillations occur at 188 and 457 hertz. Furthermore, the amplitude of the two pressure components are nearly the same inside the burner at x/LC = 0.0. Thus, it appears as if a large amount of energy is being released to sustain the plenum chamber resonance at the same magnitude as the combustor resonance inside the burner itself. Upstream in the plenum chamber, the pressure oscillations exist primarily at 188 hertz as shown by the acoustic model computation (Figures 4.3 and 4.4) for this operating condition. The fluctuating combustion process adds energy to the acoustic field in a manner to sustain the large amplitude resonance oscillations in the plenum chamber. A much smaller energy input is required to maintain the combustor resonance at the same magnitude as the plenum resonance in the burner.

As the flow speed is increased to 40 m/sec the pressure oscillations (Figure 4.18) inside the combustor do not appreciably change in frequency content or magnitude. However, the light radiation measurements (Figures 4.32 to 4.34) indicate the heat release is somewhat different. At the position nearest the flameholder, x/LC = 0.094, the fluctuations at 188 hertz are approximately equal to the fluctuations at 457 hertz. The magnitude of light oscillations become larger as the vortex moves downstream. In fact, the magnitude of the oscillations at x/LC = 0.344 is 5.6 times larger than the magnitude of the oscillations at x/LC = 0.094. At the higher velocity, 40 m/sec, the

magnitude of the 188 hertz radiation measurements are smaller than the 22 m/sec counterpart at each measurement location. This seems appropriate because the flow visualization indicates the vortex travels about 20 percent farther downstream at the higher velocity. Consequently, the vortex formed at 40 m/sec is not as large at the observation point as a vortex formed at 22 m/sec, and thus, the emission measurements are somewhat smaller at these locations. However, the flow visualization records also indicate that not all the combustible mixture is burnt within the vortical structure formed when the dump plane velocity is 40 m/sec. Some gas passes over the vortex and is burned further downstream.

Therefore, the overall effect of increasing flow speed on the 188 hertz light fluctuation is to decrease the quantity of heat released by the burning in the vortex at the plenum chamber resonance frequency, i.e., the instability frequency. The light fluctuations decrease at least by a factor of two which appears to affect the magnitude of the pressure oscillations measured within the combustor. Figures 4.18 and 4.17 show that the magnitude of the 188 hertz pressure oscillation at the 40 m/sec dump plane velocity is about 12 percent below the same frequency oscillation at 22 m/sec. Since this is not a huge decrease in the pressure oscillation, the data would indicate that there exists some threshold in which the quantity of heat, being added periodically to the flow field at the instability frequency, will produce an actual combustion instability. If the fluctuating heat added at a mode capable of producing large velocity fluctuations near the flameholder is above some threshold value, then a combustion instability may result. The unstable flow field formed under such conditions is weakly dependent

upon the mean flow velocity. Of course at some point, the mean flow speed will be increased to a value such that the energy supplied during vortex burning will be insufficient to sustain the relatively large velocity perturbations, and the instability will die out.

The experimental results indicate that the heat addition to the flow field occurs in phase with the acoustic pressure oscillations during the time the vortex forms, grows, and impinges against the lower combustor wall. For example, Figure 4.51 shows the flame radiation and pressure oscillation when the velocity of the gas entering the combustor is 22 m/sec. The three sets of curves show the light radiation and filtered pressure oscillation at three measurement locations. Heat is released more or less at a single frequency of 188 hertz (Figures 4.29 and 4.30), while the pressure oscillations occur at two frequencies, 188 and 457 hertz (Figure 4.17). Consequently, comparing oscillations at the heat release frequency requires filtering the pressure signal to highlight the low-frequency pressure component, and the pressure traces in Figure 4.51 are filtered. The upper two curves of this figure show the time sequential heat release rate at $x/LC = 0.094$ and the filtered pressure oscillation at the dump plane, $x/LC = 0$. The local heat release rate and pressure oscillation are just about in phase at this location. Furthermore, Figure 4.92 shows the location of the vortex relative to the light emission measurements. The peak emission occurs when the vortex passes the measurement station and falls as the vortex travels downstream. It is interesting to note that a small rise in emission is observed as the flame surface, preceding the next oncoming vortex, passes the observation window. As this flame surface passes, emission decreases until the next vortex moves past the photomultiplier's view.

Thus, the heat release is connected to burning within the vortex, and at x/LC = 0.094, the vortex is at a position such that the local pressure oscillation and heat release rate are in phase.

The Rayleigh criterion (Strehlow 1979) states that energy supplied to the acoustic field amplifies, or drives, the pressure oscillation if the local energy release is positively correlated with the naturally available presure fluctuation. Mathematically, the criterion may be expressed as:

$$\Delta E_{cycle} = \int_{cycle} p'q' \, dt \; .$$

Since the 188 hertz pressure oscillation and flame emission are approximately in phase at x/LC = 0.094, the integral is positive, and energy is supplied to the oscillating flow field.

Farther downstream at x/LC = 0.188, the middle set of curves in Figure 4.51 show the simultaneous light and pressure oscillations for this instability case. The figure reveals that the pressure is still primarily in phase with the heat addition at this location. The local magnitude of the pressure oscillation is about the same, since the wavelength of the disturbance is over 33 centimeters, but the magnitude of the heat release rate is twice as large as it was at x/LC = 0.094 (Figures 4.29 and 4.30). Since the heat release rate and pressure are primarily in phase, the net energy addition to the flow field as indicated by the Rayleigh criterion is larger, and more energy is being fed into the acoustic field as the vortex impinges against the wall.

At the farthest downstream measurement location, x/LC = 0.344, the last set of curves in Figure 4.51 shows the light emission and pressure oscillation almost totally out of phase. Even though the heat released

at this location is over 5 times larger than at x/LC = 0.094, no net driving results. In fact, the evaluation of the integral yields a negative energy change. Thus, energy is being removed locally from the acoustic field, tending to damp out the oscillations. Figure 4.92 indicates the burning vortex has not yet reached this downstream light observation position within the period of oscillation associated with the 188 hertz oscillation. As the gas is convected farther downstream, the local pressure oscillation falls as the gas approaches the exit of the burner. Visual observation of the flame inside the combustor indicates that the burning is nearly completed within the initial 20 centimeters of the combustor, as no visible flame is observed farther downstream. Consequently, energy addition or abstraction to the acoustic field is small at the rear portion of the combustor, and the main features of the energy supply mechanism are represented by measurements of the pressure and emission at the three locations discussed.

Figure 4.52 shows the simultaneous emission and pressure measurements for vortices formed at 188 hertz when the flow speed is increased to 40 m/sec. This figure and Figures 4.32 to 4.34 indicate that the heat is released periodically at 188 hertz as in the 22 m/sec case. Pressure and heat release are in phase at the first two measurement positions, x/LC = 0.094 and 0.188, as before. However, in this higher speed case, the pressure and heat release are somewhat in phase at the farthest downstream light measurement location, x/LC = 0.344. As mentioned earlier, the vortex moves slightly farther downstream as the mean flow speed increases, and the increasing vortex travel shows up in this measurement. Further downstream, the pressure

and heat addition are out of phase and energy is removed from the acoustic field. So, the method of energy addition to the mean flow field is similar to the 22 m/sec vortex shedding instability.

The measurements obtained for the 188 hertz vortex shedding at 22 and 40 m/sec are performed under steady state conditions in that the pressure oscillation and vortex formation are repeatable and continuous. Thus overall, no net energy is added to the system. Since the Rayleigh criterion can only be invoked locally, it provides the means to identify local regions of energy input or extraction. Consequently, the data indicate that burning within the vortex, from the time of initial vortex formation till after wall impingement, supplies net positive energy to the flow field. Consequently, this region can be identified as the key energy input device sustaining the large pressure fluctuations, which, in turn, generate sizeable velocity perturbations at the rear edge of the flameholder.

The third instability case of interest is the 520 hertz vortex shedding. Figures 4.63 to 4.65 show the light radiation results from the experimental test at the three standard measurement locations. Major fluctuations in flame radiation occur at 520 and 457 hertz. From the eigenvalue computations, both the 520 and 457 hertz oscillations are system resonant modes, with the 457 hertz oscillation a system mode associated with the combustor. Two major frequencies are dominant in both the emission and pressure spectra, whereas before, during 188 hertz shedding, the major fluctuation in light emission occurred at the shedding frequency.

Since the velocity fluctuations sustained at the dump plane are approximately equal to the mean flow speed for both the 22 m/sec, 188

hertz instability case and the 50 m/sec, 520 hertz instability case, a comparison between the light emission results is informative. During the 188 hertz shedding, the magnitude of the light oscillations (Figures 4.29 to 4.31) increases as the vortex travels downstream. The opposite is found during 520 hertz shedding (Figures 4.63 to 4.65), where the light intensity decreases at each successive downstream measurement location. One possible reason for the difference is the strength of the velocity fluctuation creating the vortex. The velocity fluctuation during 520 hertz shedding is 2.3 times larger than the velocity fluctuation at 188 hertz shedding. The vortex reaches the lower combustor wall in a shorter time and in a shorter distance (Figure 4.84 and 4.82). The wall impingement location is near the radiation observation position at x/LC = 0.094 for the 520 hertz shedding, and near the observation point at x/LC = 0.188 for the 188 hertz shedding. Notice that the magnitude of light fluctuation at x/LC = 0.094, for the 520 hertz shedding, is nearly equal to the amplitude of the 188 hertz oscillation at x/LC = 0.188. Consequently, the light emissions at both shedding frequencies are close to the same value for the point at which the vortex impinges against the combustion chamber wall.

Even though the magnitudes of the light radiation measurements at the shedding frequency are nearly equal at impingement, the amplitude of the resultant pressure oscillations are much different. During 520 hertz shedding, the amplitude of the pressure oscillations at 520 hertz are about 7 times larger than the 188 hertz pressure oscillations at the dump plane. The analytical computation of the acoustic pressure distribution in the system show that, at the frequency of instability, the maximum pressure oscillation occurs in the plenum chamber for the

188 hertz instability (Figure 4.3), and in the combustor during the 520 hertz instability (Figure 4.7). These pressure data imply that energy addition, for the 520 hertz instability, occurs in the section of the apparatus where the maximum pressure fluctuation occurs. In contrast, the energy input, provided by the combustion, is removed from the location of maximum pressure oscillation for the 188 hertz instability.

In addition, the computed acoustic velocity distributions for these two instabilities show that the velocity fluctuation, inside the combustor near the flameholder (x/LC slightly larger than 0.0), are quite different at the two frequencies of instability. For the 188 hertz instability, Figure 4.4 shows that the velocity fluctuation near the flameholder is nearly equal to the fluctuation at the exit of the combustor, because the wavelength of the disturbance is very long, on the order of 4 meters. However, Figure 4.8 shows that the velocity fluctuation is near the minimum value close to the flameholder during the 520 hertz instability. Consequently, the pressure oscillations required to produce a large velocity fluctuation in the vicinity of the flameholder needs to be substantially larger to support instabilities at 520 hertz, and the experimental pressure results indicate that this is indeed the case.

The data also suggest that not only is the pressure oscillation larger during the 520 hertz instability, but that the energy supplied to the acoustic field is greater for this instability, and produces the large velocity fluctuation which creates a vortex that forms, grows, and reaches the combustor wall in less than one-half the time. The Rayleigh criterion states the energy supplied to the acoustic field is related to the product of the magnitude of the heat release rate and pressure

oscillation. As mentioned, the heat released at the shedding frequency is approximately the same for both the 520 and 188 hertz instabilities, but the pressure oscillation is about an order of magnitude larger for the 520 hertz shedding. Since the evolution of the vortices during both instability cases is similar, it is reasonable to assume that the relative phase relationship between the heat release rate and pressure oscillation is the same for both cases, and, as such, the Rayleigh criterion implies that the energy supplied to the acoustic field during 520 hertz shedding is larger than during 188 hertz shedding.

Another major difference between the 520 hertz instability and the 188 instability is the quantity of heat released at the system mode associated with the combustor, 457 hertz. The light intensity measurements during the 188 hertz instability at the system mode attributed to the combustor are about constant amplitude at each measurement location (Figures 4.29 to 4.31). The magnitude of the emission at 457 hertz is an order of magnitude less than the 188 hertz emission. However, during the 520 hertz instability, the magnitude of the 457 hertz light emission is over 4 times larger at x/LC = 0.094 than the 457 hertz emission for 188 hertz vortex shedding. Downstream at x/LC = 0.344, the emission is 7.5 times larger. Consequently, the energy supplied to the 457 hertz modes is larger during the 520 hertz instability, and the measured 457 hertz pressure oscillations are over 7 times larger than those observed during the 188 hertz instability. Large quantities of heat are added to two system modes, 457 and 520 hertz, during the 520 hertz instability, but the major heat release during the 188 hertz instability occurs at a single system mode, the system resonant frequency attributed to the plenum chamber.

In Figures 4.63 to 4.65 large emissions appear to occur at 71 hertz. The 71 hertz component is due to the nonsteady nature of the heat addition process. The 520 hertz frequency is determined by analysis of the high-speed movies which have limited resolution. If the light emission data are examined closely, the spectra reveal an emission at 528 hertz. Since the difference between 520 and 528 hertz is less than 2 percent, introducing a 528 hertz component via one measurement and a 520 hertz component via another seemed cumbersome and was avoided. However, 71 hertz is the difference between light emission at 528 and 457 hertz, and obviously, the 71 hertz component in the light emission spectrum is a beat phenomenon. The amplitude of the pressure oscillations are stochastic in nature and vary with time; consequently, the 71 hertz component shows up in the experimental data as a result of the unsteady nature of the process.

The final instability mode for which emission data was gathered is the off-stoichiometric, 40 m/sec, 449 hertz instability case. Figures 4.60 to 4.62 show the light emission characteristics of the flame during 449 hertz vortex shedding. A single dominant heat release at 449 hertz, the system mode sensitive to combustor conditions, is present at all 3 measurement locations. The magnitudes of the light emissions at 449 hertz are not substantially different than the corresponding emission measurements, at the system resonance attributed to the combustor mode of 457 hertz, encountered during the 520 hertz instability. The table below lists the Fourier coefficients for the light intensity, at the system resonance attributed to the combustor, for the 3 measurement locations of both instabilities.

Light Emission	Fourier Coefficients at Combustor Resonance	
	520 hertz shedding (50 m/sec, phi=1)	449 hertz shedding (40 m/sec, phi=.7)
I′(.094)	.069	.077
I′(.188)	.071	.102
I′(.344)	.119	.120

As the table illustrates, the lean mixture ratio does not greatly affect the light intensity, i.e., the heat release rate fluctuations, at the system mode influenced by the combustor. However, the mixture change eliminates heat release at 520 hertz, and the 520 hertz vortex shedding ceases. Instead, vortices form at 449 hertz, whose evolution, as mentioned earlier, is different from any of the other three instabilities.

A third form of information about the vortex is obtained by making a quantitative analysis of the flow visualization records, in order to have some feel for the speed at which the vortex travels downstream. The high-speed motion pictures are used to compute the vortex velocity. Two characteristic points are traced throughout the formation cycle so that the movement of the vortex can be analyzed. First, the outer combustion front which preceds the vortex is used to find the approximate point at which the vortex reaches the combustor wall. This outer front as defined is shown in Figure 4.91. The second point, or inner front, is also shown in the same figure. It is the location of the front portion of the vortex. A frame-by-frame analysis of the

movies yields the position of these fronts at discrete points in time. Consequently, the velocity of the fronts can be computed by determining the distance traveled between two movie frames, and dividing this distance by the time interval between frames.

An example of a computed velocity diagram is shown in Figure 4.87, for the 188 hertz, 22 m/sec instability case. The solid line drawn through the circled data points represents the velocity time history of the inner front, and the line through the triangled points represents the velocity of the outer front. The flow is nearly stopped at time equal to zero, and accelerates as the vortex begins to form. After the vortex is formed, both fronts propagate downstream at nearly constant velocity. The inner and outer fronts move at approximately the same speed from time equal to 1.8 msec to about three-quarters of the way through the cycle. At this point in time, the two curves diverge. The outer front undergoes an acceleration and the velocity increases, while the inner front velocity decreases. The divergence in the two curves corresponds to the point in the cycle at which the vortex reaches the lower combustor wall. The enhanced mixing which occurs at this point rapidly combines fresh reactants with hot burnt products, and rapid combustion takes place in the region between the inner and outer fronts. Consequently, the volumetric expansion of this region causes the inner front to slow and the outer front to accelerate. The emission measurements indicate that large quantities of heat are released during this process, which provides energy for reinforcement of the system resonant frequency associated with the plenum chamber.

Figure 4.88 shows the front movement for the 188 hertz instability when the dump plane velocity is increased to 40 m/sec and the

equivalence ratio is one. The vortex evolution at 40 m/sec is similar to the 22 m/sec evolution so that this velocity diagram is not unlike the one constructed for the 22 m/sec instability (Figure 4.87). The point in time at which the velocity of the outer front becomes constant is just about the same as found for the 22 m/sec , 188 hertz instability. Furthermore, the duration of the constant velocity vortex propagation is nearly the same for both 188 hertz instabilities. The actual velocity magnitudes of the two instabilities during this constant velocity propagation are similar: 20 m/sec for the situation in which the inlet velocity is 22 m/sec, and 25 m/sec for the case in which the inlet velocity is 40 m/sec. The inner and outer fronts diverge as the vortex nears the combustor wall. The time at which the inner and outer fronts diverge appears to be somewhat earlier in the higher speed case. However, at the higher velocity, the inner front is not as clearly defined (Figure 4.83); therefore, pinpointing the location of the inner front from the shadowgraphs left room for error. Consequently, the location of the actual point of divergence may be somewhat inaccurate. Nevertheless, the two fronts do diverge, indicating the presence of volumetric expansion between the two fronts, as the vortex impinges against the wall and rapid combustion occurs.

Figure 4.89 shows the front movements as the geometry is changed so that a combustion instability is produced at 520 hertz. The curves drawn through the data points are only a crude estimate of the front propagations because scattering among the data points is substantial. A vortex cycle occurs every 1.9 milliseconds. Thus, the high-speed camera could only capture about 17 frames per cycle as compared to 45 frames for the low-speed 188 hertz instability. Consequently, the time

resolution is much coarser, and the definition of the actual fronts is difficult because of image blurring created by the high velocity gas movement. Nevertheless, an attempt is made to trace the movement of the inner and outer fronts. The results, Figure 4.89, show the same general trend as found in the 188 hertz instabilities. The vortex forms, accelerates, and reaches a nearly constant velocity of about 40 m/sec. This speed is roughly twice the velocity measured for the 188 hertz instability. The two fronts diverge at about the same relative point in the cycle as the vortex impinges against the wall. The figure indicates that the divergence rate is larger during the 520 hertz instability. This seems appropriate because the velocity fluctuations, both measured and calculated, are substantially larger during the 520 hertz instability than the fluctuations measured during the 188 hertz instability.

As the flow speed and equivalence ratio are lowered to 40 m/sec and 0.74, respectively, Figure 4.90 shows that the vortex motion is substantially different from the three other instability cases discussed. The vortices formed during this 449 hertz instability move far more slowly than the vortices formed during the 520 hertz instability. Since the vortices move slowly and the frequency of vortex formation does not change appreciably, the motion of the vortex can be observed over two cycles of oscillation as shown in Figure 4.90. No strong divergence of the inner and outer fronts is observed within the cycle of vortex formation. In fact, the data indicate that the two fronts move along at about the same rate in the later half of the cycle.

Following the vortex through the second cycle, a divergence of the fronts seems to be indicated in the first quarter of the cycle.

However, the data show no strong divergence and the resolution is less than impressive. The two fronts then seem to exhibit no strong divergence for the remainder of the second cycle. Both fronts tend either to accelerate or decelerate in unison, although the actual velocity of the inner front appears to be less than the outer front.

The data plotted in Figure 4.90, from the high speed movies during the 449 hertz instability, indicate that the movement of the vortex during the cycle of formation is substantially different than the movement of the vortices found during the three other instability cases (Figures 4.87, 4.88, 4.89). The inconsistent vortex movement during the 449 hertz instability suggests that the burning within the vortex and its surroundings is quite different than the other instability cases. Consequently, the heat addition and energy feedback mechanism may be different in this situation.

5.3 Mechanism for Instability

The model for the feedback mechanism leading to combustion instability is based upon the large vortex and the combustion within. A large velocity fluctuation in the vicinity of the flameholder produces a large vortical structure. It grows rapidly and impinges against the lower combustor wall at an elapsed time equal to about three-quarters of the disturbance period. At impingement, vigorous mixing occurs between the remaining unburnt reactants and the hot combustion products, which produces an increase in the heat release rate. The mechanism for sustaining the resonant excitation, which triggers vortex formation via a large velocity fluctuation, is connected with burning inside the

vortex. Measurements of the light emitted from the flame show that the local pressure and radiation are basically in phase, from initial vortex formation until after the vortex has impinged against the combustor wall. In addition, the magnitude of the radiation increases rapidly as the vortex grows. If the assumption is made that the radiation fluctuations are roughly proportional to the fluctuations in the heat release rate, then as the vortex evolves, the data suggest that the amount of energy fed into the flow field continues to increase until the vortex has grown and interacted with the wall, with the maximum energy input at the impingement location. Rayleigh's criterion states that heat addition, in phase with the local pressure oscillation, places net energy into the acoustic flow field. Thus, the burning vortex is the energy input device.

When an instability is observed, it occurs at a frequency which is an acoustic resonant mode of the system. Large velocity fluctuations are produced in the vicinity of the flameholder by the acoustic field. The subsequent burning of the combustible mixture within these vortices generates unsteady heat addition. This fluctuating heat release feeds energy into the acoustic field. The excitation of naturally available acoustic modes requires a minimal energy input to produce large velocity fluctuations and hence, resonant modes are most easily excited by the energy released during combustion.

The mixture velocity does enter the problem in that the ratio of the fluctuation velocity to mean velocity, not the actual magnitude of the velocity perturbation, is important. The ratio determines whether or not a vortex is formed periodically at the frequency of the velocity fluctuation at the flameholder. So as the mean flow velocity increases,

a stronger fluctuation is required to produce a vortex. For some limiting velocity, the feedback will be too weak to produce the necessary amplitude of fluctuation and the instability will die out.

The magnitude of the velocity fluctuation seems to be directly proportional to the frequency of shedding for the vortices which are formed at stoichiometric mixture ratios. This implies that excitation of higher frequencies requires larger velocity fluctuations, and subsequently implies that the energy supplied to the acoustic field must be larger for higher frequency instabilities. The experimental data suggest that the heat released during vortex evolution is nearly the same for all shedding frequencies, but the pressure oscillations are larger at the higher instability frequencies. Evaluation of the local energy supplied to the acoustic field, employing the Rayleigh criterion, would indicate greater energy is released, when the pressure oscillation is larger, because the energy released is related to the product of the pressure oscillation and heat release rate. If the proper amount of energy can be supplied to the acoustic field in an appropriate manner, any number of system resonant modes may be driven leading to instabilities which may occur over a wide range of frequencies.

The rate of combustion and the subsequent heat released depend strongly upon the fuel type and fuel-air mixture ratio. The experimental observations indicate the interaction of the vortex with the combustor wall increases the local heat release rate. Therefore, the time delay between the mixing and combustion plays an important role in the mechanism. Remember, the chemical time can change by an order of magnitude from 0.2 milliseconds to 2 milliseconds by changing the equivalence ratio from 1.0 to 0.6. Consequently, at lean mixture

ratios, the chemical time becomes a fair fraction of the period of oscillation. For lean fuel-air ratios, the chemical time will influence the frequencies which can be sustained by the feedback mechanism. In addition, the energy available to sustain the oscillations is reduced as the fuel-air ratio is reduced, and this may affect the regimes in which the instability can exist.

The experimental results also show that the instability may be halted entirely by changing the fuel fraction of the combustible mixture. Formation of large vortical structures at an acoustic resonant frequency ceases, and a mixing layer is formed downstream of the flameholder. The experimental results reveal that the feedback mechanism proposed at the beginning of this section may be altered by the stoichiometry. The shedding frequency of the large vortices can be shifted to another system resonance frequency by decreasing the fuel-air ratio, and the mechanism sustaining the large velocity fluctuations is much different. The large vortices do not form, grow and reach the combustor wall within one period of oscillation as described by the proposed mechanism for vortices formed at stoichiometric mixture ratios. Instead, multiple vortices form and the internal feedback mechanism is altered. Nevertheless, the key to the instability, or large vortex formation, still appears to be the large velocity fluctuations present at the flameholder created by energy supplied to the acoustic resonant modes of the system by unsteady combustion within the vortex. Consequently, any number of system modes may be excited given a specific fuel type and fuel-air ratio by a variety of mechanisms. This study has attempted to explore fully one of these mechanisms in detail.

I would like to emphasize that the instability mechanism proposed

in this study is acoustic in nature, not a result of the hydrodynamic instability in the forced free shear layer. As mentioned earlier in Section 5.2.1, Michalke and Freymuth (1966) predicted the instability frequency in free shear layers by using a linearized inviscid approach. This calculation appears to predict, with good accuracy, the vortex formation in free shear layers. As low-level forcing is applied near the frequency of instability in the shear layer, vortex pairing can be enhanced (Oster and Wygnanski, 1982). Ho and Huang (1982) found that several discrete vortices, a maximum of 4, formed at the natural instability frequency of the layer and were displaced laterally to form a larger vortex as the amplitude of the forcing was increased (on the order of 2 percent). This process was referred to by them as collective interaction, and the new large vortex composed of the smaller vortices formed over a substantial downstream distance. This finding led them to propose a collective interaction in which no small vortices are formed. Instead, a large vortex is formed if the forcing level is high. No real mention of the level of forcing is given, but it is probably less than 10 percent of the free stream velocity.

In the current study, the flow is severely retarded and perhaps flow reversal occurs before the pressure peaks and begins to fall. The streamwise velocity fluctuations are of the order of the mean velocity and a shear layer as such does not even exists. Using a result formulated upon small perturbations in the shear layer velocity profile seems unwise if no such layer exist, but even if a calculation is made using this theory, the most amplified frequency would be 2510 hertz: based upon the maximum growth rate at a Strouhal number of 0.032, the average momentum thickness, and a mean velocity of 22 m/sec. The major

velocity fluctuation, i.e., forcing frequency, occurs at 188 hertz which is much less than the shear layer instability frequency.

If the natural instability frequency is 2510 hertz, then the forcing frequency would be something like the twelfth subharmonic of the natural frequency. This is far different than the third subharmonic forcing described in Ho and Huang (1982), which produced a slow aglomeration of four discrete vortices, i.e., the collective interaction process. As pointed out in Roberts (1985), it seems unreasonable to extend the findings to an infinite number of subharmonics. So overall, the data would suggest that the large vortices formed, in this study, are not created by gross deformations of the shear layer by simultaneous vortex aglomerations. But rather, the vortices form because of the periodic surging flow of reactants into the combustor created by acoustic excitation of the system.

GEOMETRIC CONFIGURATION	DUMP PLANE VELOCITY (m/sec)	EQUIVALENCE RATIO	KINEMATIC FLOW FIELD
I	22	1.0	unsteady
	22	0.64	steady
	22	1.28	steady
	40	1.0	unsteady
	50	1.0	steady
	70	1.0	steady
I (with acoustic damping)	22	1.0	steady
	40	1.0	steady
	50	1.0	steady
	70	1.0	steady
II	22	1.0	steady
	22	0.74	unsteady
	40	1.0	steady
	50	1.0	unsteady
	70	1.0	steady
III	22	1.0	steady
	40	1.0	steady
	50	1.0	steady
	70	1.0	steady

Table 5.1 Flow Field Classifications

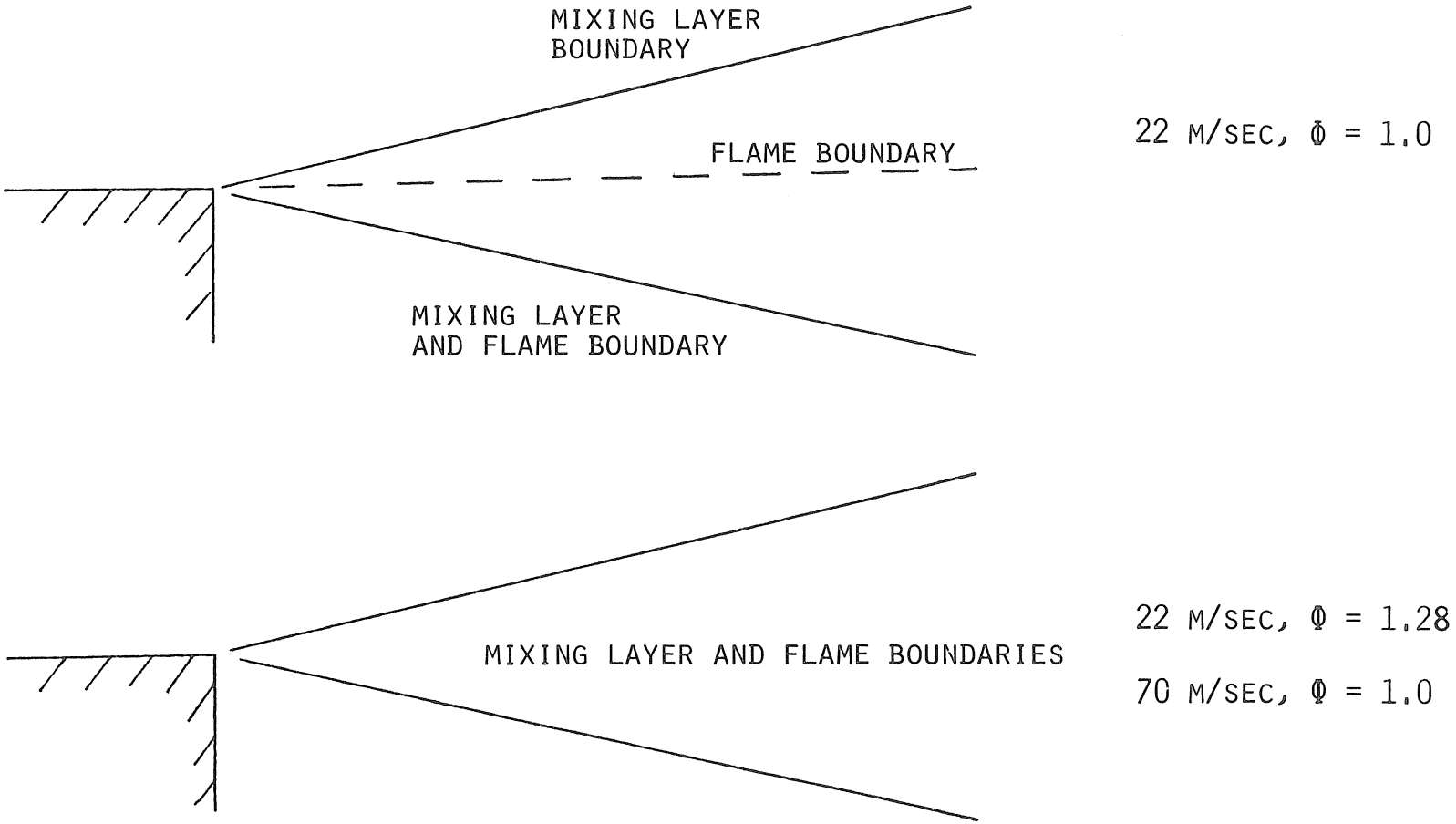

Figure 5.1 Visible Flame within the Mixing Layer

CHAPTER 6

CONCLUSIONS

An experimental investigation, of the internal feedback mechanism capable of sustaining combustion instabilities, is explored in a small laboratory combustor in which the flame is stabilized behind a rearward facing step. The local heat addition and the pressure field are examined to determine the energy release characteristics inside the combustor, and the development of the reacting, kinematic flow field is studied by employing a shadowgraph flow visualization technique. The major results and conclusions of this investigation are presented with respect to the conditions of the flow field. The main emphasis of the investigation is to study the unstable flow, but some observations of the steady flow field are notable and are highlighted.

Steady Flow Field:

Steady flow fields are produced when no large velocity fluctuations are present in the vicinity of the flameholder. A reacting, reattaching, mixing layer is formed downstream of the flameholder, and consists of discrete coherent structures. The layer growth rate is a function of flow speed and heat release within the layer. Since many parameters change as the flow speed is varied, such as the acoustic field and initial boundary layer state, no firm conclusions can be stated about the effect of flow speed on the layer growth. However, an increase in the heat release rate within layers at the same velocity conditions, decreased the growth rate of the shear layer.

The location of the visible flame, or reaction region, within the layer is a function of the fuel-air ratio of the combustible mixture. For lean mixture ratios, the visible flame resides in the lower portion of the mixing layer adjacent to the hot combustion products. However, if the mixture ratio is rich or near stoichiometric, the flame extends across the entire mixing layer.

Unstable Flow Field:

Excitation of the system's resonant modes may create combustion instabilities. In the presence of strong acoustic oscillations which accompany combustion instability, a large velocity fluctuation in the vicinity of the flameholder produces a surging flow into the combustor. This unsteady flow produces a large vortex at the frequency of the large velocity fluctuation, and the mechanism that supplies energy to the acoustic field depends upon the unsteady combustion within the vortex. Energy is supplied to the acoustic field because the heat release rate fluctuations and the pressure oscillations are in phase from initial vortex formation, until the vortex has grown, propagated downstream, and impinged against the combustor wall. Furthermore, the location of the maximum energy input appears to occur when the vortex impinges on the wall.

The motion of the vortex is a function of the instability frequency, and is meagerly affected by the mean flow speed. However, the time required for vortex impingement is determined by the magnitude of the velocity fluctuation, and the instability frequency seems to be directly proportional to the amplitude of these fluctuations. This dependence of the vortex motion upon the magnitude of the velocity

fluctuation creates the possibility of exciting a large range of system frequencies.

The mean flow velocity is important in this mechanism because the ratio of the fluctuating velocity to mean flow velocity must be substantial to produce the large vortices which sustain the instability. For some limiting velocity, the energy feedback is too weak to produce the necessary amplitude of fluctuation and the instability dies out.

The interaction of the vortex with the combustor wall is key to the mechanism, in that this interaction greatly increases the local heat release rate. Since the time delay between mixing and rapid combustion is a strong function of the initial reactant temperature, fuel type, and fuel-air ratio, these parameters affect the regimes in which the instability can exist. As the mixture ratio is changed, the instability may die out completely, or a different instability may arise driven by a different energy feedback mechanism.

APPENDIX

The acoustic pressure and velocity distributions within all the segments of the apparatus, except the inductance, i.e., the flameholder region, are described by the wave equation. In section 3.1, the matching conditions describing the change in the local acoustic pressure, or velocity, between segments was presented in a basic, preliminary form so that the underlying physical concepts were clear.

The apparatus is described with two boundary conditions and six matching conditions which collectively contain nine unknown parameters. Thus, a system of 8 equations with 9 unknown variables needs to be solved to determine the resonant frequencies of the system. The nine unknown parameters consist of the complex frequency, and eight pressure coefficients. As mentioned in section 3.2, the eight pressure coefficients were eliminated in favor of the complex frequency, which then could be found by an iterative technique. The unknown pressure coefficients may be determined by choosing a value for one of the coefficients, and solving for the others based upon this selection. The boundary and matching conditions define the relationship between the pressure coefficients at the junctions between segments of the apparatus, and these relationships were presented in basic form in the text of section 3.1. However, the complete final forms of these equations are presented on the next two pages to show the detailed relationships between the pressure coefficients, which are the basis for the equations used in the computation of the acoustic resonant frequencies, pressure, and velocity distributions.

a.) Entrance boundary condition:

$$P_3^- e^{iK_3LP} = \beta_p P_3^+ e^{-iK_3LP}$$

b.) Matching condition between the plenum chamber, section 3, and the inlet region, section 2:

$$P_3^+ = \left[1 + \frac{a_3A_2}{a_2A_3} \right] \frac{1}{2 F_{32I}} P_2^+ + \left[1 - \frac{a_3A_2}{a_2A_3} \right] \frac{F_{2I}}{2 F_{32I}} P_2^-$$

$$P_3^- = \left[1 - \frac{a_3A_2}{a_2A_3} \right] \frac{1}{2 F_{3I}F_{32I}} P_2^+ + \left[1 + \frac{a_3A_2}{a_2A_3} \right] \frac{F_{2I}}{2 F_{3I}F_{32I}} P_2^-$$

where: a_i = local acoustic velocity

A_i = cross-sectional area

$$F_{2I} = e^{iK_2LI} / e^{-iK_2LI}$$

$$F_{3I} = e^{iK_3LI} / e^{-iK_3LI}$$

$$F_{32I} = e^{iK_3LI(M_3-1)} / e^{iK_2LI(M_2-1)}$$

c.) Matching conditions across the inductance

$$P_2^+ = \left[1 - \frac{i\Omega}{2} \frac{l_e}{a_A} \frac{A_2}{A_e} \right] P_A^+ + \frac{i\Omega}{2} \frac{l_e}{a_A} \frac{A_2}{A_e} P_A^-$$

$$P_2^- = - \frac{i\Omega}{2} \frac{l_e}{a_A} \frac{A_2}{A_e} P_A^+ + \left[1 + \frac{i\Omega}{2} \frac{l_e}{a_A} \frac{A_2}{A_e} \right] P_A^-$$

with: l_e = length of the inductance segment

d.) Temperature change:

$$P_A^+ = \tfrac{1}{2} \left[1 + \frac{a_1}{a_A} \right] P_1^+ + \tfrac{1}{2} \left[1 - \frac{a_1}{a_A} \right] P_1^-$$

$$P_A^- = \tfrac{1}{2} \left[1 - \frac{a_1}{a_A} \right] P_1^+ + \tfrac{1}{2} \left[1 + \frac{a_1}{a_A} \right] P_1^-$$

e.) Combustor exit boundary condition:

$$P_1^+ \; e^{iK_1LC} = \beta_e P_1^- \; e^{-iK_1LC}$$

COMPUTER CODE FOR CALCULATION OF SYSTEM PRESSURE DISTRIBUTION

```
      PROGRAM MAIN
C
      REAL C1,C2,C3,A1AE,A2A3,LC,LI,LP,LE,M1,M2,M3,T1,T2,T3,PRES1,S,
     1     PRES2,PRES3,RHO1,RHO2,RHO3,U1M,U2M,U3M,GAMI,GAMC,UR,EPS,R
C
      COMPLEX BP,BE,X(14),OMEGA(14),FREQPR(14),F1,F3P,F32I,K1,K2,K3,
     1        W1,W2,W3,F2I,F3I,F22I,F33I,BZ,W4,W5,W6
      DIMENSION INFER(14)
      INTEGER NSIG,KN,NGUESS,N,ITMAX,IER,NFREQ,PROMPT,INDEX
C
      CHARACTER PLOT1*1/'N'/,PLOT2*1/'n'/,PLOT*1
C
      COMMON/AREA1/LC,LI,LP,LE,A1AE,A2A3
      COMMON/AREA2/C1,C2,C3,U1M,U2M,U3M,M1,M2,M3,T1,T2,T3
      COMMON/AREA3/PRES1,PRES2,PRES3
      COMMON/AREA4/BP,BE
      COMMON/AREA5/GAMI,GAMC
      COMMON/AREA6/X,NGUESS
      COMMON/AREA7/K1,K2,K3,F1,F3P,F32I,W1,W2,W3,W4,F2I,F3I,F22I,F33I
      COMMON/AREA8/R,S
C
      EXTERNAL FREQ
C
      NFREQ=1
      PROMPT=1
      INDEX=1
C
C        USE INPUT SUBROUTINE TO INPUT REQUIRED INFORMATION
C
 50   CONTINUE
C
      CALL INPUT
C
      EPS=1.0E-5
      NSIG=5
      KN=0
C
C          THIS PROGRAM PROMPTS FOR THE NUMBER OF ROOTS TO BE
C            FOUND AND ITERATIONS IN ZANLYT
C
      PRINT*,'INPUT THE NUMBER OF ROOTS TO BE FOUND BY ZANLYT'
      PRINT*,' '
      PRINT*,'MAX # IS 14, HOWEVER, IF ERROR IN CEXP CONTINUES'
      PRINT*,'AFTER REDUCING NUMBER OF ITERATIONS, REDUCE'
      PRINT*,'NUMBER OF ROOTS'
      READ*,N
C
      PRINT*,'INPUT MAX ITERATIONS FOR ZANLYT (ITMAX)'
      PRINT*,' '
      PRINT*,'TYPICALLY 10<ITMAX<50 BUT NOT NECESSARILY'
      PRINT*,'IF EXP(ARGUMENT) ERROR RESULTS TRY SMALLER ITMAX'
      READ*,ITMAX
C
      CALL ZANLYT(FREQ,EPS,NSIG,KN,NGUESS,N,X,ITMAX,INFER,IER)
C
      DO 200 I=1,N
           OMEGA(I)=X(I)/2./3.141592654
 200  CONTINUE
C
C        OUTPUT FREQUENCIES TO USER
C
```

```
      IF(IER.EQ.33) GO TO 500
C
 300  DO 400 I=1,N
           IF(I.EQ.5) PAUSE 'TO VIEW FREQUENCIES'
           IF(I.EQ.10) PAUSE 'TO VIEW FREQUENCIES'
           WRITE(6,310) I,OMEGA(I),INFER(I)
 310       FORMAT(' ','THE COMPLEX FREQUENCY',1X,I2,1X,
     1             'IS',6X,'(',F17.9,',',F17.9,')',4X,'HZ',/1X,
     1             'THIS ROOT WAS FOUND IN',3X,I5,3X,'ITERATIONS')
 400  CONTINUE
C
      GO TO 600
C
 500  WRITE(6,510)ITMAX
      WRITE(12,510)ITMAX
 510  FORMAT('0','THE ROOTS RETURNED HAD A PROBLEM WITH',
     1       'CONVERGENCE'/1X,'IN',1X,I5,2X,'ITERATIONS')
C
      GO TO 300
C
 600  CONTINUE
C
      PAUSE 'TO VIEW FREQUENCIES - OUTPUT TO FOLLOW'
C
C          OUTPUT TO USER ONLY
C
      WRITE(6,700)BP,BE
 700  FORMAT(//' ','THE COMPLEX PLENUM REFLECTANCE IS',T51,'(',F8.5,',',
     1    F8.5,')'/' ','THE COMPLEX EXIT REFLECTANCE IS',T51,'(',
     1    F8.5,',',F8.5,')')
C
      WRITE(6,710)GAMI,GAMC
 710  FORMAT(//' ','THE INLET DUCT GAMMA IS',T51,F10.4/
     1     ' ','THE COMBUSTOR GAMMA IS',T51,F10.4)
C
      WRITE(6,720)A2A3,A1AE
 720  FORMAT(//' ','THE INLET TO PLENUM AREA RATIO IS',T51,F10.4/
     1       ' ','THE INDUCTANCE AREA RATIO (>1) IS',T51,F10.4)
C
      WRITE(6,730)LI,LC
 730  FORMAT(//' ','THE LENGTH OF THE INLET IS',T51,F10.4,
     1    4X,'(FT)'/' ','THE LENGTH OF THE COMBUSTOR IS',T51,F10.4)
C
      PAUSE 'TO VIEW FREQUENCIES - OUTPUT TO FOLLOW'
C
      WRITE(6,740)LE,(LP-LI)
 740  FORMAT(' ','THE LENGTH OF INDUCTANCE IS',T51,F10.4/
     1     ' ','THE LENGTH OF THE PLENUM IS',T51,F10.4)
C
      WRITE(6,750)C1,C2,C3
 750  FORMAT(//' ','THE COMBUSTOR SONIC VELOCITY IS',T51,F10.4,
     1    4X,'(FT/SEC)'/' ','THE INLET DUCT SONIC VELOCITY IS',T51,
     1    F10.4/' ','THE PLENUM SONIC VELOCITY IS',T51,F10.4)
C
      WRITE(6,760)PRES1,PRES2,PRES3
 760  FORMAT(//' ','THE COMBUSTOR STATIC PRESSURE IS',T51,F10.4,
     1    4X,'(PSI)'/' ','THE INLET STATIC PRESSURE IS',T51,
     1    F10.4/' ','THE PLENUM STATIC PRESSURE IS',T51,F10.4)
C
      WRITE(6,770)M1,M2,M3
 770  FORMAT(//' ','THE COMBUSTOR MACH NUMBER IS',T51,F10.4/
```

```
     1     ' ', 'THE INLET DUCT MACH NUMBER IS', T51, F10.4/
     1     ' ', 'THE PLENUM MACH NUMBER IS', T51, F10.4)
C
      WRITE(6,780)T1,T2,T3
 780  FORMAT(//' ', 'THE COMBUSTOR STATIC TEMPERATURE IS', T51, F10.4,
     1     4X, '('R)'//' ', 'THE INLET STATIC TEMPERATURE IS', T51,
     1     F10.4//' ', 'THE PLENUM STATIC TEMPERATURE IS', T51, F10.4)
C
C          OUTPUT TO TAPE FILE
C
C         OUTPUT FREQUENCIES TO TAPE
C
      IF(IER.EQ.33) GO TO 900
C
 800  DO 850 I=1,N
        WRITE(12,310) I,OMEGA(I),INFER(I)
 850  CONTINUE
C
      GO TO 920
C
 900  WRITE(12,310)ITMAX
      GO TO 800
C
 920  CONTINUE
C
C           OUTPUT TO TAPE
C
      WRITE(12,700)BP,BE
      WRITE(12,710)GAMI,GAMC
      WRITE(12,720)A2A3,A1AE
      WRITE(12,730)LI,LC
      WRITE(12,740)LE,(LP-LI)
      WRITE(12,750)C1,C2,C3
      WRITE(12,760)PRES1,PRES2,PRES3
      WRITE(12,770)M1,M2,M3
      WRITE(12,780)T1,T2,T3
C
C     OUTPUT THE MODE SHAPES
C
      PRINT*,'DO YOU WANT TO PRINT P AND U AS FN(X) ? (Y OR N)'
      READ(5,1000)PLOT
 1000 FORMAT(A1)
      IF(PLOT.EQ.PLOT1) GO TO 1300
      IF(PLOT.EQ.PLOT2) GO TO 1300
      PRINT*,'ENTER NUMBER OF FREQUENCIES TO BE PRINTED (1,2,--,9)'
      READ(5,1010)NFREQ
 1010 FORMAT(I1)
C
      DO 1200 PROMPT=1,NFREQ
      WRITE(6,1100)PROMPT
 1100 FORMAT(' ', 'FREQUENCY', 2X, I2, 2X, 'HAS INDEX ? (1,2,3,---,14)')
      READ*,INDEX
      FREQPR(PROMPT)=X(INDEX)
 1200 CONTINUE
C
C     PRINT IS THE SHAPE PRINTING SUBROUTINE
C
      CALL PRESR(FREQPR,NFREQ)
 1300 CONTINUE
C
      PRINT*,'DO YOU WANT TO RUN AGAIN ? (Y OR N)'
```

```
      READ(5,1000)PLOT
      IF(PLOT.EQ.PLOT1) STOP
      IF(PLOT.EQ.PLOT2) STOP
      GO TO 50
C
      END
      SUBROUTINE CONST(Z1,Z2)
C
      REAL A1AE,A2A3,C1,C2,C3,LI,LC,LP,LE,M1,M2,M3,T1,T2,T3,PRES1,
     &RHO1,RHO2,RHO3,U1M,U2M,U3M,GAMI,GAMX,R,S,PRES2,PRES3
      COMPLEX B,BP,BE,K1,K2,K3,F1,F3P,F2I,F3I,F22I,F33I,F32I,BZ,
     &W1,W2,W3,W4,Z1,Z2
C
      COMMON/AREA1/LC,LI,LP,LE,A1AE,A2A3
      COMMON/AREA2/C1,C2,C3,U1M,U2M,U3M,M1,M2,M3,T1,T2,T3
      COMMON/AREA4/BP,BE
C
      COMMON/AREA7/K1,K2,K3,F1,F3P,F32I,W1,W2,W3,W4,F2I,F3I,F22I,
     &F33I,BZ
      COMMON/AREA8/R,S
C
      B=(0.0,1.0)
      K1=Z1/C1/(1.-M1**2.)
      K2=Z2/C2/(1.-M2**2.)
      K3=Z2/C3/(1.-M3**2.)
      F1=CEXP((-2.)*K1*LC*B)
      F3P=CEXP(2.*K3*(-LP)*B)
      F2I=CEXP((-2.)*K2*(-LI)*B)
      F3I=CEXP((-2.)*K3*(-LI)*B)
      F22I=CEXP((-M2)*K2*(-LI)*B)/CEXP(K3*(-LI)*B)
      F33I=CEXP((-M3)*K3*(-LI)*B)/CEXP(K2*(-LI)*B)
      F32I=F33I/F22I
      BZ=B*Z2*LE/(2.*C2)*A1AE
      R=(C2+C1)/(2.*C2)
      S=(C2-C1)/(2.*C2)
      W1=(R*BE*F1+S)*(1.-BZ)+BZ*(S*BE*F1+R)
      W2=(1.+BP*F3P*F3I)-(1.-BP*F3P*F3I)*C2/C3/A2A3
      W3=F2I*(-(R*BE*F1+S)*BZ+(S*BE*F1+R)*(1.+BZ))
      W4=(1.+ BP*F3P*F3I)+(1.-BP*F3P*F3I)*C2/C3/A2A3
c
      return
c
      end
C
C
C


      COMPLEX FUNCTION FREQ(Z)
C
      REAL A1AE,A2A3,C1,C2,C3,LI,LC,LP,LE,M1,M2,M3,T1,T2,T3,PRES1,
     &RHO1,RHO2,RHO3,U1M,U2M,U3M,GAMI,GAMC,R,S,PRES2,PRES3
      COMPLEX Z,B,BP,BE,K1,K2,K3,F1,F3P,F2I,F3I,F22I,F33I,F32I,BZ,
     &W1,W2,W3,W4
C
      COMMON/AREA1/LC,LI,LP,LE,A1AE,A2A3
      COMMON/AREA2/C1,C2,C3,U1M,U2M,U3M,M1,M2,M3,T1,T2,T3
      COMMON/AREA4/BP,BE
      COMMON/AREA7/K1,K2,K3,F1,F3P,F32I,W1,W2,W3,W4,F2I,F3I,F22I,F33I,BZ
      COMMON/AREA8/R,S

C
```

```
      B=(0.0,1.0)
      K1=Z/C1/(1.-M1**2.)
      K2=Z/C2/(1.-M2**2.)
      K3=Z/C3/(1.-M3**2.)
      F1=CEXP((-2.)*K1*LC*B)
      F3P=CEXP(2.*K3*(-LP)*B)
      F2I=CEXP((-2.)*K2*(-LI)*B)
      F3I=CEXP((-2.)*K3*(-LI)*B)
      F22I=CEXP((-M2)*K2*(-LI)*B)/CEXP(K3*(-LI)*B)
      F33I=CEXP((-M3)*K3*(-LI)*B)/CEXP(K2*(-LI)*B)
      F32I=F33I/F22I
      BZ=B*Z*LE/(2.*C2)*A1AE
      R=(C2+C1)/(2.*C2)
      S=(C2-C1)/(2.*C2)
      W1=(R*BE*F1+S)*(1.-BZ)+BZ*(S*BE*F1+R)
      W2=(1.+BP*F3P*F3I)-(1.-BP*F3P*F3I)*C2/C3/A2A3
      W3=F2I*(-(R*BE*F1+S)*BZ+(S*BE*F1+R)*(1.+BZ))
      W4=(1.+ BP*F3P*F3I)+(1.-BP*F3P*F3I)*C2/C3/A2A3
C
      FREQ=W1*W2-W3*W4
C
C
C     PRINT*,K1,K2,K3,'///',F1,F3P,F2I,'///',F3I,F22I,F33I,'///',
C    &F32I,BZ,'///',
C    &R,S,'///',W1,W2,'///',W3,W4,'///',FREQ,'//////////'
C
      RETURN
      END


      SUBROUTINE INPUT
C
      REAL C1,C2,C3,A1AE,A2A3,LC,LI,LP,LE,M1,M2,M3,T1,T2,T3,PRES1,
     &PRES2,PRES3,RHO1,RHO2,RHO3,U1M,U2M,U3M,GAMI,GAMC,UR
C
      COMPLEX BP,BE,X(14)
C
      CHARACTER IT1*1/'N'/,IT2*1/'n'/,IT3*1
C
      INTEGER NGUESS
C
      COMMON/AREA1/LC,LI,LP,LE,A1AE,A2A3
      COMMON/AREA2/C1,C2,C3,U1M,U2M,U3M,M1,M2,M3,T1,T2,T3
      COMMON/AREA3/RHO1,RHO2,RHO3,PRES1,PRES2,PRES3
      COMMON/AREA4/BP,BE
      COMMON/AREA5/GAMI,GAMC
      COMMON/AREA6/X,NGUESS
C
      PRINT*,'DO YOU WANT DEFAULT DATA INPUT? (Y OR N)'
      READ(5,100) IT3
100   FORMAT(A1)
      IF(IT3.EQ.IT2) GO TO 200
C
      C1=2460.
      C2=1100.
      C3=1100.
C
      BP=(1.,0.)
      BE=(-1.,0.)
C
      LC=1.3333
```

```
      LI=1.7292
      LE=0.25
      LP=4.5625
C
      A2A3=.1061
      A1AE=4.
C
      U1M=100
      U2M=25.
      U3M=2.5
C
      PRES1=14.7
      PRES2=14.7
      PRES3=14.7
C
      GAMI=1.4
      GAMC=1.3
C
      GO TO 500
C
  200 PRINT*,'INPUT THE PLENUM SONIC VELOCITY'
      READ*,C3
      PRINT*,'INPUT THE INLET SONIC VELOCITY'
      READ*,C2
      PRINT*,'INPUT THE COMBUSTOR SONIC VELOCITY'
      READ*,C1
C
      PRINT*,'INPUT THE INLET/PLENUM AREA RATIO'
      READ*,A2A3
      PRINT*,'INPUT THE INDUCTANCE AREA RATIO (>1)'
      READ*,A1AE
C
      PRINT*,'INPUT THE PLENUM COMPLEX REFLECTANCE'
      READ*,BP
      PRINT*,'INPUT THE EXIT COMPLEX REFLECTANCE'
      READ*,BE
C
      PRINT*,'INPUT THE PLENUM LENGTH (TO DUMP PLANE)'
      READ*,LP
      PRINT*,'INPUT THE INLET DUCT LENGTH'
      READ*,LI
      PRINT*,'INPUT THE COMBUSTOR LENGTH'
      READ*,LC
      PRINT*,'INPUT INDUCTANCE LENGTH'
      READ*,LE
C
      PRINT*,'INPUT THE PLENUM MEAN VELOCITY'
      READ*,U3M
      PRINT*,'INPUT THE INLET MEAN VELOCITY'
      READ*,U2M
      PRINT*,'INPUT THE COMBUSTOR MEAN VELOCITY'
      READ*,U1M
C
      PRINT*,'INPUT THE PLENUM STATIC PRESSURE'
      READ*,PRES3
      PRINT*,'INPUT THE INLET STATIC PRESSURE'
      READ*,PRES2
      PRINT*,'INPUT THE COMBUSTOR STATIC PRESSURE'
      READ*,PRES1
C
      PRINT*,'INPUT INLET GAMMA'
```

```
      READ*,GAMI
      PRINT*,'INPUT COMBUSTOR GAMMA'
      READ*,GAMC
C
 500  CONTINUE
C
      UR=53.3
C
      T1=C1**2./(GAMC*UR*32.2)
      T2=C2**2./(GAMI*UR*32.2)
      T3=C3**2./(GAMI*UR*32.2)
C
      RHO1=PRES1/UR/T1
      RHO2=PRES2/UR/T2
      RHO3=PRES3/UR/T3
C
      M1=U1M/C1
      M2=U2M/C2
      M3=U3M/C3
C
 520  PRINT*,'DO YOU WANT DEFAULT FREQ GUESSES ? (Y OR N)'
      READ(5,100) IT3
C
      IF(IT3.EQ.IT1) GO TO 550
      IF(IT3.EQ.IT2) GO TO 550
C
      X(1)=(50.,0.01)
      X(2)=(120.,0.01)
      X(3)=(180.,0.01)
      X(4)=(250.,0.01)
      X(5)=(300.,0.01)
      X(6)=(375.,0.01)
      X(7)=(425.,0.01)
      X(8)=(480.,0.01)
      X(9)=(540.,0.01)
      X(10)=(620.,0.01)
C
      NGUESS=10
      GO TO 600
C
 550  PRINT*,'INPUT NUMBER OF GUESSES TO BE ENTERED'
      READ*,NGUESS
C
      DO 575 I=1,NGUESS
          PRINT*,'INPUT COMPLEX FREQ GUESS NUMBER  ',I
              READ*,X(I)
 575  CONTINUE
C
 600  CONTINUE
C
      DO 700 I=1,NGUESS
          X(I)=X(I)*2.*3.141592654
 700  CONTINUE
      RETURN
      END

      SUBROUTINE PRESR(FREQPR,NFREQ)
C
      REAL C1,C2,C3,U1M,U2M,U3M,M1,M2,M3,T1,T2,T3,DUMMY,X1,X2,X3,
     1     LC,LI,LP,LE,A1AE,A2A3,P1I,P2I,P3I,P1R,P2R,P3R,PRES,
     1     P1MAG,P2MAG,P3MAG,P1PHAS,P2PHAS,P3PHAS,R,S,FUDGE,
```

```
     1      PRES1,PRES2,PRES3,IPHA
C
      COMPLEX OMEGA(14),FREQPR(14),FREPLO(14),BE,BP,K1,K2,K3,
     1        F1,F3P,F32I,W1,W2,W3,Z1,Z2,B,E11,E12,E21,E22,E31,
     1        E32,W5,W6,OMEGA1,OMEGA2,P1,P2,P3,W4,
     1        F2I,F3I,F22I,F33I,BZ,EIWT
C
      CHARACTER IT1*1/'n'/,IT2*1/'N'/,IT3*1
C
      INTEGER  NFREQ,ndata
C
      COMMON/AREA1/LC,LI,LP,LE,A1AE,A2A3
      COMMON/AREA2/C1,C2,C3,U1M,U2M,U3M,M1,M2,M3,T1,T2,T3
      COMMON/AREA3/RHO1,RHO2,RHO3,PRES1,PRES2,PRES3
      COMMON/AREA4/BP,BE
      COMMON/AREA7/K1,K2,K3,F1,F3P,F32I,W1,W2,W3,W4,F2I,F3I,F22I,F33I,BZ
      COMMON/AREA8/R,S
C
      DO 50 I=1,NFREQ
      OMEGA(I)=FREQPR(I)/2./3.1415926
      FREPLO(I)=FREQPR(I)
   50 CONTINUE
C
      DO 700 I=1,NFREQ
      PRINT*,'THE COMPLEX FREQ TO BE PRINTED IS',OMEGA(I)
      PRINT*,'**'
      PRINT*,'DO YOU WANT TO CHANGE THE DAMPING TERM ? (Y OR N)'
      READ(5,75)IT3
   75 FORMAT(A1)
C
      IF(IT3.EQ.IT1) GO TO 100
      IF(IT3.EQ.IT2) GO TO 100
C
      FREQPR(I)=REAL(FREQPR(I))
      PRINT*,'INTER DESIRED INLET AND PLENUM DAMPING FACTOR'
      READ*,DUMMY
      FREQPR(I)=FREQPR(I)+(0.0,1.0)*DUMMY*2.*3.1415926
C
      FREPLO(I)=REAL(FREPLO(I))
      PRINT*,'INTER DESIRED COMBUSTOR DAMPING FACTOR'
      READ*,DUMMY
      FREPLO(I)=FREPLO(I)+(0.0,1.0)*DUMMY*2.*3.1415926
  100 CONTINUE
C
      Z1=FREQPR(I)
      Z2=FREPLO(I)
      CALL CONST(Z1,Z2)
      B=(0.0,1.0)
      E11=(1.-M1)*K1*B*LC
      E12=-(1.+M1)*K1*B*LC
      E21=(1.-M2)*K2*B*LC
      E22=-(1.+M2)*K2*B*LC
      E31=(1.-M3)*K3*B*LC
      E32=-(1.+M3)*K3*B*LC
C
C
C     PRINT*,W4,F32I,W3,W2,W1
C
C
      W5=W1*2./W4/F32I
      W6=BP*F3P*W5
```

```
C
C      PRINT*,K1,K2,K3,'///',F1,F3P,F2I,'///',F3I,F22I,F33I,'///',
C     *F32I,BZ,'///',R,S,'///',W1,W2,W3,'///',W4,W5,W6,'///',
C     *E11,E12,E31
C
       PRINT*,'PICK ndata (20,30,40,50,60,70,80,90)'
       READ*,ndata
C
       X1=0.
       X2=(-LI)/LC
       X3=(-LP)/LC
       PRINT*,'ENTER TIME PHASE IN DEGREES, FOR MODES USE T=0 THEN CORREC
      &T TO GET PHASE 0 OR 180 DEGREES'
       READ*,IPHA
       EIWT=CEXP(B*IPHA*3.1415926/180.)
       OMEGA1=FREQPR(I)/2./3.1415926
       OMEGA2=FREPLO(I)/2./3.1415926
       WRITE(12,150)OMEGA1,OMEGA2
  150  FORMAT(1X,//,1X,'THE INLET & PLENUM FREQUENCY IS',T40,'(',F9.4,
     1        ',',F9.4,')'//,1X,'THE COMBUSTOR FREQUENCY IS',T40,'(',
     1       F9.4,',',F9.4,')')
       WRITE(12,155)
  155  FORMAT(1X,//,1X,T6,'X POS',T20,'PR',T30,'PI',T42,
     1'P MAG',T52,'P PHASE')
C_____________________________________________________________________
C     PRESSURE CORRECTION FACTOR DETERMINED FROM EXPERIMENTAL PSD
C_____________________________________________________________________
C
       WRITE(6,160)
160    FORMAT(1X,'ENTER THE PRESSURE FOR THIS FREQUENCY')
       READ*,PRES
       FUDGE = PRES/SQRT((REAL(1+BE*F1))**2.+(AIMAG(1+BE*F1)**2.))
       WRITE(6,165)I,FUDGE
       WRITE(12,165)I,FUDGE
165    FORMAT(1X,'THE PRESSURE CORRECTION TERM FOR FREQ. NUMBER ',I1,
     &'IS',1X,F9.4)
C_____________________________________________________________________
C     STEP THROUGH EACH SEGMENT WITH 100 POINTS
C_____________________________________________________________________
       DO 200 J=1,100
          P3=(W5*CEXP(E31*X3)+W6*CEXP(E32*X3))*EIWT*FUDGE
C
          P3I=AIMAG(P3)
          P3R=REAL(P3)
C
          P3MAG=(P3I**2.+P3R**2.)**.5
          P3PHAS=ATAN2(P3I,P3R)*360./2./3.1415926
C
          X3=X3-LE/LC
C
          WRITE(ndata,170) X3,P3R,P3I,P3MAG,P3PHAS
170       FORMAT(5F12.6)
          IF(MOD(J,5).EQ.0)WRITE(12,175)X3,P3R,P3I,P3MAG,P3PHAS
175       FORMAT(1X,5(2X,F9.4))
          X3=X3+LE/LC
C
          X3=X3+.01*(LP-LI)/LC
C
  200  CONTINUE
C
               DO 225 J=1,100
```

```
C
              P2=(W1*CEXP(E21*X2)+W3/F2I*CEXP(E22*X2))*EIWT*FUDGE
C
              P2I=AIMAG(P2)
              P2R=REAL(P2)
              P2MAG=(P2I**2. +P2R**2. )**. 5
              P2PHAS=ATAN2(P2I, P2R)*360. /2. /3. 1415926
C
              X2=X2-LE/LC
C
             WRITE(ndata, 170)X2, P2R, P2I, P2MAG, P2PHAS
          IF(MOD(J, 5). EQ. 0)WRITE(12, 175)X2, P2R, P2I, P2MAG, P2PHAS
C
              X2=X2+LE/LC
C
              X2=X2+. 01*LI/LC
C
  225 CONTINUE
C
                DO 250 J=1, 100
C
                P1=(CEXP(E12*X1)+BE*F1*CEXP(E11*X1))*EIWT*FUDGE
                P1I=AIMAG(P1)
                P1R=REAL(P1)
                P1MAG=(P1I**2. +P1R**2. )**. 5
                P1PHAS=ATAN2(P1I, P1R)*360. /2. /3. 1415926
C
                WRITE(ndata, 170)X1, P1R, P1I, P1MAG, P1PHAS
           IF(MOD(J, 5). EQ. 0)WRITE(12, 175)X1, P1R, P1I, P1MAG, P1PHAS
C
                X1=X1+. 01
C
  250 CONTINUE
C
  700 CONTINUE
C
C
      RETURN
C
      END
```

COMPUTER CODE FOR CALCULATION OF SYSTEM VELOCITY DISTRIBUTION

```
      PROGRAM MAIN
C
      REAL C1,C2,C3,A1AE,A2A3,LC,LI,LP,LE,M1,M2,M3,T1,T2,T3,P1,P2,P3,
     1     RHO1,RHO2,RHO3,U1M,U2M,U3M,GAMI,GAMC,UR,EPS,R,S
C
      COMPLEX BP,BE,X(14),OMEGA(14),FREQPR(14),F1,F3P,F32I,K1,K2,K3,
     1        W1,W2,W3,F2I,F3I,F22I,F33I,BZ,W4,W5,W6
      DIMENSION INFER(14)
      INTEGER NSIG,KN,NGUESS,N,ITMAX,IER,NFREQ,PROMPT,INDEX
C
      CHARACTER PLOT1*1/'N'/,PLOT2*1/'n'/,PLOT*1
C
      COMMON/AREA1/LC,LI,LP,LE,A1AE,A2A3
      COMMON/AREA2/C1,C2,C3,U1M,U2M,U3M,M1,M2,M3,T1,T2,T3
      COMMON/AREA3/RHO1,RHO2,RHO3,P1,P2,P3
      COMMON/AREA4/BP,BE
      COMMON/AREA5/GAMI,GAMC
      COMMON/AREA6/X,NGUESS
      COMMON/AREA7/K1,K2,K3,F1,F3P,F32I,W1,W2,W3,W4,F2I,F3I,F22I,F33I
      COMMON/AREA8/R,S
C
      EXTERNAL FREQ
C
      NFREQ=1
      PROMPT=1
      INDEX=1
C
C        USE INPUT SUBROUTINE TO INPUT REQUIRED INFORMATION
C
 50   CONTINUE
C
      CALL INPUT
C
      EPS=1.0E-5
      NSIG=5
      KN=0
C
C         THIS PROGRAM PROMPTS FOR THE NUMBER OF ROOTS TO BE
C           FOUND AND ITERATIONS IN ZANLYT
C
      PRINT*,'INPUT THE NUMBER OF ROOTS TO BE FOUND BY ZANLYT'
      PRINT*,' '
      PRINT*,'MAX # IS 14, HOWEVER, IF ERROR IN CEXP CONTINUES'
      PRINT*,'AFTER REDUCING NUMBER OF ITERATIONS, REDUCE'
      PRINT*,'NUMBER OF ROOTS'
      READ*,N
C
      PRINT*,'INPUT MAX ITERATIONS FOR ZANLYT (ITMAX)'
      PRINT*,' '
      PRINT*,'TYPICALLY 10<ITMAX<50 BUT NOT NECESSARILY'
      PRINT*,'IF EXP(ARGUMENT) ERROR RESULTS TRY SMALLER ITMAX'
      READ*,ITMAX
C
      CALL ZANLYT(FREQ,EPS,NSIG,KN,NGUESS,N,X,ITMAX,INFER,IER)
C
      DO 200 I=1,N
         OMEGA(I)=X(I)/2./3.141592654
 200  CONTINUE
C
C        OUTPUT FREQUENCIES TO USER
C
```

```
      IF(IER.EQ.33) GO TO 500
C
 300  DO 400 I=1,N
           IF(I.EQ.5) PAUSE 'TO VIEW FREQUENCIES'
           IF(I.EQ.10) PAUSE 'TO VIEW FREQUENCIES'
           WRITE(6,310) I,OMEGA(I),INFER(I)
 310       FORMAT(' ','THE COMPLEX FREQUENCY',1X,I2,1X,
     1             'IS',6X,'(',F17.9,',',F17.9,')',4X,'HZ',/1X,
     1             'THIS ROOT WAS FOUND IN',3X,I5,3X,'ITERATIONS')
 400  CONTINUE
C
      GO TO 600
C
 500  WRITE(6,510)ITMAX
      WRITE(12,510)ITMAX
 510  FORMAT('0','THE ROOTS RETURNED HAD A PROBLEM WITH',
     1       'CONVERGENCE'/1X,'IN',1X,I5,2X,'ITERATIONS')
C
      GO TO 300
C
 600  CONTINUE
C
      PAUSE 'TO VIEW FREQUENCIES - OUTPUT TO FOLLOW'
C
C          OUTPUT TO USER ONLY
C
      WRITE(6,700)BP,BE
 700  FORMAT(//' ','THE COMPLEX PLENUM REFLECTANCE IS',T51,'(',F8.5,',',
     1    F8.5,')'/' ','THE COMPLEX EXIT REFLECTANCE IS',T51,'(',
     1    F8.5,',',F8.5,')')
C
      WRITE(6,710)GAMI,GAMC
 710  FORMAT(//' ','THE INLET DUCT GAMMA IS',T51,F10.4/
     1    ' ','THE COMBUSTOR GAMMA IS',T51,F10.4)
C
      WRITE(6,720)A2A3,A1AE
 720  FORMAT(//' ','THE INLET TO PLENUM AREA RATIO IS',T51,F10.4/
     1       ' ','THE INDUCTANCE AREA RATIO (>1) IS',T51,F10.4)
C
      WRITE(6,730)LI,LC
 730  FORMAT(//' ','THE LENGTH OF THE INLET IS',T51,F10.4,
     1    4X,'(FT)'/' ','THE LENGTH OF THE COMBUSTOR IS',T51,F10.4)
C
      PAUSE 'TO VIEW FREQUENCIES - OUTPUT TO FOLLOW'
C
      WRITE(6,740)LE,(LP-LI)
 740  FORMAT(' ','THE LENGTH OF INDUCTANCE IS',T51,F10.4/
     1    ' ','THE LENGTH OF THE PLENUM IS',T51,F10.4)
C
      WRITE(6,750)C1,C2,C3
 750  FORMAT(//' ','THE COMBUSTOR SONIC VELOCITY IS',T51,F10.4,
     1    4X,'(FT/SEC)'/' ','THE INLET DUCT SONIC VELOCITY IS',T51,
     1    F10.4/' ','THE PLENUM SONIC VELOCITY IS',T51,F10.4)
C
      WRITE(6,760)P1,P2,P3
 760  FORMAT(//' ','THE COMBUSTOR STATIC PRESSURE IS',T51,F10.4,
     1    4X,'(PSI)'/' ','THE INLET STATIC PRESSURE IS',T51,
     1    F10.4/' ','THE PLENUM STATIC PRESSURE IS',T51,F10.4)
C
      WRITE(6,770)M1,M2,M3
 770  FORMAT(//' ','THE COMBUSTOR MACH NUMBER IS',T51,F10.4/
```

```
     1     ' ','THE INLET DUCT MACH NUMBER IS',T51,F10.4/
     1     ' ','THE PLENUM MACH NUMBER IS',T51,F10.4)
C
      WRITE(6,780)T1,T2,T3
 780  FORMAT(//' ','THE COMBUSTOR STATIC TEMPERATURE IS',T51,F10.4,
     1     4X,'(''R)'//' ','THE INLET STATIC TEMPERATURE IS',T51,
     1     F10.4//' ','THE PLENUM STATIC TEMPERATURE IS',T51,F10.4)
C
C          OUTPUT TO TAPE FILE
C
C         OUTPUT FREQUENCIES TO TAPE
C
      IF(IER.EQ.33) GO TO 900
C
 800  DO 850 I=1,N
         WRITE(12,310) I,OMEGA(I),INFER(I)
 850  CONTINUE
C
      GO TO 920
C
 900  WRITE(12,310)ITMAX
      GO TO 800
C
 920  CONTINUE
C
C           OUTPUT TO TAPE
C
      WRITE(12,700)BP,BE
      WRITE(12,710)GAMI,GAMC
      WRITE(12,720)A2A3,A1AE
      WRITE(12,730)LI,LC
      WRITE(12,740)LE,(LP-LI)
      WRITE(12,750)C1,C2,C3
      WRITE(12,760)P1,P2,P3
      WRITE(12,770)M1,M2,M3
      WRITE(12,780)T1,T2,T3
C
C     OUTPUT THE MODE SHAPES
C
      PRINT*,'DO YOU WANT TO PRINT P AND U AS FN(X) ? (Y OR N)'
      READ(5,1000)PLOT
 1000 FORMAT(A1)
      IF(PLOT.EQ.PLOT1) GO TO 1300
      IF(PLOT.EQ.PLOT2) GO TO 1300
      PRINT*,'ENTER NUMBER OF FREQUENCIES TO BE PRINTED (1,2,--,9)'
      READ(5,1010)NFREQ
 1010 FORMAT(I1)
C
      DO 1200 PROMPT=1,NFREQ
      WRITE(6,1100)PROMPT
 1100 FORMAT(' ','FREQUENCY',2X,I2,2X,'HAS INDEX ? (1,2,3,---,14)')
      READ*,INDEX
      FREQPR(PROMPT)=X(INDEX)
 1200 CONTINUE
C
C     PRINT IS THE SHAPE PRINTING SUBROUTINE
C
      CALL VELOC(FREQPR,NFREQ)
 1300 CONTINUE
C
      PRINT*,'DO YOU WANT TO RUN AGAIN ? (Y OR N)'
```

```
      READ(5,1000)PLOT
      IF(PLOT.EQ.PLOT1) STOP
      IF(PLOT.EQ.PLOT2) STOP
      GO TO 50
C
      END
      SUBROUTINE CONST(Z1,Z2)
C
      REAL A1AE,A2A3,C1,C2,C3,LI,LC,LP,LE,M1,M2,M3,T1,T2,T3,P1,P2,P3,
     &RHO1,RHO2,RHO3,U1M,U2M,U3M,GAMI,GAMX,R,S
      COMPLEX B,BP,BE,K1,K2,K3,F1,F3P,F2I,F3I,F22I,F33I,F32I,BZ,
     &W1,W2,W3,W4,Z1,Z2
C
      COMMON/AREA1/LC,LI,LP,LE,A1AE,A2A3
      COMMON/AREA2/C1,C2,C3,U1M,U2M,U3M,M1,M2,M3,T1,T2,T3
      COMMON/AREA4/BP,BE
C
      COMMON/AREA7/K1,K2,K3,F1,F3P,F32I,W1,W2,W3,W4,F2I,F3I,F22I,
     &F33I,BZ
      COMMON/AREA8/R,S
C
      B=(0.0,1.0)
      K1=Z1/C1/(1.-M1**2.)
      K2=Z2/C2/(1.-M2**2.)
      K3=Z2/C3/(1.-M3**2.)
      F1=CEXP((-2.)*K1*LC*B)
      F3P=CEXP(2.*K3*(-LP)*B)
      F2I=CEXP((-2.)*K2*(-LI)*B)
      F3I=CEXP((-2.)*K3*(-LI)*B)
      F22I=CEXP((-M2)*K2*(-LI)*B)/CEXP(K3*(-LI)*B)
      F33I=CEXP((-M3)*K3*(-LI)*B)/CEXP(K2*(-LI)*B)
      F32I=F33I/F22I
      BZ=B*Z2*LE/(2.*C2)*A1AE
      R=(C2+C1)/(2.*C2)
      S=(C2-C1)/(2.*C2)
      W1=(R*BE*F1+S)*(1.-BZ)+BZ*(S*BE*F1+R)
      W2=(1.+BP*F3P*F3I)-(1.-BP*F3P*F3I)*C2/C3/A2A3
      W3=F2I*(-(R*BE*F1+S)*BZ+(S*BE*F1+R)*(1.+BZ))
      W4=(1.+ BP*F3P*F3I)+(1.-BP*F3P*F3I)*C2/C3/A2A3
c
      return
c
      end
C
C
C
      COMPLEX FUNCTION FREQ(Z)
C
      REAL A1AE,A2A3,C1,C2,C3,LI,LC,LP,LE,M1,M2,M3,T1,T2,T3,P1,P2,P3,
     &RHO1,RHO2,RHO3,U1M,U2M,U3M,GAMI,GAMC,R,S
      COMPLEX Z,B,BP,BE,K1,K2,K3,F1,F3P,F2I,F3I,F22I,F33I,F32I,BZ,
     &W1,W2,W3,W4
C
      COMMON/AREA1/LC,LI,LP,LE,A1AE,A2A3
      COMMON/AREA2/C1,C2,C3,U1M,U2M,U3M,M1,M2,M3,T1,T2,T3
      COMMON/AREA4/BP,BE
      COMMON/AREA7/K1,K2,K3,F1,F3P,F32I,W1,W2,W3,W4,F2I,F3I,F22I,F33I,BZ
      COMMON/AREA8/R,S
```

```
C
      B=(0.0,1.0)
      K1=Z/C1/(1.-M1**2.)
      K2=Z/C2/(1.-M2**2.)
      K3=Z/C3/(1.-M3**2.)
      F1=CEXP((-2.)*K1*LC*B)
      F3P=CEXP(2.*K3*(-LP)*B)
      F2I=CEXP((-2.)*K2*(-LI)*B)
      F3I=CEXP((-2.)*K3*(-LI)*B)
      F22I=CEXP((-M2)*K2*(-LI)*B)/CEXP(K3*(-LI)*B)
      F33I=CEXP((-M3)*K3*(-LI)*B)/CEXP(K2*(-LI)*B)
      F32I=F33I/F22I
      BZ=B*Z*LE/(2.*C2)*A1AE
      R=(C2+C1)/(2.*C2)
      S=(C2-C1)/(2.*C2)
      W1=(R*BE*F1+S)*(1.-BZ)+BZ*(S*BE*F1+R)
      W2=(1.+BP*F3P*F3I)-(1.-BP*F3P*F3I)*C2/C3/A2A3
      W3=F2I*(-(R*BE*F1+S)*BZ+(S*BE*F1+R)*(1.+BZ))
      W4=(1.+ BP*F3P*F3I)+(1.-BP*F3P*F3I)*C2/C3/A2A3
C
      FREQ=W1*W2-W3*W4
C
C
C     PRINT*,K1,K2,K3,'///',F1,F3P,F2I,'///',F3I,F22I,F33I,'///',
C    &F32I,BZ,'///',
C    &R,S,'///',W1,W2,'///',W3,W4,'///',FREQ,'//////////'
C
      RETURN
      END


      SUBROUTINE INPUT
C
      REAL C1,C2,C3,A1AE,A2A3,LC,LI,LP,LE,M1,M2,M3,T1,T2,T3,
     &P1,P2,P3,RHO1,RHO2,RHO3,U1M,U2M,U3M,GAMI,GAMC,UR
C
      COMPLEX BP,BE,X(14)
C
      CHARACTER IT1*1/'N'/,IT2*1/'n'/,IT3*1
C
      INTEGER NGUESS
C
      COMMON/AREA1/LC,LI,LP,LE,A1AE,A2A3
      COMMON/AREA2/C1,C2,C3,U1M,U2M,U3M,M1,M2,M3,T1,T2,T3
      COMMON/AREA3/RHO1,RHO2,RHO3,P1,P2,P3
      COMMON/AREA4/BP,BE
      COMMON/AREA5/GAMI,GAMC
      COMMON/AREA6/X,NGUESS
C
      PRINT*,'DO YOU WANT DEFAULT DATA INPUT? (Y OR N)'
      READ(5,100) IT3
100   FORMAT(A1)
      IF(IT3.EQ.IT2) GO TO 200
C
      C1=2460.
      C2=1100.
      C3=1100.
C
      BP=(1.,0.)
      BE=(-1.,0.)
C
```

```
      LC=1.3333
      LI=1.7292
      LE=0.25
      LP=4.5625
C
      A2A3=.1061
      A1AE=4.
C
      U1M=100
      U2M=25.
      U3M=2.5
C
      P1=14.7
      P2=P1
      P3=P1
C
      GAMI=1.4
      GAMC=1.3
C
      GO TO 500
C
 200  PRINT*,'INPUT THE PLENUM SONIC VELOCITY'
      READ*,C3
      PRINT*,'INPUT THE INLET SONIC VELOCITY'
      READ*,C2
      PRINT*,'INPUT THE COMBUSTOR SONIC VELOCITY'
      READ*,C1
C
      PRINT*,'INPUT THE INLET/PLENUM AREA RATIO'
      READ*,A2A3
      PRINT*,'INPUT THE INDUCTANCE AREA RATIO (>1)'
      READ*,A1AE
C
      PRINT*,'INPUT THE PLENUM COMPLEX REFLECTANCE'
      READ*,BP
      PRINT*,'INPUT THE EXIT COMPLEX REFLECTANCE'
      READ*,BE
C
      PRINT*,'INPUT THE PLENUM LENGTH (TO DUMP PLANE)'
      READ*,LP
      PRINT*,'INPUT THE INLET DUCT LENGTH'
      READ*,LI
      PRINT*,'INPUT THE COMBUSTOR LENGTH'
      READ*,LC
      PRINT*,'INPUT INDUCTANCE LENGTH'
      READ*,LE
C
      PRINT*,'INPUT THE PLENUM MEAN VELOCITY'
      READ*,U3M
      PRINT*,'INPUT THE INLET MEAN VELOCITY'
      READ*,U2M
      PRINT*,'INPUT THE COMBUSTOR MEAN VELOCITY'
      READ*,U1M
C
      PRINT*,'INPUT THE PLENUM STATIC PRESSURE'
      READ*,P3
      PRINT*,'INPUT THE INLET STATIC PRESSURE'
      READ*,P2
      PRINT*,'INPUT THE COMBUSTOR STATIC PRESSURE'
      READ*,P1
C
```

```
      PRINT*,'INPUT INLET GAMMA'
      READ*,GAMI
      PRINT*,'INPUT COMBUSTOR GAMMA'
      READ*,GAMC
C
 500  CONTINUE
C
      UR=53.3
C
      T1=C1**2./(GAMC*UR*32.2)
      T2=C2**2./(GAMI*UR*32.2)
      T3=C3**2./(GAMI*UR*32.2)
C
      RHO1=P1/UR/T1
      RHO2=P2/UR/T2
      RHO3=P3/UR/T3
C
      M1=U1M/C1
      M2=U2M/C2
      M3=U3M/C3
C
  520 PRINT*,'DO YOU WANT DEFAULT FREQ GUESSES ? (Y OR N)'
      READ(5,100) IT3
C
      IF(IT3.EQ.IT1) GO TO 550
      IF(IT3.EQ.IT2) GO TO 550
C
      X(1)=(50.,0.01)
      X(2)=(120.,0.01)
      X(3)=(180.,0.01)
      X(4)=(250.,0.01)
      X(5)=(300.,0.01)
      X(6)=(375.,0.01)
      X(7)=(425.,0.01)
      X(8)=(480.,0.01)
      X(9)=(540.,0.01)
      X(10)=(620.,0.01)
C
      NGUESS=10
      GO TO 600
C
 550  PRINT*,'INPUT NUMBER OF GUESSES TO BE ENTERED'
      READ*,NGUESS
C
      DO 575 I=1,NGUESS
          PRINT*,'INPUT COMPLEX FREQ GUESS NUMBER  ',I
              READ*,X(I)
 575  CONTINUE
C
 600  CONTINUE
C
      DO 700 I=1,NGUESS
          X(I)=X(I)*2.*3.141592654
 700  CONTINUE
      RETURN
      END

      SUBROUTINE VELOC(FREQPR,NFREQ)
C
      REAL C1,C2,C3,U1M,U2M,U3M,M1,M2,M3,T1,T2,T3,DUMMY,X1,X2,X3,FUDGE,
     &     LC,LI,LP,LE,A1AE,A2A3,P1I,P2I,P3I,P1R,P2R,P3R,PRES,IPHA,
```

```
     &      P1MAG, P2MAG, P3MAG, P1PHAS, P2PHAS, P3PHAS, R, S, RHO1, RHO2, RHO3
C
      COMPLEX OMEGA(14), FREQPR(14), FREPLO(14), BE, BP, K1, K2, K3,
     &         F1, F3P, F32I, W1, W2, W3, Z1, Z2, B, E11, E12, E21, E22, E31, ETA,
     &         E32, W5, W6, OMEGA1, OMEGA2, P1, P2, P3, W4,
     &         F2I, F3I, F22I, F33I, BZ, EIWT
C
      CHARACTER IT1*1/'n'/, IT2*1/'N'/, IT3*1
C
      INTEGER  NFREQ, ndata
C
      COMMON/AREA1/LC, LI, LP, LE, A1AE, A2A3
      COMMON/AREA2/C1, C2, C3, U1M, U2M, U3M, M1, M2, M3, T1, T2, T3
      COMMON/AREA3/RHO1, RHO2, RHO3, P1, P2, P3
      COMMON/AREA4/BP, BE
      COMMON/AREA7/K1, K2, K3, F1, F3P, F32I, W1, W2, W3, W4, F2I, F3I, F22I, F33I, BZ
      COMMON/AREA8/R, S
C
      DO 50 I=1, NFREQ
      OMEGA(I)=FREQPR(I)/2./3.1415926
      FREPLO(I)=FREQPR(I)
   50 CONTINUE
C
      DO 700 I=1, NFREQ
      PRINT*, 'THE COMPLEX FREQ TO BE PRINTED IS', OMEGA(I)
      PRINT*, '**'
      WRITE(6, 55)
55    FORMAT(1X, 'ENTER THE PRESSURE FOR THIS FREQUENCY')
      READ*, PRES
      FUDGE = PRES/ SQRT((REAL(1.+BE*F1))**2.+(AIMAG(1.+BE*F1))**2.)
      PRINT*, 'DO YOU WANT TO CHANGE THE DAMPING TERM ? (Y OR N)'
      READ(5, 75)IT3
   75 FORMAT(A1)
C
      IF(IT3.EQ.IT1) GO TO 100
      IF(IT3.EQ.IT2) GO TO 100
C
      FREQPR(I)=REAL(FREQPR(I))
      PRINT*, 'INTER DESIRED INLET AND PLENUM DAMPING FACTOR'
      READ*, DUMMY
      FREQPR(I)=FREQPR(I)+(0.0, 1.0)*DUMMY*2.*3.1415926
C
      FREPLO(I)=REAL(FREPLO(I))
      PRINT*, 'INTER DESIRED COMBUSTOR DAMPING FACTOR'
      READ*, DUMMY
      FREPLO(I)=FREPLO(I)+(0.0, 1.0)*DUMMY*2.*3.1415926
  100 CONTINUE
C
      Z1=FREQPR(I)
      Z2=FREPLO(I)
      CALL CONST(Z1, Z2)
      B=(0.0, 1.0)
      E11=(1.-M1)*K1*B*LC
      E12=-(1.+M1)*K1*B*LC
      E21=(1.-M2)*K2*B*LC
      E22=-(1.+M2)*K2*B*LC
      E31=(1.-M3)*K3*B*LC
      E32=-(1.+M3)*K3*B*LC
C
      W5=W1*2./W4/F32I
      W6=BP*F3P*W5
```

```
C
C
      PRINT*, 'PICK ndata (20, 30, 40, 50, 60, 70, 80, 90)'
      READ*, ndata
C
      X1=0.
      X2= -LI/LC
      X3= -LP/LC
      PRINT*, 'ENTER TIME PHASE IN DEGREES, FOR MODES USE T=0 THEN CORREC
     &T TO GET PHASE OF 0 OR 180 DEGREES'
      READ*, IPHA
      EIWT=CEXP(B*IPHA*3. 1415926/180. )
      OMEGA1=FREQPR(I)/2. /3. 1415926
      OMEGA2=FREPLO(I)/2. /3. 1415926
      WRITE(12, 150)OMEGA1, OMEGA2
  150 FORMAT(1X, //, 1X, 'THE INLET & PLENUM FREQUENCY IS', T40, '(', F9. 4,
     1        ', ', F9. 4, ')'//, 1X, 'THE COMBUSTOR FREQUENCY IS', T40, '(',
     1        F9. 4, ', ', F9. 4, ')')
      WRITE(12, 155)
  155 FORMAT(1X, //, 1X, T6, 'X POS', T20, 'UR', T30, 'UI', T42,
     1'U MAG', T52, 'U PHASE')

         DO 200 J=1, 100
         P3=(W5*CEXP(E31*X3)-W6*CEXP(E32*X3))*EIWT*32. 2*FUDGE/(RHO3*C3)
C
         P3I=AIMAG(P3)
         P3R=REAL(P3)
C
         P3MAG=(P3I**2. +P3R**2. )**. 5
         P3PHAS=ATAN2(P3I, P3R)*360. /2. /3. 1415926
C
         X3=X3-LE/LC
C
         WRITE(ndata, 170) X3, P3R, P3I, P3MAG, P3PHAS
170      FORMAT(5F12. 6)
         IF(MOD(J, 5). EQ. 0)WRITE(12, 175)X3, P3R, P3I, P3MAG, P3PHAS

  175    FORMAT(1X, 5(2X, F9. 4))
C
         X3=X3+LE/LC
C
         X3=X3+. 01*(LP-LI)/LC
C
  200 CONTINUE
C
            DO 225 J=1, 100
C
            P2=(W1*CEXP(E21*X2)-W3/F2I*CEXP(E22*X2))*EIWT*32. 2*FUDGE/
     & (RHO2*C2)
C
            P2I=AIMAG(P2)
            P2R=REAL(P2)
            P2MAG=(P2I**2. +P2R**2. )**. 5
            P2PHAS=ATAN2(P2I, P2R)*360. /2. /3. 1415926
C
            X2=X2-LE/LC
C
            WRITE(ndata, 170)X2, P2R, P2I, P2MAG, P2PHAS
         IF(MOD(J, 5). EQ. 0)WRITE(12, 175)X2, P2R, P2I, P2MAG, P2PHAS
C
            X2=X2+LE/LC
```

```
C
              X2=X2+.01*LI/LC
C
  225 CONTINUE
              X2=X2-LE/LC
              P2R=P2R*A1AE
              WRITE(ndata,170)X2,P2R,P2I,P2MAG,P2PHAS
              X2=X1-.01
              WRITE(ndata,170)X2,P2R,P2I,P2MAG,P2PHAS

C
                DO 250 J=1,100
C
                P1=(-CEXP(E12*X1)+BE*F1*CEXP(E11*X1))*EIWT*32.2*FUDGE/
     & (RHO1*C1)
C
                P1I=AIMAG(P1)
                P1R=REAL(P1)
                P1MAG=(P1I**2.+P1R**2.)**.5
                P1PHAS=ATAN2(P1I,P1R)*360./2./3.1415926
C
                WRITE(ndata,170)X1,P1R,P1I,P1MAG,P1PHAS
          IF(MOD(J,5).EQ.0)WRITE(12,175)X1,P1R,P1I,P1MAG,P1PHAS
C
                X1=X1+.01
C
  250 CONTINUE
C
  700 CONTINUE
C
C
      RETURN
C
      END
```

List of References

Bendat, J.S., and A.G. Piersol (1971), Random Data: Analysis and Measurement Procedures, Wiley, New York.

Beranek, L.L. (1954), Acoustics, McGraw-Hill, New York.

Brigham, E.O. (1974), The Fast Fourier Transform, Prentice-Hall, New Jersey.

Brown, G.L., and A. Roshko (1974), "On Density Effects and Large Structure in Turbulent Mixing Layers," J. Fluid Mech., 64, 775-816.

Currie, I.G. (1974), Fundamentals of Fluid Mechanics, McGraw-Hill, New York.

Eaton, J.K., and J.P. Johnston (1980), "Turbulent Flow Reattachment: An Experimental Study of the Flow and Structure Behind a Backward-Facing Step," Report MD-39, Stanford University.

Eaton, J.K., and J.P. Johnston (1981), "A Review of Research on Subsonic Turbulent Flow Reattachment," AIAA J., 19, 1093-1099.

Freymuth, P. (1966), "On Transition in a Separated Laminar Boundary Layer," J. Fluid Mech., 25, 683-704.

Ganji, A.T., and R.F. Sawyer (1980), "Turbulence, Combustion, Pollutant, and Stability Characterization of a Premixed, Step Combustor," NASA Contractor Report 3230.

Ho, Chin-Ming, and Lein-Saing Huang (1982), "Subharmonics and Vortex Merging in Mixing Layers," J. Fluid Mech., 119, 443-473.

Ho, Chin-Ming, and P. Huerre (1984), "Perturbed Free Shear Layers," Ann. Rev. Fluid Mech., 16, 365-424.

Humphrey, J.W. (1983), "Computation of One-Dimensional Acoustic Modes as Applied to Ramjet Inlet/Combustors," NWC Memorandum 5164.

Huot, J.P., D. Frost, and C. Lim (1982), "Radiation from Flames," Ae 104 Report, California Institute of Technology.

Hurle, I.R., R.B. Price, T.M.Sugden, and A. Thomas (1968), "Sound Emission from Open Turbulent Premixed Flames," Proc. Roy. Soc., 303, 409-427.

Ishikawa, N. (1983), "Experimental Study of Jet Mixing Mechanisms in a Model Secondary Combustor," AIAA J., 21, 565-571.

John, R.R., E.S. Wilson, and M. Summerfield (1955), "Studies of the Mechanism of Flame Stabilization by a Spectral Intensity Method," Jet Propulsion, 25, 535-537.

John, R.R., and M. Summerfield (1957), "Effect of Turbulence on Radiation Intensity from Propane-Air Flames," Jet Propulsion, 27, 169-179.

Jones, R.E., A.M. Trout, J.D. Wear, and B.J. McFride (1984), "Combustion Gas Properties," NASA Tech. paper 2359.

Keller, J.O., L. Vaneveld, D. Korschelt, G.L. Hubbard, A.F. Ghoniem, J.W. Daily, and A.K. Oppenheim (1982), "Mechanism of Instabilities in Turbulent Combustion Leading to Flashback," AIAA J., 29, 254-262.

Liepmann, H.W., and A. Roshko (1957), Elements of Gasdynamics, Wiley, New York.

Michalke A. (1964), "On the Viscid Instability of Hypervelocity-tangent Profiles," J. Fluid Mech., 19, 543-546.

Michalke A. (1965), "On Spatially Growing Disturbances in an Inviscid Shear Layer," J. Fluid Mech., 23, 521-544.

Michalke A., and P. Freymuth (1966), "The Instability and the Formation of Vortices in a Free Boundary Layer," AGARD Conf. Proc. No. 4, Separated Flows - part 2, 575-595.

Moore, R.K. (1960), Traveling-Wave Engineering, McGraw-Hill, New York

Nayfeh, A.H., and D.T. Mook (1979), Nonlinear Oscillations, Wiley, New York.

Oates, G.C. (1978), "The Aerothermodynamics of Aircraft Gas Turbine Engines," Report Number TR 78-52, Air Force Aero-Propulsion Laboratory.

Oatnes, R.K., and L. Enochson (1978), Applied Time Series Analysis, Wiley, New York.

Oppenheim, A.K. and A.F. Ghoniem (1983), "Aerodynamic Features of Turbulent Flames," AIAA paper 83-0470.

Oster, D., and I. Wygnanski (1982), "The Forced Mixing Layer Between Parallel Streams," J. Fluid Mech., 123, 91-130.

Pitz, R.W. (1981), "An Experimental Study of Combustion: The Turbulent Structure of a Reacting Shear Layer formed at a Rearward-Facing Step," Ph.D. Thesis, University of California, Berkeley.

Pitz, R.W., and J.W. Daily (1983), "Combustion in a Turbulent Mixing Layer Formed at a Rearward-Facing Step," AIAA J., 21, 1565-1570.

Radio Corporation of America (1970), Photomultiplier Manual, RCA, New Jersey.

Roberts, F.A. (1985), "Effects of a Periodic Disturbance on Structure and Mixing in Turbulent Shear Layers and Wakes," Ph.D. Thesis, California Institute of Technology.

Rogers, D.E. (1954), "An Experimental Investigation of High Frequency Combustion Instability in a Fuel-Air Combustor, A.E. Thesis, California Institute of Technology.

Rogers, D.E., and F.E. Marble (1956), "A Mechanism for High-Frequency Oscillations in Ramjet Combustors and Afterburners," Jet Propulsion, June, 456-462.

Schadow, K.C., K.J. Wilson, J.E. Crump, and J.B. Foster (1984), "Interaction Between Acoustics and Subsonic Ducted Flow with Dump," AIAA 22nd Aerospace Sciences Meeting.

Strehlow, R.A. (1979), Fundamentals of Combustion, Kreiger, New York.

Vaneveld, L., K. Hom, and A.K. Oppenheim (1984), "Secondary Effects in Combustion Instabilities Leading to Flashback," AIAA J., 22, 81-83.

Weinberg, F.J. (1963), Optics of Flames, Butterworths, Washington.

Weinberger, J.F. (1965), Partial Differential Equations, Wiley, New York.

White, F.M. (1974), Viscous Fluid Flow, McGraw-Hill, New York.

Williams, G.C., H.C. Hottel, and A.C. Scurlock (1949), "Flame Stabilization and Propagation in High Velocity Gas Streams," Third Symp. on Combustion, 21-40.

Yang, B.T., and M.H. Yu (1983), "The Flowfield in a Suddenly Enlarged Combustion Chamber," AIAA J., 21, 92-97.

Zukoski, E.E. (1954), "Flame Stabilization on Bluff Bodies at Low and Intermediate Reynolds Numbers," Ph.D. Thesis, California Institute of Technology.

Zukoski, E.E., and F.E. Marble (1955), "The Role of Wake Transition in the Process of Flame Stabilization on Bluff Bodies," Combustion Researches and Reviews, AGARD, Butterworths, London, 167-180.

Zukoski, E.E., and F.E. Marble (1956), "Experiments Concerning the Mechanism of Flame Blowoff from Bluff Bodies," Proc. Gas Dynamics Sym. on Aerothermochenistry, Northwest University Press, 205-210.